

UNCLASSIFIED

AD NUMBER
ADB269253
NEW LIMITATION CHANGE
TO Approved for public release, distribution unlimited
FROM Distribution authorized to U.S. Gov't. agencies only; Proprietary Info.; Sep 2000. Other requests shall be referred to U.S. Army Medical Research and Materiel Command, 504 Scott St., Fort Detrick, MD 21702-5012.
AUTHORITY
USAMRMC ltr, 21 Feb 2003

THIS PAGE IS UNCLASSIFIED

Award Number: DAMD17-98-1-8177

TITLE: Visual Servoing for Optimization of Anticancer Drug Uptake in
Human Breast Cancer Cells

PRINCIPAL INVESTIGATOR: Daniel E. Callahan, Ph.D.

CONTRACTING ORGANIZATION: University of California at Berkeley
Berkeley, California 94720

REPORT DATE: September 2000

TYPE OF REPORT: Annual

PREPARED FOR: U.S. Army Medical Research and Materiel Command
Fort Detrick, Maryland 21702-5012

DISTRIBUTION STATEMENT: Distribution authorized to U.S.
Government agencies only (proprietary information, Sep 00).
Other requests for this document shall be referred to U.S.
Army Medical Research and Materiel Command, 504 Scott Street,
Fort Detrick, Maryland 21702-5012.

The views, opinions and/or findings contained in this report are those of
the author(s) and should not be construed as an official Department of the
Army position, policy or decision unless so designated by other
documentation.

20010817 043

NOTICE

USING GOVERNMENT DRAWINGS, SPECIFICATIONS, OR OTHER DATA INCLUDED IN THIS DOCUMENT FOR ANY PURPOSE OTHER THAN GOVERNMENT PROCUREMENT DOES NOT IN ANY WAY OBLIGATE THE U.S. GOVERNMENT. THE FACT THAT THE GOVERNMENT FORMULATED OR SUPPLIED THE DRAWINGS, SPECIFICATIONS, OR OTHER DATA DOES NOT LICENSE THE HOLDER OR ANY OTHER PERSON OR CORPORATION; OR CONVEY ANY RIGHTS OR PERMISSION TO MANUFACTURE, USE, OR SELL ANY PATENTED INVENTION THAT MAY RELATE TO THEM.

LIMITED RIGHTS LEGEND

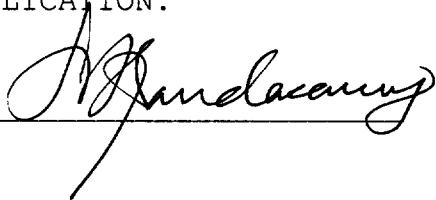
Award Number: DAMD17-98-1-8177

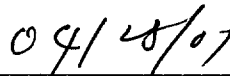
Organization: University of California at Berkeley

Location of Limited Rights Data (Pages):

Those portions of the technical data contained in this report marked as limited rights data shall not, without the written permission of the above contractor, be (a) released or disclosed outside the government, (b) used by the Government for manufacture or, in the case of computer software documentation, for preparing the same or similar computer software, or (c) used by a party other than the Government, except that the Government may release or disclose technical data to persons outside the Government, or permit the use of technical data by such persons, if (i) such release, disclosure, or use is necessary for emergency repair or overhaul or (ii) is a release or disclosure of technical data (other than detailed manufacturing or process data) to, or use of such data by, a foreign government that is in the interest of the Government and is required for evaluational or informational purposes, provided in either case that such release, disclosure or use is made subject to a prohibition that the person to whom the data is released or disclosed may not further use, release or disclose such data, and the contractor or subcontractor or subcontractor asserting the restriction is notified of such release, disclosure or use. This legend, together with the indications of the portions of this data which are subject to such limitations, shall be included on any reproduction hereof which includes any part of the portions subject to such limitations.

THIS TECHNICAL REPORT HAS BEEN REVIEWED AND IS APPROVED FOR PUBLICATION.





REPORT DOCUMENTATION PAGE			Form Approved OMB No. 074-0188	
Public reporting burden for this collection of information is estimated to average 1 hour per response, including the time for reviewing instructions, searching existing data sources, gathering and maintaining the data needed, and completing and reviewing this collection of information. Send comments regarding this burden estimate or any other aspect of this collection of information, including suggestions for reducing this burden to Washington Headquarters Services, Directorate for Information Operations and Reports, 1215 Jefferson Davis Highway, Suite 1204, Arlington, VA 22202-4302, and to the Office of Management and Budget, Paperwork Reduction Project (0704-0188), Washington, DC 20503				
1. AGENCY USE ONLY (Leave blank)	2. REPORT DATE September 2000	3. REPORT TYPE AND DATES COVERED Annual (1 Sep 99 - 31 Aug 00)		
4. TITLE AND SUBTITLE Visual Servoing for Optimization of Anticancer Drug Uptake in Human Breast Cancer Cells		5. FUNDING NUMBERS DAMD17-98-1-8177		
6. AUTHOR(S) Daniel E. Callahan, Ph.D. and Bahram Parvin, Ph.D.				
7. PERFORMING ORGANIZATION NAME(S) AND ADDRESS(ES) University of California at Berkeley Berkeley, California 94720 E-MAIL: DECallahan@lbl.gov		8. PERFORMING ORGANIZATION REPORT NUMBER		
9. SPONSORING / MONITORING AGENCY NAME(S) AND ADDRESS(ES) U.S. Army Medical Research and Materiel Command Fort Detrick, Maryland 21702-5012		10. SPONSORING / MONITORING AGENCY REPORT NUMBER		
11. SUPPLEMENTARY NOTES This report contains colored photos				
12a. DISTRIBUTION / AVAILABILITY STATEMENT DISTRIBUTION STATEMENT: Distribution authorized to U.S. Government agencies only (proprietary information, Sep 00). Other requests for this document shall be referred to U.S. Army Medical Research and Materiel Command, 504 Scott Street, Fort Detrick, Maryland 21702-5012.			12b. DISTRIBUTION CODE	
13. ABSTRACT (Maximum 200 Words) The purpose of this two-year IDEA proposal is to gather preliminary data that demonstrate the feasibility of a new class of <i>in vitro</i> drug response and chemosensitivity assays. Our objectives are to develop an instrument (a visual servoing optical microscope, or VSOM) in a stepwise fashion and gather preliminary data to aid future development of cell culture techniques and fluorescence assays. Our goal is to demonstrate the feasibility of using VSOM technology to analyze the heterogeneity and physiological characteristics of tumor cells from individual breast cancer patient biopsies. We believe that the VSOM will be extremely useful in developing new VSOM chemosensitivity fluorescence assays for a variety of breast cancer drugs. At the conclusion of this grant, we will have preliminary data that demonstrate the use of a VSOM doxorubicin chemosensitivity assay based on the dynamic physiological responses of single cells.				
14. SUBJECT TERMS Breast Cancer			15. NUMBER OF PAGES 151	
			16. PRICE CODE	
17. SECURITY CLASSIFICATION OF REPORT Unclassified	18. SECURITY CLASSIFICATION OF THIS PAGE Unclassified	19. SECURITY CLASSIFICATION OF ABSTRACT Unclassified	20. LIMITATION OF ABSTRACT Unlimited	

NSN 7540-01-280-5500

Standard Form 298 (Rev. 2-89)
Prescribed by ANSI Std. Z39-18
298-102

Table of Contents

<u>Section</u>	<u>Page</u>
Cover.....	
SF 298.....	2
Table of Contents.....	3
Introduction.....	4
Body.....	5
Key Research Accomplishments.....	18
Reportable Outcomes.....	19
Conclusions.....	20
References.....	21
Appendix A: Figure Legends.....	21
Appendix B: Figures.....	25
Appendix C: Poster Presentation, Era of Hope Meeting.....	43
Appendix D: Biophysical Society Abstract.....	
Appendix E: Protocol for Returning to the Same Set of Cells Repeatedly....	
Appendix F: VSOM Experimental Log and Bioinformatics Template.....	
Appendix G: Patent Disclosure (Includes recent grant proposals).....	

Introduction

The purpose of this IDEA proposal is to gather preliminary data that demonstrate the feasibility of visual servoing optical microscope (VSOM) technology, experiments and assays. We hope to use VSOM in future studies to rapidly analyze large populations of living cells that have been freshly derived from human breast cancer tissue biopsies. This could lead to rapid advances in in vitro chemosensitivity testing and would represent a large step toward our ultimate goal of chemotherapy regimens tailored to the individual breast cancer patient. We believe the rapid analysis of dynamic physiological responses on a patient-by-patient, tumor-by-tumor, and cell-by-cell basis will provide critical information for individualized cancer chemotherapy. Such assays could produce detailed and distinct physiological fingerprints that are highly predictive of an individual patient's response (both normal and tumor cell response) to a particular anti-cancer drug, particular combination of drugs, or particular sequence of drug exposures.

Visual servoing (VS) is a term from the field of robotic vision, and it refers to the dynamic manipulation of experimental parameters based on analysis of digital image content. A VSOM assay consists of (i) real-time observations of individual cell responses to a series of applied stimuli (ii) adaptive, and intelligent adjustment of experimental parameters to achieve experimental goals. In VSOM assays, the flow rates of computer-controlled syringes are adjusted based on observation and quantification of cell responses in a cell chamber (see **Era of Hope Poster, Appendix C**). On-line image segmentation and analysis of many single cell responses is required for VSOM experiments, with subsequent software control of the syringes. We have met these requirements in experiments where we monitor up to 1000 living cells. In Year 2, we believe we have demonstrated the feasibility of a new class of in vitro drug response and chemosensitivity assays; namely, VSOM assays that are based on a series of quantified, dynamic physiological responses of intelligently perturbed single cells.

An ideal VSOM chemosensitivity assay does not irreversibly perturb living cells, and it allows one to make predictions of drug sensitivity based on specific physiological characteristics of individual cells. We believe our technology will allow us to rapidly (i) develop new in vitro fluorescence assays that can be used to predict chemosensitivity (ii) develop selective culture conditions for specific subpopulations of cells, i.e, primary culture tumor cells (iii) demonstrate a new paradigm in in vitro chemosensitivity testing. This new paradigm is visual servoing for knowledge-based interrogation of individual living cancer cells.

Several aspects of our approach are novel. We have combined sophisticated robotic vision techniques, digital video microscopy and biophysics to monitor and automatically respond to the responses of hundreds of living cells. We have successfully demonstrated VSOM technology by analyzing the heterogeneity and physiological characteristics of mixed populations of drug-sensitive (DS) and multidrug resistant (MDR) human breast cancer cells in real-time. This demonstrates the advantages of a VSOM doxorubicin chemosensitivity assay based on the dynamic physiological responses of single cells. These results indicate our approach will be extremely useful for developing new VSOM chemosensitivity fluorescence assays for a variety of breast cancer drugs. In addition, we have begun to develop assays for cell proliferation in living cells, which, together with assays for apoptosis, will allow us automatically and intelligently design the appropriate microenvironmental conditions for the propagation of primary human breast tumor cells.

Body

The funding for our original 3-year IDEA proposal was cut 33%, and the time for completion was reduced to 2 years. However, we requested and obtained a no-cost extension so that we may complete and publish several critical aspects of this research in Year 3, as originally proposed. Thus, we present the results of **Year 2** in this Annual Report, and will submit a Final Report at the end of Year 3. Our Technical Objectives (as stated in the Two Year Revised Statement of Work) were:

- 1) **Technical Objective 1** (Tasks 1-5, System Development) : Develop an automated VSOM system.
- 2) **Technical Objective 2** (Tasks 6 –10, Biological Experiments): (a) identify subpopulations of MDR cells in mixtures of DS and MDR human breast cancer cells, (b) characterize differences in the physiology of DS and MDR human breast cancer cells, (c) identify and characterize physiological differences between normal, immortally transformed, and tumorigenically transformed human mammary epithelial cells (HMECs).

Another important goal was to use preliminary data to obtain new funding, and we have successfully obtained new DOE Medical Applications Program funding for this research (**included in Appendix G: Automated Imaging System for Guiding Antisense Compounds to Specific mRNA targets in Living Cells, 74655**, Office of Biological and Environmental Research (OBER) of the Office of Science (OS), U.S. Department of Energy (DOE)). In addition, we have applied for a DoD Clinical Bridge Grant so that we can bring this innovative technology and a new approach to chemosensitivity testing into the clinic where it could improve clinical outcomes for breast cancer patients (**included in Appendix G: Rapid Discovery of Physiological Characteristics Which Distinguish Malignant and Nonmalignant Human Breast Epithelial Cells, BC000508**, Breast Cancer Research Program, Congressionally Directed Medical Research Program 2000). As discussed in this grant proposal, we are now able to integrate a Cancer Biologist into our effort, in a way that directly addresses problems with primary breast cancer and metastatic cell culture techniques. In this grant, we also address the basic limitations of cell-line *in vitro* chemosensitivity and predictive assays, and we propose a detailed 3-year strategy for bringing this technology into clinical trials.

Technical Objective 1 (Tasks 1-5, System Development)

Task 1: Develop a graphical user interface (GUI) for a prototype, non-automated VSOM system.

It was necessary to break the VSOM GUI development into two separate projects: one for on-line experiment control and data acquisition, and a separate one for off-line data reduction, annotation, archiving, and visualization. As shown in **Figure 1 (Appendix B)**, we have created a JAVA-based GUI for the latter project. This program is referred to as a Java Command File Generator (JCFG), and it is currently being used to aggregate annotation data from different sources (user input, laboratory notebooks, local MS Access databases, ICS image header, pump logs, recipe files, etc.) into a label-based, ASCII text command file that can easily be converted to an XML format. This command file is currently accessed by a variety of PC-based data reduction and visualization programs. It is also accessed by our current UNIX-based Image Library (ImgLib) software, and various (local, in-house) image processing routines written using a custom, compiled C version of Scil Image (TNO Institute of Applied Physics, Delft, The Netherlands). Various PC-based image processing (Corel PhotoPaint), video editing (Ulead Media Studio Pro), and plotting packages (Sigma Plot, SPSS Inc., Chicago, IL) equipped with Visual Basic automation features also access these portable text files. The JCFG was produced using Visual Cafe, Database Edition (Symantec). Obviously, our current level of funding does not allow us to build all the capabilities found in PC software into a VSOM GUI at the present time. However, we have adopted a common approach of building platform independent Java-based GUIs that can aggregate annotation data collected from separate locations. This allows the Biology and Biophysics group (Drs. Callahan, Yaswen, Dairkee) to use PC and MacIntosh host computers in addition to the UNIX-based Sparcstations used by the Computer Science and Bioinformatics group (Dr. Parvin). In addition, user interfaces that have been previously used and tested by the Biology and Biophysics group can be easily integrated Dr. Parvin's more sophisticated Bioinformatics System (DeepView), if they have been developed in Java. We have recently received funding

(Automated Imaging System for Guiding Antisense Compounds to Specific mRNA targets in Living Cells) that will support this integration and development work with Dr. Parvin and Deep View.

We are currently developing visualization and interactive data features that include the ability to retrieve image data from the storage system, overlay the cell number label and the final cell outline produced by VSOM algorithms on any combination of image channels, plot time-dependent cell responses, and display cell responses as time-lapse digital video. As we demonstrate throughout this report, it is difficult to visualize and interact with the large number of cell responses that are collected across multiple channels, even when the analysis is performed off-line with color-coded, 3D graphs and time-lapse, enhanced digital video. One approach we are taking is testing and developing analysis and visualization of our data with currently available PC-based scientific software packages, and then building similar functionality into Deep View. The current Java VSOM Results Browser (**Figure 2**) is an example of this approach. Data from experiment "WA3" is shown. (We will present data from this particular experiment, WA3, using a variety of visualization and analysis tools throughout this report). The details of experiment WA3 are presented later in this report.

The following is an overview of VSOM system integration and algorithm development from a Computer Science perspective. It should be noted that several Computer Science and Bioinformatic projects supported the development of tools and infrastructure that are now available to our VSOM system. The basic VSOM target instrument is an inverted optical microscope. We have developed a plugin that interfaces this instrument to DeepView (See <http://vision.lbl.gov/>). DeepView is a channel for distributed microscopy and informatics, and it is funded through the DOE National Collaboratory program. DeepView provides a scalable interface for adding any instrument into its framework. It also provides the means for data transfer and viewing over the wide area network. The system has a generic graphical user interface that interacts with the target instrument through advertisement of its properties. In the case of VSOM, related properties are computer controlled syringes, shutters, an XY stage, a Z-axis focus motor, a filter wheel, and camera control parameters. This concept of advertising capabilities (functionalities) of an instrument leads to a more uniform interface and reduces maintenance cost through software reusability. One way to achieve this is through implementing a plugin, which has been accomplished for VSOM.

The current functional architecture for visual servoing is shown in **Figure 3A**. It consists of an image-acquisition module, image-analysis module, servoing, and archive. The image-acquisition module provides the means for time-lapse high resolution video microscopy with six fluorescence excitation filters. This module has a recipe manager to allow either manual or preprogrammed capture of images at different temporal and excitation frequencies. This recipe is expressed in XML notation that provides semantic interoperability. The analytical module integrates a unique segmentation algorithm that provides a feature-based summary of images based on size, location, response, and the bounding contours. The servoing module controls the concentration of various compounds in the cell chamber by controlling the flow in any of the four syringes that sit next to the microscope. The servoing provides three operational modes with each mode subsequently registered with the recipe-manager: (1) a static recipe in which the flow rate of each syringe, its start point in time, and its duration is specified; (2) a dynamic recipe in which the flow rate and its duration are altered as a function of a particular response of the cells under observation; and (3) a modulating recipe under program control that turns the flow on and off at a specified frequency. The archival system stores the images, the computed responses, and annotation data in a flat file environment.

The user can enter a recipe for a particular experiment. The recipe allows for (a) controlling the perfusion rate(s) into the cell chamber, (b) setting camera exposure times, (c) selecting the location of the optical filter wheel, and (d) setting the sampling rate for data collection. There are currently two operational VSOM software packages for image acquisition and control. These are called "VX5" and "ADR". VX5 is for static recipe control of the system, while ADR can run dynamic recipe visual-servoing experiments locally or over the network. In **Figure 3C**, a sample XML recipe file for a VX5 run is shown, together with an example of data found in the pump log (**Figure 3B**), and an example of an ICS digital image header (**Figure 3D**).

It should be noted that image and experimental annotation features are being developed simultaneously with new VSOM imaging protocols. For example, our preliminary results have indicated that it is necessary to return

repeatedly to the same set of cells after the dish has been returned to the incubator for 24-48 hrs. In order to successfully predict the ultimate biological endpoints induced by the stimuli we apply and the physiological responses we observe, we require this functionality. One approach currently under development is shown schematically in **Figure 4**, where a cell response is logged on the basis of the cell's 2D location in the dish. Using adaptive visual servoing principles for XY stage control, one can then return the dish to the microscope stage days later and return to the same field of cells. Cells that have disappeared (perhaps via apoptotic digestion), lost viability, moved, or divided can then be tallied. As seen schematically in **Figure 4**, a fiduciary mark "+" is etched in a plastic, 35 mm cell culture dish under sterile conditions. The (0,0) mark is recorded by the VX5 program, which then keeps track of the relative x,y position of the pertinent camera field of view. A detailed protocol for acquiring VSOM data, and then repeatedly returning to the same field of view is presented in **Appendix E**.

Task 2: Optimize algorithms for detecting individual cells in transmitted light by analyzing image data off-line.

Recently, we have developed three new techniques. One is based on a new regularized edge detector based on supremum, the second on a vector representation of the underlying image followed by feature extraction in vector space, and the third on a geometric and texture model of a cell and its interaction with neighboring cells. The new regularized edge detector has its root in visualization of 3D objects; however, we have also found it to be applicable to segmentation of scientific images. The vector representation of images has its root in analysis of spatio-temporal satellite images. Current segmentation results for living cells are shown in **Figure 5A-F**. For an introduction and overview of fluorescence microscope digital imaging, see the **Era of Hope Poster in Appendix C**.

A regularized edge detector based on supremum: We have developed a technique that accurately delineates target nuclei and their boundaries from background. This technique (a regularized edge detector based on supremum) is superior to our previous method that relied on a parametric description of target nuclei in the form of a projection of a sphere, better known as hough transform. Current regularization techniques attempt to minimize an integral such as $\int_R |\nabla f|^2$. Yet, this formulation has no control on the local property of f . In other words, the global average of $|\nabla f|$ may be small, but locally f may change sharply. A way to overcome this issue is to minimize $|\nabla f|$ at every point, which leads to minimization of the supremum of $|\nabla f|$. It is natural to consider the functional $H_N(f) = \sup_R |\nabla f|$ as a "limit" of the sequence of functionals

$$H_N(f) = \left(\int_R |\nabla f|^{2N} dx \right)^{\frac{1}{2N}}, \quad N=1,2,3,\dots \quad (1)$$

The Euler equation for the minimization of the functional $H_N(f)$ can be expressed as:

$$|\nabla f|^{2(N-2)} \left\{ \frac{1}{2(N-1)} |\nabla f|^2 \nabla f + f_x^2 f_{xx} + 2f_x f_y f_{xy} + f_y^2 f_{yy} \right\} = 0 \quad (2)$$

where a subscript indicates a derivative, such as $f_x = \frac{\partial f}{\partial x}$, $f_{xy} = \frac{\partial^2 f}{\partial x \partial y}$. By removing the first coefficient and letting $N \rightarrow \infty$, we have

$$f_x^2 f_{xx} + 2f_x f_y f_{xy} + f_y^2 f_{yy} = 0 \quad (3)$$

Equation (3) is called the Infinite Laplacian Equation (ILE), which has been studied widely in the literature. Some important properties of the equation (2) are: (1) there is at most one solution and if we redefine the

"solution" in a suitable weak sense, then a continuous solution to C^1 does exist; (2) the trajectory of the gradient of f is either a convex curve or a straight line; and (3) there are no stationary points $|\nabla f| = 0$ in R .

The rationale for optimality of the supremum is based on the "equal importance criterion". This criterion asserts that *every point in R is equally important and contributes similarly to the estimation process. Any other assumption means that we need to know some additional information about the curve.* It is easy to verify that ILE is equivalent to the follow equation:

$$\mathfrak{T}'(f) = \nabla(|\nabla f|) \cdot \frac{\nabla f}{|\nabla f|} = 0 \quad (4)$$

which implies that along each trajectory of the gradient of f , the magnitude of the gradient is a constant. Although the overall integral of $|\nabla f|$ may be larger, the supremum is smaller and the gradient is more likely to concentrate at a smaller range. It is interesting to note that Equation 3 is equivalent to the zero-crossing ($f_{xx} + f_{yy} = 0$) in the local coordinate system, where the local coordinate system is defined by ∇f . The edge detection results reveal closed regions. These regions correspond to spatial blobs that are further filtered for size, response, and convexity constraint. An example is show in **Figure 5A,B**.

Tensor-based feature analysis: Vector field analysis is a well-studied technique in computer vision and pattern recognition as well as other classic fields such as mathematics and physics. Many concepts and tools have been developed for motion based applications. Our work extends the current state of the art to segmentation and interpretation of scientific images. Given an intensity image $f_0(x, y)$, there exists a natural vector field derived from the intensity image, which corresponds to the gradient field rotated by $\pi/2$:

$$\mathbf{v} = \left(-\frac{\partial f_0}{\partial y}, \frac{\partial f_0}{\partial x} \right) \quad (5)$$

The problem here is that the vector field \mathbf{v} is noisy, and some type of regularization needs to be introduced. This can be expressed as

$$\min_{\mathbf{u}} \iint \|\mathbf{u} - \mathbf{v}\|^2 + \alpha^2 \|\nabla \mathbf{u}\|^2 dx dy \quad (6)$$

where \mathbf{u} is the regularized vector field. An elliptic PDE can be solved iteratively. A first order approximation can be computed by a simple linear (Gaussian) scale space model:

$$f(\cdot; t) = g(\cdot; t) * f_0(\cdot) \quad (7)$$

where

$$g(x, y; t) = \frac{1}{2\pi t} e^{-\frac{x^2 + y^2}{4t}} \quad (8)$$

is the Gaussian kernel with standard deviation $\sigma = \sqrt{2t}$.

Singularities of the vector field then provide a compact abstraction for the dense vector representation. These singularities can be characterized by point or linear features. Point features include vortices. An example of such a vector field and its singularities (vortices) on a synthetic scene is shown in on **Page 10 (A-D) of the Era of Hope Poster (Appendix C)**. On page 10 of the poster, vector field analysis on a synthetic image is shown in four steps: (A) original image; (B) vector field corresponding to the gradient field; (C) detection of vortices from the vector field; (D) localization results. Once these patterns are detected, the corresponding objects can be extracted. Rao used local Jacobian for feature extraction from the underlying vector field to detect singularities. Our approach is more robust and provides a measure for the size of the vortex as well. The vortex size

complements localization of convex blobs even though they are connected (or touching one another). This is based on *Jordan index* to localize singularities in the underlying vector field. Let $F = (u, v)$ be a vector field and J be a Jordan curve with no critical point on it. The index of J is defined by

$$\text{Index}(J) = \frac{1}{2\pi} \oint \frac{u dv - v du}{u^2 + v^2} \quad (9)$$

At each point P , we choose a small circle of radius R (denoted by J_P^R) around P and compute $\text{Index}(J_P^R)$. The flow field (u, v) can then be classified according to:

1. The index of a vortex is equal to +1 (the classification of singular points in a vector field has been given in the literature).

Note that there is no node in the vector field because its divergence is zero everywhere, i.e.,

$$\text{div} \mathbf{v} = \frac{\partial}{\partial x} \left(-\frac{\partial f}{\partial y} \right) + \frac{\partial}{\partial y} \frac{\partial f}{\partial x} = 0 \quad (10)$$

The vortex size is then estimated by a simple search technique. If a point (x, y) is a vortex, then its size $R^*(x, y)$ can be defined as

$$R^*(x, y) = \max \{ R \mid \text{Index}(J_{(x,y)}^R) = 1 \} \quad (11)$$

In other words, $R^*(x, y)$ is the largest R such that the index of $J_{(x,y)}^R$ remains to be 1. Being an integral of the first order partial derivatives, the Jordan index is, in some sense, a function of the intensity image. In contrast, other techniques are based on high order derivatives, which are bound to be more noisy. **Page 10 (A-D) of the Era of Hope Poster (Appendix C)** show the result of vortices and region segmentation on a synthetic image. **Figures 5C,D** show results on the nuclei of living and lysed cells labeled with the fluorescent dye Hoechst 33342. **Figures 5E,F** show results on living cells imaged using a 20X phase contrast object and transmitted light. The later result is significant because current techniques for segmenting individual cells require fluorescence imaging, which adds a layer of complexity to the design of experiments involving living cells.

NOTE: Figures 5E,F are the only digital images presented in this report that were not acquired using a 10X, NA 0.5 Zeiss Fluor Objective. All images are 1024x1024, and the CCD chip in our camera has pixels of the size 6.8x6.8 μ . Thus, all images taken at 10X show a field of view that is approximately 700 μ high and 700 μ wide.

Geometric and texture model: Although the previous techniques are applicable for localizing nuclei, a more advanced technique is needed for a more detailed segmentation at higher imaging resolutions. This is based on a geometric model of the cell, its texture in various compartments, and the relationship of its features with respect to one another. The geometric model is expressed as a graph, and the texture is computed using an array of orientation and scale specific filters. These local feature activities help collect an ensemble of information that is further refined with dynamic programming. Our preliminary result, shown on Page 10 (E) of the Era of Hope Poster (Appendix C), indicates reasonable segmentation of nucleus and cytoplasm, which can be used as a basis for computing responses in each of these compartments. Furthermore, responses can be annotated with a proximity filter (distance transform) to reveal whether responses in the cytoplasm have a preferred localization or are diffused.

Tasks 3-5: Demonstrate visual servoing using computer-controlled syringes and a DS/MDR model cell system.

A matched pair of drug-sensitive (DS) and multidrug resistant (MDR) cell lines were used. Both the DS cell line (MCF-7 WTC) and the MDR cell line (MCF-7 ADR) were obtained from Dr. Amadeo Parissenti (North Eastern Ontario Regional Cancer Centre (NEORCC), Sudbury, ONT, Canada). Both our lab and Dr. Parissenti tested these cell lines using a β -test kit for a MultiDrug Resistance (MDR) Assay being developed by Molecular Probes (Eugene, OR). As discussed in our Year 1 Annual Report, a similar set of matched MCF-7 cell lines obtained from an LBNL colleague (Dr. Ruth Lupu) did not demonstrate differential accumulation of calcein or Lysotracker Red (LTR). Dr. Parissenti obtained his cell lines directly from the published originator (Dr. Kenneth Cowan), and verified differential calcein accumulation via two distinct MDR mechanisms using the same MDR Assay β -test kit that Molecular Probes had provided to us. The β -test kit is being developed for use with a flow cytometer, and Dr. Parissenti performed his verification tests using flow cytometric methods. This provides us with an opportunity to compare VSOM results with flow cytometric results. In addition, we have compared VSOM results with results obtained using a fluorescence multiwell plate reader (Cytofluor 4000). The choice of this assay is based on its ability to demonstrate the abilities of the VSOM system with this set of cell lines. It is not necessarily the best protocol or assay for rapidly and accurately determining the relative amounts of Pgp and MRP molecules per cell.

VSOM, Cytofluor 4000, and Digital Imaging Tests of Molecular Probes MDR Assay β -Test Kit:

Principles of the kit: The acetoxymethyl ester (AM) derivative of the intensely fluorescent dye, calcein (CAM), is a relatively nonfluorescent, nonpolar, lipophilic molecule that can normally diffuse passively across the plasma membrane. Once inside the cell, the AM group is cleaved from CAM by intracellular esterases. The resulting molecule, calcein, is negatively charged, hydrophilic, and is normally retained within the cell. However, most cells have the ability to produce on demand (overexpress), a variety of transmembrane proteins that are energy (ATP) -dependent transporters, or pumps. Once one or more of these proteins is overexpressed, the cell is said to have acquired the multidrug resistance (MDR) phenotype. Interestingly, any given MDR protein has a broad spectrum of substrates (including many anticancer drugs and fluorescent dyes) that can be actively extruded, thus protecting the cell from possible cytotoxic effects. Depending on the MDR molecule, the substrate may be intercepted while passing through the plasma membrane, or the substrate may be internalized before it is pumped out. Substrates that can be extruded by a given MDR protein need not be related structurally, or functionally. The model cell system we have chosen for these MDR studies is the MCF-7 Wild Type Cowan (MCF-7 WTC) and the MCF-7 Adriamycin (doxorubicin) -resistant line MCF-7 ADR. MCF-7 ADR cells are known to express both the 170 kDa P-glycoprotein (Pgp) and the 190 kDa Multidrug Resistance Protein (MRP). Separate genes code for these two different proteins. The drug cross-resistance profiles, or spectra, of these two proteins overlap, but are not identical. In addition, these two different proteins have different sensitivities to various inhibitors, and this is the basis of the assay studied here.

Doxorubicin (DOX, the anticancer drug Adriamycin) is a fluorescent molecule. DOX efflux is the classical functional assay for MDR, but it suffers from low sensitivity, unless UV excitation light is used. We have substituted DOX for CAM in several experiments, and have little problem detecting its signal. We may use DOX in place of CAM, which is now patented for MDR assays (one must buy the kit, if one wants to use CAM to perform MDR assays). However, CAM is now favored by most researchers, and we used CAM for most of our studies in Year 2.

Calcein accumulates intracellularly at a rate that is dependent on several factors: (i) external CAM concentration, (ii) temperature, (iii) number and type of MDR pumps in the cell membrane which can extrude CAM, (iv) the general metabolic state of cell, including energy charge and endogenous esterase activity, (v) presence or absence of MDR pump inhibitors such as MK-571 ("MK"), vanadate, cyclosporin A, probenecid, or verapamil ("V"), (vi) the kinetics and mechanism of inhibition (e.g., competitive vs. noncompetitive inhibition, etc.).

Experimental Details: A schematic for VSOM study WA3 is given in **Figure 6A**. This experiment consisted of two VSOM runs, Run #1 for MCF-7 WTC (DS) cells, and Run #2 for MCF-7 ADR (MDR) cells. Cells were grown in 35mm cell culture dishes (Nunc, Δ) in DMEM containing 10% FBS, and 1:100 pen/strep. Cells were allowed to plate at least 24 h before each run. Runs took place sequentially, on the same day. Cells

were rinsed with "D-PBS containing high glucose and sodium pyruvate" (DPBS_GP, or BUFF), and were then incubated for 1 h in DPBS_GP containing Hoechst 33342 (H42), which is membrane permeable and labels the nuclei of living cells. Cells were then placed in a temperature-controlled microperfusion chamber (**Figure 6G, and Era of Hope Poster, pages 3 and 4**) and the VSOM run was begun. For both runs, an initial buffer perfusion (BUFF) was used to wash out the H42 incubation solution, followed by perfusion of a CAM (only) solution. **Figure 9** gives detailed information on the syringes, composition of perfusion solutions, flow rates, and perfusion intervals used in this study. **Pages 3 and 4 in the Era of Hope Poster (Appendix C)** contain overview photos of the VSOM system. Continuing in **Figure 6A**, one can see that the CAM (only) perfusion is followed by a BUFF (buffer, DPBS_GP) perfusion. Next, a CAM+MK perfusion is performed, followed by a buffer perfusion. The final exposure is to a CAM+V solution, followed by a buffer wash. Total time elapsed is 110 min, or 1.8h (6600 sec). As depicted in **Figure 6A**, the DS cells rapidly accumulate calcein during the initial CAM (only) perfusion, while MDR cells accumulate little or no calcein due to the presence of both the Pgp and MRP transmembrane proteins. Both Pgp and MRP can intercept CAM in the plasma membrane, before it reaches the inside of the cell, where it is digested to form calcein. Interestingly, MRP can also extrude calcein from the interior of the cell, while the Pgp protein cannot. MK-571 is a specific inhibitor of MRP; thus, during the perfusion of CAM+MK, MDR cells begin to accumulate calcein, while DS cells are not greatly perturbed. Verapamil inhibits both Pgp and MRP; thus, when CAM+V is perfused MDR cells should (theoretically) equilibrate to the same intracellular calcein concentration as DS cells during this final perfusion. By comparing the fluorescence intensity of cells after CAM+MK perfusion to the fluorescence intensity after CAM+V perfusion, one can determine the relative amounts of MRP and Pgp pumps on a per cell basis.

One important fact, not noted in **Figure 9**, is that all CAM solutions (CAM, CAM+MK, CAM+V) contain between 0.1 and 0.5% DMSO. Concentrated stock solutions of CAM, MK, and V are prepared in DMSO, because they have limited solubility in water. Small aliquots of the stock solution(s) are then added to DPBS_GP. The scientific staff at Molecular Probes have informed us that there are some toxicity issues involving DMSO, even at these low concentrations. Furthermore, these toxicity issues can be a function of the particular lot of DMSO used.

Cytofluor Experiment WA1: As mentioned above, we have also attempted to implement this MDR assay using living cells in 24-well plates. This assay more closely follows the Molecular Probes protocol suggested for flow cytometric studies because cells are only exposed to a single MDR modulator (MK or V). However, in addition to using CAM as a fluorescent probe, we also used DOX as a fluorescent probe (both at 0.25 μ M) in a separate set of plates. On Day 1, DS (MCF-7 WTC, 2 plates) and MDR (MCF-7 ADR, 2 plates) cells were plated in 24-well plates at a density of 5 $\times 10^4$ cells/well or 2.8 $\times 10^4$ cells/cm². In addition, a concentration ladder of wells was generated that received from 0 to 1 $\times 10^5$ cells/well. The layout for all four plates is shown in **Figure 7A**. An 8-channel, automated electronic pipettor with a programmable console (Electrapette, Matrix Technologies, Lowell, MA) was used in these experiments to reduce pipetting errors. Aliquots were drawn from a Wheaton sterile reservoir ("V-shaped" bottom) (**Figure 6B**). Cells were then grown in 5% CO₂ in DMEM containing 10% FBS and Pen-Strp. On Day 3, media was removed and wells were rinsed with DPBS_GP. Solutions of CAM, CAM+MK, or CAM+V and solutions of DOX, DOX+MK, or DOX+V were then added to the appropriate wells of the appropriate plates for a 1h exposure at 37°C, 5% CO₂. Control wells received CAM (only) or DOX (only) solution. After a 1h exposure, all wells were rinsed with DPBS_GP (containing 1:100 pen-strep), and plates containing living, exposed cells were read on a temperature-controlled multichannel fluorescence plate reader at 37°C (**Figure 6C**). After this first set of measurements, plates were returned to the incubator for an additional 24h. On Day 5, living cells were triple stained with H42, CAM, and Ethidium homodimer (EH, a red fluorescent indicator for the nuclei of dead cells), giving blue, green, and red fluorescence, respectively, on separate channels. After this second set of measurements, cells were fixed and on Day 6, cells were stained with DAPI (a DNA stain), and a third set of fluorescence measurements were acquired.

Experiment **WA1** was designed to show many of the strengths of multiwell plate assays. On Day 3, multiple readings (of whole cell populations) were taken at different positions within each well, and replicate samples were measured in adjacent wells. Thus, the calcein accumulation for each exposure condition was easily obtained. Readings were corrected for background fluorescence using an average background value given by the four blank (no cells) wells. All four plates could be rapidly read (<5min per plate) with the lids on. The lids can be left on

because fluorescence excitation occurs from the bottom and measurements are taken through the bottom of the plate. All plates could then be returned to the incubator for several days. On Day 5, it was then possible to relabel the plates using three different fluorescence dyes. **H42** was used to label cell nuclei (blue channel), thus giving an idea of total cell number per plate. **CAM** (only) and **EH** gave green and red readings, respectively, that indicate the relative number of live and dead cells (**EH** only stains the nuclei of non-viable cells). On Day 6, fixed cells could once again be stained with **DAPI** so that the relative number of cells per well could be obtained for purposes of normalizing observed fluorescence to relative number of cells present.

Results from experiment **WA1** are shown below in **Table 1**.

TABLE 1

<u>PLATE</u>	<u>EXPOSURE</u>	<u>DAY 3: Signal (490nm) ± STD</u>	<u>DAY 5: Signal (490nm) ± STD</u> <u>(all plates, 1.0 µM CAM, 1 hr)</u>
WTC_CAM (DS)	Control	398 ±86	4822 ±973
	MK-571	553 ±24	4951 ±427
	Verapamil	567 ±558	4997 ±599
MDR_CAM (MDR)	Control	305 ±61	1658 ±36
	MK-571	211 ±175	1588 ±158
	Verapamil	164 ±134	1373 ±178
WTC_DOX (DS)	Control	n.o.	6598 ±429
	MK-571	n.o.	6356 ±458
	Verapamil	n.o.	6556 ±733
MDR_DOX (MDR)	Control	n.o.	1965 ±49
	MK-571	n.o.	1641 ±400
	Verapamil	n.o.	1682 ±242

Normalization of signal in the 490nm channel using **H42** (360nm channel), **CAM/EH** ratio (live/dead ratio, 490nm/530nm channel), or **DAPI** fluorescence(360nm channel) did not improve standard deviation values (data not shown). As seen in the Day 3 column of **Table 1**, the signal observed in the 490 channel was weak (blank wells gave a reading of 40 ± 1). The weak fluorescence exhibited by DOX in the 490 channel was not observable (n.o.) above background. These values represent the fluorescence signal of calcein or DOX after 1h exposures at 0.25 µM. The values in the Day 5 column represent calcein accumulation in cells that were incubated for 1h with 1.00 µM. Unfortunately, in no instance was it possible to observe a statistically significant difference between MK and V exposed cells. However, (Day 5) **DS** cells consistently incorporated more calcein than MDR cells when the four-fold higher CAM incubation was used. The lower CAM concentration (0.25 µM) used on Day 3 is the concentration recommended for the **MK** and **V** concentrations used (10 µM and 50 µM, respectively), and this is sufficient signal for flow cytometry analysis. The signal due to this lower concentration is also easily detected in our VSOM experiments (below). Thus, the fluorescence plate reader (Cytofluor 4000, PE Biosystems, Foster City, CA) is significantly less sensitive than VSOM or flow cytometry. However, as shown in **Figure 6F**, multiwell plates can be easily mounted on our computer controlled scanning stage. VSOM technology could be used to automatically acquire many multichannel images in each well of interest. It is interesting to note some aspects of this approach (using a microscope to read multiwell plates) have been recently patented (*System for cell-based screening*, US5989835, Inventor(s): Dunlay; R. Terry, Pittsburgh, PA, Taylor; D. Lansing, Pittsburgh, PA., Applicant(s): Cellomics, Inc., Pittsburgh, PA., Nov. 23, 1999. See www.cellomics.com, and <http://www.delphion.com/> for more information)

There is currently great commercial interest in the development of fluorescence assays for microplate readers (See Cortese, J.D., "At the Speed of Light" *The Scientist*, pp18-21, July 10, 2000, www.the-scientist.com). A great deal of progress has been made in the automation of these systems for high-throughput screening (HTS). These robotic systems are fully capable of performing the precisely timed solution exchanges and multichannel fluorescence detection that are a feature of VSOM fluorescence assays. We believe one important application of our VSOM technology will be in the design of sophisticated assays that be implemented by these high-throughput systems.

Digital Imaging Test Experiment WA2: The protocol shown in **Figure 6A**, and used in experiment WA1 (Cytofluor Test of MDR Assay β -Test kit) was repeated here using cells plated in four 35mm circular cell culture dishes. DOX was not used in this study, and the WA1 protocol was followed only up to Day 3, at which point digital images were obtained from dishes (**Figure 8, Experiment WA2**). In this color-coded representation of gray-scale images, low intensity pixels have been assigned "colder" colors (black, purple, blue) while "warmer" colors (yellow, red, white) have been assigned to the higher intensity pixels. As shown in the bar, the warmer colors indicate higher levels of intracellular calcein. MDR (MCF-7 ADR) incubated with CAM (only) are shown in **Figure 8A**. These cells accumulate relatively little calcein, while MDR cells incubated with CAM+MK (**Figure 8B**) show greater accumulation, and MDR cells treated with CAM+V show the highest degree of calcein accumulation (**Figure 8C**). **Figure 8D** is an image of DS (MCF-7 WTC) cells stained with CAM (only). These digital images show good agreement with the expected behavior of the β -Test kit assay (**Figure 6A**).

VSOM Experiment WA3: The MDR Assay β -Test kit was also tested in a VSOM experiment (WA3). **Figure 9** is a schematic diagram of this VSOM experiment, which is also depicted in **Figure 6A**. Pumps are turned on and off at specified flow rates according to a pre-programmed recipe, or based on real-time analysis of individual cell responses. It should be noted, as shown in **Figure 9**, that the CAM, V, and MK concentrations are the same as those used in experiments WA1 and WA2. The three exposures to CAM are 900s (20min) each, and thus the total exposure to CAM is 60min, or 1hr. The black windows at the bottom of the figure show the mean response of all cells in the field of view. This mean response plot is displayed on the computer screen during the VSOM experiment, and digital images from one or more channels (transmitted light is usually one of the channels displayed) are displayed on the screen as well. The plot and images are continuously refreshed and updated during the experiment. As seen in the two plots recorded for MCF-7 WTC (DS, run #1) and MCF-7 ADR (MDR, run #2), DS cells (upper plot) accumulated more calcein (240 ± 82 , $N=336$) than did the MDR cells (103 ± 80 , $N=161$). This is in agreement with the relative differences in calcein accumulation observed between DS and MDR cells in the multiwell plate experiments (Table 1: $1658/4822 = 0.34$, $1965/6598 = 0.30$; VSOM: $103/240 = 0.43$) which represent an average over many cells. However, as shown in **Figure 10**, (DS cells, Run #1) the mean cellular fluorescence of each cell is monitored during VSOM experiments, and deviations from the mean can be easily detected. For example, the arrow in **Figure 10** indicates several cells that began to lose viability and plasma membrane integrity. Such cells are unable to retain calcein, and it leaks out, causing the fluorescence signal to drop. It is possible that this is an effect related to the DMSO toxicity discussed above. It should be noted that the current VSOM system could easily terminate the exposure/perfusion as soon as a single cell death is noted.

Figure 11 shows four selected single cell responses from **Run #2, experiment WA3**. These response curves are good examples of the underlying principle of the β -Test kit shown schematically in **Figure 6A** (MDR, RUN #2). In two of the response curves (**Figure 11, red**) the cells do not accumulate calcein until verapamil (V) exposure during the operation of Syringe 4 (**Figure 9**). Thus, we can infer that these cells only express Pgp pumps, because the pumps are not inhibited by MK-571 (MK). It can clearly be seen that none of these cells were present in the DS cell population (**Figure 10**). Further, after CAM+V exposure, one of the cells rapidly accumulates calcein until its mean cellular fluorescence falls within one standard deviation of the mean response of cells observed for DS cells (**Figure 10**). If we assume all other factors are the same then one would predict that the second cell contains fewer Pgp molecules. The remaining two curves (**Figure 11, blue**) show additional responses during CAM (only) and CAM+MK exposures, requiring a additional analysis. Obviously, the actual situation is much more complicated than depicted in **Figure 6A**. The curves we observe cannot be explained in terms of the presence or absence of only two pump types, neither having the ability to extrude internalized

calcein. This is the type of detailed physiological information that flow cytometric assays and multiwell plate assays cannot provide, and it demonstrates that our VSOM technology has the capabilities we initially predicted.

For example, detailed rate information on calcein accumulation and retention is available throughout the VSOM experiment. For the blue response curves, one can calculate a rate of calcein accumulation during the three CAM perfusions, and one can calculate a rate of calcein retention during BUFF perfusions. Calcein accumulation is occurring in the 1500, 3500, and 5500s time periods, and plateaus corresponding to excellent calcein retention are observed in the 2500, 4500, 6500 time intervals. As noted above, some MDR pumps have the ability to extrude calcein after it has been internalized in the cell. The ability of DS cells to extrude internalized calcein is apparent during the 2500s period (**Figure 10**) corresponding to BUFF perfusion; however, 2 MDR cells (**Figure 11, blue**) do not have this ability.

Experiment WA4: We have also performed VSOM experiments where only CAM (at the four-fold higher concentration of 1.0 μ M) is perfused. The first perfusion interval of such an experiment is shown in **Figure 12**, where the same data is presented using a variety of 3D perspectives. As seen earlier (**Figure 11, blue**), a significant subpopulation of calcein-accumulating cells is present, and these cells demonstrate varying degrees of calcein accumulation during a 2100s exposure. In this experiment CAM solutions were not flushed from the chamber between CAM, CAM+MK, and CAM+V exposures. Cells were allowed to sit in contact with these solutions between perfusion intervals. Portions of this experiment are presented in the **Biophysical Society Abstract (Appendix D)**. The experiment ended after 1100s of exposure(s), and although the cells remained viable, significant membrane blebbing was observed.

Technical Objective 2 : Biological Experiments

Tasks 6 –7: In our original three-year proposal, we proposed to study only the ~~MCF-7~~ WTC (DS) and MCF-7 ADR (MDR) model system during our preliminary VSOM system development studies. However, it was suggested that additional cell lines might give more pertinent biological information and might yield important biological results more quickly. Thus, the funding was reduced 33%, and the number of cell lines to be studied was doubled.

As we discuss in our Clinical Bridge Grant Proposal (**Included in Provisional Patent application, Appendix G: Rapid Discovery of Physiological Characteristics Which Distinguish Malignant and Nonmalignant Human Breast Epithelial Cells, BC000508**, Breast Cancer Research Program, Congressionally Directed Medical Research Program 2000), it may be necessary to reproduce the low pH environment seen by tumor cells in vivo, if we are to successfully culture primary breast tumor cells in vitro. Our objectives are to demonstrate and verify that VSOM can rapidly discover and optimize, on a tumor-by-tumor basis, microenvironmental conditions suitable for the successful in vitro propagation and chemosensitivity testing of primary human breast tumor cells. Our specific aims are to (a) rapidly and automatically develop in vitro microenvironments that favor the propagation of primary breast tumor cells, (b) rapidly develop new in vitro fluorescence assays that predict cell behavior on the basis of early physiological responses to applied stress (c) improve VSOM technology in order to achieve our objectives and specific aims. A great deal of progress has been made in primary culture of malignant human breast epithelial cells (BECs). Currently, there is great interest in the unique physiology of solid tumors, and it is likely that a sub optimal, nutritionally depleted environment exists in breast tumors. This environment is believed to consist of regions of low oxygen (hypoxia), low pH, low levels of glucose, and high levels of metabolic waste. It has been demonstrated that when such conditions are simulated in culture, it is possible to isolate relatively pure populations of primary breast tumor cells. Nonmalignant cells are unable to survive these initial, hostile environmental conditions. Thus, an additional benefit is that nonmalignant epithelium with its higher proliferation rate, is not present and is not able to overgrow the tumor cells which have a slower proliferation rate. A common misconception is that malignant BECs proliferate more rapidly than nonmalignant BECs. It should also be noted that drug resistance in tumor cells may depend on and be the result of the stress of a hostile microenvironment. For this reason, accurate measurements of drug resistance may require that the assays be performed on cells in the proper microenvironment. It is interesting to note that some of the most successful in vitro chemosensitivity tests involve the culture of cells in tiny capillary tubes that are sealed at both

ends and incubated for 14 days (see below). The resulting microenvironment is likely to be even more hostile than those generated using the sandwiched coverslip technique.

We immediately encountered pH-related cell propagation effects when we began studies on human mammary epithelial cell (HMEC) lines. Normal HMECs (184SK), and immortally transformed HMECs (184B5) provided by our LBNL collaborator, Dr. Paul Yaswen, have been studied. We have successfully conducted VSOM studies on these cell lines. However, as seen in **Figure 13 (blue circles)**, MCF-7 WTC and MCF-7 ADR cells grown in DMEM (containing a bicarbonate buffer) and HMECs (**Figure 13, red triangles**) grown in MEGM (containing both a bicarbonate buffer and a HEPES buffer) show very different pH behavior as a function of incubator CO₂ levels. In addition, the pH range tolerated by each cell type varies (**vertical arrows in Figure 13**). The net effect is that there is not a common CO₂ level that allows these different cells types (in separate flasks, in the media that each prefers) to simultaneously propagate in a single incubator. The more normal HMECs tolerate a much narrower range of pHs than do the MCF-7 cancer cells. None of the cell lines prefer a lower pH environment (<7.1). If it is true that successful propagation of human tumor breast epithelial cells requires pHs < 7.0, then it is clear why previous in vitro chemosensitivity assays have not been successful. Most media and cell incubation conditions have been designed for pHs > 7.0. Thus, when human tumor biopsy specimens are cultured in these conditions, it is the normal cells that attach and proliferate, not the tumor cells. Chemosensitivity tests are then unknowingly conducted on normal cells, rather than the tumor cells. This may be the reason for the previous failure of these assays during clinical trials.

Figure 14 is an example of the behavior observed when an attempt is made to propagate cells at an unfavorable pH. In this case, MCF-7 WTC cells incubated at CO₂ levels that produce a pH >7.4 (on average) in DMEM successfully attach, spread out, and proliferate on the plastic tissue culture ware surface (**Figures 14 A,B**). However, at pHs < 7.2, these cells round up, and do not do attach well(**Figures 14 A,B**). A similar effect is seen if MCF-7 ADR are plated under conditions where the pH > 8.0. In this case, the cells never successfully attach or proliferate, while MCF-7 WTC cells grow well. It should be noted that these type of morphological transformations can be quantified by a VSOM system with the ability to segment cells in transmitted light. The images in **Figure 14** were acquired by placing a T-25 tissue culture flask on the microscope using the appropriate stage mounting plate (**Figure 6F**). In the future, we believe the VSOM system will be able to repeatedly image many fields of cells in a closed tissue flask. The flask could then be returned to the incubator for a suitable period. Our ability to segment cells in transmitted light means that cell shapes, locations and relative positions could be saved, so that when one returned the flask to the microscope, the VSOM system would return to the same field(s) of cells, acquired new images, and quantify any morphological changes. This is an example of a more mechanical visual servoing application, where the system would relocate the same field of cells, even if cell numbers, relative positions, and shapes had changed.

Tasks 8-9: The goal of these tasks was to find and exploit differences between cell types to give a growth advantage to specified cells (i.e., primary breast tumor cells), while giving a growth disadvantage to other cells (i.e., normal mammary epithelial cells). In addition to the morphological indications (discussed above) that cells have attached and have begun dividing, we wish to develop VSOM fluorescence assays that can quantify the proliferation rate of living cells on a cell-by-cell basis.

Experiment HM1: BrdU Proliferation Assay for Living Cells

The power of any VSOM predictive assay is improved if specific cell responses can be correlated with specific biological endpoints. Several fluorescence assays for apoptosis exist, but there are few fluorescence assays for living cells that can measure important parameters, such as BrdU incorporation, which can be used to quantify DNA synthesis or cell proliferation. In experiment **HM1**, we demonstrate an image ratioing technique that can detect the proliferation state of living cells by quantifying the amount of BrdU incorporation. The protocol for this assay is illustrated in **Figure 7B**, and is adapted from the published protocol used by our collaborator, Dr. Paul Yaswen (Stampfer, M.R. et al, *Exp. Cell Res.* **208**, 175-188 (1993)). We used the same cell lines and media; however, for DNA synthesis assays, we substituted 5-bromo-2'-deoxy uridine (**BrdU**) for [³H]-thymidine. We performed these experiments using a 5-bromo-2'-deoxy uridine labeling and detection kit (No.

1296736, Boehringer Mannheim). Thus, after a VSOM experiment we were able to fix the cells and verify VSOM results (based on digital image ratioing) using traditional indirect immunofluorescence assays.

Principles of Assay: Cells that have been stimulated to grow (proliferate) synthesize twice their normal complement of DNA in preparation for cell division. These actively growing cells can take the nucleotides A,T, C, or G from the extracellular media and use them to construct DNA. However, when BrdU is present, it is used instead of T to synthesize DNA. Thus, if one exposes a population of cells to BrdU for a short period (1 h), the subpopulation of cells that were synthesizing DNA during that 1 h period will incorporate the most BrdU into their nuclear DNA. This is referred to as a pulse-labeling experiment. The goal of this experiment was to determine whether the ratio of Hoechst 33342 (**H42**) and Syto 16 (**S16**) fluorescence emission intensities is useful for determining the amount of BrdU incorporation on a cell by cell basis. **H42** and **S16** stain the nuclei of living or fixed cells. **H42** fluorescence emission is quenched (reduced) if the DNA contains incorporated BrdU. The fluorescence emission of **S16** is not affected by the presence of incorporated BrdU. Thus, the ratio of H42/S16 fluorescence intensities (calculated on a pixel by pixel basis using digital images) should be proportional to the amount of BrdU incorporated into each cell's DNA.

Three dishes of 184B5 cells were used in these experiments (**Figure 7B**). For the first 48 hrs, two dishes received MEBM (Mammary Epithelial Cell Basal Medium, CC-3151, Clonetics, San Diego, CA) while the third dish received MEGM (Mammary Epithelial Cell Growth Media, MEGM, CC-3051, Clonetics). These are serum free formulations. MEGM contains bovine pituitary extract (BPE), hydrocortisone, human epidermal growth factor (EGF), and insulin, while MEBM does not. Thus, for the first 48hrs, Dish 3 received all the factors commonly required for propagation, while Dishes 1 and 2 did not. MEBM only supports cells at a basal level of metabolism and is not intended to support cell attachment or propagation. After 48hrs, Dish #2 was refed with MEGM (this two step process is referred to as "MEBM+EGF"), Dish #3 was also refed with MEGM, but Dish #1 received MEGM-hEGF (BPE, hydrocortisone, and insulin were present). The Dish #1 treatment is referred to as "MEBM-EGF". As seen in fig. 4 of the Stampfer paper (184B5 cells), DNA synthesis reaches a peak approximately 18hrs after feeding, with MEGM cells showing the greatest amount of DNA synthesis, followed by MEBM+EGF cells which show decreased DNA synthesis. Cells maintained in MEBM-EGF show little DNA synthesis. These results were obtained using [³H]-thymidine. In our experiments, we pulse-labeled with BrdU for 1 hr, and then dual-stained the living cells with **H42** and **S16**. One digital image was acquired of cells with 360nm excitation (**H42** signal), and a second was acquired at 490nm excitation (**S16** signal). These images were processed and ratioed on a pixel by pixel basis. The resulting ratio values were then color coded as shown in **Figure 15**. As seen in this figure, our results agree with those obtained by traditional [³H]-thymidine incorporation assays. MEGM cells (Dish 3) showed the greatest degree of BrdU incorporation, followed by MEBM+EGF cells (Dish #2), with MEBM-EGF cells(Dish #1) showing little BrdU incorporation.

To further verify these observations, the cells were fixed with 70% ethanol and 50mM glycine, pH2.0 at -30 °C, and indirect immunofluorescence staining was performed. After this staining, cells were restained with **H42** and **S16** to see if fixed cells labeled with the anti-BrdU antibody also had low **H42** fluorescence, indicative of BrdU quenching. As seen in **Figures 7C,D**, there was some evidence of this effect. **Figure 7D** shows a combined color image of triple-stained cells. The MEGM cells exhibited the greatest amount of BrdU staining (red cells circled in white). If one examines the same cells in the blue channel, (**Figure 7C**) one can see the general trend that cells that stain for BrdU exhibit lower H42 fluorescence signal.

Experiment HM2: Visualization of Intracellular Calcium Levels and mRNA Response in Living Cells

One goal of these Tasks was to correlate several biological responses simultaneously during VSOM experiments. In experiment **HM2**, we dual-stained 184B5 cells with FURA-PE3 (green: a calcium-sensitive fluorescence probe) and LDS-751 (red: a DNA and RNA binding fluorescence probe with a very different emission wavelengths, depending on whether it is bound to DNA or RNA). Cells were then sequentially stimulated with 2μM thapsigargin (TG) and 5μM ionomycin (ION) (**Figures 16, 17**). Both of these compounds are known to elevate intracellular calcium. As seen in **Figure 16**, the red RNA signal due to LDS-751 increases greatly for all the cells after intracellular calcium has been elevated. The fluorescence signal of LDS-751 when bound to DNA is emitted in the infrared; thus, the nuclei of these cells do not exhibit any red signal. The 3D

graphs inset in **Figure 16** are zoomed up in **Figure 17**. The LDS-751 response for all cells is shown in **Figure 17A**, while selected responses are shown in **Figure 17B**. As seen in the selected responses, some cells exhibit a second response to **ION** after the initial **TG** stimulation, and some do not. In addition, some cells respond more quickly to **TG** than do others. Our goal in the next year is to closely track these cells and determine if their ultimate biological fate (proliferation, apoptosis, or differentiation) is closely correlated to perturbations in intracellular calcium levels. In addition, we wish to use VSOM to "clamp" the intracellular calcium concentrations (and/or pH) to values that will selectively induce proliferation or apoptosis in different cell types.

Key Research Accomplishments

- **Demonstrated the predicted VSOM capabilities**
- **Demonstrated a new class of drug response and chemosensitivity assays**
- **Demonstrated that VSOM is superior to multiwell plate MDR assays**
- **Obtained two new grants using VSOM preliminary data**
- **Reduced VSOM patent to practice**
- **Demonstrated that living cells can be segmented using transmitted light only**
- **Demonstrated Image Ratioing BrdU Proliferation Assay for Living Cells**
- **Imaged mRNA response to high calcium in TG-stimulated HMEC cells**

Reportable Outcomes

Presentations (included in Appendix C):

Callahan, D.E., and Parvin, B. Quantitation of Single Cell Responses using Fluorescence Microscopy, *Proceedings: Era of Hope Department of Defense Breast Cancer Research Program Meeting, Volume 2, page 709*. Atlanta, GA, June 8-11, 2000, Poster Number: CC-5.

Abstracts (included in Appendix D):

Callahan, D.E., and Parvin, B. Visual Servoing for the Detection, Quantitation, and Modulation of Specific Cell Responses in Subpopulations of Multidrug Resistant (MDR) Human Breast Cancer Cells, to be presented, Biophysical Society Annual Meeting 2001, Boston, MA, February 17-21, 2001, Abstract Number: 3275.

Provisional Patent Application (included in Appendix G):

Callahan, D.E., and Parvin, B. A Method for Knowledge-Based Discovery and Optimization of Differences Between Cell Types, LBNL Provisional Patent Application: submitted: June 8, 2000, reduced to practice: September 22, 2000.

Grants Submitted and Pending (Grants #1, #2, #4 (below) are included in Appendix G)

1. *Rapid Discovery of Physiological Characteristics Which Distinguish Malignant and Nonmalignant Human Breast Epithelial Cells*

Proposal ID number: BC000508
Amount: \$505,324
submitted: June 6, 2000 to:
Congressionally Directed Medical Research Program 2000
Breast Cancer Research Program
"Clinical Bridge Grant"
Berkeley Lab Proposal BG 00-297(00)
Principal Investigators: Callahan, D.E., and Parvin, B.

Grants Submitted and Funded:

2. *Automated Imaging System for Guiding Antisense Compounds to Specific mRNA Targets in Living Cells*

Amount: \$1,188,146
submitted: May 27, 2000 to:
DOE OBER Program "Imaging Gene Expression in Health and Disease"
Berkeley Lab Proposal LAB00-13
Principal Investigators: Parvin, B., Callahan, D.E., Barcellos-Hoff, M.H., and Taylor, S.

3. *Quantitative Spatial and Temporal Resolution of Multicellular Interactions*

Amount: \$240,000
submitted: May 16, 2000 to:
Lawrence Berkeley National Laboratory
"Laboratory Directed Research and Development Grant: Strategic Initiative"
Principal Investigators: Barcellos-Hoff, M.H., Callahan, D. E., Parvin, B., and Sudar, D.

Grants Submitted and Not Funded:

4. Predictive Testing for the Individual Breast Cancer Patient

Amount: \$1,116,897

submitted: January 13, 2000 to:

California Breast Cancer Research Program

"New Scientific Perspectives Research Collaboration"

Principal Investigators: Callahan, D.E., Parvin, B.

Berkeley Lab Proposal BG-00-021(00)

Conclusions

The VSOM demonstrations we present here clearly show the feasibility and advantages of VSOM MDR assays. We have demonstrated a rapid VSOM fluorescence assay for doxorubicin chemosensitivity that can identify a subpopulation of cells in a much larger population of cells. In this VSOM fluorescence assay, for this model cell system, optimizing the retention of calcein is equivalent to optimizing the uptake and cytotoxicity of the anticancer drug doxorubicin. It appears unlikely that a single MDR kit, single set of inhibitors, single set of concentrations and exposure times will be able to deal with the wide range of MDR proteins that are overexpressed to varying extents in multidrug resistant tumor cells. VSOM technology offers the advantage of intelligent adaptation during ongoing quantification of dynamic cell responses. This means that an assay could be modified on-line, intelligently and automatically, on a specimen-by-specimen, or patient-by-patient basis. The number and type of exposures, the order and duration of exposures, the compounds and the concentrations used can be optimized during the assay in order to efficiently and rapidly obtain the physiological information necessary to select the best chemotherapeutic drugs for that patient. We believe we have demonstrated that 1 MDR cell out of 1000 DS cells can easily be detected and stimulated repeatedly, for hours, in order to determine the number and type of MDR proteins expressed at the cell surface. Thus, we believe we have demonstrated the technical feasibility of in vitro, VSOM assays that could be used to design breast cancer chemotherapy for the individual patient.

References (none)

Appendix A: Figure Legends

NOTE: Figures 5E,F are the only digital images presented in this report that were not acquired using a 10X, NA 0.5 Zeiss Fluar Objective. All images are 1024x1024, and the CCD chip in our camera has pixels of the size 6.8x6.8 μ . Thus, all images taken at 10X show a field of view that is approximately 700 μ high and 700 μ wide.

Figure 1: Screen snapshots of the Java Command File Generator (JCFG). (A) Opening dialog box (B) Assignment of perfusion runs as a treatment, or exposure of a specific cell type (C) Assignment of a group of images to an perfusion interval (D) Expanded tree view of C.

Figure 2: A single screen snapshot of multiple Netscape Browser windows that automatically open during use of the **Java VSOM data browser**. Window A presents a tree structure for an image directory, and the opposite frame in window A displays a thumbnail of the ICS image. By clicking on *Pop-Up Full-Size JPEG*, one can bring up the 1024x1024 image in window B, and by clicking on *Show Image with Segmentation*, one can bring up the image for a given channel in window D (cell nuclei in channel 0: 360nm excitation of Hoechst 33342). If one then clicks on an individual cell in Window D, the time-dependent mean cellular fluorescence is plotted (in Window C) for that cell (arrow in D) in the current channel. The calcein fluorescence response seen in channel 1 (490nm excitation) is shown, and the image displayed is one acquired at an early time point. The fluorescence signal plotted in Window C thus reflects calcein accumulation in a single cell over a 6600s time period (110 min, or 1.8h). Data from Experiment **WA3** is shown.

Figure 3: (A) The functional architecture of the **Deep View Bioinformatics system** is shown. Examples of (B) the Pump Log, (C) an XML recipe file, and (D) an ICS image header are presented.

Figure 4: A schematic diagram illustrating the use of an etched culture dish for the purpose of establishing a **frame of reference for cell location** in the dish. As discussed in **Appendix E**, our goal is to annotate each cellular response with the actual physical location of that cell in the dish. This will give us the ability to return to the same field of cells days later, in order to determine the ultimate biological fate of each cell

Figure 5: These are examples of two of the three different image segmentation algorithms that are currently under development. One is based on a new regularized edge detector based on supremum, the second on a vector representation of the underlying image followed by feature extraction in vector space.
(A,B) Regularized edge detector based on supremum: nuclei of living **184B5** cells stained with Syto16 are shown. The same cells exhibit mRNA staining in another channel, as seen in **Figure 16**.
(C,D) Vector representation of the underlying image followed by feature extraction in vector space (fluorescence image): Nuclei of living MCF-7 cells stained with Hoechst 33342.
(E,F) Vector representation of the underlying image followed by feature extraction in vector space (transmitted light image): Phase-contrast images of living MCF-7 cells taken at 20X.

The third image segmentation algorithm is based on a geometric and texture model of a cell and its interaction with neighboring cells. An example is found on Page 10 (E) of the Era of Hope Poster (Appendix C).

Figure 6: (A) Schematic description of VSOM experiment **WA3**. This experiment consisted of two VSOM runs, Run #1 for MCF-7 WTC (**DS**) cells, and Run #2 for MCF-7 ADR (**MDR**) cells. Each downward arrow indicates a different perfusion state. Curved arrows indicate the extrusion of calcein-AM (CAM)

from the cell. Green indicates intracellular accumulation of free calcein due to esterase cleavage of AM group from CAM. Blue indicates Hoechst 33342 (H42) -labeled cell nuclei. The nuclei of DS and MDR cells are represented as "|||" and "+", respectively.

Compare this schematic to **Figure 9**, where more detailed information (on the syringes, composition of perfusion solutions, flow rates, and perfusion intervals used in the study) is given.

(B) Preparation of multiwell plates in a sterile hood using a programmable, multichannel pippetor.

(C) Multiwell plate being pulled into a temperature-controlled, fluorescence multiwell plate reader (Cytofluor 4000).

(D) VSOM scanning stage without a stage plate mount inserted. Silver areas represent modifications made so that temperature controlled microperfusion chamber could be mounted.

(E) Blow-up of a stage plate mount used for chambered coverslips. Both 2-well and an 8-well chambered coverslips are shown without lids.

(F) A variety of stage plate mounts used for different sizes of tissue culture flasks, dishes, and multiwell plates.

(G) Temperature-controlled microperfusion chamber modified for mounting on the inverted microscope shown in D.

Figure 7: Protocols for (1) Cytofluor 4000 Test (WA1) of Molecular Probes MDR Assay β -Test Kit, and (2) BrdU Incorporation Test for Proliferation in Living Cells (**HM1**)

(A): Layout of plates for the MDR fluorescence assay (experiment **WA1**) that employed living cells in 24-well plates. Each treatment group appears in quadruplicate. A concentration ladder of cells, and blank wells are also shown. Results appear in **Table 1, page 12**.

(B): Flow chart representation of the protocol used for the BrdU ratio imaging test (experiment **HM1**).

(C): The blue channel of the color image shown in D (**HM1**). Fixed cells (nuclei) stained with H42 are shown. Red nuclei that are circle in white in D are circled in blue in this figure.

(D): Fixed and triple-stained 184B5 cells from **HM1**. Cells were pulse-labeled with BrdU for one hour. Three digital images were obtained on the red, green, and blue channels (570, 490, and 360nm fluorescence excitation, respectively). These three images were combined into the full color image shown here. Red fluorescence indicates indirect immunofluorescence detection of incorporated BrdU using an anti-BrdU antibody. Green fluorescence represents the Syto16 nuclear stain (**S16**, which also stains RNA to some extent). Blue fluorescence represents the nuclear stain Hoechst 33342 (**H42**). From these digital images, there are two ways to quantify BrdU incorporation: (i) anti-BrdU antibody detection, represented by the intensity of red fluorescence (ii) calculation of the ratio of blue nuclear fluorescence intensity (**H42**) divided by green nuclear fluorescence intensity (**S16**) on a pixel by pixel basis (image ratioing). **H42** is quenched by BrdU incorporation, while **S16** is not. Thus, the nuclei that appear red here (circled in white), should exhibit lower **H42** fluorescence in the blue channel (C), where they appear circled in blue.

Figure 8: Digital Imaging Test of Molecular Probes MDR Assay β -Test Kit (**Experiment WA2**). The protocol shown in **Figure 6A** (also used in experiment **WA1**, Cytofluor 4000 Test of MDR Assay β -Test kit) was repeated here using cells plated in four 35mm circular cell culture dishes. In this color-coded representation of gray-scale images, low intensity pixels have been assigned "colder" colors (black, purple, blue) while "warmer" colors (yellow, red, white) have been assigned to the higher intensity

pixels. As shown in the bar, the warmer colors indicate higher levels of intracellular calcein. (A) MDR (MCF-7 ADR) incubated with CAM (only). These cells accumulate relatively little calcein. (B) MDR cells incubated with CAM+MK. (C) MDR cells treated with CAM+V (D) Image of DS (MCF-7 WTC) cells stained with CAM (only). These digital images show good agreement with the expected behavior of the β -Test kit assay (Figure 6A).

Figure 9: This diagram gives detailed information on the syringes, composition of solutions in the syringes, flow rates, and perfusion intervals used in VSOM experiment WA3. This experiment consisted of two VSOM runs, Run #1 for MCF-7 WTC (DS) cells, and Run #2 for MCF-7 ADR (MDR) cells. These two runs were performed, one after the other, on the same day. Both runs used the pump schedule. At the end of each run, the plot which was displayed on the computer screen was saved. The plots for Runs #1 and 2 are shown in black windows at the bottom of the figure. The red line in each case represents the average of all the cell responses in the entire field of view. As seen in these two plots recorded for MCF-7 WTC (DS, run #1) and MCF-7 ADR (MDR, run #2), DS cells (upper plot) accumulated more calcein (240 ± 82 , $N=336$) than did the MDR cells (103 ± 80 , $N=161$). This is in agreement with the relative differences in calcein accumulation observed between the same DS and MDR cells in the multiwell plate experiments which represent an average over many cells.

Figure 10: The individual cell responses of each DS cell in Run #1 (Experiment WA3) are shown in green. The mean response \pm standard deviation of all the cells is shown overlaid in black. During VSOM experiments the mean cellular fluorescence of each cell is monitored, and deviations from the population mean can easily be detected. For example, the arrow indicates several cells that began to lose viability and plasma membrane integrity. Such cells are unable to retain calcein and the fluorescence signal drops. It should be noted that (1) the largest number of cells observed to date in a single field is 1000 (2) the current VSOM system could easily terminate or modify the exposure/perfusion as soon as a single cell death is noted (3) the current VSOM system could easily detect a single MDR cell (Figure 11, red curves) out of 1000 DS cells. This is because there is no overlap between such cell responses between 1000 and 5000s.

Figure 11: Selected individual cell responses from four cells in Run #2 (Experiment WA3). This is the type of detailed physiological information that flow cytometric assays and multiwell plate assays cannot provide, and it demonstrates that our VSOM technology has the capabilities we initially predicted. Detailed rate information on calcein accumulation and retention is available throughout the VSOM experiment. For the blue response curves, one can calculate a rate of calcein accumulation during the three CAM perfusions, and one can calculate a rate of calcein retention during BUFF perfusions. Calcein accumulation is occurring in the 1500, 3500, and 5500s time periods, and plateaus corresponding to excellent calcein retention are observed in the 2500, 4500, 6500 time intervals. For the red curves, no calcein accumulation occurs until 5000s, when CAM+V is perfused.

Figure 12: Calcein accumulation in 65 MCF-7 ADR (MDR) cells during Calcein-AM (CAM) perfusion (VSOM Experiment WA4). CAM (at the four-fold higher concentration of $1.0 \mu\text{M}$) was perfused. The first perfusion interval this experiment is shown, and the same data is presented using a variety of 3D perspectives. As seen earlier (Figure 11, blue), a significant subpopulation of calcein-accumulating (DS) cells is present, and these cells demonstrate varying degrees of calcein accumulation during a 2100s exposure. Portions of this experiment are presented in the **Biophysical Society Abstract (Appendix D)**. Cells that accumulate calcein are not multi-drug resistant. Four views of the same data are shown. (A) Selected responses of 14 cells that accumulated calcein. 3D response curves are color coded according to intensity (B) All 65 cell responses shown (C) All 65 cell responses viewed end-on (D) 2D projection of data shown in 3D in C.

Figure 13: MCF-7 Cells vs. HMECs: pH is a function of CO_2 , Buffering System(s) and Metabolism. MCF-7 cells (WTC and ADR, blue circles) grown in DMEM (containing a bicarbonate buffer) and HMECs (red triangles) grown in MEGM (containing both a bicarbonate buffer and a HEPES buffer) show

different pH behavior as a function of incubator CO₂ levels. As indicated by the vertical arrows, the pH range tolerated by each cell type varies. The pH zone common to both cell types is shown in green. There is not a common CO₂ level that allows these different cell types (in separate flasks, in the media that each prefers) to simultaneously propagate in a single incubator. The more normal HMECs tolerate a much narrower range of pHs than do the MCF-7 cancer cells. None of the cell lines prefer a lower pH environment (<7.1).

Figure 14: Transmitted light images of MCF-7 WTC cells propagated in media of varying pH. Images were acquired by placing a T-25 tissue culture flask on the microscope using the appropriate stage mounting plate (**Figure 6F**).

(A,B) MCF-7 WTC cells incubated at CO₂ levels that produce a pH >7.4 (on average) in DMEM successfully attach, spread out, and proliferate on the plastic tissue culture ware surface.

(C,D) At pHs < 7.2, MCF-7 WTC cells round up, and do not do attach well. A similar effect is seen if MCF-7 ADR are plated under conditions where the pH > 8.0.

Figure 15: Color coded ratioed images of 184B5 cells (Experiment HM1). Living cells were pulse-labeled with BrdU for 1 hr, and then dual-stained with H42 and S16. One digital image was acquired of cells using 360nm excitation (H42 signal), and a second was acquired using 490nm excitation (S16 signal). These images were processed and ratioed on a pixel by pixel basis. The resulting ratio values were then color coded as indicated by the bar. MEGM (complete) cells showed the greatest amount of DNA synthesis, followed by MEGM+EGF cells which show decreased DNA synthesis. Cells maintained in MEGM-EGF show little DNA synthesis. Our results agree with those obtained by traditional [³H]-thymidine incorporation assays.

Figure 16: Experiment HM2: HMECs (184B5 cells) were dual stained with FURA-PE3 (green: a calcium-sensitive fluorescence probe) and LDS-751. Cells were sequentially stimulated with 2μM thapsigargin (TG) and 5μM ionomycin (ION). Both of these compounds are known to elevate intracellular calcium. The red mRNA signal due to LDS-751 increases greatly for all the cells after intracellular calcium had been elevated. The fluorescence signal of LDS-751 when bound to DNA is emitted in the infrared; thus, the nuclei of these cells do not exhibit any red signal. The 3D graphs inset in **Figure 16** are zoomed up in **Figure 17**.

Figure 17: Experiment HM2: (A) The LDS-751 response for all cells is shown in **Figure 16**, (B) selected responses taken from panel A. As seen in the selected responses, some cells exhibit a second response to ION after the initial TG stimulation, and some do not. In addition, some cells respond more quickly to TG than do others.

Appendix B: Figures

[illegible]

New Specimen Treatment

headsheadsheads

1DMC7ADRB1, H42 washout BUFF
 1DMC7ADRB2, 0.25UM CAM penus
 1DMC7ADRB3, 0.25UM CAM washo
 1DMC7ADRB4, 0.25UM CAM+10UM
 1DMC7ADRB5 CAM+MK571 washo
 1DMC7ADRB6, 0.25UM CAM+50UM
 1DMC7ADRB7 CAM+VER washout

Images

dc102000bp2.0083.1_X1cs
 dc102000bp2.0084.1_X1cs
 dc102000bp2.0085.1_X1cs
 dc102000bp2.0086.1_X1cs
 dc102000bp2.0087.1_X1cs
 dc102000bp2.0088.1_X1cs
 dc102000bp2.0089.1_X1cs
 dc102000bp2.0090.1_X1cs
 dc102000bp2.0091.1_X1cs
 dc102000bp2.0092.1_X1cs
 dc102000bp2.0093.1_X1cs
 dc102000bp2.0094.1_X1cs
 dc102000bp2.0095.1_X1cs
 dc102000bp2.0096.1_X1cs
 dc102000bp2.0097.1_X1cs
 dc102000bp2.0098.1_X1cs
 dc102000bp2.0099.1_X1cs
 dc102000bp2.0100.1_X1cs
 dc102000bp2.0101.1_X1cs
 dc102000bp2.0102.1_X1cs
 dc102000bp2.0103.1_X1cs
 dc102000bp2.0104.1_X1cs
 dc102000bp2.0105.1_X1cs
 dc102000bp2.0106.1_X1cs
 dc102000bp2.0107.1_X1cs
 dc102000bp2.0108.1_X1cs
 dc102000bp2.0109.1_X1cs
 dc102000bp2.0110.1_X1cs

Expand Tree

☐ dc102000bp2.0032.1_X1cs
☐ dc102000bp2.0033.1_X1cs
☐ dc102000bp2.0034.1_X1cs
☐ dc102000bp2.0035.1_X1cs
☐ dc102000bp2.0036.1_X1cs
☐ dc102000bp2.0037.1_X1cs
☐ dc102000bp2.0038.1_X1cs
☐ dc102000bp2.0039.1_X1cs
☐ dc102000bp2.0040.1_X1cs
☐ dc102000bp2.0041.1_X1cs
☒ 1DMC7ADRB4, 0.25UM CAM+10UM MK571 penus
☐ dc102000bp2.0042.1_O1cs
☐ dc102000bp2.0043.1_O1cs
☐ dc102000bp2.0044.1_O1cs
☐ dc102000bp2.0045.1_O1cs
☐ dc102000bp2.0046.1_O1cs
☐ dc102000bp2.0047.1_O1cs
☐ dc102000bp2.0048.1_O1cs
☐ dc102000bp2.0049.1_O1cs
☐ dc102000bp2.0050.1_O1cs
☐ dc102000bp2.0051.1_O1cs
☐ dc102000bp2.0052.1_O1cs
☐ dc102000bp2.0053.1_O1cs

Number of treatment groups

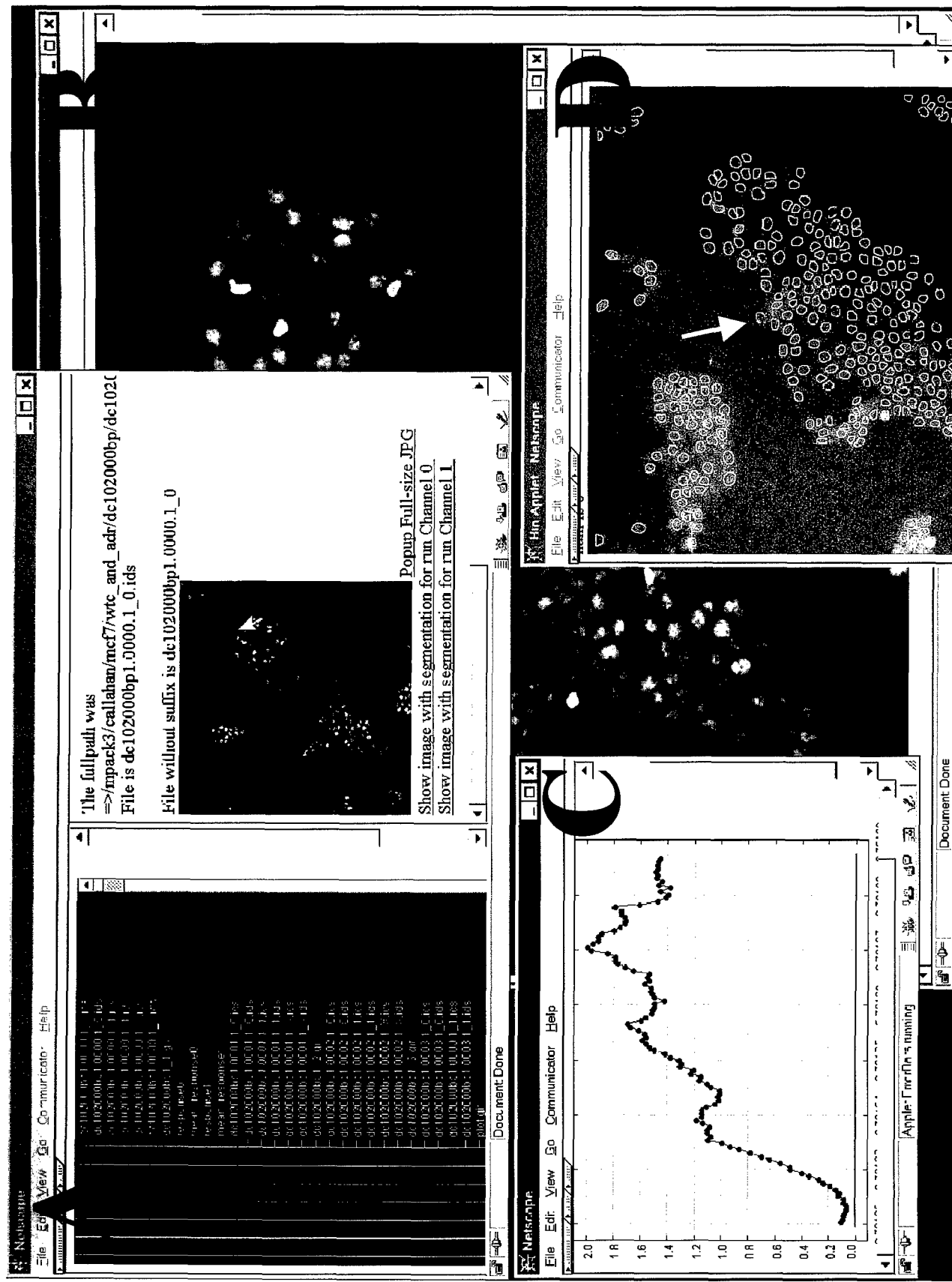
7

☐ Write to database?

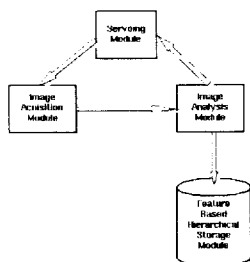
Back

Done

Annual Report: Callahan, Parvin Page 26



JAVA VSOB Results Browser: Window A presents a tree structure for an image directory, and the opposite frame in window A displays a thumbnail of the ICS image. By clicking on Pop-Up Full-Size JPEG, one can bring up the 1024x1024 image in window B, and by clicking on Show Image with Segmentation, one can bring up the image for that channel in window D (Channel = 0 here for 360 excitation of H42). If one then clicks on an individual cell in Window D, the time-dependent mean cellular fluorescence is plotted for that cell (arrow) in the current image (channel 1 image in this case; an early time point). The signal reflects calcein accumulation in a single cell.



(A) Functional Architecture

```

<Pump_state
  current_time_secs="965701306"
  current_time_uses="64660"
  pumpnumber="0"
  syringe_0_rate="2.100000"
  syringe_0_rate_units="ml/mn"
  syringe_1_rate="2.700000"
  syringe_1_rate_units="ml/mn"
  syringe_0_diameter="26.000000"
  syringe_1_diameter="26.000000"
  running_or_stopped="Stopped"
  mode="Proportional"
  direction="Parallel"

```

```

/>
<Pump_state
  current_time_secs="965701306"
  current_time_uses="374190"
  pumpnumber="1"
  syringe_0_rate="2.300000"
  syringe_0_rate_units="ml/mn"
  syringe_1_rate="0.000000"
  syringe_1_rate_units="ml/mn"
  syringe_0_diameter="27.000000"
  syringe_1_diameter="25.000000"
  running_or_stopped="Stopped"

```

(B) Small Selection from "Pump Log"

```

<StackAcquisition
  SINGLE or MULTIPLE stack_acquisition="MULTIPLE"
  seconds_interval_between_multiple_stacks="300"
  TOTAL_TIME or NUM_STACKS to_stop_multiple_stack_acquisition="TOTAL_TIME"
  total_time_seconds_then_stop="7200"
  num_stacks_then_stop="1" >

  <Channel
    filterWheelPosition="0"
    headerInfo_wavelength="360nm"
    headerInfo_filenameChannelChar="0"
    description="H42"
    ACTIVE="yes"
  >
  <exposureTime_ms> 200</exposureTime_ms>
</Channel>

  <Channel
    filterWheelPosition="1"
    headerInfo_wavelength="490nm"
    headerInfo_filenameChannelChar="1"
    description="null"
    ACTIVE="yes"
  >
  <exposureTime_ms> 1000</exposureTime_ms>
</Channel>

  <Channel
    filterWheelPosition="2"
    headerInfo_wavelength="570nm"
    headerInfo_filenameChannelChar="2"
    description="null"
    ACTIVE="yes"
  >
  <exposureTime_ms> 1000</exposureTime_ms>
</Channel>

  <Channel
    filterWheelPosition="3"
    headerInfo_wavelength="380nm"
    headerInfo_filenameChannelChar="3"
    description="null"
    ACTIVE="yes"
  >
  <exposureTime_ms> 500</exposureTime_ms>
</Channel>

  <Channel
    filterWheelPosition="4"
    headerInfo_wavelength="340nm"
    headerInfo_filenameChannelChar="4"
    description="null"
    ACTIVE="yes"
  >
  <exposureTime_ms> 500</exposureTime_ms>
</Channel>

  <Channel
    filterWheelPosition="5"
    headerInfo_wavelength="OPEN"
    headerInfo_filenameChannelChar="5"
    description="null"
    ACTIVE="no"
  >
  <exposureTime_ms> 100</exposureTime_ms>
</Channel>

  <Channel
    filterWheelPosition="6"
    headerInfo_wavelength="TRANS"
    headerInfo_filenameChannelChar="X"
    description="brightfield"
    ACTIVE="yes"
  >

```

(C) XML "Recipe" File

```

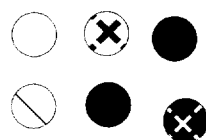
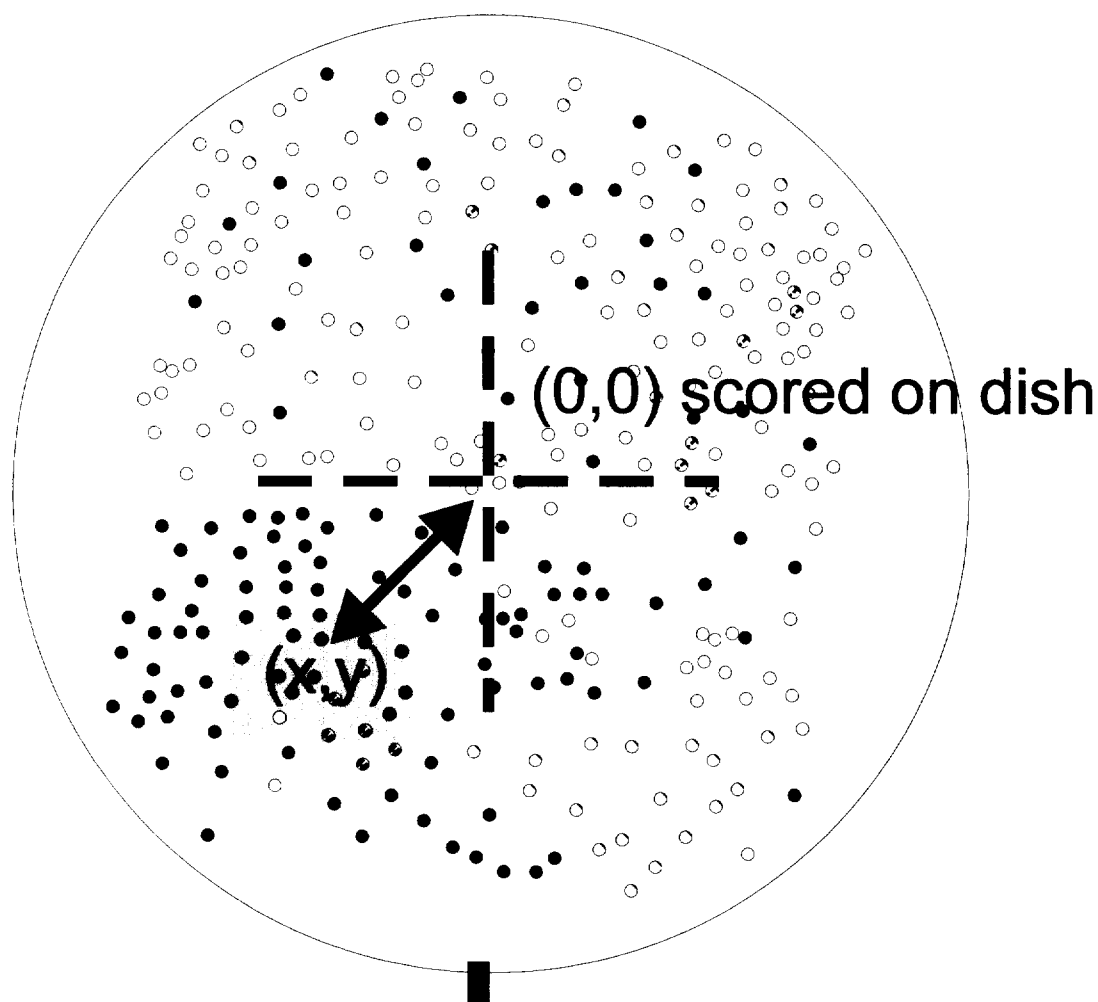
ics_version 1.0
filename de051300dc.01.1
layout parameters 4
layout order bits x y z
layout sizes 16 1024 1024 5
layout coordinates video
layout significant_bits 16
representation format integer
representation sign signed
representation compression compress
representation byte_order 2
representation SCIL TYPE g3d
parameter origin 0 160 6 0
parameter scale 1 0.68000001 0.68000001 0
parameter labels intensity x-pos y-pos probe
parameter units relative microns microns undefined
parameter exptype beads
parameter exptarget other
parameter probe dapi_360 fite_490 tr_570 fura2_380 fura2_340
parameter target other other other other
parameter exposure_time 1.00 1.00 1.00 1.00 1.00
history date Sat May 13 23:50:22 2000
history computer Sun Spare Ultra 170
history laboratory I.B.N.L. Life Sciences Division
history operator Daniel E Callahan
history microscope Zeiss Axiovert135TV
history objective Zeiss Fluor 10x 0.50NA
history camera .dev.sdv0
history software SCIL-Image 1.3
history comments New Xe lamp, base mounted camera

```

(D) ICS Image Header File

FIGURE 3

KEEP TRACK OF CELL LOCATIONS (LOCATION OF MICROSCOPIC FIELD OF VIEW) DURING EXPERIMENTS



DIFFERENT TYPES OF LIVING CELLS.

(x,y)

1024x1024

ONE FIELD OF VIEW IN A PETRI DISH. KEEP TRACK OF RELATIVE POSITION OF CELLS DURING TIME LAPSE EXPERIMENT. BE ABLE TO RETURN TO THIS FIELD OF VIEW DAYS LATER.

FIGURE 4

IMAGE SEMENTATION RESULTS

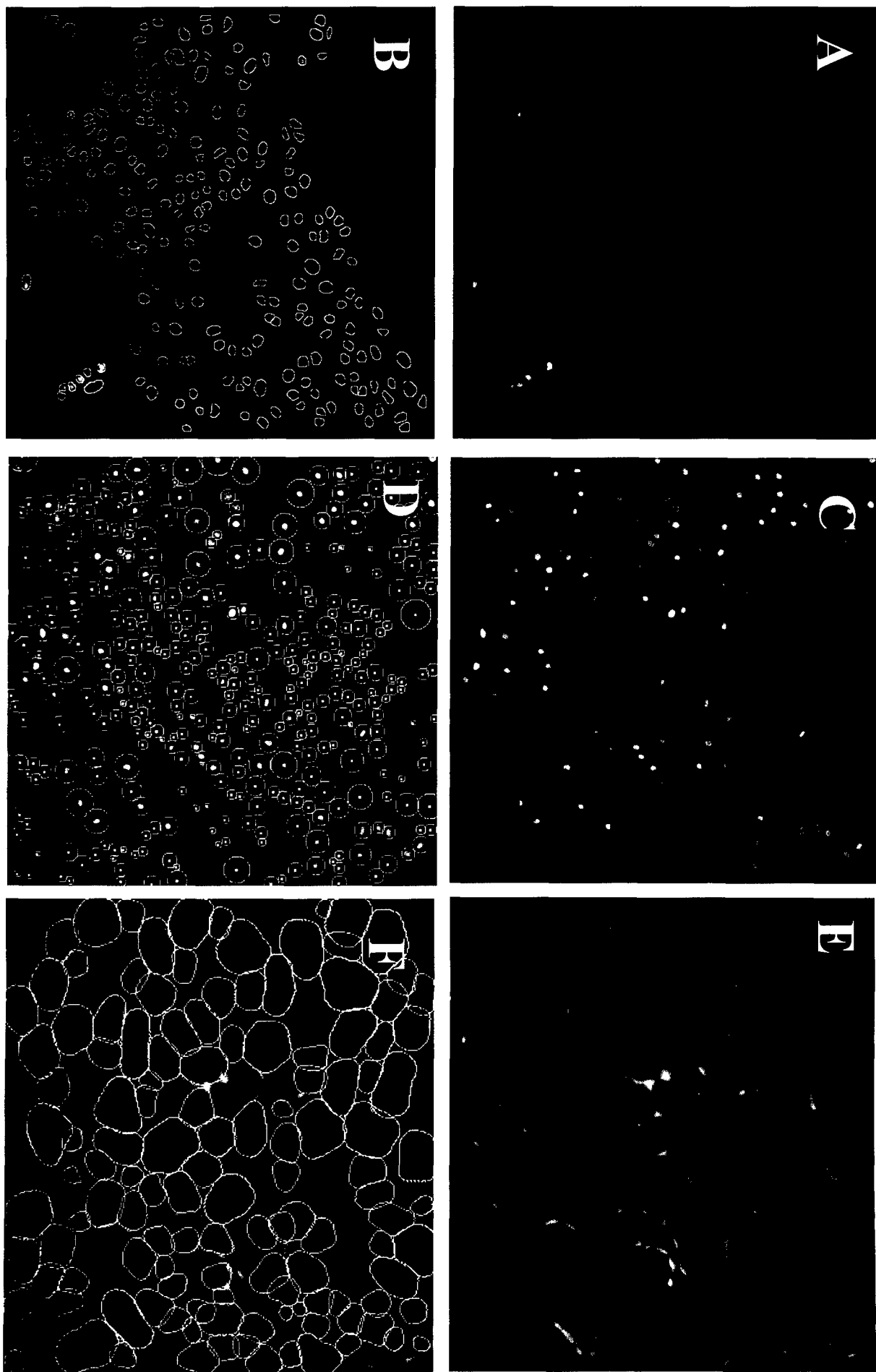


FIGURE 5

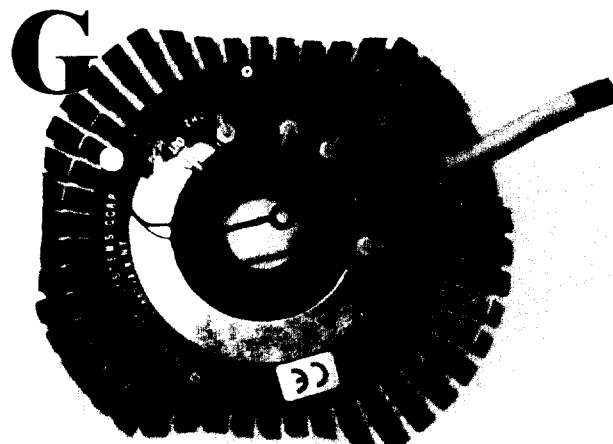
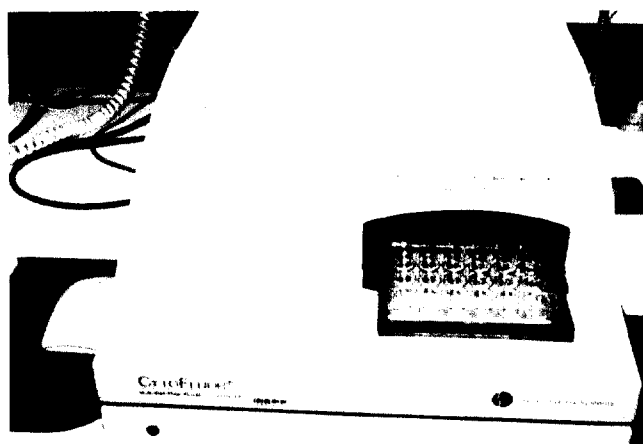
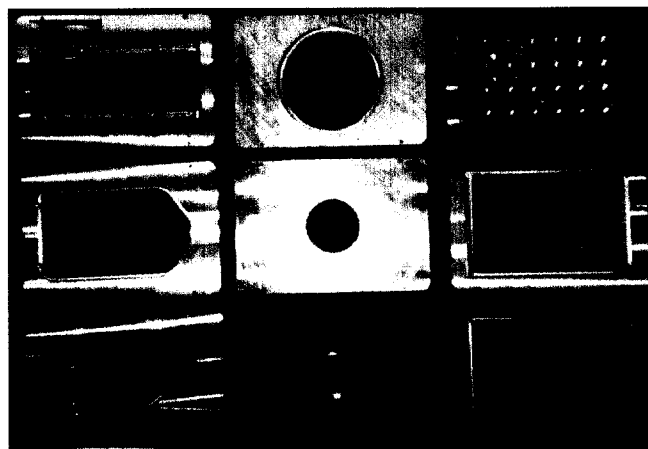
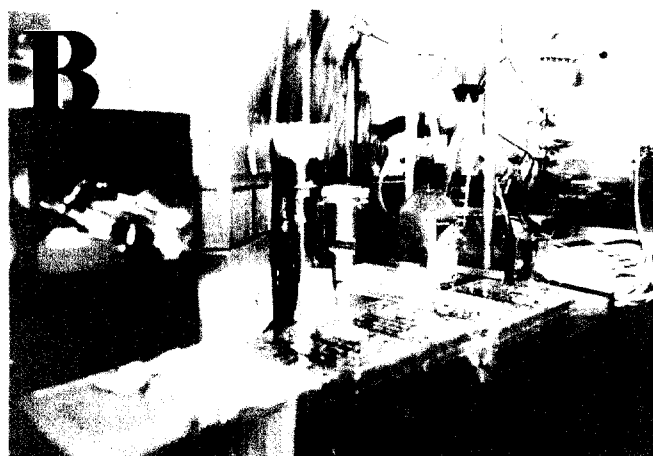
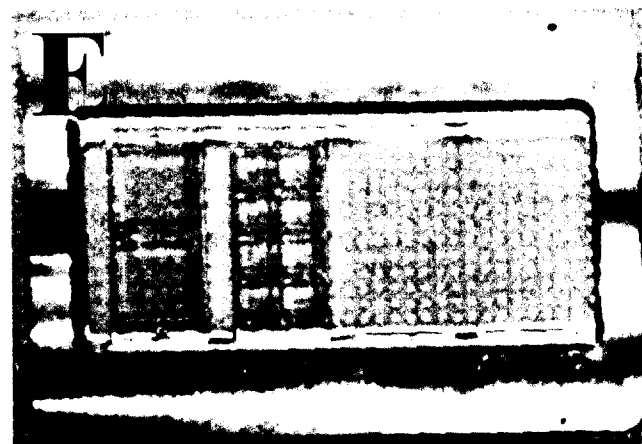
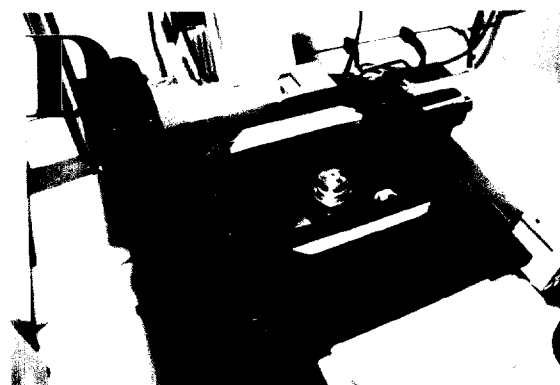
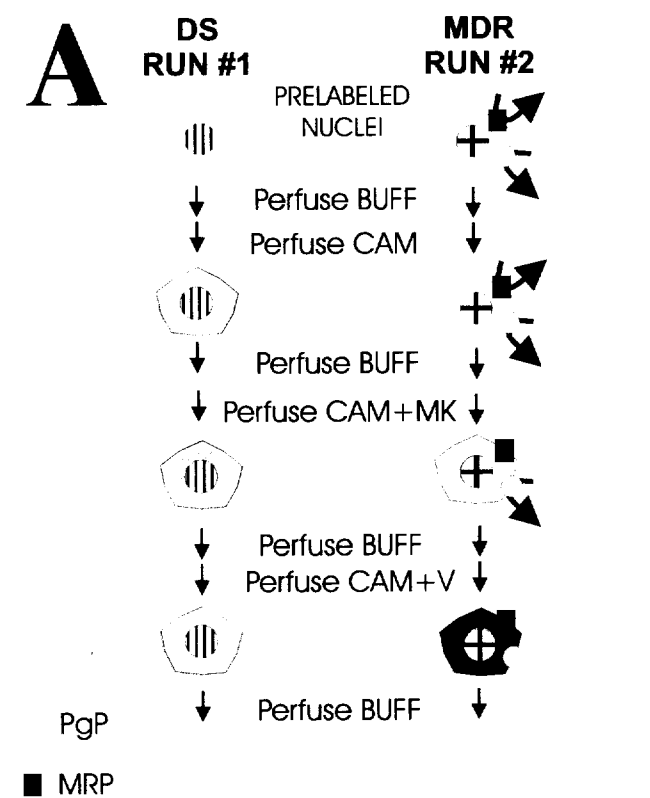
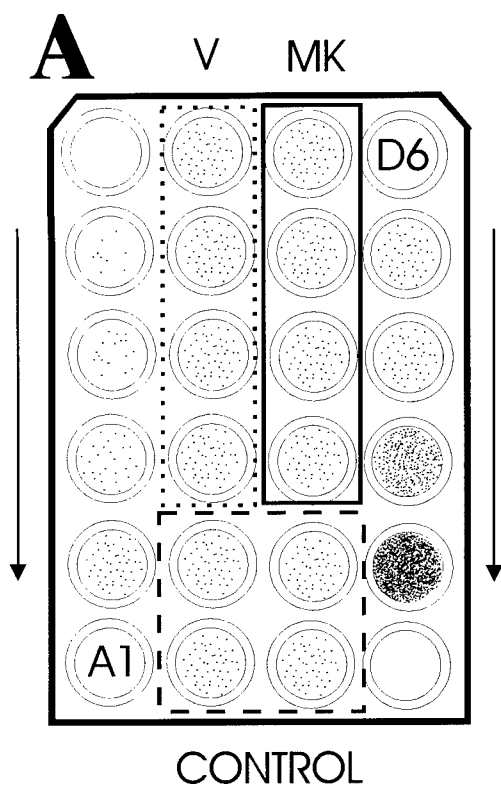
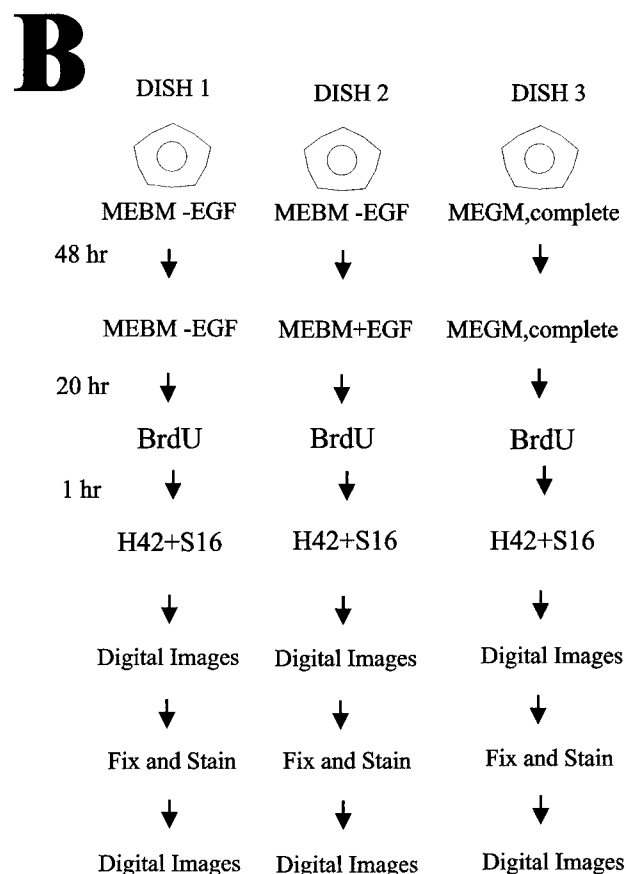


FIGURE 6



Layout of the four plates used in experiment WA1. (**Control**, CAM (only), 4 wells; **V**, CAM+Verapamil, 4 wells; **MK**, CAM+MK-571, 4 wells; **A1** and **D6** are array designations for 2 of the 4 blank wells.) Black dots in each well represent relative cell density.



BrdU Incorporation Assay

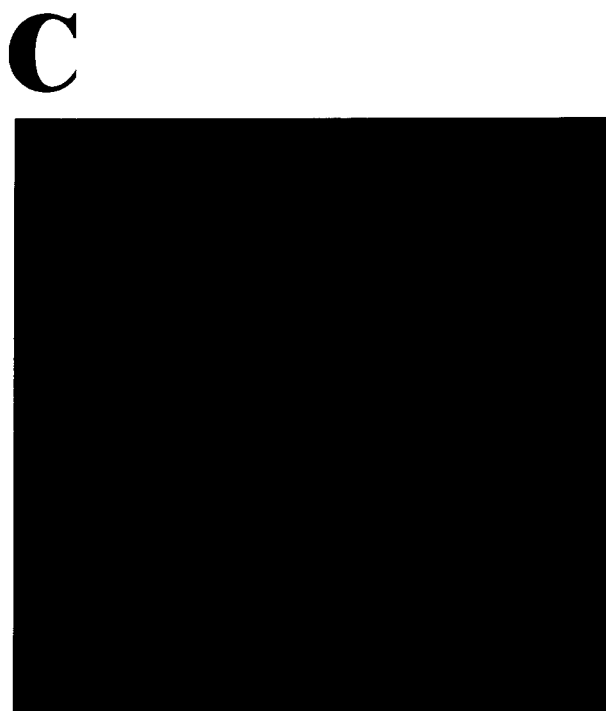
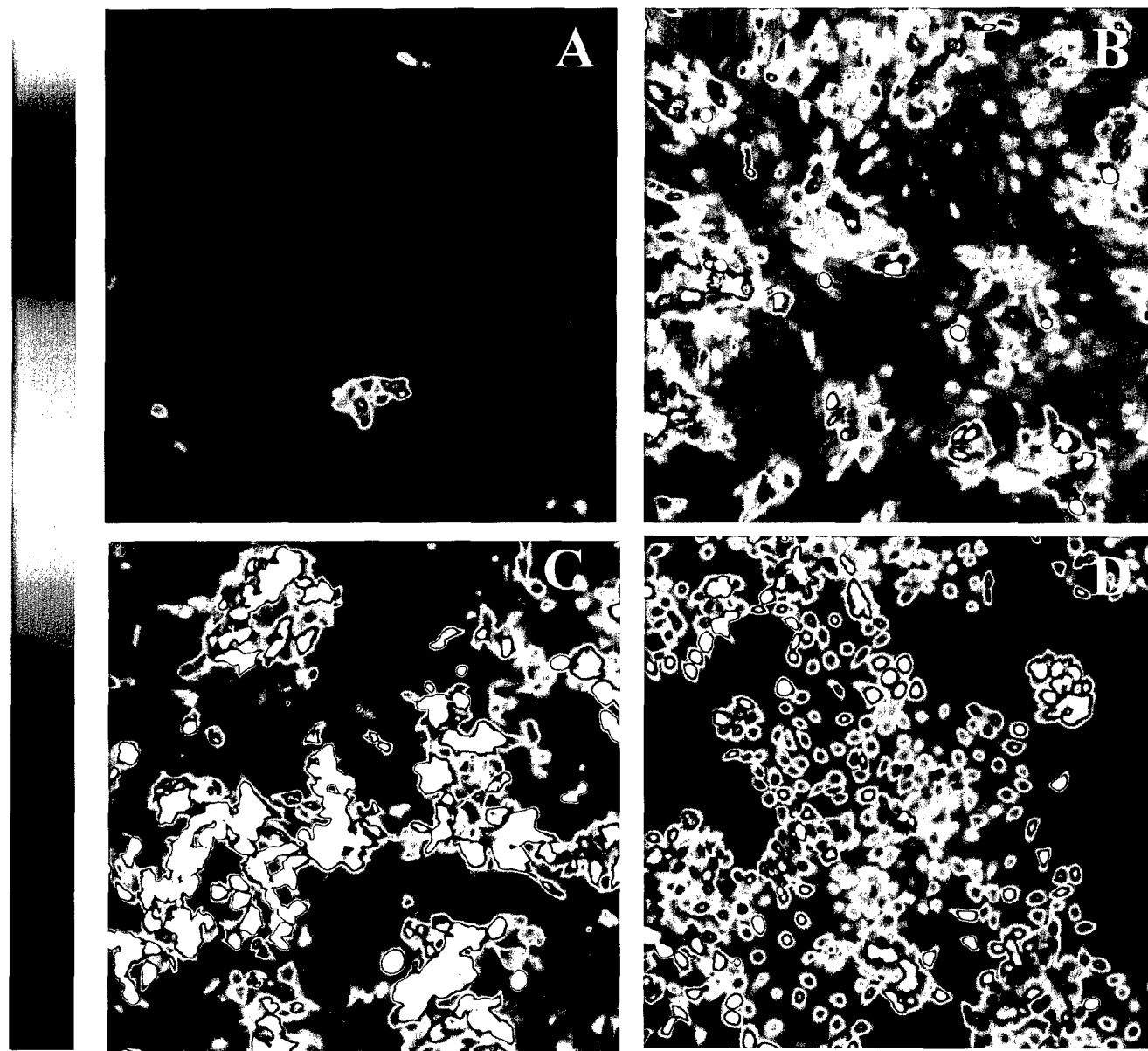


FIGURE 7

**High
Calcein**



**Low
Calcein**

FIGURE 8

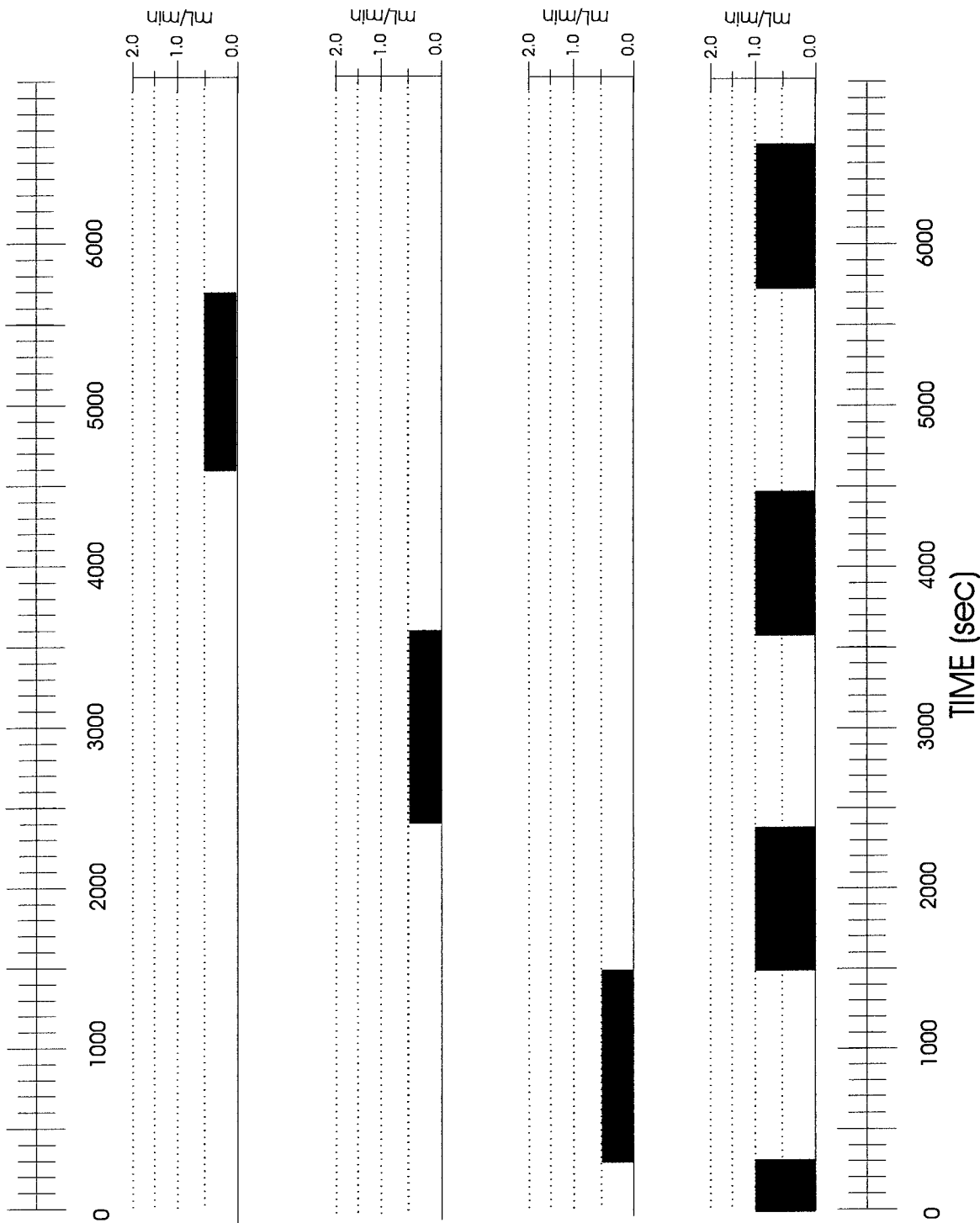


FIGURE 9

FIGURE

Diagram of Pump Schedule and screen snapshots of Calcein-AM accumulation for entire fields of cells of MCF-7 WTC (run1) and MCF-7 ADR (run2). In the screen snapshots, the mean fluorescence intensity is calculated for each cell, and then the average intensity for all the cells is plotted on the screen throughout the experiment.

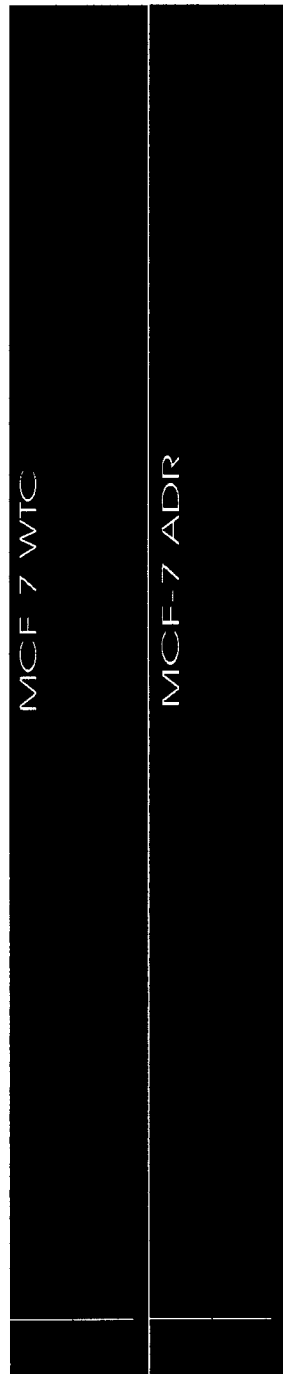
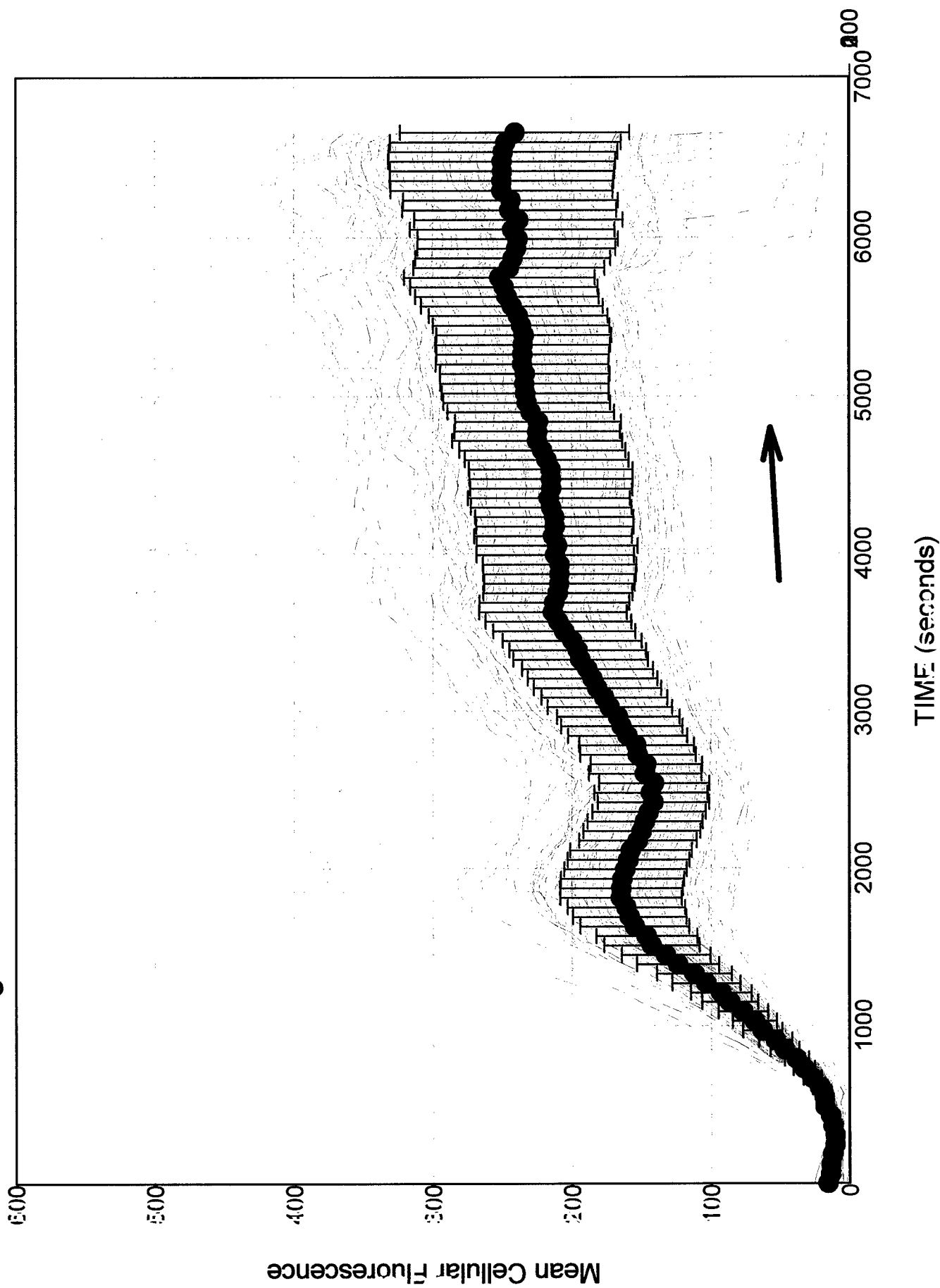


FIGURE 10

MCF-7 WTC: Individual cell responses shown in green.
Average \pm Standard Deviation of all cells is shown in black.



MCF-7 ADR: Modulation of MDR. Four Individual Cell Responses Shown.
RED : Cells that accumulated Calcein only when Verapamil was present.
BLUE: Cells that demonstrated additional responses.

NOTE: There is a considerable lag between the time when the pump is turned on (at 0.5 or 1.0 mL/min) and the time when the solution reaches and equilibrates with the solution in the cell chamber.

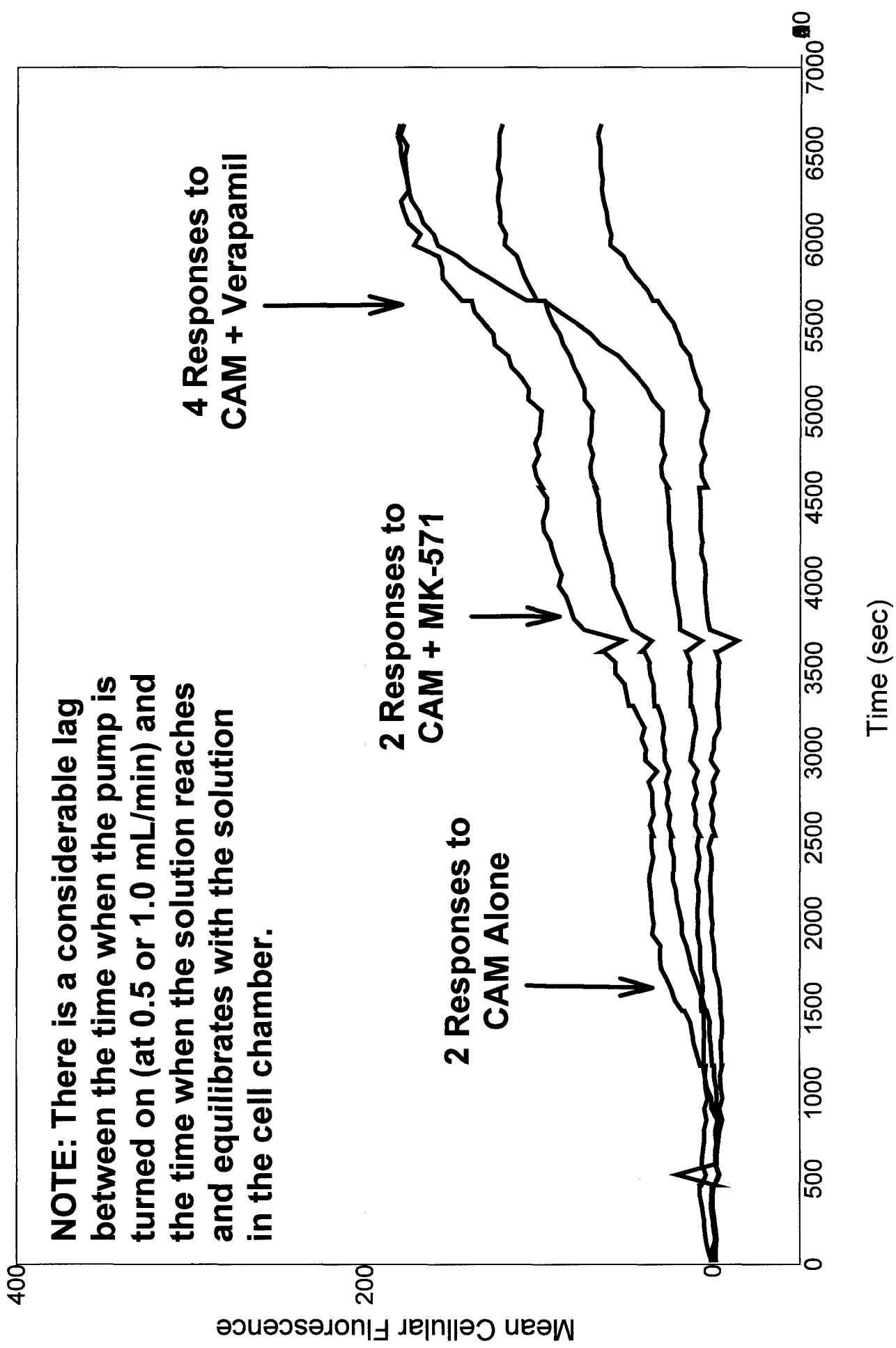


FIGURE 11

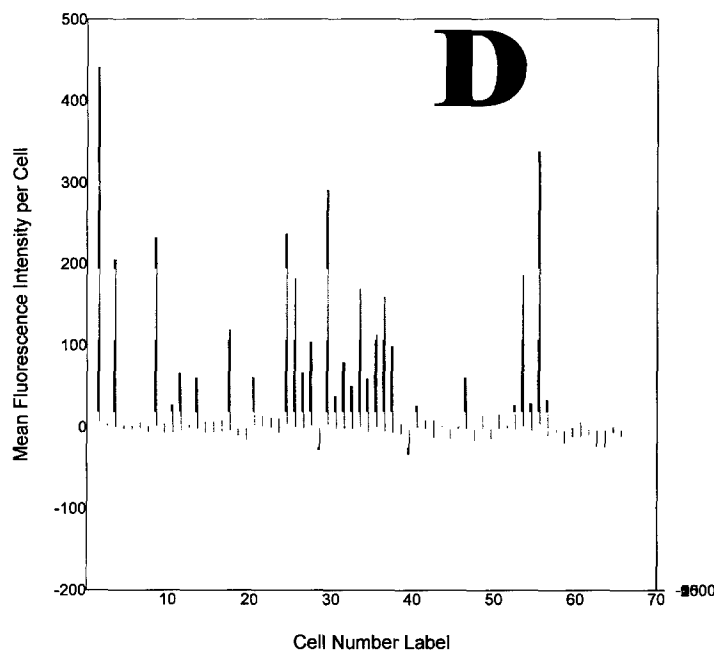
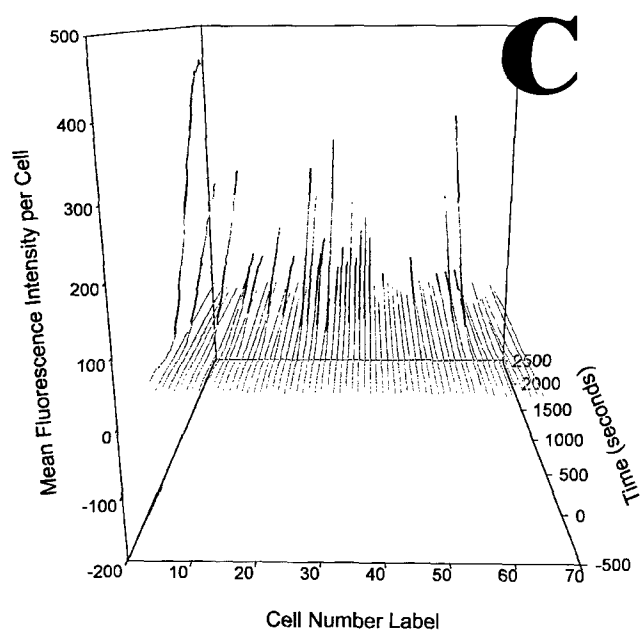
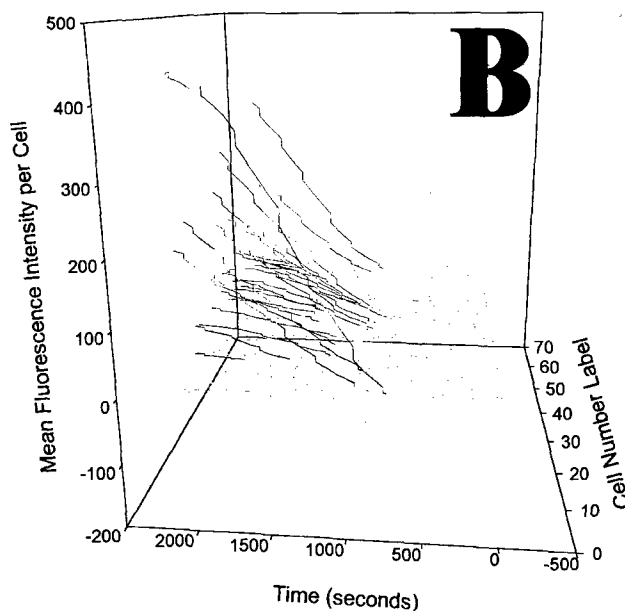
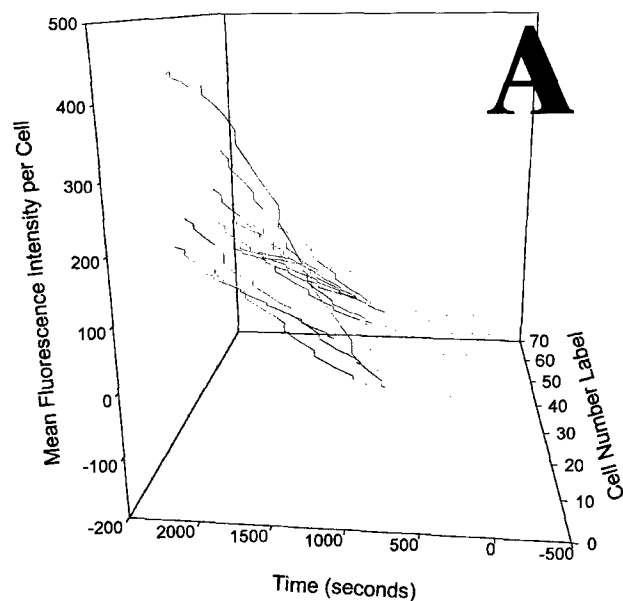


FIGURE : Calcein accumulation in 65 MCF-7adr cells during Calcein-AM perfusion. Cells that accumulate calcein are not multi-drug resistant. Four views of the same data are shown. (A) Selected responses of 14 cells that accumulated calcein. 3D response curves are color coded according to intensity (B) All 65 cell responses shown (C) All 65 cell responses viewed end-on (D) 2D projection of data shown in 3D in C.

FIGURE 12

pH is function of CO₂, Buffering, System(s) and Cell Metabolism

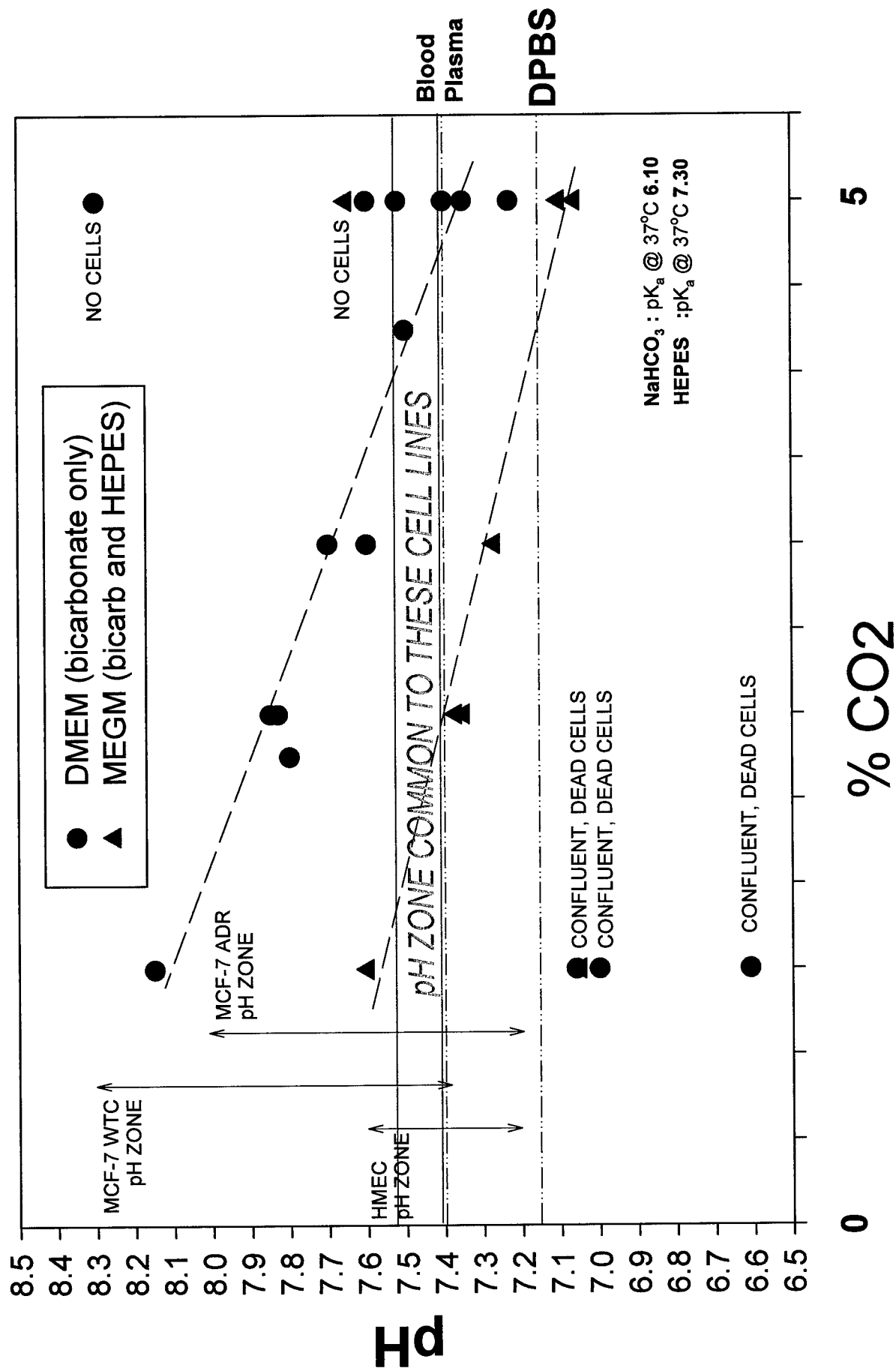


FIGURE 13



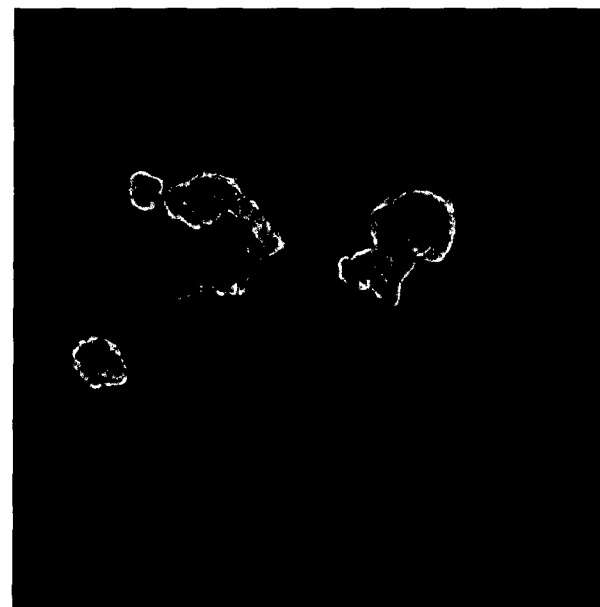
**A. MCF-7 WTC
in DMEM, pH > 7.2**



**C. MCF-7 WTC
in MEGM, pH < 7.2**



**B. MCF-7 WTC
in DMEM, pH > 7.2**



**D. MCF-7 WTC
in MEGM, pH < 7.2**

FIGURE 14

LIVING CELLS STAINED WITH NUCLEAR STAINS Hoechst 33342 and Syto 16

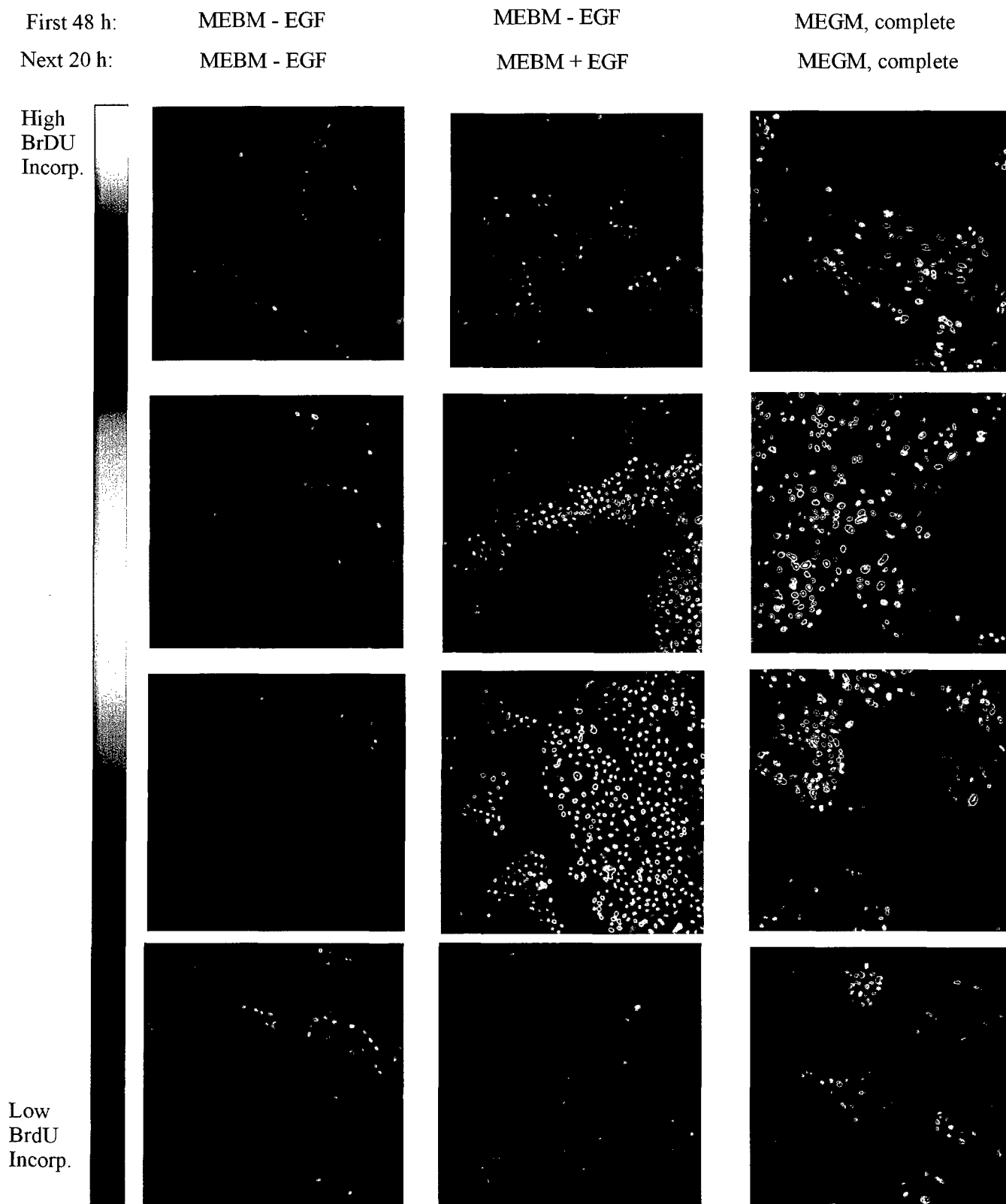


FIGURE 15

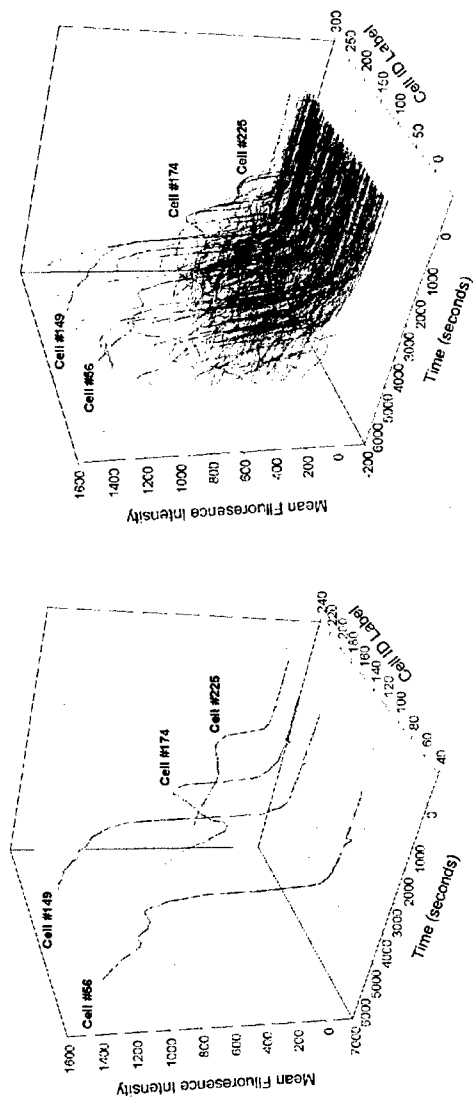
184B5 Cells pre-loaded
with FURA-PE3 (2uL/3mL) and
LDS-751 (1:19; 1uL/3ml)

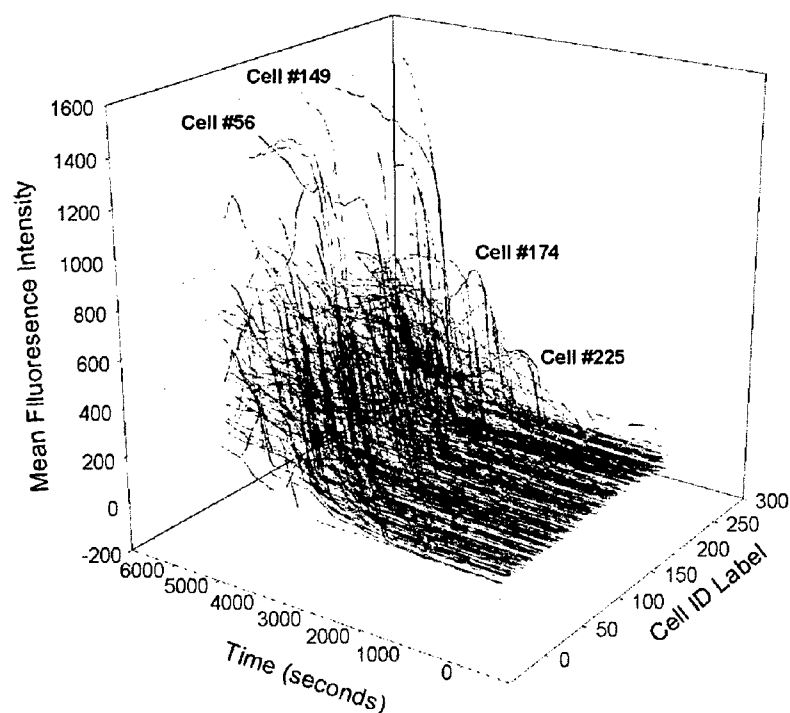
473 sec

184B5 Cells prestained with
FURA-PE3, and LDS-751
30 mins after stimulation with
2 uM thapsigargin

2645 sec

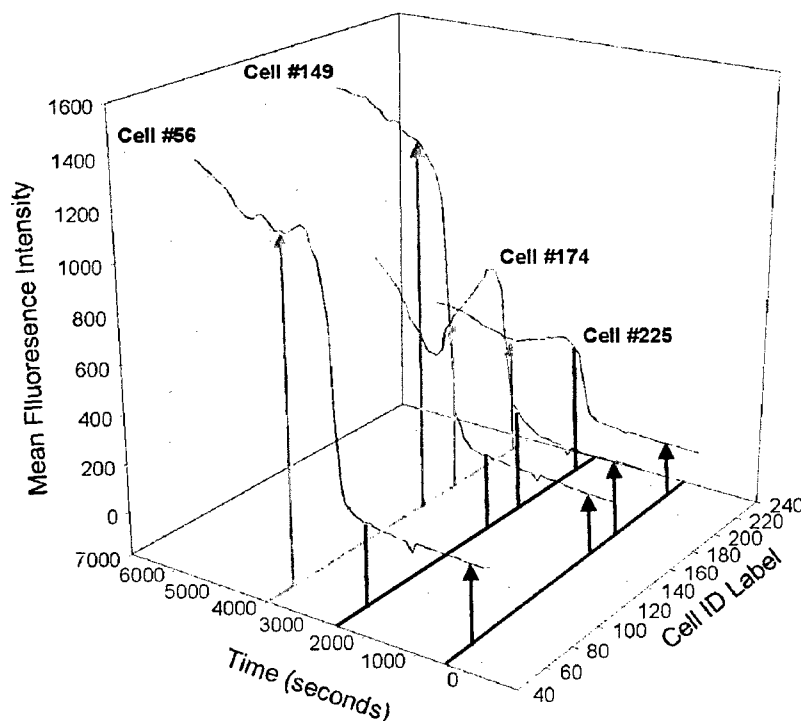
FIGURE 16





A

Single cell responses of 225 184B5 cells. These cells were shown in the two previous images at $t=473$ sec and $t=2645$ sec. A heterogeneous set of responses can be seen. Four of these responses are colored black and shown in greater detail below.



B

Selected cell responses to (a) RED: 2 μ M thapsigargin(TG) (473s, 1 mL/min, 45 mL) and (b) GREEN: 5 μ M ionomycin (3941s, 1 mL/min, 15 mL). Some cells exhibit a second response to ionomycin (174, 255), and some do not (56, 149). In addition, Some cells (225) respond more quickly to TG than others (56, 149, 174).

FIGURE 17

Appendix C: Era of Hope Poster

Callahan, D.E., and Parvin, B. Quantitation of Single Cell Responses using Fluorescence Microscopy, *Proceedings: Era of Hope Department of Defense Breast Cancer Research Program Meeting, Volume 2, page 709*. Atlanta, GA, June 8-11, 2000, Poster Number: CC-5.

ABSTRACT

The purpose of this two-year IDEA proposal is to gather preliminary data that demonstrate the feasibility of a new class of in vitro drug response and chemosensitivity assays. Our objectives are to develop an instrument (a visual servoing optical microscope, or VSOM) in a stepwise fashion and gather preliminary data to aid future development of cell culture techniques and fluorescence assays. Our goal is to demonstrate the feasibility of using VSOM technology to analyze the heterogeneity and physiological characteristics of tumor cells from individual breast cancer patient biopsies. We believe that the VSOM will be extremely useful in developing new VSOM chemosensitivity fluorescence assays for a variety of breast cancer drugs. VSOM fluorescence assays are based on the dynamic physiological responses of single cells. In these assays, computer controlled syringes inject various substances into a temperature controlled microperfusion chamber. We are currently observing the single cell responses of up to 500 cells in five separate channels. The following cell types have been examined: MCF-7 (human breast cancer cell line, drug sensitive, or DS), MCF-7adr (multi-drug resistant, or MDR, version of MCF-7), 184SK (normal human mammary epithelial cells, or HMECs), and 184B5 (immortally transformed HMECs). At the present time, we have quantified the uptake and retention of the fluorescent compounds FURA-2AM, calcein-AM, LysoTracker-Red, and Hoechst 33342 in all the cell types. We have also documented the effects of ionomycin, thapsigargin, and 4-Br-A23187 in 184SK and 184B5 cells labeled with FURA-2AM and LDS-751. We have the infrastructure in place to handle very large amounts of digital video data and perform on-line analysis and intelligent instrument control. Once the VSOM is fully automated it will be extremely useful for dissecting complex biochemical pathways, isolating and optimizing important environmental variables, and designing fluorescence assays for specific cell types or for breast cancer drug chemosensitivity.

The U.S. Army Medical Research and Materiel Command under DAMD17-98-1-8177 supported this work.

1 Tumor cells from breast cancer patient
(Surgical Discard, FNA)

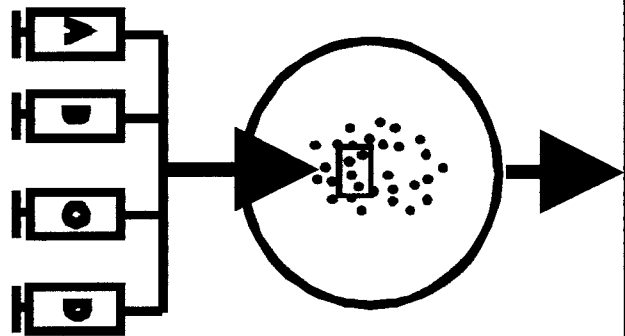


2 Isolation and Culture of Primary Breast Tumor Cells

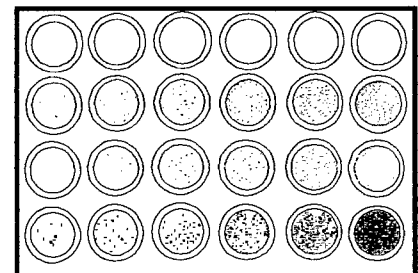
(Dairkee, et al., *Cancer Res.*, **57**, 1590 (1997), Li, et al., *Cancer Res.*, **58**, 5271 (1998))



3 VSOM
Microenvironmental
Analysis, Stimulation,
and Expansion of Cells



4 Multiwell Plate Analysis
under VSOM-Optimized
Environmental Conditions





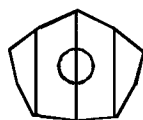
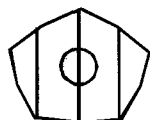
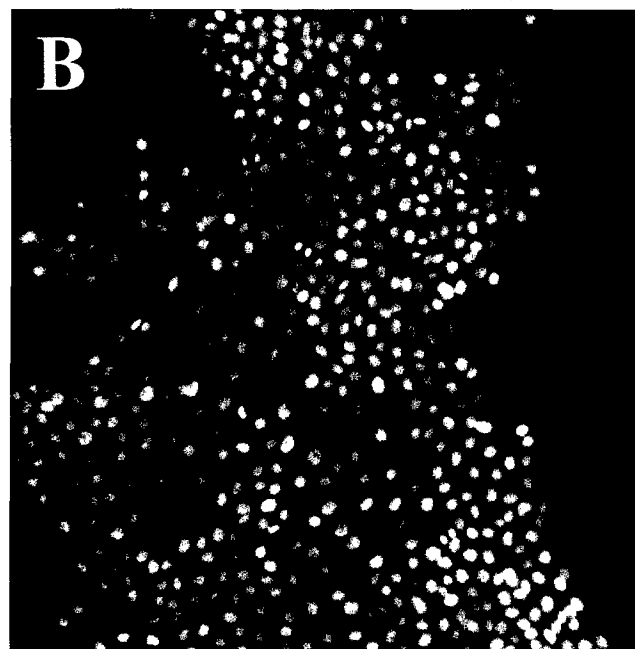
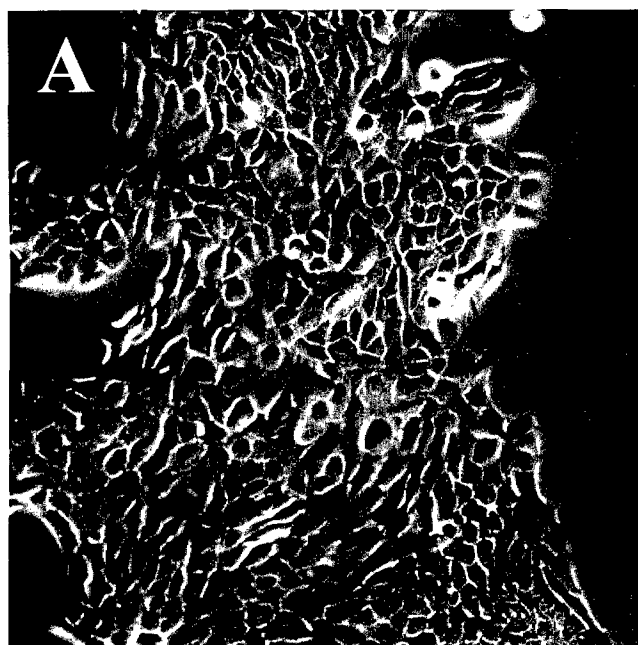
- (A) Microperfusion Chamber With Probes and Vacuum Aspirator**
- (B) Computer-controlled xy scanning stage with plate insert.**



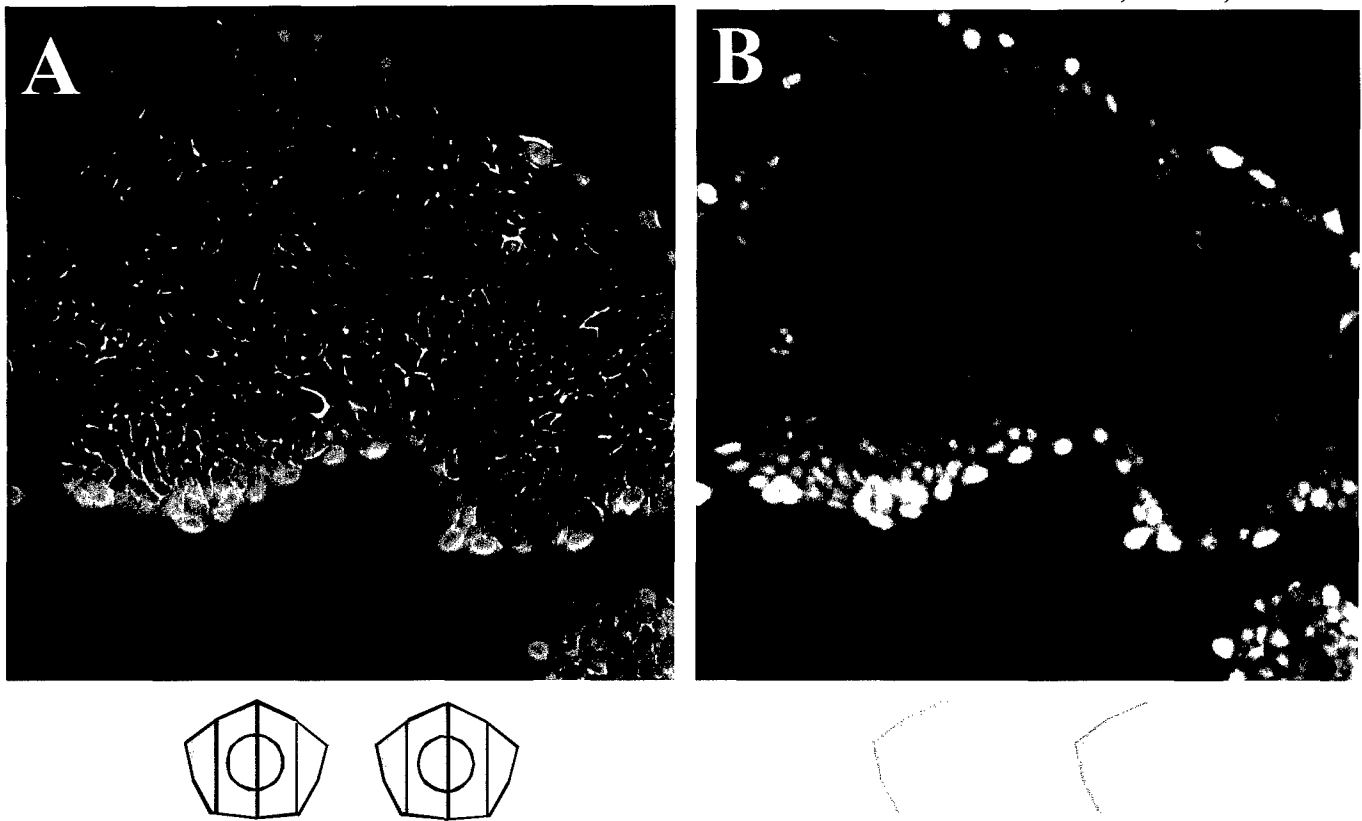
VSOM: Zeiss Inverted Fluorescence Microscope with Four Computer-Controlled Syringe Pumps leading to a temperature-controlled micro-perfusion chamber mounted on a computer-controlled xy scanning stage.

Visual Servoing Optical Microscopy (VSOM) for A New Class of Predictive In Vitro Drug Response and Chemosensitivity Assays

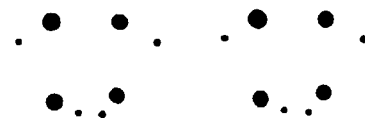
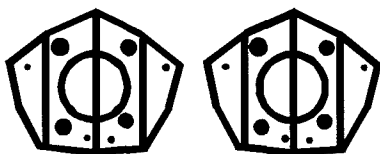
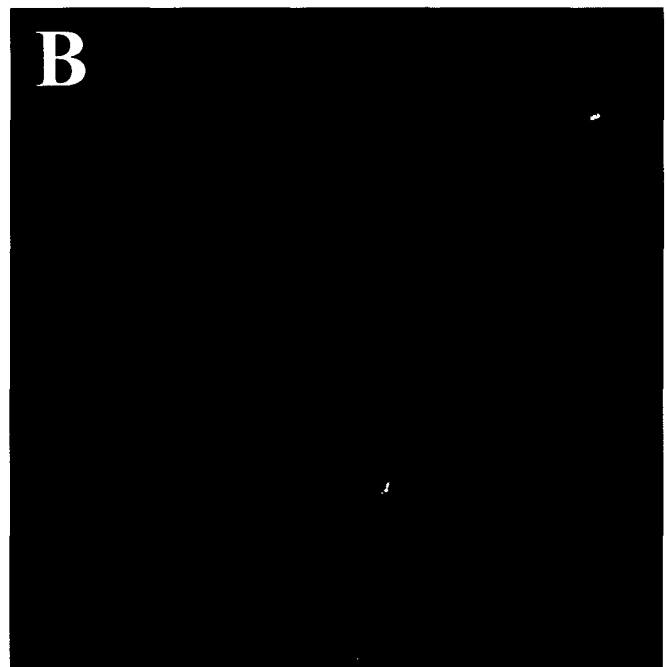
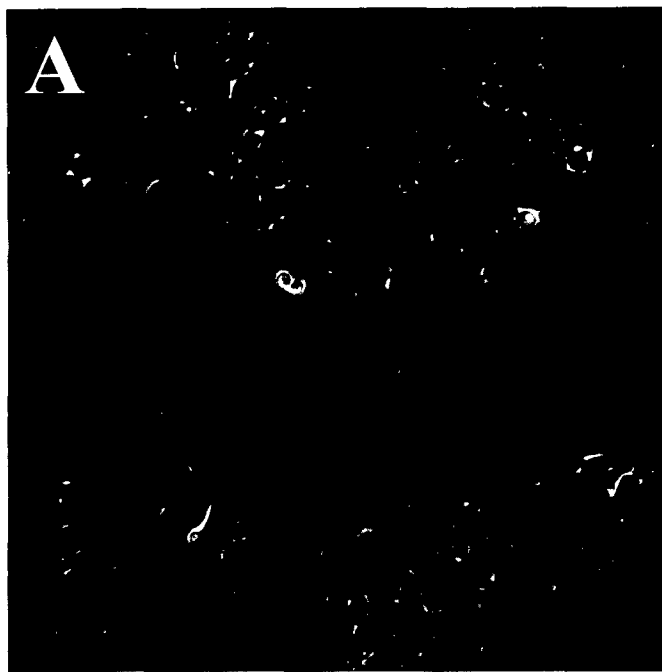
- Hundreds of individual, living cells closely monitored
- Quantification of dynamic physiological responses in multiple channels
- Real-time digital image segmentation and analysis
- Intelligent, repetitive computer-applied cell stress and cell stimulation
- Ability to return the same field of cells for long term studies



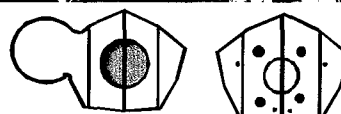
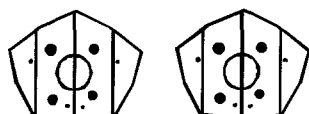
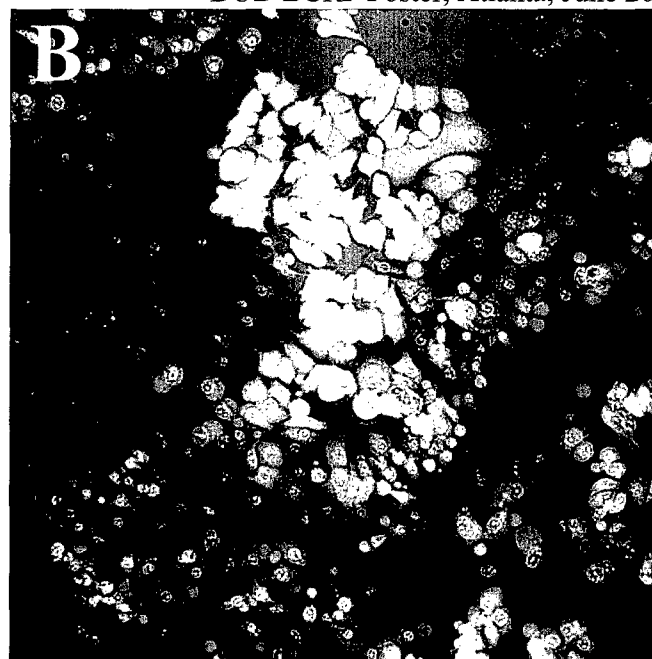
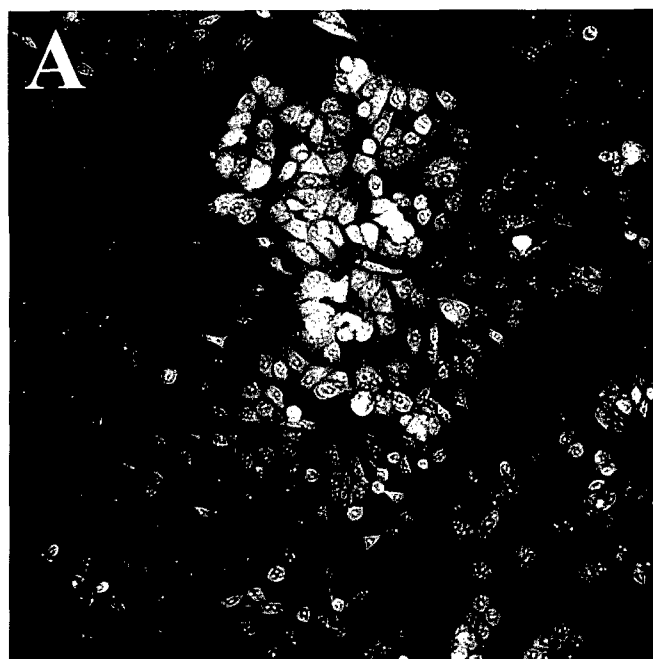
LIVING CELLS: DNA in nucleus labeled with blue fluorescent dye
(A) A two-channel digital image: (i) transmitted light + (ii) blue fluorescence
(B) One channel image: blue fluorescence only
(human mammary epithelial cells at 10X, Hoechst 33342).



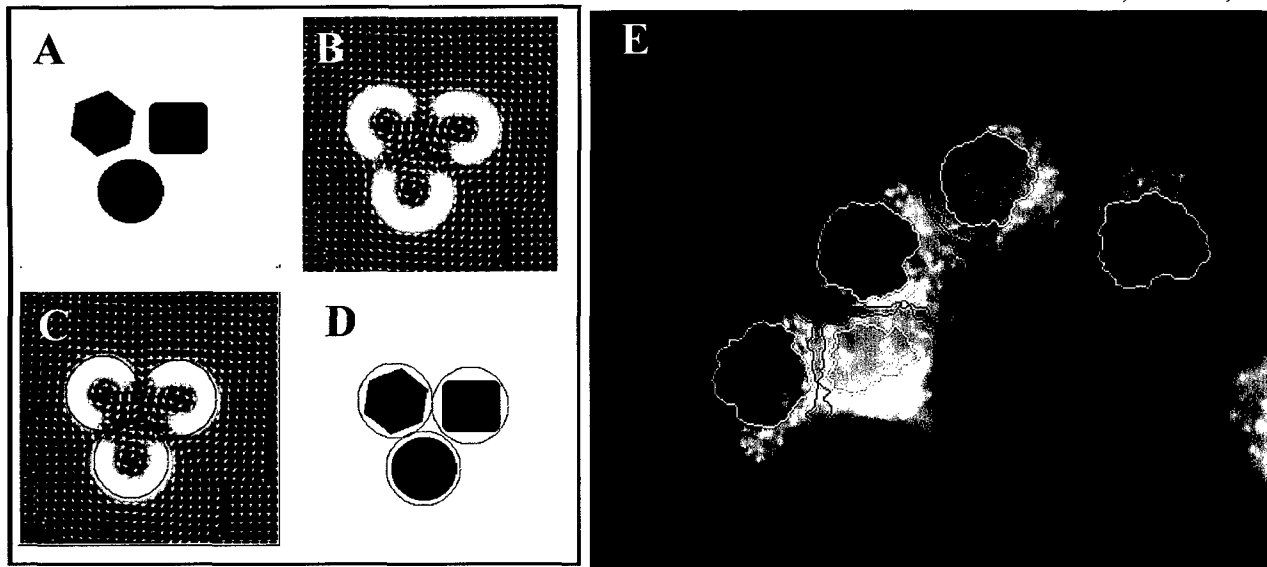
LIVING CELLS: Cytoplasm labeled with green cell viability dye.
(A) A two-channel digital image: (i) transmitted light + (ii) green fluorescence (B) One channel image: green fluorescence only (human mammary epithelial cells at 10X, Calcein-AM).



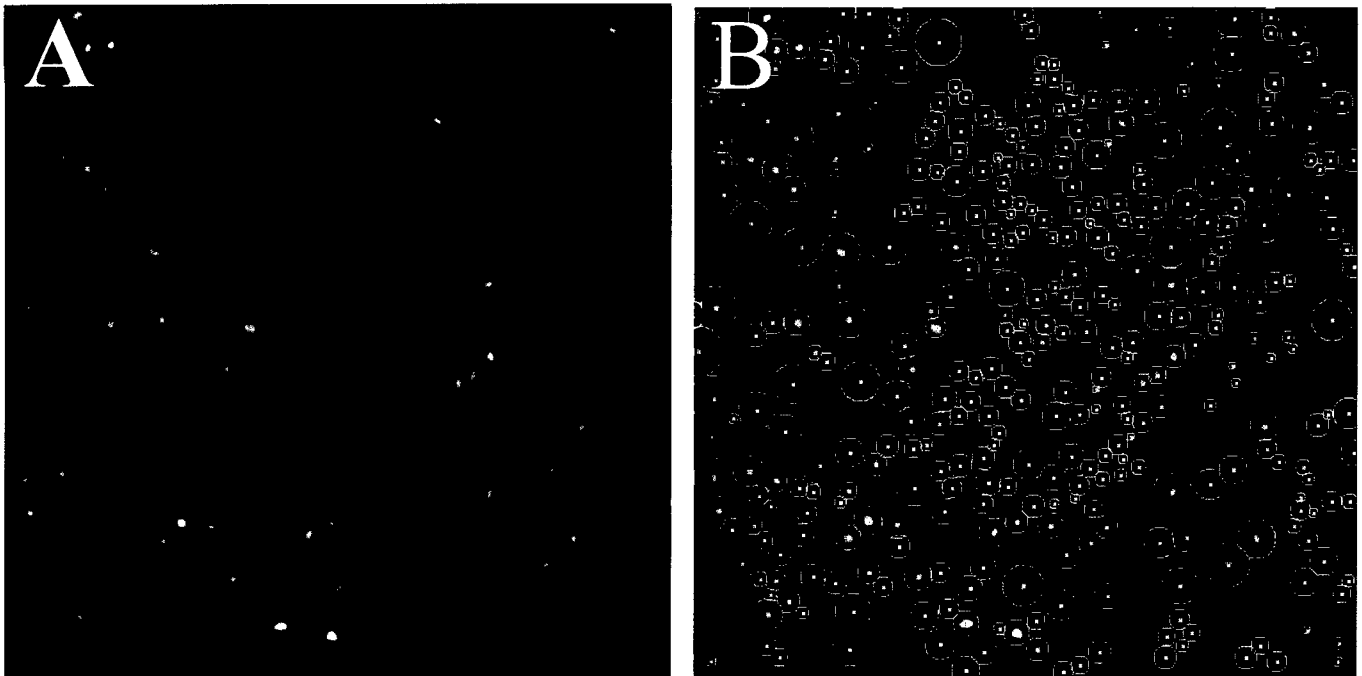
LIVING CELLS: Lysosomes labeled with acidotropic red dye.
(A) A two-channel digital image: (i) transmitted light + (ii) red fluorescence **(B) One channel image: red fluorescence only**
(human mammary epithelial cells at 10X, Lysotracker-Red).



CELL DEATH DURING UV IRRADIATION: Cytoplasm labeled with green and red cell viability dyes. Nucleus stained with blue dye. Four channel images shown (red, green, blue, and transmitted light). (A) All cells viable (B) Membrane blebbing and loss of red and green cell viability stains, nuclei still blue. Dynamic process was monitored. (human cancer cell line, MCF-7 at 10X, Hoechst 33343, LysoTracker-Red, Calcein-AM, brightfield transmitted light).

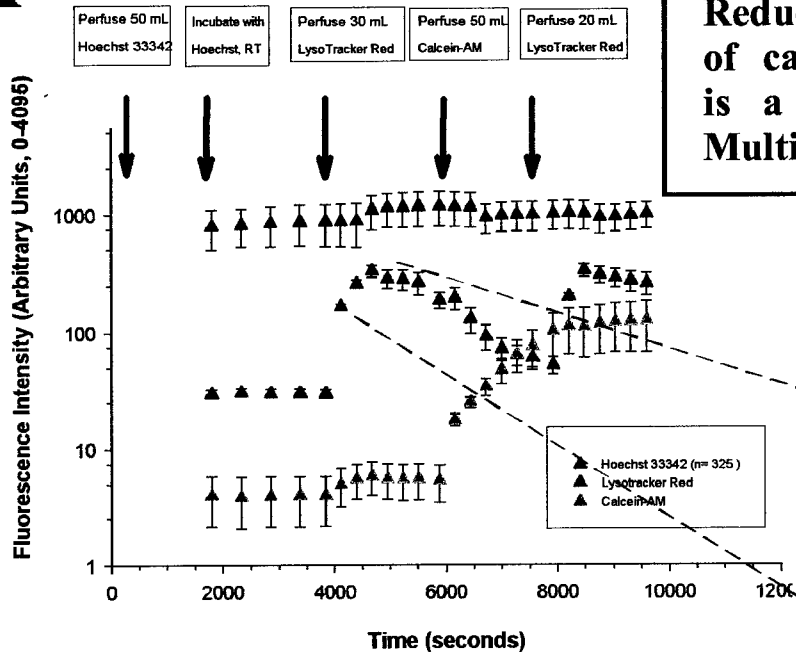


ADVANCED CELL DETECTION AND TRACKING: We continue to improve our quantitative image processing and image segmentation algorithms. (A-D) Test case for vector representation of digital images and feature extraction in vector space (vortex detection). (E) MCF-7 cells stained with TMRE, a mitochondrial and cytoplasm stain useful for monitoring the membrane potential of the mitochondrial and plasm membrane (63X, oil immersion objective). Our goal is non-invasive segmentation of each cell and its important subcompartments and organelles. This is demonstrated for the nuclear and cytoplasmic compartment in E.

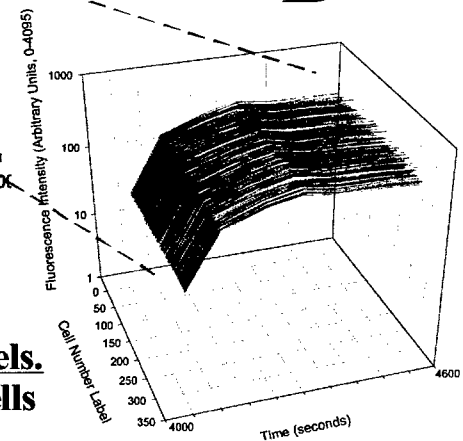


DETECTION AND QUANTITATION OF FLUORESCENCE INTENSITY IN THE NUCLEAR SUBCOMPARTMENT OF INDIVIDUAL LIVING CELLS. Rapid and accurate image segmentation is required for VSOM experiments. In order to monitor physiological responses in individual cells, we often quantify changes in the mean fluorescence intensity of individual cells or cell compartments.

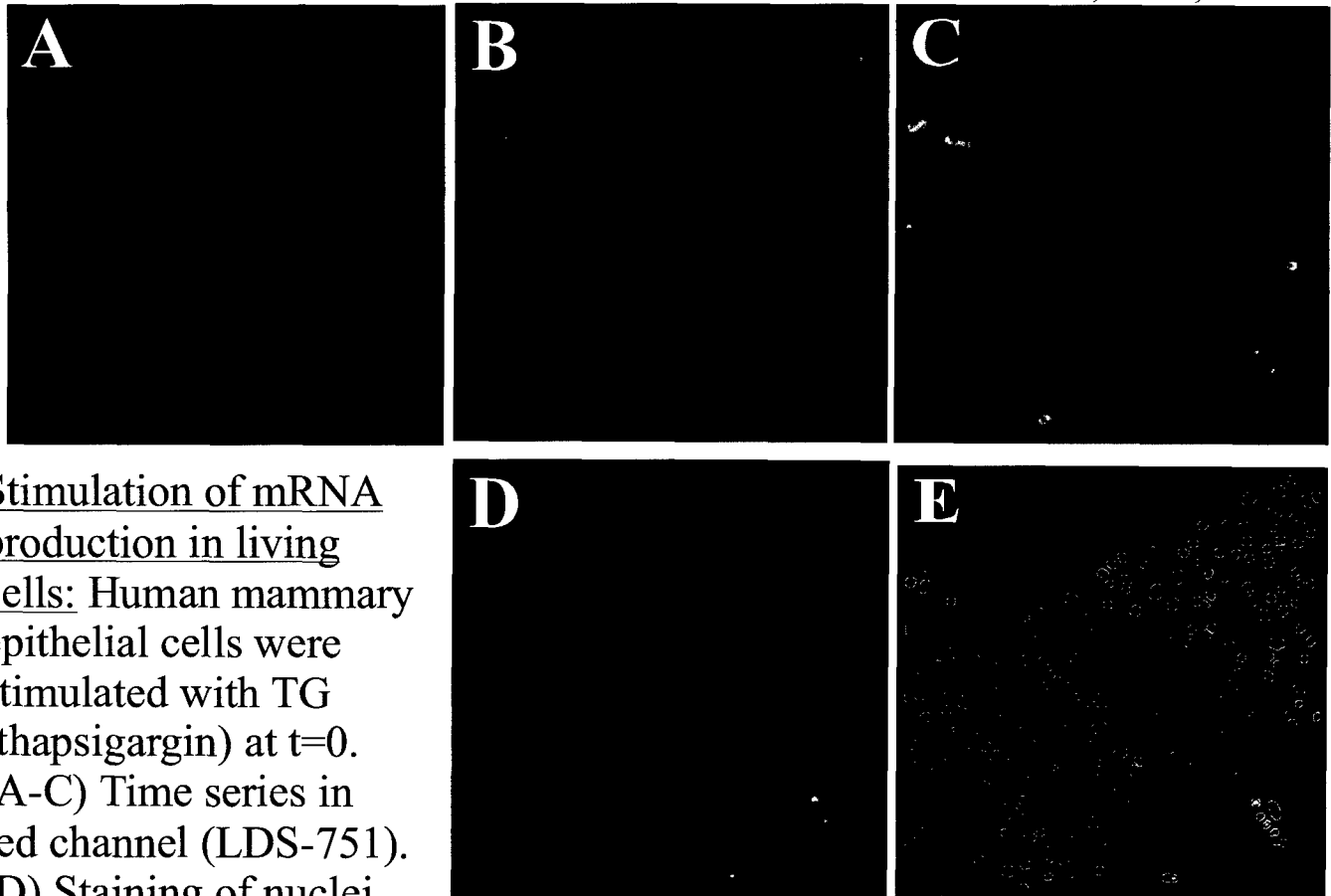
(A) This is one frame, and one channel (blue) of a time-lapse experiment. These are the nuclei of the blue channel for the MCF-7 cells shown in Figure 9B. (B) Nuclei of detected using the vortex method shown in Figure 10 A-D.

A

Reduced uptake and retention of calcein-AM (green curve) is a common indicator of Multidrug Resistance (MDR).

B

Physiological Responses of hundreds of living MCF-7 cells quantified in three separate channels.
(A) Mean fluorescence intensity of individual cells +/- standard deviation for blue, green, and red channels (B) Blow-up of one small region of the red response curve. Hundreds of individual cell responses are monitored.



Stimulation of mRNA production in living cells: Human mammary epithelial cells were stimulated with TG (thapsigargin) at $t=0$. (A-C) Time series in red channel (LDS-751).

(D) Staining of nuclei in green channel using Syto16. (E) Detection of cells using vortex method. Time elapsed between A-C is approximately 2 hrs.

Conclusions

- 1) VSOM assays are feasible as originally envisioned.
- 2) We are now ready to undertake several new steps in the continuing development of VSOM technology, assays, and optimized microenvironments.
 - a) Revisit the same field of cells after cells have been returned to a controlled environment for long-term incubation. This is necessary for verifying the predictive power of early cell responses.
 - b) Move from established cell line models to new studies on primary breast tumor cells.
 - c) Perform automated "clamping" perfusion studies for precise control of intracellular ionic environment (e.g., intracellular calcium levels).
 - d) Design microenvironments that increase proliferation rate of primary breast tumor cells in culture.
 - e) Verify VSOM results using multiwell plate systems.
 - f) Begin to populate a modern object-oriented database with single cell responses to stress and various stimuli
 - g) Perform Multi-Field (MF) VSOM in order to monitor several fields of cells at the same time.

Acknowledgements:

Research funded by the Department of Defense, Breast Cancer Research Program, under the U.S. Army Medical Research and Materiel Command, contract number DAMD17-98-1-8177.

Appendix D: Biophysical Society Abstract

Callahan, D.E., and Parvin, B. Visual Servoing for the Detection, Quantitation, and Modulation of Specific Cell Responses in Subpopulations of Multidrug Resistant (MDR) Human Breast Cancer Cells, to be presented, Biophysical Society Annual Meeting 2001, Boston, MA, February 17-21, 2001, Abstract Number: 3275.

VISUAL SERVOING FOR THE DETECTION, QUANTITATION, AND MODULATION OF SPECIFIC CELL RESPONSES IN SUBPOPULATIONS OF MULTIDRUG RESISTANT (MDR) HUMAN BREAST CANCER CELLS.

Daniel E. Callahan, Bahram Parvin: Lawrence Berkeley National Laboratory, Cell and Molecular Biology Department, 1 Cyclotron Road, Berkeley, CA 94720

MDR can be dependent on transmembrane proteins (e.g., PgP and MRP) that extrude foreign compounds. Expression of these proteins is indicated by reduced accumulation of calcein. An automated digital imaging fluorescence microscope was used to perfuse calcein-AM (CAM, 0.25 μ M) containing modulating agents MK-571 (10 μ M) or verapamil (50 μ M) into a microperfusion cell chamber. MK-571 is a specific inhibitor of MRP, while verapamil inhibits both PgP and MRP. MCF-7ADR cells labeled with Hoechst 33342 were observed at 35°C. Mean fluorescence intensity per cell (MI, calcein) was calculated in real-time and software operation of syringe pumps was based on these calculations; hence, the term *visual servoing*. The protocol found in an MDR Beta-Test Kit (Molecular Probes, Eugene, OR), was modified. Images were acquired during perfusion intervals (1) 0-2100s, CAM, (2) 8600-11000s, CAM+MK-571, and (3) 14000-16000s, CAM+verapamil. All cells responded by 3. Subpopulations expressing MRP and/or PgP can be inferred based on responses where $\Delta MI > 200$ (FIG1): (a) Responses in 1 (no PgP or MK-571) (b) None until 2 (MRP) (c) None in 1 or 2 (PgP only) *Funded by Department of Defense, DAMD17-98-1-8177 & U.S. Department of Energy DE-ACO3-76SF00098.*

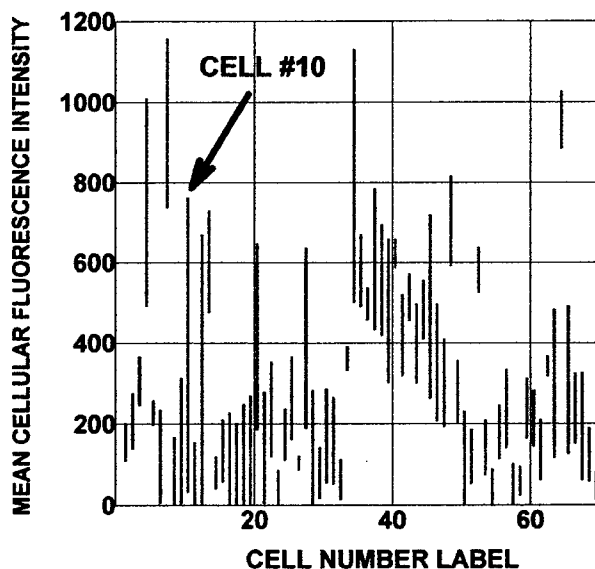


FIGURE 1: CAM+MK-571 perfusion, interval 2 (8600 - 11000s).
The 2D projection of MI versus time for 69 cells is shown. Time axis is perpendicular to the plane of the page. The increase in MI due to calcein accumulation was greater than 200 in 30 cells, due to inhibition of MRP by MK-571. Three digital images (channels) were acquired every 60s. The MI of cell #10, for example, increased from 30 to 760 (arrow) during this 2400s perfusion interval.

Appendix E: Imaging Protocol for Returning to the same set of cells Repeatedly

I. Goal of these experiments:

The goal of these experiments is to (i) make observations on one or more sets of living cells in a cell culture dish on a moveable microscope stage, (ii) remove the dish (moving the stage during the interim) and return it to the incubator, (iii) replace the dish, (iv) automatically return to the same set of cells, (v) make more observations, (vi) remove dish, and (vii) repeat this process as many times as desired. The responses of the set of cells (500-1000 cells at 10X magnification) are observed as various compounds are perfused into the dish. A stack of images (consisting of a specified number of channels) is acquired one or more times at a specified intervals for a specified length of time. An editable (text) recipe file specifies experimental parameters. For "snapshots" only one image stack is acquired. For "time-lapse" experiments, a complete stack of images is acquired at regular intervals. Several time-lapse experiments may be performed (in sequence) on the same set of cells before removing the dish (user should not move stage or dish between these sequential time-lapse experiments). The dish will be removed from the microscope stage to the incubator for hours or days. When the dish returned to the microscope stage, the cells may still be alive, or they may be dead (as in "fixed and stained"). If the cells are dead, time-lapse experiments are not performed. However, in this case, surrounding fields of cells will also be imaged (by taking "snapshot" image stacks) to verify that the single set of cells monitored repeatedly was representative of many surrounding sets of cells.

II. Definitions:

Channel: The channel specifier is designated in our filenames by: _0, _1, _2, _3, _4, _5, and _X. The numbers refer to a specific position on the optical filter wheel, and the _X refers to a transmitted light image. The identity of the optical filter at each position in the filter wheel is noted in the header of each image according to wavelength. The type of transmitted light used is not specified.

Examples:

dc122999dc2.0001.1_0.ics: This image was acquired with the filter wheel in position "0". If one looks in the image header, one will see that the filter at this position is a 360nm fluorescence excitation filter.

dc122999dc2.0001.1_X.ics: An image acquired by opening the transmitted light shutter. This image may be phase contrast, DIC, bright field, etc.

Notes:

The (maximum wavelength) identities of the optical filters at each position of the filter wheel are contained in the editable config text file (below).

Set of Cells: All the cells visible in a particular field of view in a digital image at a specific magnification. Over the course of hours and days, single living cells may enlarge and divide into two cells, cells may disintegrate, cells may die and float away, and individual living cells may also move. The initial location of a set of cells is specified as a location relative to a (0,0) point which is a "+" (crosshairs) symbol physically etched on the surface of the Petri dish.

Stack of images: a collection of all the specified channels at a single time point

Example : The 7th stack in a time-lapse series of image stacks:

dc122999dc13.0007.1_0.ics
dc122999dc13.0007.1_1.ics
dc122999dc13.0007.1_2.ics
dc122999dc13.0007.1_3.ics
dc122999dc13.0007.1_X.ics

Recipe File: a text file that specifies:

Which fluorescence channels go into a complete image stack
Exposure time for each channel
Order in which image channels are acquired
Interval between acquired image stacks in time-lapse experiments.
Number of stacks to acquire.
Identity of excitation filters at each location in the filter wheel

III. Iteration Examples

1. **First Iteration:** A dish of cells that has never been imaged.
 - a. Set (0,0) mark on the computer screen using crosshairs etched on dish
 - b. Search for a set of cells to observe (various shutters will need to be opened and closed, filter wheel needs to move to different positions, and program must keep track of where user has moved relative to the (0,0) mark).
 - c. Focus, and then execute the experiment based on information in the recipe file. This first experiment will usually be a time-lapse experiment on living cells, but it could also be a series of "snapshots" of fixed and stained cells.
 - d. Re-Edit the recipe file (DO NOT MOVE CELLS OR STAGE. REFOCUSING IS ALLOWED.) and do one or more additional time-lapse experiments.
 - e. Remove cells and return cells to incubator OR, (in the case of a "snapshot" experiment) go to other locations and take more snapshots.
2. **Second Iteration:** A set of living cells has been imaged and information about their location has been stored.
 - a. Manually mount and position the dish . Acquire an initial transmitted light image of the crosshairs mark.
 - b. Click on the (0,0) mark on the screen and tell the program which set of cells these are. The program will move to the (0,0) mark and then move to the proper field of cells.
 - c. Focus, and then execute the experiment based on information in the edited recipe file. (user will need to open shutters and move the filter wheel in order to focus).
 - d. Re-Edit the recipe file (DO NOT MOVE CELLS OR STAGE. REFOCUSING IS ALLOWED.) and do one or more additional time-lapse experiments.
 - e. Remove cells and return them to the incubator OR, (in the case of a snapshot experiment) go to other locations and take more snapshots.
3. **Nth Iteration:** A set of living cells has been repeatedly imaged and information about their location has been stored. Sequence of events is similar to second iteration.

Appendix F: VSOM Experimental Log and Bioinformatics Template

Experiment:

[illegible]

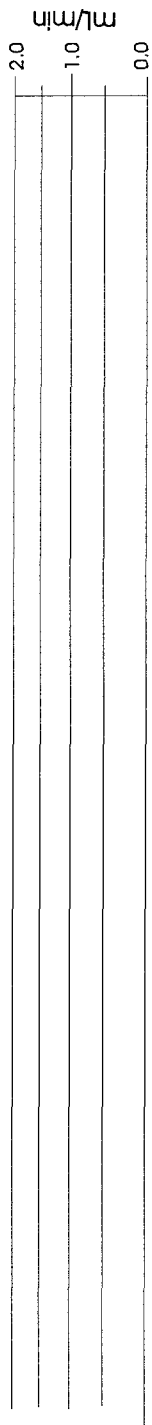
[illegible]

[REDACTED]

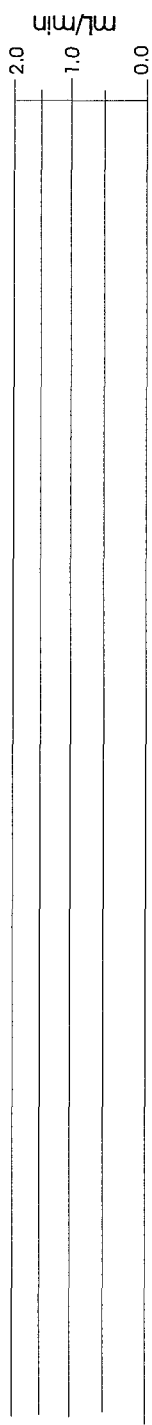
Experiment: _____

DATE: _____

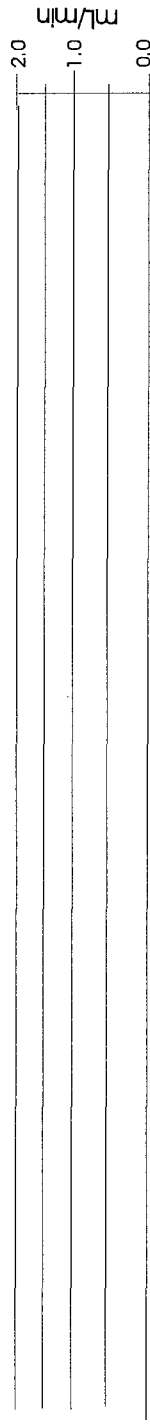
PUMP 4 ____ cc



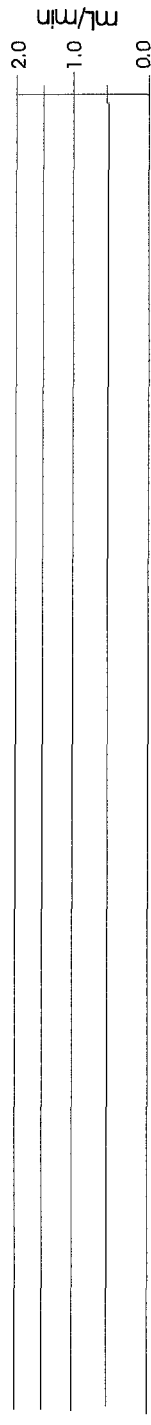
PUMP 3 ____ cc



PUMP 2 ____ cc



PUMP 1 ____ cc



PRE-TREATMENT

IMAGE ACQUISITION
INTERVALS

TIME

Appendix G: Patent Disclosure (Includes recent grant proposals)



OFFICE OF THE LABORATORY COUNSEL

Patent Department
M/S 90-1121
(510) 486-7058 phone
(510) 486-7896 fax

JUNE 20, 2000

WILLIAM DAUBENSPECK
DEPARTMENT OF ENERGY
OFFICE OF PATENT COUNSEL
MAIL STOP L-376
LIVERMORE, CA 94550

RE: IB-1559P: A Method for Knowledge-Based Discovery and Optimization of Differences Between Cell Types
Serial No.: Unassigned
File Date: 6/08/00
Inventor(s): Daniel E. Callahan
Bahram Parvin


Dear Mr. Daubenspeck:

On behalf of The Regents of The University of California, we do hereby elect to take title to the subject invention.

In addition, enclosed is a copy of a patent application in the above-identified case filed in the United States Patent and Trademark Office on 6/08/00.

Please return to us a confirmatory license to the Government for execution by the Regents.

Very truly yours,


David J. Aston
Patent Counsel

DJA/vw

Enclosure(s)

cc: Daniel C. Callahan
Bahram Parvin
Tech Transfer

DESCRIPTION:

Background of the invention Please summarize:

- 1) Technical problems overcome to make the invention,
- 2) What your invention enables people to do that couldn't be done as well before,
- 3) How people currently address the problem your invention addresses.

1. (a) Prior to this invention, it was technically difficult to digitally image large numbers of single living cells under a microscope. It was also difficult to simultaneously monitor multiple physiological responses in large numbers of single, living cells for an extended period of time, without harming the cells.

The first limitation existed because of the limited field of view at any given magnification. The field of view was further restricted by the limited size and resolution of the solid-state digital imaging device (charge coupled device) inside a given digital camera. This invention addresses these technical limitations in the following ways. (i) It rapidly, automatically, and repetitively monitors multiple fields of view (and thus larger numbers of cells) by software control of an x,y,z microscope stage (ii) It allows simultaneous remote control of multiple microscopes from a central computer.

Living cells can move or change shape. Thus, when returning to a given field of view, the software must adjust focus (z-axis control), and must make small horizontal and vertical adjustments to reacquire and reregister the field of view (x,y axis control). In addition, the original contours defining the outline of individual cells must be modified in order to track changes in cell position and shape. This is an elementary example of Visual Servoing Optical Microscopy (VSOM), where decisions regarding control of the instrument are made based on analysis of image content.

This invention allows one to define the contours of living cells using transmitted light in addition to fluorescence emission light. This allows one to track cells that do not contain a fluorescent compound. In addition, this allows one to use smaller amounts of potentially cytotoxic fluorescent labeling compounds and avoid the intense fluorescence excitation illumination required to stimulate fluorescence emission. Thus, cells can be observed for longer periods of time, and cells with specific behaviors can be retrieved individually at the end of the experiment for pooling, establishment of cell sublines, cloning, propagation towards a given differentiated state, or analysis.

In addition to monitoring a larger number of cells, this invention allows a larger number of physiological responses to be observed during a single experiment because the instrument can observe different physiological responses in different channels (almost simultaneously) by rapidly cycling the imaging from transmitted light to fluorescence emission light of different wavelengths.

2 "A Method for Knowledge-Based Discovery and Optimization of Differences Between Cell Types"

1. (b) A technical limitation of implementing knowledge-based, multi-channel, multi-field, multi-microscope Visual Servoing Optical Microscopy (VSOM) was the fact that the method is memory and CPU-intensive, and the proper computer hardware may not be located near the microscope or microscopes.

Often, the local computers (the clients) that control local microscope peripherals such as scanning stages, filter wheels, perfusion pumps, robotic arms, shutters, cameras, etc. will not have sufficient memory, software, or CPU resources to perform VSOM rapidly and efficiently. To overcome this limitation, our method allows VSOM to be performed by remote control, over the Internet, by a more powerful central computer (the server) located in a different geographical location. The server can perform (or distribute) the more CPU intensive tasks and can serve as a central location for a very large database of current and previous cellular responses.

This type of VSOM benefits greatly from network access to a powerful central server and a large central database of previously observed single cell responses (with previously observed correlations across multiple channels of information). During the course of the experiment, the system repeatedly detects cells, logs and analyzes all the observed cell responses across all channels, compares current cell responses, makes correlations across current channels of information and consults a database of previously observed cell responses and previously observed correlations across different channels of information. Then, during the course of a single experiment, the system makes a series of knowledge-based decisions on how to adjust experimental parameters in order to achieve the objective of the current experiment.

2. This invention allows multiple, complete experimental cycles during the course of a single, relatively short experiment. This greatly accelerates the process of searching for, discovering and optimizing differences between different cell types. Relatively low numbers of cells are required, and because individual cell responses are monitored, specimens submitted for analysis may contain several different types of cells.

For large numbers of individual living cells, the ability to rapidly make automated, knowledge-based decisions on how to alter experimental parameters during the course of the experiment was not available prior to our invention. The ability to perform many "test/ store/ analyze/ learn/ redesign/ retest" cycles during the course of a single experiment will allow many experiments and applications that were not previously feasible. When cells remain viable and an experiment remains in progress and on-line, correlations between past and future responses to stimuli are maintained on a cell-by-cell basis. Various and repeated computer-generated stimuli can be applied and repeated during a single experiment using a relatively small sample of cells. This is a tremendous advantage when searching for and optimizing differences between cell types.

3. How do people currently address the problem your invention addresses?

Currently, large numbers of single cell responses are obtained taking a single measurement, or "snap-shot" of cell status, response, or identity at a single instant. For microscope studies, cells are often fixed (killed and preserved) and stained. A large number of cells can then be scanned and multi-channel fluorescence and transmitted light images can be obtained and analyzed. The cells are dead and cannot be repeatedly stimulated. In microscope studies of living cells, only a limited number of cells (a single field) can be observed during stimulation. However, the images

3 "A Method for Knowledge-Based Discovery and Optimization of Differences Between Cell Types"

are usually analyzed (often days) after the experiment. Thus, it is not possible to make rapid, automated decisions on how to alter experimental parameters during the course of the experiment.

Ongoing fluorescence signals from an entire population of living cells can be detected using a multi-well fluorescence plate reader. Single cell responses cannot be observed. One potential use of VSOM is the discovery and optimization of fluorescence assays that are suitable for multi-well plate readers. Multi-channel fluorescence signals from individual living cells can be detected at a single instant using flow cytometry. The cells can be sorted according to fluorescence signal and can be recovered. However, the cells flow rapidly past a detector, and a single (perhaps multi-channel) measurement is taken. Individual cells are not tracked for any length of time, and repeated observations of the same cell, with correlations between past and present responses, is not possible. However, another potential use of VSOM is the discovery and optimization of fluorescence assays that are suitable for flow cytometry and fluorescence activated cell sorting.

List uses of the invention - research, commercial, pilot plant, etc.: Think as broadly as possible.

1) Fluorescence Assays: As discussed above, many instruments currently exist that can take advantage of new, cell-type specific fluorescence assays. These instruments and assays are currently in use in hospitals and other diagnostic laboratories. These assays are useful in human, animal, and plant cell studies. The invention described here will also benefit from any newly discovered fluorescence assays.

Examples: (a) The detection and discrimination between normal, premalignant, malignant, or multi-drug resistant cancer cells derived from a human tissue biopsy. (b) The design of protocols that selectively label rare cell types such as stem cells, or fetal cells in maternal blood. Such protocols could be modified to work with radioactive labels, also. (c) The design and application of assays that suggest a chemotherapeutic regimen, or combination of drugs, that are tailored to an individual patient or an individual tumor within a patient. (d) Assays useful for screening large numbers of potential drug, insecticide, or herbicide candidates. (e) Assays useful for screening large numbers of potential agents useful for cell proliferation, cytotoxicity, or differentiation. (f) other cell-type specific fluorescence diagnostic tests.

2) Design of in vitro tissue culture conditions that are cell-type specific

With development of suitable fluorescence assays, this invention can be used to design in vitro tissue culture conditions that lead to the proliferation of a specific cell type, either by giving a growth advantage to this cell type, or by designing environmental conditions or protocols that are cytotoxic to other cell types present in the culture. For example, it is often difficult to propagate tumor cells from patient biopsies in culture so that the characteristics of that patient's tumor cells can be studied. Normal cells often grow more easily in vitro than tumor cells. Other types of cells are difficult to grow in culture, and this invention would allow one to rapidly develop suitable environmental conditions or growth maintenance protocols for the specific cell types of interest. In addition, cell culture conditions suitable for guiding cells to a specific differentiated end-point could be designed using this invention. Thus, the conditions necessary to guide stem cells or embryonic cells to a final desired end point could be developed using this invention.

3) Design and application of other in vitro diagnostic tests

With development of suitable fluorescence assays, this invention could be used to develop and execute many types of rapid in vitro tests. For example, if several potential tissue or bone marrow donors existed for a certain patient, the various donor's cells could be mixed with the patient's immune cells and observations could be made, on the single cell level, of the immune rejection response generated by each potential donor's cells. In addition, these types of tests could be performed in the presence of drugs (or drug candidates) designed to suppress transplant rejection. Such tests could allow one to choose the proper donor for a patient, and the proper anti-rejection drug or drugs for the patient.

Identify companies that might be interested in licensing this technology.

Companies that provide scientific instruments for medical or scientific applications would be interested in this technology. Especially companies specializing in cytometry and diagnostic applications; these companies produce digital imaging microscope systems, flow cytometers, and other sophisticated medical and scientific instrumentation.

Summary of the Invention

We have developed methods, software and a process to discover, develop, and optimize fluorescence assays, protocols, and in vitro tissue culture conditions that are based on differences between cell types. This approach does not require pure populations of cells. It is well suited for relatively small samples and heterogeneous mixtures of cells. "Cell type" is a classification achieved by any observation that can separate a group of cells into multiple groups of cells, where each cell of a group has a similar property(ies) that distinguishes it from another group(s) of cells. The method requires repeated observations of relatively rapid physiological responses at the individual, single-cell level (including observations of subcellular components, changes in morphology, cell division, cell death, detachment, etc.). The term "**stimulus**" is meant to include: a single, repeated, or continuous application of a stimulus, stimuli, or combinations of stimuli. Stimuli that generate physiological responses can be mechanical, physical, chemical, or biological in nature. One distinguishing features of this method is rapid, on-line analysis of large numbers of living cells and large numbers of correlated physiological responses (including references to a database of responses, and correlation across multiple channels of image information representing different imaging modalities such as transmitted light and fluorescence emissions at a variety of excitation/emission wavelengths). Another distinguishing feature of this method is computer automation of the following: (1) repeated or continuous application of the stimulus to living cells (2) repeated or continuous detection and monitoring of one or more cellular or subcellular physiological responses to the stimulus at the single cell level using a microscope and digital imaging, (3) rapid observation of a sufficient number of individual cell responses to establish criteria suitable for (i) reliable identification of cell type(s), and/or (ii) modification of the stimulus for purposes of optimizing differences between cell types (4) rapid analysis of current and previously stored (as in a database) cell responses so that knowledge-based stimulus control decisions can be made while current cells are still available for observation and/or stimulation. Correlation of time-dependent events across multiple channels are also monitored.

We refer to the process described above as **Visual Servoing Optical Microscopy (VSOM)**. In its simplest form, VSOM uses computer vision to analyze a single field of view under a microscope

5 "A Method for Knowledge-Based Discovery and Optimization of Differences Between Cell Types"

and alter microscope peripherals until a desired goal is achieved. A trivial example is that of autofocusing. The computer moves a microscope objective up or down until a specified degree of sharpness is achieved in a digital image.

Biological systems are extremely complex and often heterogeneous in nature. Cells are continuously processing and responding to a multitude of intracellular and extracellular signals. Cells rapidly initiate responses to subtle changes in their environment; thus, a large number of experimental variables must be accounted for. In addition, individual cells of the same cell type exhibit a range of responses to the same stimulus. Thus, a large number of individual cells must be observed in order to define the distribution of responses that are possible. Current biological instrumentation (e.g. flow cytometry) makes a single (possibly multichannel) measurement on large numbers of cells as they flow past a detector. However, repeated measurements on the same cell are not possible, and an image of each cell is not obtained.

Our process relies on computer software and commercially available instrumentation to achieve the following:

(i) Detection and tracking of one or more (usually large numbers) individual (usually living) cells in one or more fields of view. This detection and tracking occurs by repeatedly obtaining one or more channels of digital image information simultaneously (or in rapid succession). Digital image information in these channels can consist of various combinations of information derived from any microscope imaging modality (e.g. transmitted light techniques such as phase contrast or differential interference contrast, fluorescence excitation/emission techniques, three-dimensional imaging, etc.)

(ii) Identification of different cell types or subpopulations of cell types.

(iii) Discovery and/or optimization of cell-type-specific physiological responses.

(iv) Knowledge-based control of the microscope and microscope peripherals to modify stimuli and selectively optimize the unique physiological response(s) of specific cell types.

(v) Allow retrieval of specific individual cells at the end of the experiment.

Publications (including LBL reports, meeting abstracts, or prior patents or patent applications) that ACTUALLY DESCRIBE or RELATE to the invention:

NOTE: No publications actually describe this invention.

These publications relate to invention:

To be presented:

Parvin, B., Taylor, J.R., Cong, G., O'Keefe, M., Barcellos-Hoff "Deep View: A Channel for Distributed Microscopy and Informatics" IEEE Conference on High Performance Computing and Networking" November 1999, Portland, OR.

6 "A Method for Knowledge-Based Discovery and Optimization of Differences Between Cell Types"

Parvin, B., Taylor, J.R., Cong, G. "Deep View: A Channel for Distributed Microscopy" International Conference on Distributed Objects, Scotland, UK, Early September, 1999.

Already Presented or Published:

Parvin, B., Taylor, J.R., Cong, G. "A Collaborative Framework for Distributed Microscopy" IEEE Conference on High Performance Computing and Networking" November 1998.

Parvin, B., Taylor, J.R., Callahan, D.E., Johnston, W.E., Dahmen, U. "Visual Servoing for Online Facilities" (1997) *IEEE Computer* 30 , 56-62.

Parvin, B., Callahan, D., Johnston, W., Maestre, M. "Visual Servoing for Micro-Manipulation", 13th Int. Conf. on Pattern Recognition, Aug 25-30, 1996, Vienna, Austria.

Parvin, B., Callahan, D., Johnston, W., Maestre, M. "Microdissection of Single DNA Molecules" Fifth DOE Human Genome Program Contractor-Grantee Workshop, Santa Fe, NM, Jan28-Feb 1. (1996)

Parvin, B., Maestre, M.F., Fish, R.H., Johnston, W. "A Method and Apparatus for Manipulation of an Object on a Microscope Stage" US Patent Application Filed April, 1995. IB-1025 and IB-1052.

Parvin, B., Taylor, B., Crowley, B., Wu, L., Johnston, W., Owen, D., O'Keefe, M.A., Dahmen, U. "Telepresence for In-Situ Microscopy" IEEE Conference on Multimedia Systems and Computers, June 1996.

Other early documentation that relates to the invention:

Callahan, D.E. and Parvin, B. (Principal Investigators), "Visual Servoing for Optimization of AntiCancer Drug Uptake in Human Breast Cancer Cells" LBNL proposal submitted to DOD/US Army Breast Cancer Research Program, Second submission, **July 1997 (funded)**.

Callahan, D.E. (Principal Investigator), "Visual Servoing for Optimization of AntiCancer Drug Uptake in Human Breast Cancer Cells" LBNL proposal submitted to DOD/US Army Breast Cancer Research Program, First submission, **July 1996 (not funded)**.

Callahan, D.E. (Principal Investigator) "Calcium Homeostasis in Normal and Transformed Mammary Cells" LBNL proposal submitted to California Breast Cancer Research Program, **January 1996 (not funded)**.

Parvin, B., (Principal Investigator) "Ordered Micro Dissection and Retrieval of DNA Molecules" NIH R01 (1R01HG01443-01) LBNL proposal submitted, **May 1995 (not funded)**

Parvin, B., Johnston, W., Dahmen, U., Callahan, D., Maestre, M., Liburdy, R. "Visual Servoing for Scientific Applications" LBNL LDRD #2 (Laboratory Directed Research and Development) proposal submitted **April 30, 1994 (funded)**

Callahan, D.E., Liburdy, R.P., Maestre, M.F., Johnston, W.E., Parvin, B., Elaydi, T.S. "Calcium Oscillations in Jurkot Cells" Internal LBNL Video V-943-13, **April 1994**.

7 "A Method for Knowledge-Based Discovery and Optimization of Differences Between Cell Types"

Johnston, W., Parvin, B., Maestre, M., Callahan, D. Liburdy, R., Dahmen, U. "Visual Servoing in a High Speed Network Environment", LBNL LDRD #1, proposal submitted **April 30, 1993 (funded)**.

Technical Abstract: *Rapid Discovery of Physiological Characteristics Which Distinguish Malignant and Nonmalignant Human Breast Epithelial Cells*, Callahan, D.E., Parvin, B., and Dairkee, S.H.

Background: Three prospective clinical trials have attempted to use in vitro chemosensitivity testing to improve patient chemotherapy response and cancer survival. The trials failed to demonstrate increased survival for patients who were administered chemotherapy based on results of in vitro chemosensitivity tests. Two in vitro chemosensitivity assays were used, the HTCA (human tumor cloning assay) and the DiSC (differential staining cytotoxicity) assay. In these two assays, the in vitro cell culture and propagation techniques used and the biological endpoints measured differ significantly. A common set of problems were noted in the data emanating from these trials. Both assays (1) are manual and labor intensive in nature, (2) are dependent on human judgment for quantitation, (3) often fail to produce any results, because tumor cells from some patients do not grow well in these in vitro systems. For reasons such as these, clinician perception and acceptance of these assays is poor; thus, patient and specimen accrual has been difficult. Our group has the expertise to address these problems using advanced cell culture techniques and innovative technology derived from the fields of robotic vision and digital imaging fluorescence microscopy. With the successful completion of our proposed studies, we expect to demonstrate that in vitro chemosensitivity tests based on a single protocol or assay will rarely be successful. We will use the clinical observations and findings that have emanated from three prospective clinical trials, and we will demonstrate a new paradigm for the scientific design of chemotherapeutic regimens tailored to the individual breast cancer patient.

Hypothesis: Our hypothesis is that previous clinical studies that sought to administer anticancer drugs based on in vitro chemosensitivity tests failed to see dramatic increases in patient response or survival for several specific reasons: (i) the microenvironment favored by tumor cells was not properly simulated in vitro (ii) the physiological responses of individual cells were not monitored closely throughout the assay, and (iii) the drug concentrations, combinations, and exposure times examined were limited, and not scientifically optimized. We further hypothesize that Visual Servoing Optical Microscopy (VSOM) can rapidly discover and exploit key physiological characteristics which distinguish malignant and nonmalignant human breast epithelial cells (BECs). In this way, VSOM will help to solve problems (i-ii), listed above.

Objective: Demonstrate and verify that VSOM can rapidly discover and optimize, on a tumor-by-tumor basis, microenvironmental conditions suitable for the successful in vitro propagation and chemosensitivity testing of primary human breast tumor cells. Our specific aims are to (a) rapidly and automatically develop in vitro microenvironments that favor the propagation of primary breast tumor cells, (b) rapidly develop new in vitro fluorescence assays that predict cell behavior on the basis of early physiological responses to applied stress (c) improve VSOM technology in order to achieve our objectives and specific aims.

Study Design: We will study a well characterized set of human malignant and nonmalignant BECs. Using our demonstrated expertise in this field, we will propagate tumor cells as monolayers, and this will allow us to perform a wide range of multicolor, multichannel VSOM fluorescence assays in a temperature-controlled microperfusion chamber. The intracellular calcium levels, levels of mRNA, and intracellular pH of individual cells will be monitored and manipulated during VSOM experiments. Early physiological responses to perturbations of the microenvironment (pH, pO₂, [Ca⁺²]_{ex}, anticancer drugs) will be stored in our bioinformatics database. The ultimate effect of these perturbations will be assessed by using VSOM to return to the same field of cells after longer-term incubations. In addition, responses that appear to predict an increase in proliferation or apoptosis will be verified in multiwell plate fluorescence assays during longer-term incubations. Proliferation, cell viability, and apoptosis will be monitored using VSOM and multiwell plate fluorescence assays.

Relevance: Factors responsible for the previously unsuccessful application of in vitro chemosensitivity testing in the clinic should become apparent during our proposed VSOM experiments. We believe VSOM technology will demonstrate a practical solution to these problems and this will necessitate new clinical trials at the end of three years. We believe clinician participation and patient accrual will improve if we can demonstrate the advantages of this improved, sophisticated approach to in vitro chemosensitivity testing.

Public Abstract: *Rapid Discovery of Physiological Characteristics Which Distinguish Malignant and Nonmalignant Human Breast Epithelial Cells*, Callahan, D.E., Parvin, B., and Dairkee, S.H.

In three clinical trials researchers have attempted to find an improved method for selecting the best chemotherapy drug or combination of drugs for their patients. Scientists and physicians know that every patient is slightly different; for example, one patient may have an adverse reaction to a drug, while another patient experiences no side effects. Doctors often deal with this problem, and they deal with it using their training, experience, and a trial-and-error method where another drug is substituted for the one that causes side effects. In the case of breast cancer, doctors must choose several drugs from a wide range of possibilities and find the combination that (1) is most effective against that patient's tumor, and (2) produces the fewest side effects in the patient. Breast tumor cells from different patients can be very different and respond differently to the same drug. Thus, for over 40 years, attempts have been made to remove tumor cells from the patient's body and test them "in vitro", which means outside the living body, in an artificial environment. This same concept is often applied to the living breast cancer patient. For example, the physician may prescribe a chemotherapy drug and find that a patient's tumor does not respond, or shrink. The physician then tries another drug for this patient, and then perhaps another. These are "in vivo" drug response tests, meaning they are performed in a living body. Unfortunately, this can be very debilitating to the patient, and there are just too many drugs and too many possible combinations to make this approach work. The potential advantage of testing the drug response of cells outside the patient's body is that a wider range of drugs can be tested, and the patient is spared a series of debilitating trial-and-error attempts. However, due to the reported shortcomings of the "first generation" of in vitro drug response tests, the entire idea of in vitro drug response testing has fallen out of favor with practicing clinicians. This has occurred to such an extent that researchers have trouble convincing clinicians to refer patients to clinical trials where "second generation" in vitro drug tests are being performed. Due to lack of support and lack of funding, many leaders in the field have left academia to continue their research at private companies, many located in Southern California (<http://www.oncodocs.com/laboratories/laboratories.html>; See also, "Pretesting Tumors", *Scientific American*, February, 1999, pp. 19-22.). Other pioneers in this field of research, who remain in academia, such as Dr. D.D. Von Hoff, currently the President of the AACR (American Association for Cancer Research), have commented that, "It is indeed a puzzle as to why in vitro predictive assays have not been integrated at least into some aspect of the care of patients with cancer." (Commentary, *Journal of the National Cancer Institute*, 82, 1990, pp. 96-101). This puzzle exists because the second generation tests have proven to be excellent at discovering which drugs have no effect on a patient's tumor cells. Thus, doctors do not have to consider these drugs when performing in vivo drug response tests on patients. This is indeed a great accomplishment considering the fact that the technology used in these second generation tests is no more advanced than what was available in the 1950s. These tests are performed manually, with a technician counting cells or colonies under a microscope. Thus, the tests are slow, labor intensive and subject to human error. In our proposed research we describe how we will apply 21st century technology to this important problem, thus creating a "third generation" of in vitro drug response tests. Previous clinical trials have provided us with a great deal of data that we will use as we improve these in vitro tests. We believe our new automated instrument, a Visual Servoing Optical Microscopy (VSOM) will be able to overcome the problems reported in the first set of clinical trials. These problems include (1) the difficulty in getting tumor cells to grow in vitro at all (2) the limited ability to observe cells at intervals during the course of the assay (3) the limited number of biological endpoints that could be observed per assay (4) the lack of automation. Our studies will demonstrate and verify that VSOM can rapidly discover and optimize, on a tumor-by-tumor basis, microenvironmental conditions suitable for the successful in vitro propagation and chemosensitivity testing of primary human breast tumor cells. Our specific aims are to (a) rapidly and automatically develop in vitro microenvironments that favor the propagation of primary breast tumor cells, (b) rapidly develop new in vitro fluorescence assays that predict cell behavior on the basis of early physiological responses to applied stress (c) improve VSOM technology in order to achieve our objectives and specific aims. We believe that successful completion of these goals will lead to new clinical trials that will demonstrate the ability of VSOM to predict patient-specific responses and establish a scientific basis for chemotherapy treatment planning.

Relevance and Impact Statement

For some types of cancer such as certain leukemias and testicular cancer, chemotherapy can cure a majority of patients. This demonstrates the potential of chemotherapy to effect a cure in some instances of cancer. However, in solid tumors such as breast, little progress has been made in improving therapy. Multidrug resistance (MDR), inherent or acquired, in solid tumors such as breast has been cited as one important obstacle preventing cures via chemotherapy. In vitro chemosensitivity assays to assess drug response and predict patient response have been in development for over forty years but a truly successful in vitro chemosensitivity test has not been developed. Our approach to in vitro drug response and chemosensitivity testing represents a radically different approach and a new paradigm. We believe our improvements in in vitro drug response and chemosensitivity assays will allow patient-directed therapies that improve clinical outcomes for breast cancer patients. Digital imaging fluorescence microscopy, real-time analysis of digital images, and bioinformatics databases have evolved to the point where a new class of experiments is possible. Visual servoing (VS), a robotic vision technique, refers to the dynamic manipulation of experimental parameters based on analysis of digital image content. In addition, a visual servoing optical microscope (VSOM) has the ability to scan back and forth across multiple fields of view and in this way monitor very large numbers or different populations of living cells. In addition, VSOM can also return repeatedly to the same field of cells to monitor changes on a cell by cell basis. This capability will help us achieve our objective of making correlations between the early physiological responses observed in cells and the future biological state or ultimate biological fate of the cells, whether this be proliferation, apoptosis, or arrest in some stage of the cell cycle. In our opinion, the most desirable predictive assays are dynamic and adaptive VSOM fluorescence assays involving the observation of a series early physiological response to intelligently chosen, computer-controlled stimuli. This approach becomes more powerful when such stimuli and perturbations are reversible and do not permanently commit the cell to a given biological path. The ability to repeatedly apply relatively innocuous stimuli and perturbations to living cells will allow us to repeatedly probe the cell for physiological characteristics that can be exploited by anticancer drugs or combinations of anticancer drugs. Our creation of a modern object-oriented database containing records of previously observed physiological cell responses will become very valuable in the future when we implement knowledge-based control of VSOM assays. The ability to access such a central database remotely from any VS-enabled microscope will make these instruments controllable over the Internet and will greatly increase their functionality while greatly decreasing the expense of these instruments and the computer power required to operate them. This will be an advantage for VSOMs located in clinics lacking the resources to build and maintain such a database. Currently, we believe that individualized patient treatment and patient-specific analysis of tumor cells begins with characterizing and then recreating the specific microenvironmental conditions necessary to propagate and amplify the cells for in vitro testing. Once this is achieved, a variety of anticancer drugs, and drug combinations can be tested using standard multiwell plates and fluorescence assays. Thus, these are the initial VSOM experiments we will perform. We believe this proposal meets the stated intent of the Bridge Award mechanism. It is likely that the successful demonstration of our technology will result in new, more successful clinical trials. Thus, the proposed research can be considered proximal to clinical trials. In addition, it may be considered a Post-Clinical Trial Follow-Up Study in the sense that it that uses the clinical observations and findings that emanated directly from three previous prospective clinical trials. While we will not use the exact tumor specimens used in the previous studies, we will use a well characterized set of malignant breast epithelial cells (BECs) derived from a range of human breast cancer patients. Nonmalignant BECs will also be studied. We will be able to determine whether the stated microenvironmental conditions employed in previous clinical trials (composition of the media, pH, pO₂, etc.) need to be altered for successful propagation and testing of primary tumor cells in culture, and we will determine the range of conditions favored by breast tumor cells from multiple individuals. In addition, we will determine whether other factors such as the drug concentrations and exposure times used in previous studies were optimal, and we will determine if any or all of such factors contributed to fact that previously clinical trials have reported little or no improvement in patient survival when chemotherapy was selected on the basis of in vitro drug-sensitivity tests.

Statement of Work

Specific Aim 1: **Rapidly and automatically develop in vitro microenvironments that favor the propagation of primary breast tumor cells**

Task 1 (months 1-12): Begin VSOM experiments using very small samples of malignant BECs derived from human patients. Initial experiments will examine the tumor cells of 10 individuals. Deposit small numbers of these cells (2000-3000 cells) onto well defined circular regions of cell culture dishes using cell sedimentation chambers. Monitor intracellular calcium levels, intracellular pH, mitochondrial membrane potential, mRNA levels, and BrdU incorporation in individual living cells as various growth stimuli and environmental stresses are applied. Observe early (8-12h) cell responses, then return cells to a controlled environment for longer experiments. Return to the same cells later (24-96h) and make correlations between initial observed responses and important biological endpoints. Do this on a cell-by-cell basis. Find conditions that result in proliferation and then amplify cells.

Task 2 (months 13-30): Using the amplified cells from Task 1, perform long-term incubation, multiwell plate surveys of nonmalignant and malignant BECs in order to verify the microenvironmental results obtained during VSOM experiments. If necessary, place special sealed gas chambers inside incubators, and perfuse the chamber with gas mixtures of known composition. The pO_2 and pCO_2 will be held constant in each gas chamber in order to generate a given pO_2 or pH in all the wells of all the plates contained in a chamber. Other experimental parameters will be varied across the wells of the plates such as $[Ca^{+2}]_{ex}$, glucose, anticancer drug concentration, and concentration of important growth stimulants such as thapsigargin. In addition to variations in the concentrations of these agents, the duration of exposure will also be varied. Plates will be removed at specified intervals and read on a fluorescence plate reader. Fluorescence assays for cell number, live/dead ratio, apoptosis, and proliferation index will be performed. Data resulting from this wider sampling of combinations of environmental stresses will also be integrated into our bioinformatics database.

Task 3 (months 31-36): Using conditions selected from Task 2, perform a limited number of clonogenic assays in soft agar and determine whether it is important to conduct in vitro drug response assays under carefully controlled microenvironmental conditions that closely reflect the in vivo tumor cell microenvironment.

Specific Aim 2: **Rapidly develop new in vitro fluorescence assays that predict cell behavior on the basis of early physiological responses to applied stress**

Task 4 (months 12-24): Perform dynamic VSOM experiments where controlled modulation of intracellular calcium, intracellular pH, and mitochondrial membrane potential is performed after exposure of cells to specific pharmacological agents. This is achieved by using computer-controlled perfusion pumps to perform buffer exchanges at specified intervals after exposure of the cells to specific pharmacological agents. These are commonly referred to as "clamping" experiments. In this way, the intracellular concentrations of specific ions can be clamped, or coupled to the extracellular concentration of ions, an experimental

parameter that is under direct computer control. Use this ability to search for cell-specific differences that can be exploited for identification purposes, or as a means to selectively perturb a specific subpopulation of cells. In addition, use this ability to more precisely relate intracellular conditions to eventual biological endpoints such as proliferation and apoptosis.

Task 5 (months 25-36): Use MF-VSOM to compare and contrast physically separated patches of cells in co-culture. One patch of cells will contain relatively pure tumor-derived BEC and the second patch of cells will be derived from matched nonmalignant peripheral tissue. By moving back and forth between the two groups of cells, MF-VSOM will automatically search for very subtle differential responses to physiological stresses that it applies automatically. Knowledge for this system control will be partially derived from the bioinformatics database. Using this technique, develop improved VSOM fluorescence assays so that it is possible to correctly identify and monitor specific subpopulations of cells within complicated mixtures of cells. An initial matched set of cells representing 10 individuals will be used.

Specific Aim 3: **Improve VSOM technology in order to achieve our objectives and specific aims.**

Task 6 (months 1-12): Perfect the VSOM ability to return to the same field of cells using a variety of vessels, such as dishes, flasks, and multiwell plates. Allow VSOM to automatically apply and detect responses to alterations in the biochemical milieu of cells during on-line VSOM experiments. Populate the bioinformatics database with single cell responses and search for correlations between observed responses and biological endpoints. Perform this off-line data mining in order to discover and optimize early physiological responses (and the relevant fluorescence assays) that have a high predictive value for specific biological endpoints.

Task 7 (months 13-24): Develop and perfect multi-field (MF) VSOM.

Task 8 (months 25-36): Develop knowledge-based algorithms for VSOM system control that take advantage of previously observed cell responses stored in our bioinformatics database.

BACKGROUND

Introduction: Recent advances in the in vitro propagation of primary breast tumor cells allow relatively small numbers of tumor cells harvested from fine-needle aspirates (FNAs) to be passaged and expanded in culture (Li et al., 1998). Moreover, the resultant cells in culture (up to 10^7 cells) closely resemble the original tumor and display one or more tumor phenotypes, including growth in soft agar. We believe the culture of primary breast tumor specimens can be further improved through the use of our new technology which is derived from the fields of robotic vision, fluorescence microscopy, biophysics, and bioinformatics. Visual servoing (VS) is a term from the field of robotic vision. In the proposed studies, VS refers to the dynamic manipulation of microenvironmental parameters based on analysis of digital image content. Our goal in the proposed research is to use visual servoing optical microscopy (VSOM) to rapidly characterize large populations of living cells that have been freshly derived from human breast cancer tissue biopsies or fine needle aspirates (FNAs). We believe VSOM chemosensitivity assays will allow critical information for individualized cancer chemotherapy to be obtained in a rapid, automated fashion. It is important to note that in vitro chemosensitivity testing originated in the 1950s, and a majority of the previous work on the development of in vitro chemosensitivity assays occurred in the late 1970s and early 1980s. This was prior to the revolution in computing power, digital imaging fluorescence microscopy, and robotic vision. The advances in these fields over the past twenty years have been impressive, and allow for the development and application of a new paradigm in the field of in vitro chemosensitivity testing. This new paradigm is based on visual servoing and adaptive, computer-controlled testing of individual, living cancer cells derived from the individual breast cancer patient.

We believe this proposal meets the stated intent of the Bridge Award mechanism. It is very likely that the successful demonstration of our technology and our new paradigm will make it imperative that new clinical trials be conducted in order to reevaluate the efficacy of in vitro chemosensitivity testing and other predictive assays for the individual breast cancer patient. Thus, the proposed research can be considered proximal to clinical trials. In addition, it may be considered a Post-Clinical Trial Follow-Up Study in the sense that it that uses the clinical observations and findings that emanated directly from three previous prospective clinical trials (Gazdar et al., 1990; Von Hoff et al., 1990; Wilbur et al., 1992). We are proposing novel technology and protocols that will improve and expand upon assays that have previously been in clinical trials (Weisenthal and Lippman, 1985). Many clinical observations and findings have emanated from these and other clinical trials, and our investigations will lead do a new understanding of these clinical data and to the development of new clinical hypotheses. In addition, our technology has high translational potential. For example, we have recently filed a provisional patent application entitled, "A Method for Knowledge-Based Discovery and Optimization of Differences Between Cell Types" (LBNL Patent Docket #S-94,163). It should be noted that several companies, located in Southern California, have recently formed for the purpose of conducting such in vitro chemosensitivity testing, also referred to as predictive testing (Strauss, 1999 February).

While we will not use the exact tumor specimens used in the previous clinical studies, we will use a set of well characterized malignant breast epithelial cells (BECs) derived from a range of human breast cancer patients. Nonmalignant BCEs will also be studied. We will be able to compare our results with data and results generated by the previous trials. For example, we will be able to determine whether the stated or implied microenvironmental conditions employed in previous clinical trials (composition of the media, pH, pO_2 , etc.) need to be altered for successful propagation and testing of primary tumor cells in culture, and we will determine the range of microenvironments favored by breast tumor cells from multiple (10-60) individuals. In addition, we will determine whether the drug concentrations and exposure times used in previous studies were optimal, and we will determine if any or all of such factors could have contributed to fact that previously clinical trials have reported little or no improvement in patient survival when chemotherapy was selected on the basis of in vitro drug-sensitivity tests.

Primary Culture of Human Breast Tumor Cells: A great deal of progress has been made in primary culture of malignant human breast epithelial cells (BECs) (Band et al., 1990; Ethier et al., 1993; Dairkee et al., 1995; Dairkee et al., 1997; Li et al., 1998). Currently, there is great interest in the unique physiology of solid tumors, and it is likely that a suboptimal, nutritionally depleted environment exists in breast tumors (Dairkee et al., 1995; Tomida and Tsuruo, 1999; Brown and Giaccia, 1998). This environment is believed to consist of regions of low oxygen (hypoxia), low pH, low levels of glucose, and high levels of metabolic waste. It has been demonstrated that when such conditions are simulated in culture, it is possible to isolate relatively pure populations of primary breast tumor cells (Dairkee et al., 1995). Nonmalignant cells are unable to survive these initial, hostile environmental conditions. Thus, an additional benefit is that nonmalignant epithelium with its higher proliferation rate, is not present and is not able to overgrow the tumor cells which have a slower proliferation rate. A common misconception is that malignant BCEs proliferate more rapidly than nonmalignant BCEs. It should also be noted that drug resistance in tumor cells may depend on and be the result of the stress of a hostile microenvironment (Tomida and Tsuruo, 1999). For this reason, accurate measurements of drug resistance may require that the assays be performed on cells in the proper microenvironment. It is interesting to note that some of the most successful in vitro chemosensitivity tests involve the culture of cells in tiny capillary tubes that are sealed at both ends and incubated for 14 days (see below). The resulting microenvironment is likely to be even more hostile than those generated using the sandwiched coverslip technique (Dairkee et al., 1995).

In Vitro Chemosensitivity Assays: The idea of using in vitro assays to select chemotherapy regimens tailored to the tumor of the individual patient is not new (DeVita, 1997). A summary of clinical correlations can be made using the following nomenclature: TP (true positive, patients who are sensitive in vitro and respond to therapy, TN (true negative, patients who are resistant in vitro and do not respond to chemotherapy, FP (false positive, patients who are sensitive in vitro but resistant clinically), FN (false negative, patients who are resistant in vitro but respond clinically), PPA (positive predictive accuracy) = $TP/(TP+FP)$, percentage of patients with sensitivity in the test who respond, NPA (negative predictive accuracy) = $TN/(TN+FN)$, percentage of patients with resistance in the test who do not respond to therapy. Correlations of in vitro test results with patient response show an overall PPA of 72% and a NPA of 90%. This corresponds to a sensitivity (ability to detect clinically responsive patients) of 85%, and a specificity of 89% (ability to detect clinically unresponsive patients). It should be noted that these numbers represent an average of 7 different assay types in studies involving 4263 patients, and results were pooled from several individual studies (DeVita, 1997). These authors have suggested that these assays be referred to as drug-response assays, rather than chemosensitivity assays, because they are more successful at predicting patient drug resistance than predicting patient response.

Clinical Trials: Three prospective clinical trials have attempted to use in vitro chemosensitivity tests to improve patient response and survival. Both have failed to demonstrate increased survival for patients who were administered chemotherapy based on results of in vitro chemosensitivity tests. Two different in vitro chemosensitivity assays were used in these studies, the HTCA (human tumor cloning assay) and the DiSC (differential staining cytotoxicity, or Weisenthal dye exclusion) assay. The in vitro cell culture and propagation techniques used and the biological endpoints measured differ significantly in these two assays. The HTCA calls for the culture of minced tumor tissue in very small capillary tubes that are sealed at both ends and then incubated for 14 days. Before this mixture of malignant and nonmalignant cells ($0.2-1.0 \times 10^5$ cells) is sealed in the tubes, the cells are exposed for 1 hour to standard anticancer agents at concentrations corresponding to one-tenth the peak plasma concentration seen in humans. Cells are then suspended in 0.3% agar and are sealed in 100 μ L capillary tubes for 14 days at 37 °C, and 7% CO₂. After 14 days, the cells are extracted from the tubes and the number of colonies are manually counted under a microscope. This capillary cloning system was selected because fewer tumor cells are initially required and the subsequent outgrowth of colonies with significant numbers of cells is seen to be improved. The DiSC assay is a nonclonogenic assay, where tumor cells are cultured in liquid medium in small, polypropylene tubes for 4-6 days order to amplify the number of cells available for testing. Drug exposures times range from 1 hr to 4 days, depending on the drug. In general, drug concentrations are empirically determined and are higher than those used in the HTCA. For example, cells were

treated with doxorubicin for 1 hr at 0.04 $\mu\text{g/mL}$ in the HTCA , but for 1 hr at 1.2 $\mu\text{g/mL}$ in the DiSC assay. In the DiSC assay, cell membrane integrity is assessed by staining dead cells in suspension with Fast Green. Acetaldehyde-fixed duck red blood cells (DRBC) are added to the culture as an internal standard, and then the entire mixture is cytocentrifuged onto a microscope slide, with the result that living cells appear clear, while dead cells and the DRBC are stained green. Slides are then counterstained with HE (haematoxylin-eosin) which stains the living cells. Cells are then identified under the microscope by a skilled technician as tumour or normal who counts cells to determine the ratio of living tumor cells over DRBC.

HYPOTHESIS/RATIONALE/PURPOSE

Our hypothesis is that previous clinical studies that sought to administer anticancer drugs based on in vitro chemosensitivity tests failed to see dramatic increases in patient response or survival for several specific reasons: (i) the microenvironment favored by tumor cells was not properly simulated in vitro (ii) the physiological responses of individual cells were not monitored closely throughout the assay, and (iii) the drug concentrations, combinations, and exposure times examined were limited, and not scientifically optimized. We further hypothesize that Visual Servoing Optical Microscopy (VSOM) can rapidly discover and exploit key physiological characteristics which distinguish malignant and nonmalignant human breast epithelial cells (BECs). In this way, VSOM will help to solve problems (i-iii), listed above.

OBJECTIVE/SPECIFIC AIMS

Demonstrate and verify that VSOM can rapidly discover and optimize, on a tumor-by-tumor basis, microenvironmental conditions suitable for the successful in vitro propagation and chemosensitivity testing of primary human breast tumor cells. Our specific aims are to:

- (1) Rapidly and automatically develop in vitro microenvironments that favor the propagation of primary breast tumor cells
- (2) Rapidly develop new in vitro fluorescence assays that predict cell behavior on the basis of early physiological responses to applied stress
- (3) Improve VSOM technology in order to achieve our objectives and specific aims.

PRELIMINARY DATA

Visual Servoing Optical Microscopy: A VSOM fluorescence assay consists of (i) real-time observations of individual cell responses to a series of environmental perturbations or stimuli (ii) real-time, automatic, and intelligent adjustment of these stimuli and environmental perturbations in order to achieve specified goals. Currently, environmental perturbations and stimuli are applied by means of computer-controlled perfusion pumps (Figure 1). Individual cell responses are monitored using a variety of fluorescence probes. An example of a specified goal might be the identification of a particular subpopulation of cells based on an observed stress response as the pH of the extracellular medium is decreased. An intelligent response of the system would be to lower the pH of the medium until the cells of interest had been identified, then return the cells to a higher pH before they are irreversibly damaged. The cells of interest would then be identified on a cell-by-cell basis, and the system could then proceed with additional tests that attempt to optimize or exploit this differential response to a low pH environment.

An ideal VSOM fluorescence assay for cell identification is performed rapidly on a complicated mixture of cells, the fluorescent probe is nontoxic to the cells, cells are identified based on characteristic physiological responses to applied stimuli or perturbations, and the stimuli or perturbations do not have an irreversible effect on the cells. In our opinion, the most desirable predictive assays would be dynamic and adaptive VSOM fluorescence assays involving the observation of a series early physiological responses to intelligently chosen,

computer-controlled stimuli. This approach becomes more powerful when such stimuli and perturbations are reversible and do not permanently commit the cell to a given biological path. The ability to repeatedly apply relatively innocuous stimuli and perturbations to living cells will allow us to repeatedly probe the cell for physiological characteristics that can be exploited by anticancer drugs or combinations of anticancer drugs. Our initial goal is to develop VSOM fluorescence assays that are highly predictive of the cell's future behavior or ultimate fate; for example, whether the cell has been sufficiently stimulated to proliferate, or whether it has been stressed to the point where apoptosis is inevitable. This capability will help us achieve our objective of making correlations between the early physiological responses observed in cells and the future biological state or ultimate biological fate of the cells, whether this be proliferation, apoptosis, or arrest in some stage of the cell cycle.

Our current VSOM is shown in Figures 1 and 2. Currently four syringe perfusion pumps are under computer control (Fig. 1A), and we have modified a temperature-controlled microincubation chamber so that it mounts firmly to our computer-controlled xy scanning stage (Fig. 2A). A vacuum powered aspirator removes excess liquid and a temperature probe provides feedback for temperature control (Fig. 2B). More details on this hardware can be found in the Facilities Description pages. As seen schematically in Figure 3, the system currently references its position relative to an extremely fine grid ("+") that is gently etched into the sterile, plastic culture dish using a glazier's microfinish wheel. The dish can then be removed and placed back into the incubator. When it is time to reimage the cells, the system is calibrated by making reference to the "+" on the dish, and the (0,0) point of the coordinate is taken to be the center of the "+". The user can easily see the etching under transmitted light for initial positioning.

A simple VSOM experiment, currently in use for determining the degree of multidrug resistance in individual MCF-7 cells, is shown schematically in Figure 4. As seen in Figure 4A, the nuclei of living cells can be prelabeled using the membrane permeable fluorescence dye Hoechst 33342 (H42). As seen in Figure 4B, after LysoTracker-Red (LT-R) fluorescence dye (a lysosome-specific organelle stain for living cells) has been perfused into the chamber, individual cell lysosomes become labeled. The mean fluorescence intensity of each cells in one field of view is monitored using multiple fluorescence channels, corresponding to multiple fluorescence excitation and emission wavelengths. These quantitative measurements for an actual experiment are shown in Figure 5 for MCF-7 cells. The error bars indicate \pm standard deviation for 325 cells. The blue symbols represent a steady H42 signal in all the cells as a function of time. However, the red signal representing LT-R uptake is seen to increase as soon as LT-R perfusion begins. At approximately 6000 s, the LT-R pump is turned off, the Calcein-AM (CAM) perfusion is begun, and green fluorescence signal begins to accumulate in the cells, while LT-R begins to be rinsed out of the cell. Calcein-AM, like LT-R is a cell viability stain that is only retained in cells with intact membranes. Multidrug-resistant, or MDR cells, however, actively pump CAM out of the cell. CAM signal appears throughout the cytoplasm as depicted in Figure 4C. When the LT-R signal drops below the CAM signal, the CAM pump is turned off, and the LT-R pump is turned back on until the LT-R intensity reaches its previous maximum.

It should be noted that an entire digital image is taken for each fluorescence channel (red, green, and blue) and an image is also taken using transmitted light. At each time point, a full-color image can be constructed as shown in Figure 7. In this experiment long exposures at 345nm light were made repetitively until the cell membrane blebbed, and the cell lysed, resulting in a loss of the red LT-R stain, and the green CAM stain. This time-dependent process, and a large number of lysed cells may be seen by comparing Figures 4A,C to Figures B, D.

We can also monitor cells in multiwell plates using either the microscope (Fig 6A) or a fluorescence plate reader (Figure 6B). The process of loading such plates with compounds such as doxorubicin (DOX) is shown in Figure 6C. We plan to control the pH and pO_2 during these plate exposures by putting the plates into special gas chambers which are then placed in the incubator (Figure 6D,E). Gas mixtures of known CO_2 and O_2 composition can then be perfused into these gas chambers to control pH and pO_2 during long term incubations. An image of MCF-7 cells in one well of a plate is shown in Figure 6F. These cells are stained with a live/dead stain (CAM, and ethidium homodimer, or EH). Thus, green cells are alive and red cells are dead. We have also developed fluorescence staining procedures for detecting mRNA expression in living cells. LDS-751

(Molecular Probes, Eugene OR) stains both DNA and RNA. However, a large spectral blue shift takes place when LDS-751 moves from being bound to DNA (infrared fluorescence emission) to being bound to mRNA. Thus, as mRNA levels increase in the cells in response to an agent that increases intracellular calcium (thapsigargin, or TG) the resulting red fluorescence becomes visible in our red channel (Figures 8A,B). It should be noted that the cells can also be labeled with FURA-2-PE3, a calcium sensitive fluorescence dye. Thus, one can observe increases in intracellular calcium at the same time one is monitoring the expression of mRNA in another channel.

Intracellular calcium is monitored by performing image ratioing. One takes a digital image at 345nm excitation, and divides this image, on a pixel-by-pixel basis, by a second image that was acquired at 385nm excitation (Negulescu et al., 1994). It has been demonstrated in T lymphocytes that one can stimulate cells with TG, and then perform perfusions with high or low calcium buffer. In this way, one can control the intracellular levels of calcium. If the levels of intracellular calcium are elevated for a sufficiently long time, subsequent gene expression can be observed in response to this perceived intracellular signal (Negulescu et al., 1994). Using the calcium image rationing technique, it has also been demonstrated that the proliferation rate of primary cultures of human mammary epithelial cells (HMECs) can be increase as intracellular levels of calcium are increased (Tannheimer et al., 1997). In this study, polycyclic aromatic hydrocarbons (PAHs) were used to elevate intracellular levels of calcium and thus generate an increase in the proliferation rate of the cells. Image ratioing can also be used to detect BrdU incorporation. As seen in Figure 9, it is possible to quantify the degree of BrdU incorporation in living cells. Using this technique, we have verified the effects of EGF stimulation on 184B5 cells, an immortalized HMEC cell line (Stampfer et al., 1993). Using the same cells (after fixation with acidic ethanol) shown in Figure 9, we also performed indirect immunofluorescence detection of BrdU incorporation using an antiBrdU antibody. Similar results were obtained (data not shown).

Image Processing

The process of visual servoing is highly dependent on our ability to detect and outline individual cells in digital images. This is referred to as "segmenting" the image. We currently use two different segmentation algorithms for stained nuclei. We are using these algorithms for our live cell studies, and for our studies of immunostained tissue sections. We will show examples of both types of images. One segmentation approach is based on a variation of Hough transform and is suitable for a large class of cells as long as they conform to a specifically parameterized geometric model. The second approach focuses on extraction of partial information corresponding to step and roof edges and then groups them through geometric reasoning (Cong and Parvin, 1999 June; Cong and Parvin, 2000). The intent is to construct a partitioning that is globally consistent. A list of step edges is constructed by thresholding raw images, recovering corresponding boundaries, and localizing concave corners from their polygonal approximation. These corners provide possible cues to the position where two adjacent nuclei may touch each other. Thresholding separates big clumps consisting of several nuclei squeezed together, but the boundaries between adjacent nuclei cannot be detected because they have higher intensities than background. The partial boundaries between adjacent nuclei can be recovered; however, by extracting crease segments (Monga et al., 1992; Thirion, 1996; Thirion and Gourdon, 1996). These crease segments correspond to trough edges (positive curvature maxima), but false creases may also be extracted in the process. Nevertheless, dealing with noise and erroneous segments is a higher-level process that is handled during the grouping process. Our system generates a number of hypotheses for possible grouping of the boundary segments. A unique feature of this system is in hyperquadric representation of each hypothesis and use of this representation for global consistency. The main advantage of such a parameterized representation (as opposed to polygonal representation) is compactness and better stability in shape description from partial information. In this fashion, each step-edge boundary segment belongs to one and only one nucleus while each trough-edge boundary segment is shared by two and only two nuclei. These initial hypotheses and their localized inter-relationship provide the basis for search in the grouping step. This is expressed in terms of an adequate cost function and minimized through dynamic programming. The final result of this computational step is then shown to an operator for verification and elimination of false alarms. An example is shown in

Figure 10, where comparison to manual segmentation is shown. A major limitation of this approach is its computational complexity. Grouping of local features is a complex process, and simpler techniques are highly desirable.

Recently, we have developed three new techniques. One is based on a regularized form, the second on a vector representation of the underlying image followed by feature extraction in vector space, and the third on a geometric and texture model of a cell and its interaction with neighboring cells. The new regularization form has its root in visualization of 3D objects; however, we have also found it to be applicable to segmentation of scientific images. The vector representation of images has its root in analysis of spatio-temporal satellite images (Yang and Parvin, 2000a; Yang and Parvin, 2000b). The detection result using the regularized form is shown in Figure 11A and B. The third approach has been developed for measuring mRNA expression. Due to space limitations we can only show our preliminary results. These preliminary results are shown in Figures 11 and 12.

PROPOSED RESEARCH AND METHODS

The cells lines available for our use have been previously described (Dairkee et al., 1995; Dairkee et al., 1997; Li et al., 1998). To summarize, the number and types of specimens available are: organoids for epithelial propagation that were derived from reduction mammoplasties (82 cases); epithelial cultures from primary breast carcinoma at passage 2 or greater (73 cases); matched epithelium from non-malignant peripheral tissue (23 cases). These human specimens are not the same ones used in the previous prospective trials, nor are they tied to a patient database. Our approach is to build on the data and findings of the previous prospective trials. This approach allows us to focus on breast cancer, rather than lung cancer (Wilbur et al., 1992; Gazdar et al., 1990), or "cancer" in general, as was the approach of the HTCA studies (Von Hoff et al., 1990). For example, in the HTCA study only 5 breast cancer specimens were used and this would not be a sufficient number of individuals for our proposed studies. For an initial estimate of how many individual specimens we will need to examine, we will perform studies on the tumor cells derived from 10 individuals. We will compare differences in the proliferation rates of tumor cells from different individuals and determine how these rates can be increased, on a per patient basis, as the microenvironment is altered. It is our hypothesis that this important experimental parameter, the microenvironment in which the drug tests are performed was not controlled closely enough in the previous studies. In order to determine how sensitive such tumor cell proliferation and drug response tests are to the preferred, or optimum, microenvironment, (which we believe will vary from individual to individual) we will use tumor cells derived from at least 10, and at most, 70 patients. In addition, we will perform parallel studies on at least 10 specimens of nonmalignant BCEs, derived from reduction mammoplasties. We expect to see much less variation in the preferred microenvironment when we examine these nonmalignant BCEs.

There are additional advantages to using well characterized primary breast tumor cells. For example, we will already have information concerning the *erb-B2*, *p53*, and *bcl-2* status of some cases (Dairkee et al., 1997). It is likely this will help us interpret observed differences in specimens; for example, the relative resistance or sensitivity of different specimens to apoptosis.

(NOTE: Due to space limitations, we will not repeat experimental details or the experimental timeline that already appears in the Statement of Work).

Experimental Approach: Our approach will be to monitor intracellular calcium levels, intracellular pH, mitochondrial membrane potentials, mRNA levels, and BrdU incorporation in individual living cells as various growth stimuli and/or environmental stresses are applied. Early physiological responses to perturbations of the microenvironment (pH, pO_2 , $[Ca^{+2}]_{ex}$, anticancer drugs) will be stored in our bioinformatics database. The ultimate effect of these perturbations will be assessed by using VSOM to return to the same field of cells after longer-term incubations. In addition, responses that appear to predict an increase in proliferation or apoptosis will be verified in multiwell plate fluorescence assays during longer-term incubations. Proliferation, cell viability, and apoptosis will be monitored using VSOM and multiwell plate fluorescence assays. This approach will allow us to: (1) develop conditions that are favorable or selective for the propagation of primary breast

tumor cells in culture, (2) develop an array of predictive assays based on observations of dynamic, early physiological events (3) document tumor cell mechanisms of resisting effects of anticancer drugs, (4) use this information to pick the proper combination of antitumor drugs

Anticancer Drugs: The drugs we will use are those that were used in all three of the previous clinical trials. Concentrations are given in $\mu\text{g/mL}$, followed by exposure time where C indicates continuous exposure for the duration of the test. Our initial experiments will use this range of concentrations and exposure times.

<u>DRUG</u>	<u>DiSC</u>	<u>HTCA</u>
cisplatin	1.65, C	0.2, 1 hr
doxorubicin	1.2, 1h	0.04, 1 hr
etoposide	41.7, C	3.0, 1hr
5-fluorouracil	20.0, C	6.0, 1hr
mitomycin C	0.30, C	0.1, 1 hr
vinblastine	0.55, C	0.05, 1 hr
vincristine	0.25, C	0.01, 1hr

Cell stresses other than anticancer drugs: Agents that increase $[\text{Ca}^{+2}]_{\text{in}}$ with used alone or in conjunction with high and low calcium buffer exchanges. These agents include TG, calcium ionophores, and PMA (phorbol 12-myristate 13-acetate), as previously described (Negulescu et al., 1994). Low pH will be induced during VSOM experiments by constant perfusion of buffers of known pH. Low pO_2 will induced during VSOM experiments by (i) perfusing solutions that were previously equilibrated to a known pO_2 by bubbling gas of known composition through the solution. In addition, gas of the proper composition will be layered over the cell chamber during the experiment. Our cell chamber is designed for this purpose.

Other agents to be investigated: EGF, TGF- β

Early responses to be monitored: intracellular calcium, intracellular pH, mitochondrial membrane potential, total mRNA levels, levels of reactive oxygen species, and changes in morphology via transmitted light observations. Intracellular calcium will be monitored using calcium ratio imaging in cells that have been pre-loaded with FURA-2-PE3. Intracellular pH will be monitored using cells labeled with BCECF, and image ratioing will be used here, also. Mitochondrial membrane potential will be monitored using TMRE, as previously described (Farkas et al., 1989). Total mRNA will be monitored using LDS-751, as described in the preliminary data section. Levels of reactive oxygen species will be monitored using a variety of fluorescence probes that are sold for this purpose by Molecular Probes (Eugene, OR). We are especially interested in the generation of reactive oxygen species generated by TGF- β .

Biological Endpoints: proliferation, apoptosis, necrosis. Proliferation will be monitored via BrdU incorporation and nuclear image ratioing as described in the preliminary data section. A wide variety of fluorescence probes are available from Molecular Probes (Eugene, OR). The live/dead assay described in the Preliminary Data section will also be used.

Multiwell Plate experiments: For long term incubations of amplified cells we will use multiwell plate assays. We will use a fluorescence plate reader, and also image cells in the individual wells as demonstrated in the Preliminary Data section. Fluorescence assays kits for cell proliferation, etc. are commercially available. In cases where pO_2 or pH must be held constant, multiwell plates will be placed in gas chambers as described in the Preliminary Data section. Gas of known O_2 and CO_2 composition will be continuously perfused into these chambers in order to control pO_2 and/or pH.

Cell Sedimentation Manifolds: We have obtained a set of homemade cell sedimentation chambers, provided to us by Dr. Mike Børens of Creative Scientific Methods, Inc. (www.creative-sci.com). The procedure for using these chambers to deposit very small numbers of cells onto small, well-defined regions of different surfaces is described on this company's website.

Fluorescence Calibrations: Multispeck beads will be used as fluorescence intensity standards (Molecular Probes, Eugene, OR). Defined standard calcium solutions are also provided by this company for calcium ratio imaging calibrations.

ACRONYMS

BEC	breast epithelial cell
$[Ca^{+2}]_{ex}$	extracellular calcium concentration
$[Ca^{+2}]_{in}$	intracellular calcium concentration
CAM	calcein-AM
DiSC	differential staining cytotoxicity
DOX	doxorubicin
DRBC	duck red blood cells
DS	drug sensitive
EH	ethidium homodimer
FN	false negative
FNA	fine-needle aspirate
FP	false positive
FURA-2-PE3	a calcium sensitive fluorescence dye
H42	Hoechst 33342
LT-R	LysoTracker Red
HMEC	human mammary epithelial cell
HTCA	human tumor cloning assay
MCF-7	a human breast cancer cell line
MDR	multidrug-resistant
NPA	negative predictive accuracy
PMA	phorbol 12-myristate 13-acetate
PPA	positive predictive accuracy
TRME	tetramethylrhodamine ethyl ester
TN	true negative
TP	true positive
TG	thapsigargin
VS	visual servoing
VSOM	visual servoing optical microscopy

REFERENCES

- Band, V., D. Zajchowski, K. Swisshelm, D. Trask, V. Kulesa, C. Cohen, J. Connolly, and R. Sager. 1990. Tumor progression in four mammary epithelial cell lines derived from the same patient. *cancer research*. 50:7351-7.
- Brown, J. M., and A. J. Giaccia. 1998. The unique physiology of solid tumors: opportunities (and problems) for cancer therapy. *cancer research*. 58:1408-16.
- Cong, G., and B. Parvin. 1999 June. Model based segmentation of nuclei. In Proceedings of the Conference on Computer Vision and Pattern Recognition.
- Cong, G., and B. Parvin. 2000. Model based segmentation of nuclei. *Journal of Pattern Recognition*.
- Dairkee, S. H., G. Deng, M. R. Stampfer, F. M. Waldman, and H. S. Smith. 1995. Selective cell culture of primary breast carcinoma. *Cancer Research*. 55:2516-9.
- Dairkee, S. H., E. C. Paulo, P. Traquina, D. H. Moore, B. M. Ljung, and H. S. Smith. 1997. Partial enzymatic degradation of stroma allows enrichment and expansion of primary breast tumor cells. *Cancer Research*. 57:1590-1596.
- DeVita, V. T., Jr. 1997. *Cancer: principles and practice of oncology*. Lippincott-Raven, Philadelphia.
- Ethier, S. P., M. L. Mahacek, W. J. Gullick, T. S. Frank, and B. L. Weber. 1993. Differential isolation of normal luminal mammary epithelial cells and breast cancer cells from primary and metastatic sites using selective media. *Cancer Research*. 53:627-35.
- Farkas, D. L., M. D. Wei, P. Febroriello, J. H. Carson, and L. M. Loew. 1989. Simultaneous imaging of cell and mitochondrial membrane potentials [published erratum appears in Biophys J 1990 Mar;57(3):following 684]. *Biophysical Journal*. 56:1053-1069.
- Gazdar, A. F., S. M. Steinberg, E. K. Russell, R. I. Linnoila, H. K. Oie, B. C. Ghosh, J. D. Cotelingam, B. E. Johnson, J. D. Minna, and D. C. Ihde. 1990. Correlation of in vitro drug-sensitivity testing results with response to chemotherapy and survival in extensive-stage small cell lung cancer: a prospective clinical trial [see comments]. *Journal Of The National Cancer Institute*. 82:117-24.
- Li, Z., V. Bustos, J. Miner, E. Paulo, Z. H. Meng, G. Zlotnikov, B. M. Ljung, and S. H. Dairkee. 1998. Propagation of genetically altered tumor cells derived from fine-needle aspirates of primary breast carcinoma. *Cancer Research*. 58:5271-5274.
- Monga, O., S. Benayoun, and O. Faugeras. 1992. From partial derivatives of 3d density images to ridge lines. In Proceedings of the Conference on Computer Vision and Pattern Recognition. 354-359.
- Negulescu, P. A., N. Shastri, and M. D. Cahalan. 1994. Intracellular calcium dependence of gene expression in single T lymphocytes. *Proceedings Of The National Academy Of Sciences Of The United States Of America*. 91:2873-7.
- Stampfer, M. R., C. H. Pan, J. Hosoda, J. Bartholomew, J. Mendelsohn, and P. Yaswen. 1993. Blockage of EGF receptor signal transduction causes reversible arrest of normal and immortal human mammary epithelial cells with synchronous reentry into the cell cycle. *Experimental Cell Research*. 208:175-88.
- Strauss, E. 1999 February. Pretesting Tumors. In Scientific American. 19-22.
- Tannheimer, S. L., S. L. Barton, S. P. Ethier, and S. W. Burchiel. 1997. Carcinogenic polycyclic aromatic hydrocarbons increase intracellular Ca²⁺ and cell proliferation in primary human mammary epithelial cells. *Carcinogenesis*. 18:1177-82.
- Thirion, J. 1996. New feature points based on geometric invariants for 3d image registration. *International Journal of Computer Vision*. 18:121-137.
- Thirion, J., and A. Gourdon. 1996. The 3d matching lines algorithm. *Graphical Models and Image Processing*. 58:503-509.
- Tomida, A., and T. Tsuruo. 1999. Drug resistance mediated by cellular stress response to the microenvironment of solid tumors. *Anti-Cancer Drug Design*. 14:169-77.
- Von Hoff, D. D., J. F. Sandbach, G. M. Clark, J. N. Turner, B. F. Forseth, M. J. Piccart, N. Colombo, and F. M. Muggia. 1990. Selection of cancer chemotherapy for a patient by an in vitro assay versus a clinician [see comments]. *Journal Of The National Cancer Institute*. 82:110-6.
- Weisenthal, L. M., and M. E. Lippman. 1985. Clonogenic and nonclonogenic in vitro chemosensitivity assays. *cancer treatment reports*. 69:615-32.
- Wilbur, D. W., E. S. Camacho, D. A. Hilliard, P. L. Dill, and L. M. Weisenthal. 1992. Chemotherapy of non-small cell lung carcinoma guided by an in vitro drug resistance assay measuring total tumour cell kill. *British Journal Of Cancer*. 65:27-32.
- Yang, Q., and B. Parvin. 2000a. Detection of singularities from sst data. In Int. Conf. on Pattern Recognition.
- Yang, Q., and B. Parvin. 2000b. Feature-based visualization of large scale geophysical data. In Proceedings of the Conference on Computer Vision and Pattern Recognition.

Cat #	Description	Price	Callahan, Daniel E.
			Subtotal
AH 73-0235	HSE-Harvard Data Acquisition Hardware, W98	\$1834.25	
AH-73-0045	PLUGSYS Basic System Case, Type 603	\$1890.00	
AH-73-0212	EMM Amplifier Module	\$1420.00	
AH-73-0215	pHMM Amplifier Module	\$1420.00	
AH-73-0210	OPPM Oxygen Partial Pressure Module	\$2060.00	
AH-73-0208	Flow-Through O2 Chemosensor	\$1515.00	
AH-73-2712	Reference Electrode	\$ 955.00	
AH-73-0213	pH Flow-Through Sensor	\$1384.60	
AH-73-2711	Flow-Through Biosensor for glucose, L-Lactate, etc.	\$1515.00	
AH-73-0642	Flow-Through Sensor for Calcium Ion	\$1696.83	\$15690.68

Equipment budget justification:

We have requested \$15,700 for biosensors and the associated electronics necessary for on-line monitoring of important microenvironmental parameters during VSOM experiments. The sensors we have chosen are ZABS flow-through sensors that can be connected in series to our perfusion lines. Thus, we will be able to continuously monitor and log several important properties of the medium just before it reaches the cells. There is not enough room to place all these sensors in the actual cell perfusion chamber, due to the presence of the large transmitted light condenser, the temperature probe, and the vacuum aspirator. Therefore, we will monitor pH, L-lactate (or glucose), extracellular calcium, and pO_2 of the medium as it is continuously perfused into our microincubation chamber. The electronics package (PLUGSYS) we have selected is modular in design and the basic system case has sufficient slots to hold the various amplifier modules necessary for the measurement of pH, pO_2 , calcium, and other biological molecules such as glucose or L-lactate. The PLUGSYS system case is also compatible with the data acquisition hardware we have chosen, which includes a PCI A/D converter board for a PC. This equipment will provide important, real-time data for VSOM system control, and will allow us to continuously monitor and log microenvironmental parameters that are important for the execution and interpretation of our proposed experiments.

Supply budget justification:

A significant portion of the requested supply money is for the purchase of fluorescence dyes from Molecular Probes (Eugene, OR). For example, a great deal of the fluorescent dye calcein-AM is consumed during on-line VSOM experiments where 100 mL of a 1.0 μM solution is perfused through the cell chamber during a single experiment. In addition, this compound must be repeatedly added to all the wells of multiwell plates in many of our proposed experiments. The cost of this compound is \$142 for 1 mg (Catalog #C-3099, 1mg, MW =994g/mole). In addition, a significant amount of sterile culture work will be performed on-site at LBNL, and the sterile serological pipettes, tissue culture flasks, media, serum, multiwell plates, and tissue culture dishes are expensive consumables. In addition, we require sterile syringes and tubes of various sizes, special pipette tips and sterile reservoirs for our multichannel pipettor, 0.2 μm syringe filters for the preparation of sterile solutions, sterile chambered coverslips for high-resolution, high magnification oil-immersion objective studies of cells, and replacement arc lamps and excitation filters for the fluorescence microscope.

Personell and subcontract budget justification:

This is a multi-institution, multi-disciplinary proposal. Dr. Callahan's effort is required at the 50% level. He will coordinate, schedule, and perform the VSOM experiments and the multiwell plate fluorescence assays on-site at LBNL using living, human BECs cells provided by Dr. Shanaz H. Dairkee. Dr. Callahan will test, modify and refine VSOM fluorescence assays and protocols and integrate the various hardware components into a functioning system. Dr. Callahan will test and help refine the VSOM image analysis, data reduction, and system control software provided by Dr. Bahram Parvin. These evaluations will be conducted both on-line during VSOM experiments, and off-line after the experiments are completed. Dr. Callahan will make the image data and analysis results available to all members of the group. Dr. Callahan will manage and backup the data using magnetic tape, and will keep records of experiments performed, summaries of results, and records that track data sets stored on-line and off-line. Dr. Callahan will also coordinate the overall group effort regarding publications, and presentations and will publish biological results in the relevant biological journals. Dr. Parvin's effort is required at the 10% level. Dr. Parvin will provide software necessary to improve the existing VSOM system software, and will publish computer science results in the relevant computer science journals. Dr. Parvin will eventually control the VSOM system remotely, and will store digital images, single cell responses, and relevant experimental parameters directly into a modern, object-oriented bioinformatics database. Dr. Parvin will make this database available to other members of the group and this will allow them to examine and visualize the multidimensional data in ways that will generate novel experimental insights. Dr. Shanaz Dairkee will provide a variety of well-characterized human BECs, both malignant and nonmalignant, for VSOM and multiwell plate experiments. Her effort is required at the 10% level. In addition to cells, she will provide critical cancer cell biology and cell culture expertise to the group and will help design and interpret experiments on a regular basis. She will also monitor the group's progress from the perspective of a cancer biologist, and will help set experimental priorities so that important biological results are rapidly and efficiently generated. (Modify text for Dr. Dairkee)

FACILITIES

Laboratory Space: Dr. Callahan's shared lab space consists of 600 sq. ft. containing 4 work benches, refrigerators and freezers, 2 sinks, laminar flow hood, 3 incubators, cell culture hood, chemical storage, networked Pentium computers and printers. Major equipment includes a computer controlled fluorescence multiwell plate reader (Cytofluor 4000) and Cytocalc software, automatic microplate strip washer, PCR thermocycler (Crocodile II), gel electrophoresis apparatus, Nikon inverted phase microscope, Coulter counter, balances, water baths, centrifuges, table top and ependorf centrifuges. In addition, Dr. Callahan has a complete wet laboratory and cell culture facility that is dedicated to VSOM studies. This facility is immediately adjacent to the Life Sciences Microscope Resource (LSMR).. In addition, he is part of the Barcellos-Hoff Group and has access to all her labs and equipment

Dr. Callahan has access to several computers. He shares a Pentium III PC and a Sparstation Ultra 1 with members of the Barcellos-Hoff research group, and also has access to the shared SUN Sparstations in the Life Sciences Microscope Resource. All the computers are networked and have access to the centrally located (Building 50) LBNL software farm and other computer resources located in Dr. Parvin's building at the LBNL Supercomputing Center (NERSC).

Digital Imaging Fluorescence Microscopy: Studies will be performed at the Life Sciences Microscope Resource (LSMR, in room 174, Building 74) using our Visual Servoing Optical Microscope (VSOM). This Zeiss Axiovert 135 H/DIC, TV inverted microscope is used for transmitted light (phase and DIC) and multicolor fluorescence microscopy. It is equipped with a computer controlled xy scanning stage, z-axis stepping motor, and six position filter wheel. A 12-bit Xillix CCD camera (Xillix Technologies, Vancouver, BC) containing a Kodak KAF-1400 CCD chip (1317x1035 pixels, 7x7 micron pixel size) will be used for these studies. This camera has a readout rate of 8 MHz (approximately four full size images per sec). Images from the cameras are readout directly into a Sparstation Ultra 1, a multitasking UNIX workstation that can store or transfer images across the network during the course of the experiment. A 100 BaseT network line links the LSMR computers and microscope to the computers of the Imaging Technology and Distributed Computing Group (Dr. B. Parvin, Building 50). A Mass Storage System for digital images is also available at the LBNL Supercomputer Center (NERSC, Building 50). The VSOM system is built around an inverted microscope and a vibration isolation table is installed. This inverted microscope has a base port so that cameras mounted below obtain better fluorescence signal. In addition, the inverted design allows perfusion of living cells, with cells located on the bottom of a microperfusion cell chamber. With this design it is possible to switch from fluorescence to transmitted light detection (phase or DIC) and verify cell locations, morphology, etc. This is achieved with a computer controlled transmitted light shutter. A computer controlled epifluorescence shutter is also available in the filter wheel. Operation of the system (control of shutters, filter wheel, xy stage, z-axis motor, images acquisition) can be automated using the software SCIL Image (TNO Institute of Applied Physics, Delft, The Netherlands), or using the VSOM software of Dr. Parvin.. Two computer controlled, dual syringe pumps (Harvard 33, Harvard Apparatus) are available. Syringes do not have to be the same size. Each syringe has its own, computer controlled block so that perfusion rates can be controlled independently. An open, perfusion microincubator (PDMI-2, Harvard Apparatus) has been mounted on the Zeiss Axiovert. A bipolar temperature controller (TC-202) is available for use with the PDMI-2. This is a Peltier electronic instrument that delivers and adjusts DC current to the microincubator to control temperature. A "Bath" type thermistor (BSC-T3, 36K Ohms total) is used with the PDMI-2. A manual and/or computer controlled microcapillary positioner (Model MP-185 Motorized Huxley-Wall Type Micromanipulator from Sutter Instrument Co., Novato, CA) is available for microdissection work.

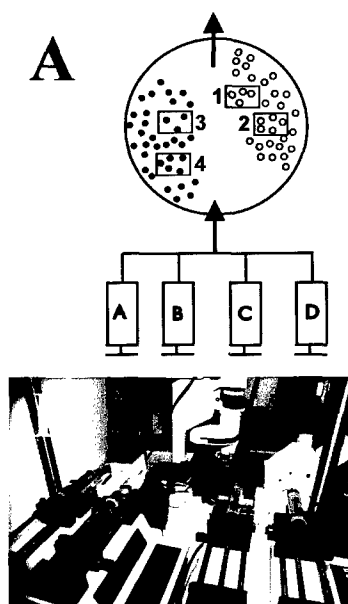


FIGURE 1: (A) Schematic of cells in co-culture undergoing perfusion. Four fields of view are being monitored (gray squares). Cell type 1 on the left, cell type 2 on right. (B) Current VSOM system with four computer-controlled syringes and an inverted, Zeiss Axiovert fluorescence microscope.

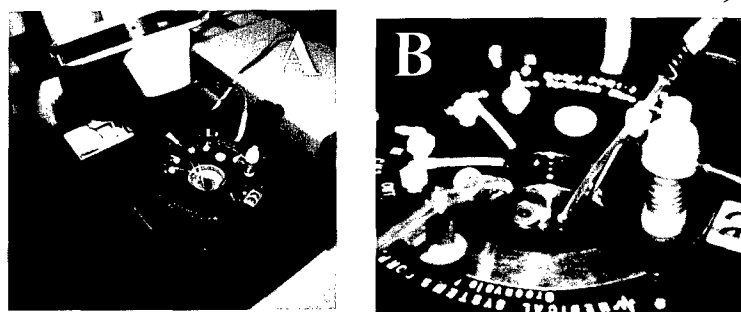


FIGURE 2: Microperfusion chamber mounted on Zeiss Axiovert. (A) Transmitted light condenser tilted back to show chamber. (B) Close-up of chamber showing vacuum aspirator (red base), temperature probe (blue base), and other perfusion input lines.

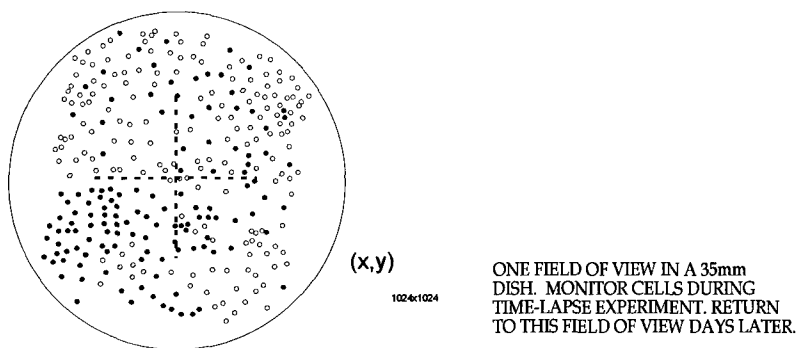


FIGURE 3: Schematic of current approach for linking early responses to eventual cell fate on a cell-by-cell basis. Use VS to return repeatedly to same field of cells after additional time in incubator. Cross-hairs are etched into surface of plate (red).

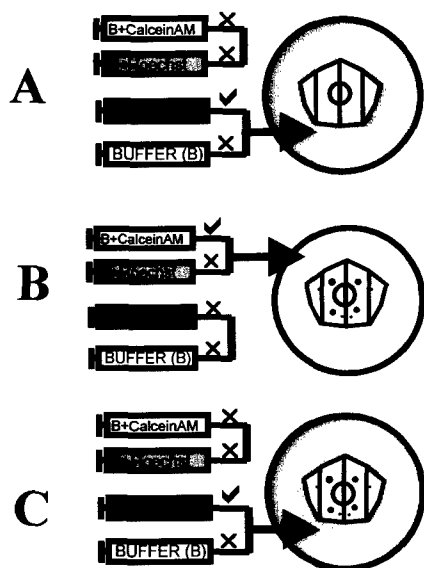


FIGURE 4: Schematic of VSOM experiment. (A) Cell nuclei pre-labeled with Hoechst 33342, begin Lyso-Tracker Red perfusion (B) Cell lysosomes labeled, begin calcein-AM perfusion (C) relabeled lysosomes. Actual experimental data of this experiment shown in Figure 5.

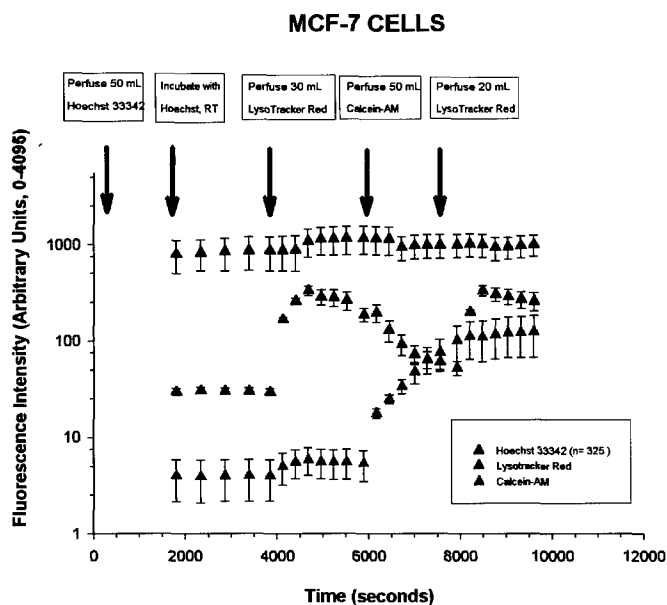


FIGURE 5: Actual experimental results for the experiment depicted in Figure 4. 325 cells were monitored in the red, green, blue, and transmitted light channels. Error bars indicate +/- standard deviation.

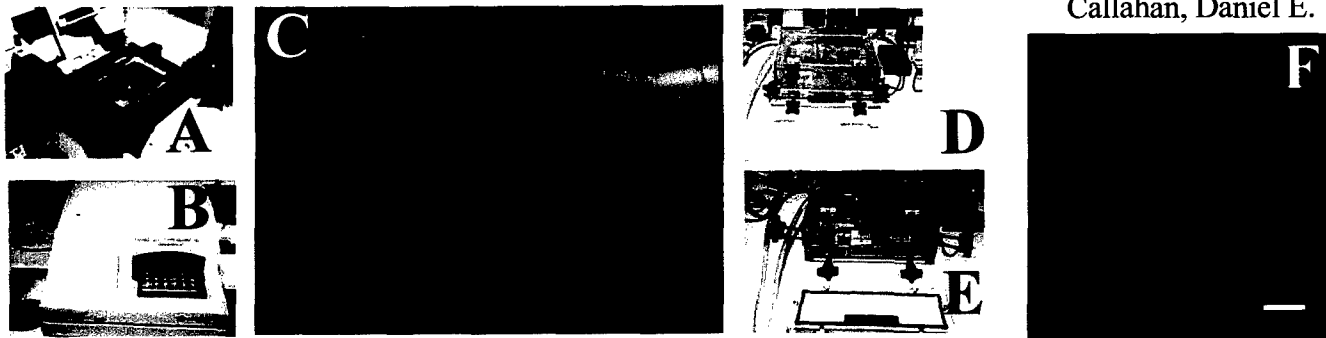


FIGURE 6: Use of multiwell fluorescence plates. (A) Stage holder for using plates on microscope. (B) Cytofluor fluorescence plate reader (C) Loading plates in sterile hood using multichannel pipetter (red outline) (D) Gas chamber for incubator (front lid sealed) (E) Lid open (F) Image of living cells in one well of a plate, acquired using live/dead stain 10X objective. (All images on page at same magnification.)

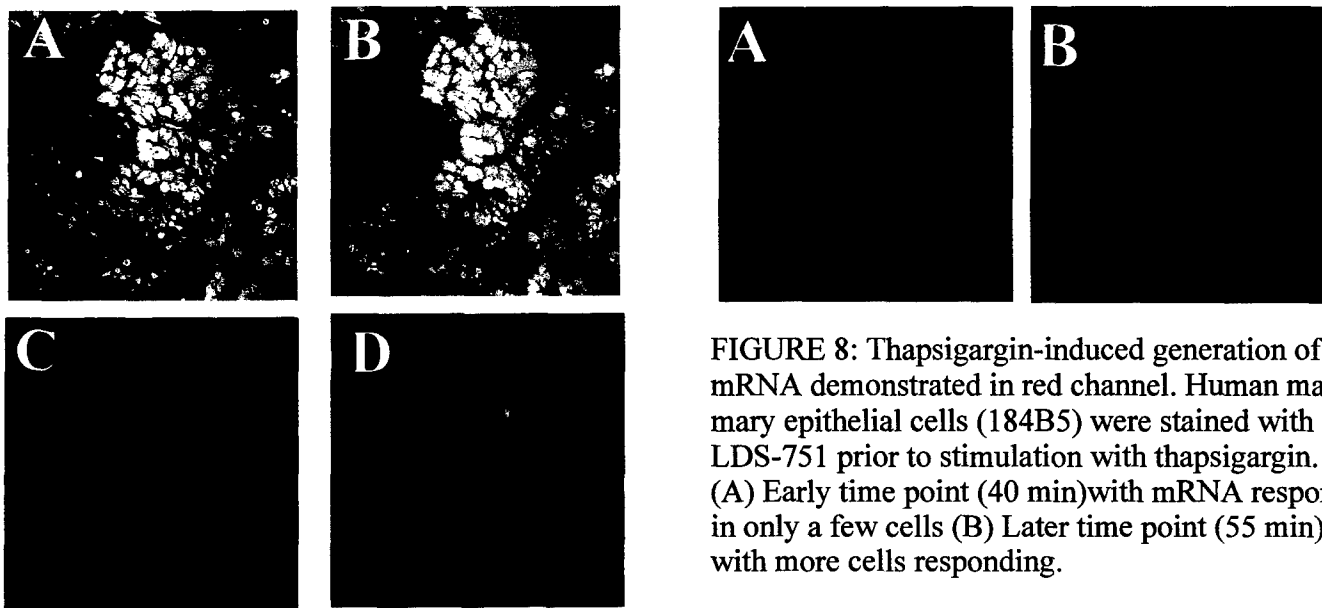


FIGURE 8: Thapsigargin-induced generation of mRNA demonstrated in red channel. Human mammary epithelial cells (184B5) were stained with LDS-751 prior to stimulation with thapsigargin. (A) Early time point (40 min) with mRNA response in only a few cells (B) Later time point (55 min) with more cells responding.

FIGURE 7: Selected images from a stress response, time-lapse experiment on MCF-7 cells. Images A and C and B and D are the same. However, A and B have the transmitted light image overlaid on the combined red, green, and blue channels which represent LysoTracker Red, Calcein-AM, and Hoechst 33342 fluorescence, respectively. Cells were stressed by low calcium buffer and excessive UV illumination. Lysed cells with blebbing membrane and no green dye may be observed in the image from the later time point, image B/D.

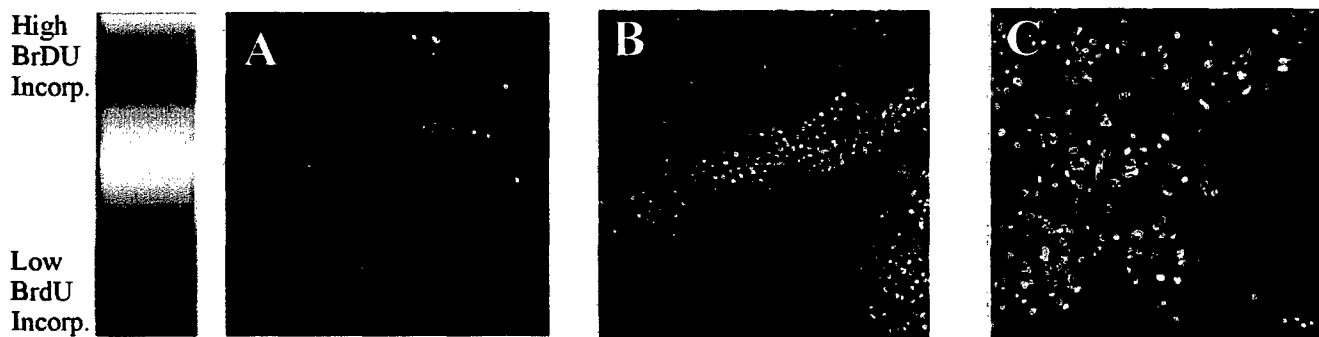


FIGURE 9: Quantitation of BrdU incorporation using dual-stained, living cells and image-ratio technique. Cells were pulse-labeled with BrdU for 1 hr, then were dual-stained with Hoechst 33342 and Syto16. Images acquired with 360 and 490nm excitation, respectively, were ratioed on a pixel by pixel basis and color-coded. Three separate dishes of HMECs (184B5) in images A, B, and C: (A) Cells deprived of EGF for 72hr. (B) Cells deprived of EGF for 48 hr, then received EGF 24 hrs ago (C) Cells that were never deprived of EGF and were refed 24 hrs ago. Results agree with Stampfer, et al. *Exp Cell Res.*, 208:175-188 (1993).

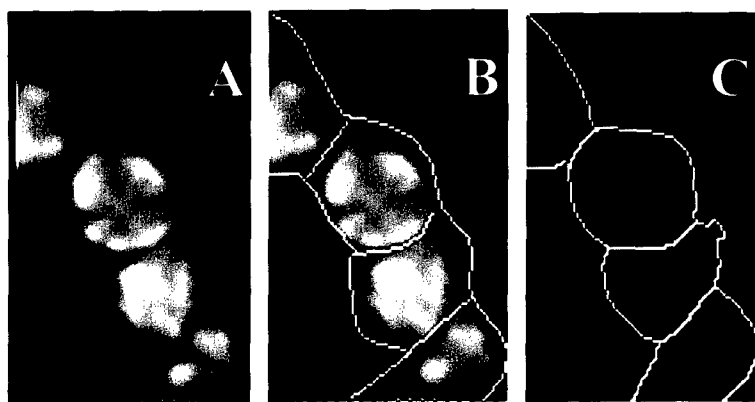


FIGURE 10: Example of nucleus segmentation in tissue sections stained with DAPI. (A) original (B) segmentation by hand (C) one of our segmentation algorithms

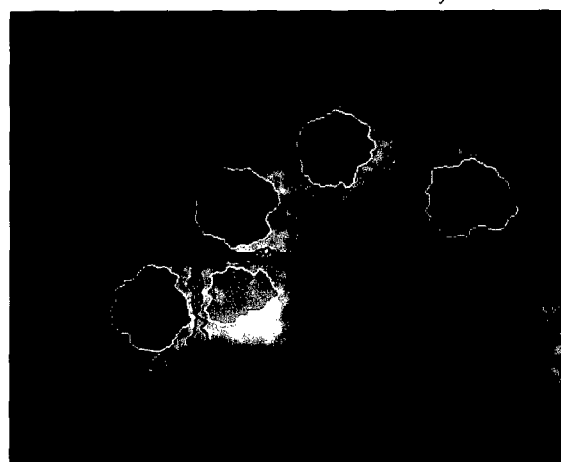


FIGURE 11 Living MCF-7 cells stained with TMRE. Both the plasma and motchondrial membrane potential can be calculate from this image (Farkas, et al.). 63X, oil objective used.

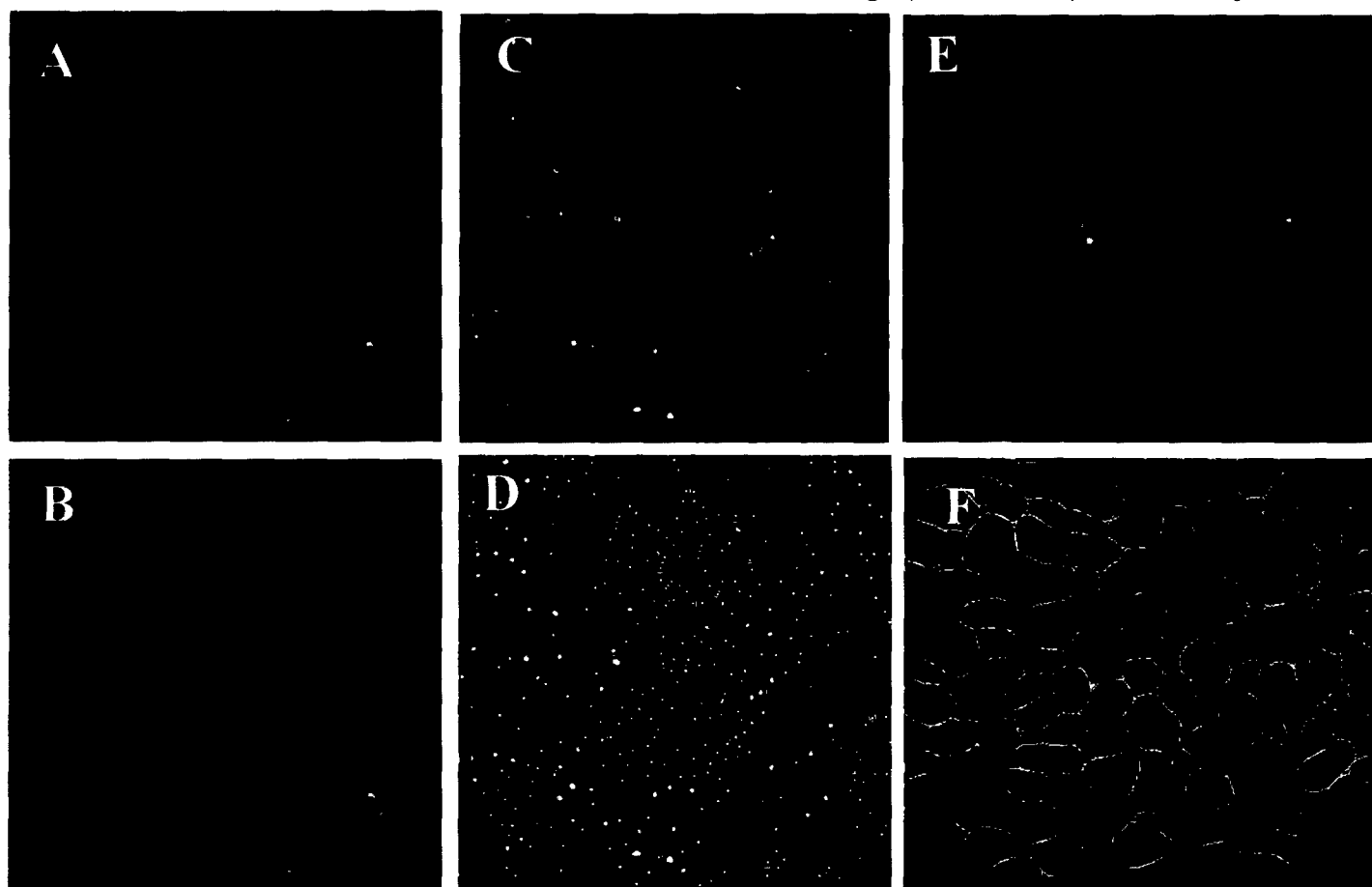


FIGURE 12: These are examples of three different image segmentation algorithms that are currently under development. (A,B) Nuclei of living 184B5 cells stained with Syto16. The same cells exhibit mRNA staining in another channel, as shown in Figure 8. (C,D) Nuclei of living MCF-7 cells stained with Hoechst 33342. This is the blue channel of the cells seen in Figure 7. (E,F) Segmentation of cells using transmitted light only. Our goal is to be able to segment cells in the transmitted light channel, and thus avoid staining the cells in any way. At the present time, our algorithms are only working with phase-contrast images taken at 20X. We hope to improve this algorithm until we can segment cells at 10X, using only brightfield illumination. The use of phase contrast objectives is not recommended for sensitive fluorescence studies of living cells..

FORM 3

This form is required for all applications

SCIENTIFIC ABSTRACT

Predictive Testing for the Individual Breast Cancer Patient

Project Title (Do not exceed 60 characters and spaces)

Life Sciences/Information and Computing Sciences, Lawrence Berkeley National Laboratory

Department and Organization (if applicable)

Our goal in the proposed research is to use visual servoing optical microscopy (VSOM) to rapidly analyze large populations of living cells that have been freshly derived from human breast cancer tissue biopsies. We believe the rapid analysis of dynamic physiological responses on a patient-by-patient, tumor-by-tumor, and cell-by-cell basis will provide critical information for individualized cancer chemotherapy. We have assembled a multidisciplinary team with expertise in engineering, computer sciences, digital imaging, cell biophysics, and cancer biology. The successful accomplishment of the research objectives proposed here would represent an important advance in in vitro chemosensitivity testing and would represent a large step toward our ultimate goal of chemotherapy regimens tailored to the individual breast cancer patient. Visual servoing (VS) is a term from the field of robotic vision. In our case, it refers to the dynamic manipulation of experimental parameters based on analysis of digital image content. A VSOM fluorescence assay consists of (i) real-time observations of individual cell responses to a series of applied stimuli (ii) automatic, and intelligent adjustment of experimental parameters to achieve experimental goals. Our immediate goal is to develop a wide range of VSOM fluorescence assays that rapidly (1-8 hrs) produce detailed and distinct physiological fingerprints that are highly predictive of an individual patient's response (both normal and tumor cell response) to a particular anti-cancer drug, particular combination of drugs, or particular sequence of drug exposures. An ideal VSOM fluorescence assay does not irreversibly perturb living cells, and it allows one to make predictions of drug sensitivity based on specific physiological characteristics of individual cells.

Hypothesis: We believe our technology will allow us to rapidly (i) develop new in vitro fluorescence assays that can be used to predict chemosensitivity (ii) develop selective culture conditions for specific subpopulations of cells, i.e, primary culture tumor cells (iii) demonstrate a new paradigm in in vitro chemosensitivity testing. This new paradigm is visual servoing for knowledge-based interrogation of individual living cancer cells.

FORM 4

This form is required for all applications

LAY ABSTRACT

Predictive Testing for the Individual Breast Cancer Patient

Project Title (Do not exceed 60 characters and spaces)

Life Sciences/Information and Computing Sciences, Lawrence Berkeley National Laboratory

Department and Organization (if applicable)

Several companies have recently been formed to pursue the idea of testing each individual breast cancer patient's tumor cells in a test tube or dish outside the patient's body (<http://www.oncodocs.com/laboratories/laboratories.html>). Such tests are performed on each patient's cancer cells in order to determine the best drug regimen for that particular patient. This type of testing is referred to as "in vitro" chemosensitivity testing or "predictive testing". The goal of our proposed research is to demonstrate the feasibility of a new class of in vitro drug response and chemosensitivity assays. Our objectives are to develop a computer controlled microscope (a visual servoing optical microscope, or VSOM) that can rapidly and automatically test a patient's cancer cells prior to the selection of an anti-cancer drug regimen. We believe our instrument will not only be useful for the ultimate application of such tests; it will also be useful for the development of additional tests that are more sensitive and precise. Our goal is to build the instrument and perform several demonstrations that will get other scientists and funding agencies excited about our new approach. Several aspects of our approach are unique. We have combined sophisticated robotic vision techniques, digital video microscopy and biophysics to actually observe the responses of hundreds of living cells in a variety of colors. The different colors represent glowing fluorescent tracers within the living cells. In these assays, computer controlled syringes inject various substances into a temperature controlled cell chamber. We are currently observing the single cell responses of up to 500 cells in three or four different colors. In addition, we can observe the traditional, transmitted light image of all the cells. In one model system, we propose to study normal human mammary epithelial cells. In a second model system, (drug sensitive and multi-drug resistant human breast cancer cell lines; MCF-7 cells) our results indicate that current fluorescence assays for multidrug resistance are indeed in need of improvement. We will attempt to develop improved versions of these tests in this three year grant.

FORM 5

This form is required for all applications.

RESPONSIVENESS to the PRIORITY ISSUE and AWARD TYPE

This information is used for the programmatic review (see Section 3 in the application packet.).

1. Indicate the one (1) BCRP priority issue targeted best by this application (see Section 2):

- | | |
|---|---|
| <input type="checkbox"/> Health Care Delivery and Health Policy | <input type="checkbox"/> Socio-cultural, Behavioral, and Psychological Issues |
| <input type="checkbox"/> Biology of the Normal breast | <input type="checkbox"/> Prevention |
| <input type="checkbox"/> Etiology | <input type="checkbox"/> Earlier Detection |
| X Innovative Treatment Modalities | <input type="checkbox"/> Pathogenesis |

2. Indicate the award type for this application:

- | | |
|---|--|
| <input type="checkbox"/> SPRC Exploratory Award | X SPRC Full Research Award |
| <input type="checkbox"/> TRC Pilot | <input type="checkbox"/> TRC Full Research Award |
| <input type="checkbox"/> IDEA-I | <input type="checkbox"/> IDEA-II |
| <input type="checkbox"/> New Investigator | <input type="checkbox"/> Postdoctoral Fellowship |
| <input type="checkbox"/> Training Program | <input type="checkbox"/> RFA |

Discuss how the priority issue and award type are targeted by the research project and how they are responsive to the mission of the BCRP in reducing impact of breast cancer in California. Use one (1) continuation page (5A), as needed.

The title of our proposed research is "Predictive Testing for the Individual Breast Cancer Patient". In the proposed research, we are targeting Priority Issue 7, "Innovative Treatment Modalities: Search for a Cure". Specifically, we are proposing a new, rational therapeutic approach for tailoring drug combinations to individuals using a novel approach to in vitro chemosensitivity testing. We have constructed a Visual Servoing Optical Microscope (VSOM), and will use it to design, execute, and archive the results of VSOM fluorescence assays. This is a new technology and a new approach to testing living cells. An important feature of VSOM fluorescence assays is the ability of the system to interact with an ensemble of living cells in an intelligent fashion, during the course of each assay. This approach combines sophisticated robotic vision techniques with biophysical models of single-cell responses to applied stimuli. A currently funded breast cancer researcher (Dr. D.E. Callahan) with extensive experience with biophysical studies of cancer cells will be working with a computer vision expert (Dr. B. Parvin). Thus, we have chosen to apply for a Scientific Perspectives Research Collaboration (SPRC) Award. This will allow a breast cancer researcher (Dr. Callahan) an excellent opportunity to continue to work with Dr. Parvin and continue to integrate him into the ongoing breast cancer research in our Life Sciences Division. We have new tools and theories to apply to the field of breast cancer research. The technology revolution that has produced robotic vision, powerful computers, massive storage capabilities, object-oriented databases, and Internet connectivity has not yet been fully applied to current problems in breast cancer research. What is required are scientists who are willing to bridge the gaps between computer science, molecular and cell biology, DNA and gene technologies, medicine, physiology, chemistry, and biophysics.

Our team of scientists at Lawrence Berkeley National Laboratory (LBNL) has unique resources, expertise and experience. We often work together in large multi-disciplinary teams. Phase 1 of our VSOM project is nearly complete. Drs. Parvin and Callahan are midway through a 2-year Department of Defense breast

cancer IDEA grant, "Visual Servoing for Optimization of Anti-Cancer Drug Uptake in Human Breast Cancer Cells". In this grant, we have constructed a VSOM and are in the process of demonstrating a new approach to disease prevention that will identify and characterize drug sensitive and drug resistant tumor cells on a patient-by-patient and tumor-by-tumor basis. We believe we are responsive to the SPRC award type. We have a strong commitment to breast cancer research because it is the focus of our Division and our Department. There are many future opportunities for interaction with the other breast cancer researchers in our building and this will be our focus for the foreseeable future

FORM 6

This form is required for all applications.

STATEMENTS for the ADDITIONAL CRITERIA

- This information is used for the programmatic review (see Section 3).
- You may add one continuation page (page 6A) to this form.

Discuss how your project addresses the following BCRP programmatic criteria

Multidisciplinary Approach: (incorporation of researchers and methods from several fields)

We have a truly multidisciplinary team and meet the additional criteria for a full SPRC grant. We have obtained pilot data, established a solid organizational infrastructure, and developed protocols (administrative, financial, etc.) for collaboration between Computer Scientists and Biologists. Many obstacles to such collaboration have been overcome during the last several years. For example, it is difficult to compete with the overwhelming demand for computer scientists of the highest caliber, as may be seen by their cost to the project. In addition, computer scientists and biologists at LBNL are physically separated on a large campus and have very different administrative structures, cultures, and vocabularies. Even their computer platforms (Sun/UNIX vs. PC/Windows) are quite different and can hinder collaborations. We have a proven track record of collaboration. Drs. Parvin (Information and Computing Sciences Division, ICSD) and Callahan (Life Sciences Division, LSD) have spent over 5 years introducing the animal, cell and cancer biologists in our Division to multi-channel (multi-color) digital imaging fluorescence microscopy. The Life Sciences Microscope Resource (LSMR), under the direction of Dr. Mary Helen Barcellos-Hoff (our colleague and consultant on this grant) has helped cancer biologists move from selective photographic documentation of biological phenomena in cells and tissue to quantitative biology with non-biased sampling methods and statistical analysis of digital image information. In addition, the computer scientists and biophysicists have come to appreciate the most complex and most pertinent biological systems (tissue and animals) and have learned to focus more intently on the rapid production of important biological results. These interactions have produced several fruitful collaborations between our Divisions, several of which are currently in progress. The Parvin/Callahan/Barcellos-Hoff research partnership obtained funding using the LSMR as a method of collaboration and has now moved on to a second level of collaboration. The second phase involves shared equipment in the LSMR, compatible software packages and image formats, custom-written software, graphical user interfaces, image libraries, databases and seamless network connectivity. This research collaboration is underway, and is taking place on different computer platforms and operating systems.

Translational Potential: (potential to be used for direct and immediate impact on breast cancer)

Several companies currently perform in vitro chemosensitivity testing. Such tests are being performed on patient's biopsied cancer cells in order to determine the best drug regimen for that particular patient. Also, health insurance companies are beginning to

pay for this testing (See <http://www.oncodocs.com/laboratories/laboratories.html> and Scientific American, Feb. 1999 article). We plan to demonstrate the application of VSOM assays in traditional multiwell plate fluorescence assays in order to verify the translational potential of information obtained using a VSOM. It should be possible to replicate many of our timed agent exposures and buffer exchanges manually in multiwell plates. Thus, the improved tests would be widely available immediately and our customized hardware would not be required. However, we believe that a VSOM will be very useful for executing fluorescence assays, not just developing them. Thus, we have filed an LBNL Patent Disclosure: "A Method for Knowledge-Based Discovery and Optimization of Differences Between Cell Types" Callahan, D.E., and Parvin, B. September 9, 1999. We are very interested in working with commercial companies and making this technology available as soon as possible.

In addition, any VSOM information we can obtain regarding selective media conditions for the propagation of primary human breast cancer cells would also be of immediate and practical value to researchers, new drug developers, and in vitro chemsensitivity testing companies.

Focus on Underserved Populations: (potential to reduce disparities in incidence and treatment)

A flexible chemotherapeutic regimen designed for each individual breast cancer patient, rather than the representative "average" population would reduce disparities in the treatment of breast cancer. Average population results will often work better for majorities rather than minorities. "Minority" in this sense can mean any minority, including women who are not sensitive or are hypersensitive to standard drugs, or women with a unique genetic disposition or other complicating factor that will never be represented in a large study.

Title: **Visual Servoing for Knowledge-Based
Interrogation of Living Human Cancer Cells**

Institution: Lawrence Berkeley National Laboratory

PI: **Bahram Parvin**

Position of PI: Staff Scientist

Co-PI: **Dan Callahan and Ge Cong**

Address: M.S. 50B-2239
Lawrence Berkeley National Laboratory
Berkeley, CA 94720

Telephone: 510-486-6203

FAX: 510-486-6363

Email: parvin@george.lbl.gov

Requested funding: Year 1 (\$224,777), Year 2 (\$218,608), Total (\$443,385)

Use of human subject: None

Use of vertebrate animals: None

man-02/1999

Signature:

Date:

1 Introduction

Visual servoing [15] refers to the dynamic manipulation of experimental parameters (in this case, the concentrations of anti-cancer drugs or other agents) based on the analysis of image content. Our goal is to use visual servoing optical microscopy (VSOM) to rapidly analyze large populations of living and cultured human cells that have been freshly derived from cancer tissue biopsies. We believe the rapid analysis of dynamic physiological responses on a patient-by-patient, tumor-by-tumor, and cell-by-cell basis will provide critical information for individualized cancer chemotherapy. We have assembled a multidisciplinary team with expertise in engineering, computer sciences, imaging, cell biophysics, and cancer research. The successful accomplishment of the research objectives proposed here would represent an important achievement in biomedical engineering. A VSOM fluorescence assay consists of (i) real-time observations of individual cell responses to a series of applied stimuli (ii) automatic, and intelligent adjustment of experimental parameters to achieve experimental goals. An ideal VSOM fluorescence assay does not irreversibly perturb living cells, and it allows one to make correlations between specific physiological characteristics of a cell and the subsequent sensitivity of the cell to anti-cancer drugs, or other agents. Our long range goal is to develop a wide range of VSOM fluorescence assays that rapidly (1-6 hrs) produce detailed physiological VSOM "fingerprints" of a large population of cells on a cell-by-cell basis. We believe our technology will allow us to develop specific VSOM assays that are highly predictive of an individual patient's response (tumor and normal cell chemosensitivity) to a particular anti-cancer drug, or combinations of drugs. We also believe our technology will allow us to rapidly develop optimized culture conditions for specific subpopulations of cells. There will be three phases in the proposed research, and three funded programs will be leveraged to meet the program goals.

Phase 1: Initial construction of a database consisting of baseline data collected during VSOM assays that target specific physiological responses and specific cellular compartments in model cell systems.

Phase 2: Refinement of this database by modifying experimental parameters during real-time experiments until the assay reaches the desired level of predictive power in model cell systems.

Phase 3: Intelligent, knowledge-based, real-time analysis of unknown, paired specimens (e.g., physically separated normal and tumor cell populations). This will require automatic application of the proper VSOM assays in the proper order, using the appropriate experimental parameters. The end result of such an analysis will be a report that compares the effects of different drugs (or other agents) on the two populations. These comparisons will be based on proliferation, apoptosis, or any other pertinent cellular responses that can be monitored during the experiment.

Visual servoing aims at automated manipulation of instrument control parameters based on automatic visual-scene interpretation. A simple example of visual servoing is autofocusing for an optical microscope, where the microscope objective is moved automatically along the Z direction to compensate for defocus. In this context, defocus is quantified and the Z-axis is moved under computer control for optimum focus. A more complex example includes drift compensation or motion detection as a function of external stimuli for dynamic experiments [12]. This system (currently in use at LBNL) not only detects motion in the scene, but also records and logs pertinent attributes, e.g. size, shape, response, direction of motion. This information is then compared to attributes of similar events that are stored in a database. Another benefit of this level of automation is that these dynamic experiments can be conducted remotely over the wide area network [15]. Automatic drift compensation provides a stationary view of the experiment and eliminates the need for high speed network and/or quality of service.

The proposed research requires close collaboration between biologists and computer scientists. The investigators, listed in this proposal, have a proven track record of scientific collaboration [11, 15].

From a computer science perspective, the following components are needed to achieve the research objectives: (1) computer control of the microscope and syringes, (2) segmentation of cells imaged on single or multiple channels, (3) annotation of the assay used in a particular experiment, (4) automated annotation of cell responses as a function of a schedule, (5) offline correlation, clustering, and learning techniques that compare the differences between two cell types as a function of an assay, and (6) online learning techniques for dynamic control and estimation of a policy (schedule) to elicit distinct responses from two physically separated cell types. The interaction between various system components are shown in Figure 1. These requirements leverage three research programs performed under other grants that are funded through DOE-MICS (*DOE2000 Material and MicroCharacterization Collaboratory*), DOE-OBER (*An Imaging Bioinformatic System for Studying the effect of Low Dose Radiation*), and a DOD Breast Cancer research grant (*Visual Servoing for Anti Cancer Drug Uptake*). The first grant provides the basis for remote collaborative microscopy, seamless data acquisition, and instrument control. The second grant provides the imaging bioinformatic component for annotating data and images and the needed core technology for segmentation of cells. The third grant provides a platform for VSOM that will be available at the end current fiscal year. Our current VSOM grant (funded by the DOD Breast Cancer Research) does not include: (1) database component and population of that database with cell responses, (2) learning, clustering, and data mining in that database, (3) real-time analysis and manipulation of physically separated population of cells, (4) segmentation of cells using data fusion technique (images acquired on multiple channels), (5) incorporation of large number of syringes, and (6) study of mitochondrial physiologies. We are confident that by coupling this proposal with our currently funded programs, a new biomedical technology can be demonstrated so that drug therapy can be tailored to an individual patient.

Section 2 provides an overview of the system architecture. Section 3 provides the review of core technology for segmentation of cells. Section 4 introduces two classes of learning in our system. Section 5 summarizes the experimental protocol.

2 System Architecture

The current trend in telepresence, distributed control, and computation research is to bring experts and facilities together from geographically dispersed locations [15, 18, 19]. The natural evolution of this research is to construct a scalable system for collaboration and to leverage either legacy or new computational toolkits to support novel scientific applications based on capabilities in real-time control and steering, visualization, and simulation. Under the DOE2000 program, the Berkeley team has developed a collaborative system [16] for remote microscopy. The software architecture for this Enterprise-wide information service is shown in Figure 2. Our system uses an extensible object oriented framework so that applications can be rapidly assembled, maintained, and reused. These objects may reside on any host and can be listed, queried, and activated in the system.

Our system consists of three service categories that interact with the object request broker (ORB): Instrument Services (IS), Exchange Services (ES), and Computational Services (CS). These core services are specified with an interface that is language independent. Instrument Services provide a scalable means of instrument control and interaction through an object hierarchy. Exchange Services provide a scalable mean to collect data and push them to users or other application software, e.g. analytical or storage facilities. Computational Services provide means for distributed image analysis, visualization, simulation, etc. The important issue is that the architecture shown in Figure 2 is distributed. For

example, complex image segmentation servers are registered with a symmetric multiprocessing system, where simple instrument control are registered with the local host near the microscope. All objects in this architecture are remotely accessible. As a result, other investigators will be able to conduct an experiment and view/share their results.

¶

3 Segmentation

Automatic delineation of cell nuclei and cytoplasm is an important step in mapping cell responses into specific cellular compartments. This computational component interacts with the Instrument Services to acquire image data from one channel or multiple channels (by rotating the filter wheel or opening and closing shutters). A brief review of the segmentation tool kits is provided [3, 4].

3.1 Segmentation of Nuclei from Single Channel

Presently, VSOM supports Hough transform to detect and track circular objects (cells or nuclei). The technique works well for both transmitted and fluorescence light images. Under our current DOE-OBER grant, we have developed a new method to localize clumped nuclei in a tissue section. This method focuses on delineation of individual nuclei that are observed with an epi-fluorescence microscope. The nuclei of interest reside in a ring of cells that surround a particular type of capillary in the tissue. The intent is to build the necessary computational tools for large scale population studies and hypothesis testing. These nuclei are clumped together, thus, making quick delineation infeasible. An example is shown in Figure 3(a)(b). Previous efforts in this area have been focused on thresholding, local geometries, and morphological operators for known cell size [20, 22]. Others have focused on an *Optimal Cut Path* that minimizes a cost function in the absence of shape, size, or other information [10, 8, 26]. These algorithms developed for tissues will be useful when segmenting adjacent cultured cells into nuclear and cytoplasmic region.

Our current research focuses on extraction of partial information corresponding to step and roof edges and then group them through geometric reasoning [3, 4]. The intent is to construct a partitioning that is globally consistent. A list of step edges is constructed by thresholding raw images, recovering corresponding boundaries, and localizing concave corners from their polygonal approximation. These corners provide possible cues to where two adjacent nuclei may touch each other. Thresholding separates big clumps consisting of several nuclei squeezed together, but the boundaries between adjacent nuclei cannot be detected since they have higher intensities than background. However, the partial boundaries between adjacent nuclei can be recovered by extracting crease segments [9, 24, 23], as shown in Figure 3(d). These crease segments correspond to trough edges (positive curvature maxima), but false creases may also be extracted in the process. Nevertheless, dealing with noise and erroneous segments is a higher-level process that is handled during the grouping process. Our system generates a number of hypotheses for possible grouping of the boundary segments. A unique feature of this system is in hyperquadric representation of each hypothesis and the use of this representation for global consistency. The main advantage of such a parameterized representation (as opposed to polygonal representation) is compactness and better stability in shape description from partial information. In this fashion, each step-edge boundary segment belongs to one and only one nucleus while each trough-edge boundary segment is shared by two and only two nuclei. These initial hypotheses and their localized inter-relationship provides the basis for search in the grouping step. This is expressed in terms of an adequate cost function and minimized through dynamic programming. The final result of this computational step

is then shown to an operator for verification and elimination of false alarms. An example is shown in Figure 4, where comparison to manual segmentation is shown.

3.2 Segmentation of Cells from Multiple Channels

Another tedious type of data collection is in the analysis of multichannel images. In this scenario, a sample is imaged with different dyes and filters to accentuate different components of the cells. Here, the system must be able to analyze several channels of data simultaneously, select a specific location in the cytoplasmic region, and make repeated measurements. An efficient approach to fusing of images based on a Bayesian framework has been developed. This approach can also be extended to 3D (with confocal microscopes) as demonstrated by our earlier work [14]. The purpose of data fusion is complementary processing of different modalities for segmentation and labeling. From this perspective, the segmentation procedure should label each pixel in the data volume accordingly. However, there are a number of ambiguities that can complicate the labeling process. These ambiguities can arise from purely local processing and the absence of any high level feedback. The sources for the ambiguities include corruption of data by noise, performance limitation of algorithms for extracting local features, and existence of nonessential features that impede the labeling task. One aspect of region segmentation is in estimating the average intensity of each region. This is done by analyzing the histogram. The initial position of the peaks in the histogram are approximated and then refined with least square approximation. The next step of the computational process is to use these peaks as cluster centers to enforce local consistency in the image space. Here, a Bayesian framework is used to label images based on their multiple channel information. Specifically, we use Bayesian hierarchical model with three levels of hierarchy. The first level is a model for the underlying classification, Z . Under ideal condition, observing Z under M different modalities (here, there are three fluorescence images corresponding to blue, green, and red fluorescence emission, respectively) specifies an ideal representation, X_i , of the data that are corrupted by different types of noise in the imaging system. The third level of the hierarchy correspond to the actual observation of data Y_i . The first level uses Markov Random Field (MRF) with prior probability density function in the form of Ising model with a positive parameter β . This parameter encourages cooperation among nearby pixels. In a Bayesian framework, β may assume prior ignorance about the scene content. The second level models X as conditionally independent given Z , i.e., $P(X_1, \dots, X_M|Z) = P(X_1|Z) \dots P(X_M|Z)$. This is reasonable since if a classification is labeled as cytoplasm then the ideal response of the green channel (cytoplasm) and the blue channel (nuclei) will not affect each other. Finally, the third level of hierarchy, Y_i , is modeled as a Gaussian distribution. As a result, Y_i will be a locally blurred representation of X_i . The full model can be written as

$$P(Z, X_i|Y_i) = \prod P(Y_i|Z) \prod P(X_i|Z)P(Z) \quad (1)$$

We use maximum a posteriori (MAP) estimates to obtain X_i and Z . However, since MAP computation is inherently infeasible, we use numerical approximation based on iterative conditioning modes (ICM) [1] to find the local optimum. An example of three channel fluorescence image processing is shown in Figures 5.

4 Learning from cell responses

There will be two categories of learning in our system corresponding to offline and online learning. Offline learning is performed when a schedule for an assay is designed and entered into the system control panel (its GUI). Massive amounts of data are then collected as the system records the response of each cell to VSOM assay stimuli. On the other hand, online learning attempts to illicit a certain cell response based on historical data (in the archive) and current summary of cell responses under observation. These learning techniques have a common thread in that they try to cluster and learn behavior in a multi-dimensional space as measured by fluctuations in the fluorescence intensity emanating from different cellular compartments as a result of applied stimuli (compounds being injected into the cell chamber). All measurements are made relative to the system's initial state. Formally, the observed intensity is a multivariable function defined as

$$I_t = f(\text{CellType}, \text{Dye}, [\text{Dye}], \text{Channel}, \frac{\partial I}{\partial t}, \frac{\partial \text{Flow}_{c_i}}{\partial t}, T) \quad (2)$$

Where I is the mean fluorescence intensity observed in the cytoplasm at time t , $\text{Dye} = \{a \text{ fluorescence dye etc.}\}$, $\text{Channel} = \{\text{Red, Green, Blue, etc.}\}$, T is temperature, and $\frac{\partial \text{Flow}}{\partial t}$ corresponds to changes in the flow of compounds (e.g., Nigericin, Valinomycin, plain buffer) being injected. An Schema will be developed to capture this time varying information to store the observations into a database for subsequent knowledge discovery. Each experimental cycle represents a possible schedule in an assay (I_t for $t = 0 \dots n$) that generates a fingerprint for each observed cell. These individual responses provide a compact representation of intra-cellular activities in the image space. This information will be stored and then visualized per cell, population of cells, cell types, etc.

4.1 Offline Learning

Statistical techniques to track and to form clusters on the basis of their state and action will be developed. We will use entropy minimization and a numerical iterative hierarchical clustering (NIHC) algorithm. The NIHC starts with randomly assigning data to clusters in a B-tree structure and iteratively reducing the total Gaussian entropy of the tree. Additionally, K-mean approximation will be used for state approximation. Co-occurrence statistics of the dynamic labels over all sequence patterns will then be calculated to establish an equivalence class.

Alternatively, a cell response and its corresponding attributes (dynamic annotations) generates a representation within a sequence. This representation can then be used to construct joint co-occurrence statistics in that sequence. These statistics can be used to create a binary tree classification of the representation. The main utility of this method is in detecting and classifying correlated sequences. Additionally, once a model is established, co-occurrence statistics provides a mean to detect outliers.

4.2 Online Learning

The intent is to illicit a certain response in order to differentiate between two cell populations. This is often referred to as reinforcement learning in the literature, which may be modeled as a markov decision process (MDP). A particular MDP is defined by its state (current observed intensity and its gradient) and action set (concentration of compounds in the cell chamber as dictated by their corresponding flow rate). The reward in such a system can be measured as the global intensity difference and its episodic gradient between two cell population types. Furthermore, the transition probabilities (of markov decision process)

can be computed from observations made from the same assay in the database. These transition probabilities provide the enabling technology for an optimal policy (schedule). In general, such a policy can be expressed as dynamic programming, Monte Carlo methods, and temporal difference learning. Dynamic programming requires a model of cell response. Such a model can be hypothesized from the database. Presumably, as the database expands, models may become more accessible. Monte Carlo methods do not require a model, but they are not suitable for step-by-step incremental computation. On the other hand, temporal methods require no model and are fully incremental. The PI has extensive experience in expressing a policy based on dynamic programming [4, 13, 17]. However, all 3 methods are applicable to our research agenda. For example, Monte Carlo techniques can be used in one incremental step (or one episode) if a sample transition probabilities (not a complete one) exists. Finally, temporal differencing is the combination of Monte Carlo and dynamic programming, i.e., learning directly from raw experience without the model, and then updating estimates based in part on learned estimates.

5 Experimental Design

Experiments will be performed at the Life Sciences Microscope Resource (LSMR, <http://mhbbh1.lbl.gov/lsmr>) using our VSOM (Figures 6a-g). This Zeiss Axiovert 135 H/DIC inverted microscope is used for transmitted light (phase and DIC) and multicolor fluorescence microscopy. It is equipped with a computer controlled xy scanning stage (Figure 6b), z-axis stepping motor (Figure 6f), and a six position filter wheel (Figure 6d). A 12-bit Xillix CCD camera (Xillix Technologies, Vancouver, BC) containing a Kodak KAF-1400 CCD chip (1317x1035 pixels, 7x7 micron pixel size) will be used for these studies (Figure 6a). This camera has a readout rate of 8 MHz (approximately four full size images per sec). The intensified video camera (Model CCU-84, Pulnix America, Inc. and robotic arm (Model MP-185 Motorized Huxley-Wall Type Micromanipulator from Sutter Instrument Co., Novato, CA) used for our automated DNA microdissection work [11] can be seen in Figures 6e and 6g, (respectively).

For the work proposed here, we will use a recently acquired (Peltier) temperature controlled microperfusion chamber (PDMI-2 open chamber with TC-202 Bipolar temperature controller, Harvard Apparatus/Medical Systems Research Products, Holliston, MA) (See Figure 7, bottom right). We have also recently acquired one computer-controlled dual-syringe pump (Pump-33, Harvard Apparatus/Medical Systems Research Products, Holliston, MA) (See Figure 7, top left). The inverted design of our microscope allows perfusion of living cells, with immobilized cells imaged from below. An oil-immersion objective can be seen under the microscope coverslip in Figure 6h. Cells may be grown in 35mm Petri dishes or grown on circular coverslips and viewed from below. A cell chamber with a circular coverslip base is seen disassembled in Figure 7 (bottom left). With this inverted microscope design, it is possible to switch from fluorescence to transmitted light detection (phase or DIC) and verify cell locations and morphology. This is achieved with a computer controlled transmitted light shutter (Figure 6c). A computer controlled epifluorescence shutter is also available in the filter wheel (Figure 6d). VSOM operation of the system (control of shutters, filter wheel, xy stage, z-axis motor, Xillix camera) will be soon be automated via a software control panel (i.e., a Java-based graphical user interface or GUI).

5.1 Mitochondrial Membrane Potential and Rh123

It has recently been recognized that mitochondria play a central role in the regulation of programmed cell death, or apoptosis [7]. Changes in the mitochondrial membrane potential occur during the early

stages of apoptosis. Mitochondrial defects also occur in cancer [25]. Most carcinoma-derived cell lines accumulate and retain this dye much more than do normal epithelial cells [21], and this includes the human breast cancer cell line MCF-7 [5]. The primary factor for selective accumulation and retention is the higher mitochondrial membrane potential in these cancer cell lines [5].

There are several advantages in choosing Rh123 for initial VSOM studies. Rh123 is known to localize in the mitochondria of cells, the mechanism of uptake is well understood, and many agents are available which modulate its uptake and retention [27]. In addition, the ability to take up Rh123 is a reliable indicator of cell health and viability [2], it is highly fluorescent, and its uptake can be monitored at the single cell level using fluorescence microscopy. It has often been used as a marker for multi-drug resistance (MDR).

Kinetic studies with other rhodamine dyes such as tetramethyl rhodamine ethyl ester (TMRE) have demonstrated that Rh123 has significant, non-Nernstian retention properties, because it is not as easily washed out of mitochondria as TMRE [6]. Additionally, the negatively charged compound TPB (tetraphenylborate) was shown to accelerate cationic dye permeation, probably by a complicated mechanism. We will include TPB exposures in some of our VSOM assays. It is likely that the non-Nernstian components of Rh123 retentions will contain a great deal of cell-type specific information.

5.2 Dynamics of MF VSOM experiments

Real-time experiments will be performed on separate, physically separated populations (multiple fields) of cells. Cells will be grown on microscope coverslips or in 35mm Petri dishes. A schematic of a multi-field VSOM experiment is presented in Figure 8. Several images will be acquired for one cell type on one half of the coverslip (gray boxes labeled 1 and 2 in Figure 8), and then the xy stage will bring the other half of the coverslip over the microscope objective for imaging the second cell type (gray boxes 3 and 4). The system will then return to the same fields of view on the opposite side of the coverslip, detect the same cells, and obtain the new fluorescence intensity for each cell. This side to side and field to field motion will continue throughout the experiment. At several locations on the coverslip, and at each time point, both a transmitted light image and a fluorescence image will be acquired. The boundary of each cell will be determined from the transmitted light image (phase contrast), and the amount of Rh123 in each cell will be determined from the fluorescence image. Both transmitted and epifluorescence shutters will remain closed except when images are being acquired. There will be no physical barrier between the two sides of the coverslip. Autofocusing will be performed. An example of Rh123 stained immortalized human mammary epithelial cells (A1L5BR) is shown in Figure 9.

Four or more computer-controlled syringe pumps will introduce Rh123 and/or other compounds into the cell chamber (Figure 8). By controlling the rates of perfusion of each syringe separately, a wide range of concentrations can be introduced into the cell chamber. For example, syringe A could contain a very concentrated Rh123 solution that can be diluted with buffer from syringe B (Figure 8). Buffer only from syringe B could be delivered for wash-out cycles.

Figure 10 and Table 11 (Figure 11) illustrate the type of time-dependent response curves that are expected from typical VSOM baseline experiments. The assay described in Figure 11 and illustrated schematically in Figure 10 was constructed by referring to published reports that compare the uptake and retention of Rh123 in "normal" epithelial cells (CV-1) relative to "typical" human carcinoma epithelium cells (MCF-7) [5]. The responses reported in these comparative studies were: Rh123 uptake and retention as a function of high potassium (137mM KCl, 3.6 mM NaCl), low potassium (137 mM NaCl, 3.6 mM KCl), temperature, and valinomycin exposure. Responses due to nigericin/ouabain

were also studied. Several striking differences were observed between normal and carcinoma cells. Most of the differences observed were attributed largely to differences in mitochondrial membrane potential. Although we do not expect to see exactly the same results as these authors reported, VSOM assays that target the mitochondrial are likely to reveal differences in the mitochondria physiology of our model cell systems. We will use KBMF VSOM assays to identify and optimize specific aspects of mitochondrial physiology that discriminate between cell types and predict doxorubicin sensitivity. Successful demonstration of these preliminary KBMF-VSOM assays will give us valuable insights into the strengths and weaknesses of this technology and will aid the future development of more complex KBMF-VSOM assays

5.3 Model Cell Systems

MCF-7 Model System: The MCF-7 (DS) and MCF-7adr (MDR) cell lines are an ideal model system for VSOM system development. In this model system, two fluorescence assays for drug response/multi-drug resistance are already available. These two assays are complementary and allow one to identify cell types based the retention of fluorescence dyes (calcein-AM and Lysotracker-Blue, Green, or Red) during perfusion experiments. In this model system, cells that retain calcein are drug-sensitive (DS) and lack the ability to pump out calcein. This retention of calcein (green fluorescence) is a good marker for doxorubicin cytotoxicity. On the other hand, the MDR cells in this model system possess acidified vesicles and will retain Lysotracker-Red (LT-R, red fluorescence). It has been shown that overcoming a MDR (MCF-7adr) cell's ability to pump out calcein or overcoming an MDR (MCF-7adr) cell's ability to sequester LT-R in acidified vesicles (lysosomes) are both excellent surrogate markers for doxorubicin sensitization and demonstrate the potential of VSOM fluorescence assays. We will test these cells using the Rh123 assay and attempt to make correlations across channels.

HMEC Model Cell System: The HMEC lines have been developed here at LBNL by Dr. Martha Stampfer and have been extensively characterized by our collaborator, cancer biologist Dr. Paul Yaswen (Stampfer and Yaswen, 1994). We will develop VSOM fluorescence assays that distinguish between normal finite lifespan, immortalized, and tumorigenically transformed human mammary epithelial cells (HMECs) (Stampfer and Yaswen, 1994). In addition to screening these three cell lines with currently available assays (calcein-AM/verapamil and lysotracker/monesin), we will perform Rh123 assays in a separate channel and try to make correlations across channels.

6 Milestones

Year 1: Complete integration of all system components that include (i) a specifically designed GUI, (ii) on-line image analysis software, (iii) database integration for offline analysis, (iv) effective visualization of cell responses in the model system, and (v) development of offline and online learning techniques. Demonstrate this system to other researchers and DOE program managers remotely using the architecture developed as a part of DOE2000 program.

Year 2: Complete integration and testing of offline and online learning algorithms. Collect data, populate the database with baseline assay schedules. Refine the database by altering stimuli and environmental conditions. Demonstrate successful correlations between observed mitochondrial physiological responses and doxorubicin sensitivity.

7 Budget Explanation

The proposed budget includes 3 units of computer controlled syringes to be acquired (currently, one unit has been purchased).

B. Parvin (0.25 FTE) will be the project PI, where he will have overall project responsibility. He will develop, integrate, and test proposed learning algorithms for the system. He will review all design and implementation of imaging and software component as they will be integrated. He will be responsible for demonstration of the proposed system. He will also coordinate publications of research papers for the project.

G. Cong (0.25 FTE) will be responsible for integration, testing of the imaging and database components. He will implement and modify the GUI as needed.

D. Callahan (0.4FTE) is the project Co-PI, and will be responsible for the design, implementation, and execution of VSOM fluorescence assays. He will be responsible for protocols involving cell biology and cell culture. He will specify the GUI, and populate the database with cell responses. He will execute the real-time experiments that refine the VSOM assays in the database, and will also conduct the experiments that search for differences between physically separated cell populations. He will focus on the biomedical aspects of the project and attempt to rapidly obtain important biological results.

References

- [1] J. Besag. On the statistical analysis of dirty pictures. *Journal of Royal Statistical Society B*, 48(3):259–302, 1986.
- [2] L.B. Chen, M.J. Weiss, S. Davis, R.S. Bleday, J.R. Wong, J. Song, M. Terasaki, E.L. Shepherd, E.S. Walker, and G.D. Steele. Mitochondria in living cells: effects of growth factors and tumor promoters, alterations in carcinoma cells, and targets for therapy. *Cancer Cells*, (3):433–443, 1986.
- [3] G. Cong and B. Parvin. Model based segmentation of nuclei. In *Proceedings of the Conference on Computer Vision and Pattern Recognition*, 1999.
- [4] G. Cong and B. Parvin. Model based segmentation of nuclei. In *Journal of Pattern Recognition*, 1999.
- [5] S. Davis, M.J. Weiss, J.R. Wong, T.J. Lampidis, and L.B. Chen. Mitochondria and plasma membranes potentials cause unusual accumulation and retention of rhodamine 123 in human breast adenocarcinoma-derived mcf-7 cells. *J. Biol. Chem.*, (260):13844–13850, 1985.
- [6] D.L. Farkas, M.-D. Wei, P. Febroriello, J.H. Carson, and L.M. Loew. Simultaneous imaging of cell and mitochondrial membrane potentials. *Biophys. J.*, (56):1053–1069, 1989.
- [7] D.R. Green and J.C. Reed. Mitochondria and apoptosis. *Science*, (281):1309–1312, 1998.
- [8] Y. Jin, Jayasooriah, and R. Sinniah. Clump splitting through concavity analysis. *Pattern Recognition*, 15:1013–1018, 1994.
- [9] O. Monga, S. Benayoun, and O. Faugeras. From partial derivatives of 3d density images to ridge lines. In *Proceedings of the Conference on Computer Vision and Pattern Recognition*, pages 354–359, 1992.
- [10] S. Ong, H. Yeow, and R. Sinniah. Decomposition of digital clumps into convex parts by contour tracing and labelling. *Pattern Recognition Letters*, 13:789–795, 1992.
- [11] B. Parvin, D. Callahan, W. Johnston, and M. Measter. Visual servoing for micro manipulation. In *Int. Conference on Pattern Recognition*, Austria, 1996.
- [12] B. Parvin and et al. Telepresence for in-situ microscopy. In *IEEE Int. Conference on Multimedia Systems and Computers*, Japan, 1996.
- [13] B. Parvin, C. Peng, W. Johnston, and M. Maestre. Tracking of tubular molecules for scientific applications. *IEEE Transactions on Pattern Analysis and Machine Intelligence*, 17:800–805, 1995.
- [14] B. Parvin, D. Robertson, and W. Johnston. Visualization of volumetric structures from mr images of brain. In *AAAI Symp. on Application of Computer Vision to Medical Imaging*, 1995.
- [15] B. Parvin, J. Taylor, D. Callahan, W. Johnston, and U. Dahmen. Visual servoing for on-line facilities. *IEEE Computer Magazine*, 1997.
- [16] B. Parvin, J. Taylor, and G. Cong. A collaborative framework for distributed microscopy. In *IEEE High Performance Computing and Networking*, 1998.

- [17] B. Parvin and S. Viswanatha. Optimal grouping of line segments into convex sets. In *British Machine Vision Conf.*, 1995.
- [18] C. Potter and etal. Evac: A virtual environment for control of remote imaging instrumentation. *IEEE Computer Graphics and Applications*, pages 62–66, 1996.
- [19] Young S.J. and etal. Implementing collaboratory for microscopic digital anatomy. *Int. Journal of Supercomputer Applications and High Performance Computing*, pages 170–181, 1996.
- [20] M. Sonka, V. Hlavac, and R. Boyle. *Image Processing analysis and Machine Vision*. Chapman & Hall, 1995.
- [21] I.C. Summerhayes, T.J. Lampidis, S.D. Bernal, J.J. Nadakavukaren, K.K. Nadakavukaren, E.L. Shepherd, and L.B. Chen. Unusual retention of rhodamine 123 by mitochondria in muscle and carcinoma cells. *Proc. Natl. Acad. Sci.*, (79):5292–5296, 1982.
- [22] H. Talbot and I Villalobos. Binary image segmentation using weighted skeletons. *SPIE Image algebra and morphological image processing*, 1769:393–403, 1992.
- [23] J. Thirion. New feature points based on geometric invariants for 3d image registration. *International Journal of Computer Vision*, 18(2):121–137, May 1996.
- [24] J. Thirion and A. Gourdon. The 3d matching lines algorithm. *Graphical Models and Image Processing*, 58(6):503–509, 1996.
- [25] D.C. Wallace. Mitochondrial diseases in man and mouse. *Science*, (283):1482–1488, 1999.
- [26] W. Wang. Banary image segmentation of aggregates based on polygonal approximation and classification of concavities. *Pattern Recognition*, 31(10):1502–1524, 1998.
- [27] J.R. Wong and L.B. Chen. Recent advances in the study of mitochondria of living cells. *Advances in Cell Biol.*, (2):263–290, 1988.

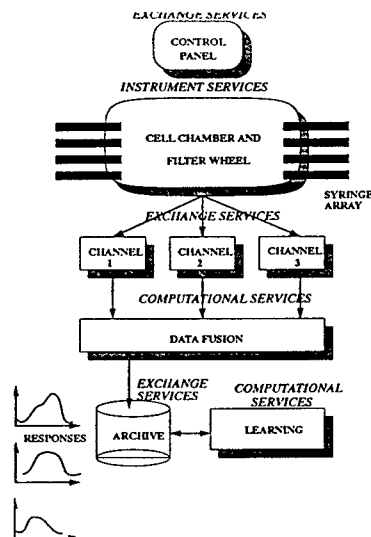


Figure 1: Interaction of various components in the knowledge based VSOM. The italic letters refer to services defined in the overall system architecture as shown in Figure 2.

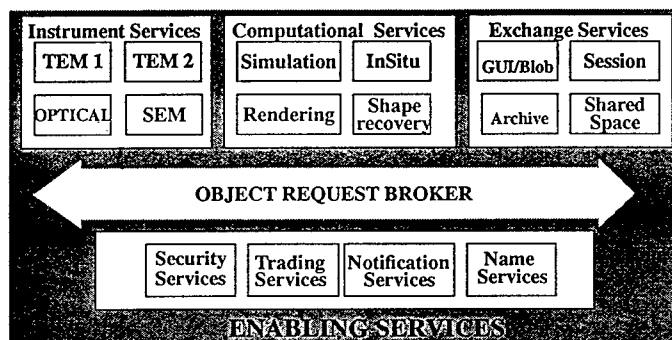


Figure 2: Interaction Between OMG defined Enabling Services and funded Services through the DOE2000 program.

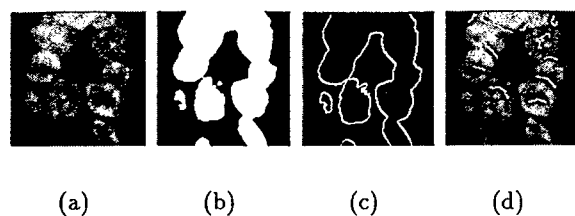


Figure 3: This example demonstrates that segmentation of nuclei with purely global or local operations is not feasible: (a) original image; (b) threshold image; (c) boundary of nuclei; and (d) local troughs.

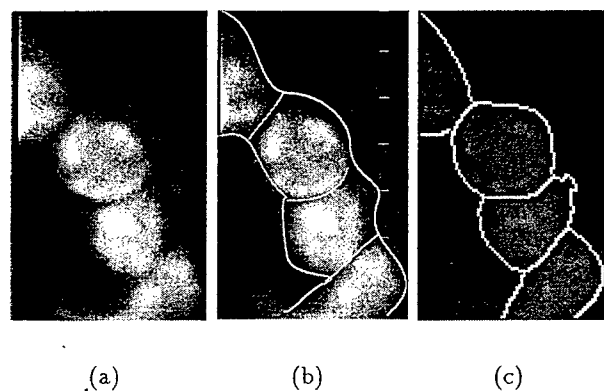


Figure 4: Segmentation results: (a) original image; (b) manual segmentation; (c) our results on segmentation of nuclei.

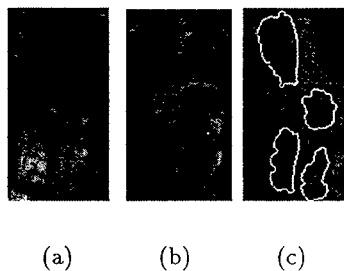


Figure 5: Multiple Channel data fusion for segmentation of nuclei: (a) DAPI image (blue channel); (b) Texas Red image (red channel); (c) segmentation results on FITC (green channel).

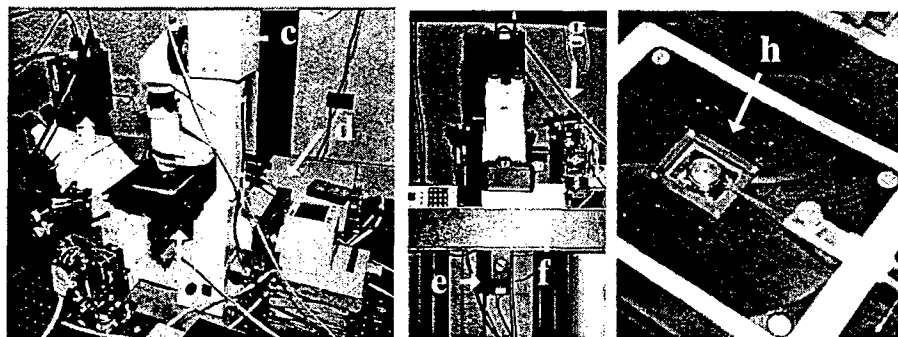


Figure 6: Components of VSOM

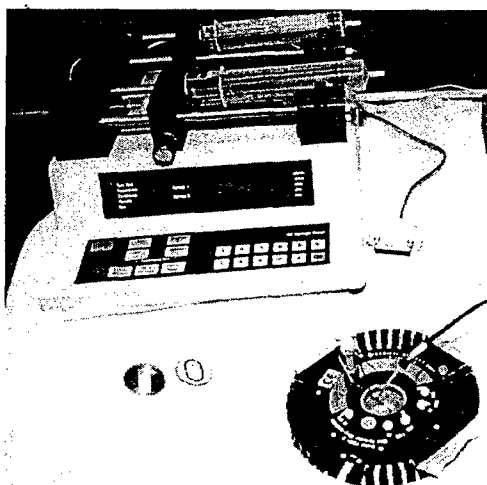


Figure 7: Pump chamber and its control system

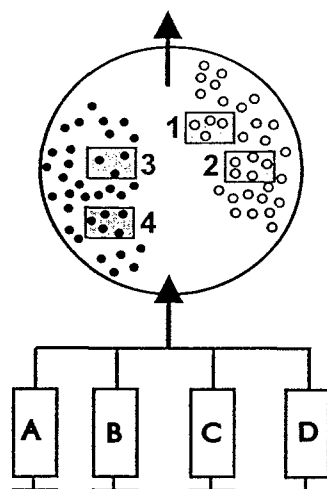


Figure 8: Schematic of multi-field VSOM

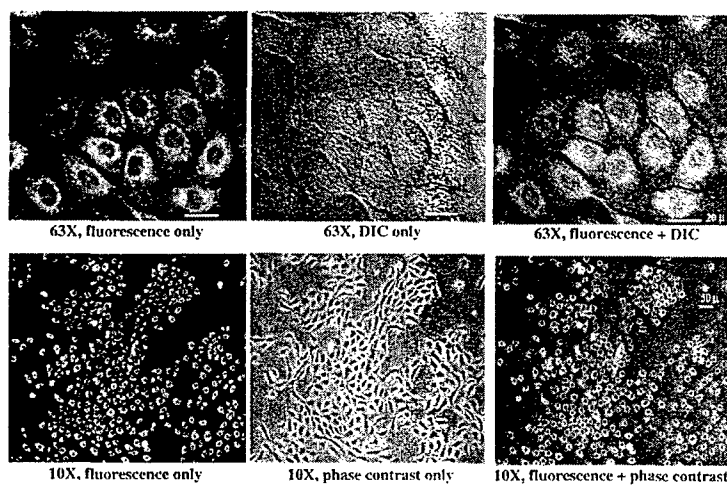


Figure 9: Cell images acquired under different imaging modalities

VSOM ASSAY BASELINE DATA EXAMPLE
5 Cell Responses shown (out of hundreds possible)
(Rh123, Valinomycin, High and Low K⁺)

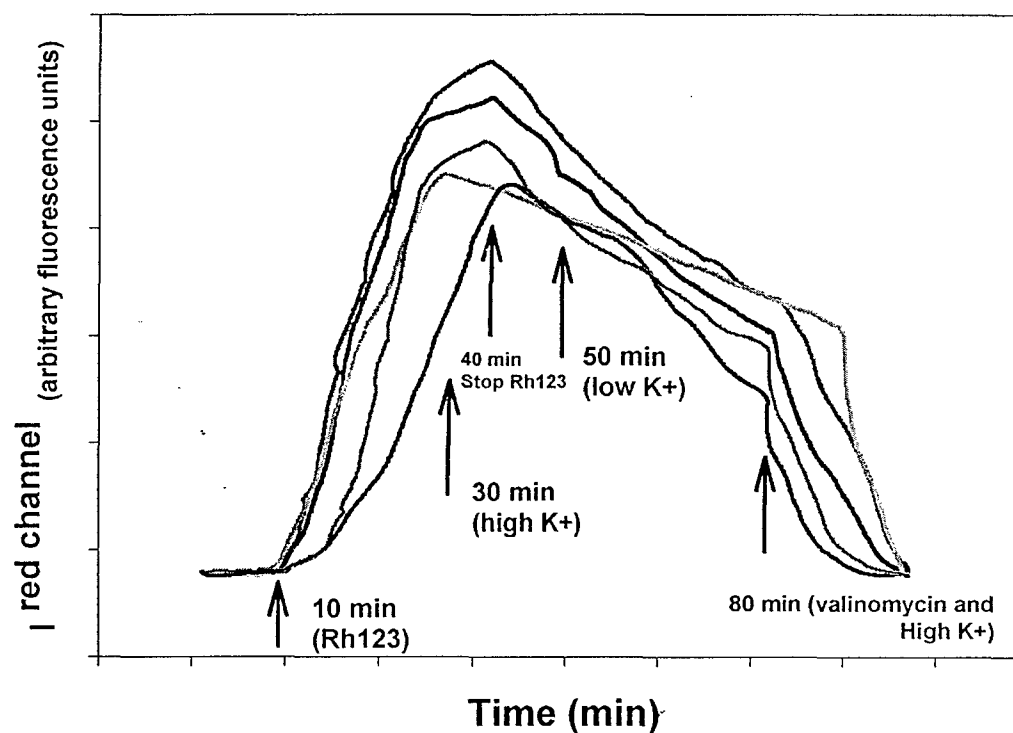


Figure 10: Cell responses containing information on mitochondrial physiology.

Phase 1: VSOM ASSAYS FOR BUILDING UP BASELINE CELL RESPONSES IN DATABASE

TIME (min)	ASSAY #X, Human Mammary Epithelial Cells: BaselineVSOM Assay for Loading DataBase: Keywords: Red, Rhodamine 123, Mitochondrial Membrane Potential, valinomycin, high/low K+, constant temp. 37 °C										
	Channel	RED									
	Compartment or Target	Syringe 01	Syringe 02	Syringe 03	Syringe 04	Syringe 05	Syringe 06	Syringe 07	Syringe 08	T (°C)	MORPHOLOGY (including Transmitted Light)
	NOTES	Media/Buffer (MCDB170 with low Na+, low K+)	Rh 123	K+ (high)	valinomycin		Na+ (normal, which is high)				partially confluent cells in isolated colonies, spread out, and touching
0	A422' cells passage 24, 1x10 ⁵ /60mm	cells in normal Na+, K+								37	
2	start buffer flow,	ON					ON			37	
10	rh123 perfusion	ON	ON				ON			37	
30	high K+	ON	ON	ON						37	
40	r123 washout	ON		ON						37	
50	low K+	ON					ON			37	
80	Valinomycin and high K+	ON		ON	ON					37	End Experiment when Fluor. is gone. Verify Morphology unchanged

Figure 11: Table 1

SC Program announcement title: "Imaging Gene Expression in Health and Disease"
LAB00-13

Title: **Automated Imaging System for Guiding
Antisense Compounds to Specific mRNA
Targets in Living Cells**

Co-PI: **Bahram Parvin, *Computing Sciences***
Address: M.S. 50B-2239
Lawrence Berkeley National Laboratory
1 Cyclotron Road
Berkeley, CA 94720

Telephone: 510-486-6203
FAX: 510-486-6363
Email: parvin@media.lbl.gov

Co-PI: **Daniel Callahan, *Life Sciences***
Co-PI: **Mary-Helen Barcellos-Hoff, *Life Sciences***
Co-PI: **Scott Taylor, *Center for Functional Imaging, Life Sciences***

Position of Co-PIs: Staff Scientist
Requested funding: Year 1 (\$387,131), Year 2 (\$393,471), Year 3(407,547)
Total (\$1,188,146)

Use of human subject: Yes
Use of vertebrate animals: None

PI Signature

Date:

Official Signature

Date:

Name: Horst Simon
Title: Division Manager
Phone: 510-486-7377
Fax: 510-486-4300
Email: HDSimon@lbl.gov

mg. 27, 2000

Contents

1	Specific aims	1
2	Narrative	1
3	Background and significance	3
3.1	Fluorescence microscope sensitivity and resolution	3
3.2	Previous collaborations and results	4
3.3	Sequestration of drugs in lysosomes	5
3.4	Previous studies in fluorescently labelled AS-ADNs	6
3.5	Visual servoing	6
3.6	Relation to other projects	7
4	Preliminary studies	8
4.1	System architecture	8
4.2	Segmentation of single-channel data	9
4.2.1	A regularized edge detector based on supremum	11
4.2.2	Tensor-based feature analysis	13
4.2.3	Geometric and texture model	14
4.3	Segmentation of multi-channel data	16
5	Research design and methods	17
5.1	Detailed segmentation	17
5.2	Feature based image storage	18
5.3	Learning from cell responses	19
5.3.1	Reinforcement learning	21
5.4	Experiments	22
5.4.1	VSOM experiments	23
5.4.2	Physiological and fluorescence assays for apoptosis in living cells	24
5.4.3	AS-ODN Delivery techniques	25

Abstract

We propose to image mRNA transcripts in real time in tissue culture and help develop antisense compounds, delivery systems, and signal amplification methods that will lead to radiolabeled antisense compounds suitable for real time medical imaging. Studies will be performed in parallel with our colleagues at the LBNL Center for Functional Imaging (CFI), who have submitted a companion grant entitled, "Strategies for Imaging Gene Expression with PET." In both proposals we will use the same three oligonucleotide sequences. We will target the same mRNA species coding for the bcl-2 protein, and we will use the same human breast cancer cell line, BT-474, as a model system. We propose to track fluorescently labeled antisense compounds within individual living cells, guide them to the appropriate target mRNA in the cell, and determine whether individual cells are affected in the manner predicted. Using digital imaging fluorescence microscopy, novel computational techniques, and bioinformatic tools, we will track the fluorescent antisense compound in one channel, while monitoring other cell responses, such as apoptosis, in separate channels. We propose to image the expression of bcl-2 at the mRNA level as a function of time, external cell stress, and antisense compound structure. We will correlate these observations with bcl-2 protein levels in each cell and the ultimate fate of each cell. We believe such experiments will provide detailed information on the biophysical properties of specific antisense compounds. This type of data acquisition will aid the intelligent design of antisense compounds useful for imaging gene expression with PET.

1 Specific aims

1. Aid the intelligent design of antisense compounds useful for imaging specific mRNA targets in living cells.
2. Collect and store detailed information on the biophysical properties of specific antisense compounds as it is guided to specific mRNA targets in the cytoplasm of living cells.
3. Construct an imaging system for automatic measurement of dynamic time varying expression of mRNA as a function of a particular antisense compound.
4. Develop and implement a policy for stepwise refinement and design of antisense compounds based on previously measured biophysical properties from the imaging system.

2 Narrative

The full potential of antisense oligodeoxyribonucleotides (AS-ODNs) has yet to be realized in living cells (in vitro) or in living tissue (in vivo). Successful demonstration of the use of fluorescently labeled AS-ODNs as real-time gene expression imaging agents in living cells in vitro will assist efforts to use AS-ODNs as selective agents for the perturbation of gene expression. In addition, data provided by our proposed experiments will be extremely valuable for the design and ongoing modifications of these agents by radiochemists, who seek to use these compounds as medical imaging agents in vivo. In our proposed fluorescence microscope studies on living cells, correlations will be made between specific chemistries and the observed behaviors of fluorescently labeled AS-ODNs. Often, fluorescently labeled antisense compounds are sequestered within non-cytoplasmic compartments of the cell (Leonetti et al., 1991 [20]; Thaden and Miller, 1993 [37]). By determining ways to release AS-ODNs from sequestration in intracellular compartments and induce redistributions within individual cells, we will learn a great deal about that compound's biophysical properties in the cell. The acquisition of this type of data will aid the intelligent design of AS-ODNs useful for imaging specific mRNA targets in living cells. Specifically, our experiments will help radiochemists decide which AS-ODN modifications and delivery methods target mRNA in the cytoplasm most effectively.

We believe we have important new technology and the interdisciplinary team necessary to make progress on these difficult technical problems. We propose to use visual servoing optical microscopy (VSOM) to automatically "guide" specific AS-ODNs to specific mRNA targets in the cytoplasm of living cells and observe the subsequent cellular response on a cell-by-cell basis. Visual servoing (a term from the field of robotic vision research) refers to dynamic control of experimental parameters based on automatic interpretation of the information contained in a stream of digital images. Our novel image processing algorithms give us the ability to automatically detect the amount of fluorescently labeled AS-ODN in the individual compartments of individual living cells in real time. Advances in the selective fluorescence staining of living cells, including the various intracellular compartments in living cells, together with advances in multicolor, digital imaging fluorescence microscopy will allow us to identify, in real time, the subcellular compartment(s) where a given

fluorescently labeled AS-ODN is located. We currently have access to a large selection of biological and chemical agents that can perturb these compartments specifically and, for example, collapse the compartmental membrane potentials that are required for proper function. Using VSOM and a set of computer-controlled perfusion pumps, we will perturb living cells in very specific ways as we continuously monitor physiological responses and correlate these responses with the movement of fluorescently labeled AS-ODNs between different compartments of the cell. Our experiments will provide details on the biophysical properties of each AS-ODN as it moves into and within the cell in response to computer-applied stimuli. We try to explain, using biophysical principles, why the compounds partition into various compartments, and predict how the compounds should be altered to prevent such problems in the future.

As documented in the extensive *in vitro* literature on this subject, fluorescently labeled AS-ODNs rarely enter the cell via simple diffusion from solution phase through the plasma membrane to an mRNA target in the cytoplasm (Shoji et al., 1991 [35]) (Thierry and Dritschilo, 1992 [38]) (Thaden and Miller, 1993 [37]). In fact, even when AS-ODNs are microinjected into the cytoplasm, they can rapidly migrate to the nucleoplasmic (nuclear) compartment. This precludes their use as a means of quantifying copy number of specific mRNA molecules in the cytoplasm. Examples of this behavior have been reported for phosphodiester (PD), phosphorothioate (PT), and methylphosphonate (MP) forms of the same fluorescently tagged 28-mer (Chin et al., 1990 [10]). This and several other technical difficulties are associated with the use of fluorescently labeled AS-ODNs for the detection or modification of gene expression. True antisense activity requires nuclease resistance, cellular uptake, and hybridization to a specific target by Watson-Crick base pairing. Other, non-antisense (non-sequence-specific) mechanisms of action by AS-ODNs are often observed (Yaswen et al., 1993 [43]). However, the exquisite sequence specificity of Watson-Crick base pairing and the tremendous sensitivity of fluorescence signal detection motivate us to overcome these problems.

One problem that must be overcome is the sequestration of AS-ODN in lysosomes. Lysosomes are acidic compartments of the cell containing a wide range of enzymes for degradation of unwanted or toxic cellular materials. Using VSOM and computer controlled perfusion pumps, we propose to track fluorescently labeled AS-ODNs within individual living cells, automatically apply the proper agent(s) at the proper concentration for the proper length of time, and in this way release the fluorescently labeled AS-ODN from cellular lysosomes. To assist us in this effort, we will develop a bioinformatics database that will record the specific perturbations applied and the resulting effect on the intracellular redistribution of fluorescently labeled AS-ODNs within the cells. Such a database will become extremely valuable for the design and ongoing modifications of these agents by radiochemists, especially as correlations are made between specific chemistries and the observed behaviors of the AS-ODNs. We believe the ability to perform data mining and visualization of multidimensional data representing actual intracellular behavior of these compounds will allow us to rapidly identify critical biological determinants of compound localization, specificity, and toxicity.

Other problems to be overcome are (a) the tendency of AS-ODNs to bind in a nonspecific manner to proteins in the nucleus and accumulate there instead of binding to mRNA targets in the cytoplasm, and (b) failure of some AS-ODNs to elicit the desired response on gene expression after they successfully reach the cytoplasm. Thus, in addition to using VSOM to guide fluorescently labeled AS-ODNs to the appropriate target mRNA sequence in the cytoplasmic compartment of

the cell, we will also use it to determine whether individual cells are perturbed in the manner predicted by the mRNA sequence targeted. Using multicolor (or, "multichannel") digital imaging fluorescence microscopy, we will monitor the fluorescent AS-ODN in one color, or "channel", while we simultaneously monitor other physiological cell responses in separate channels. In this way, we hope to successfully image expression (and alterations in expression) of specific genes at the mRNA level as a function of time, external cell stimulation, and AS-ODN chemical structure. Specifically, we will verify alterations in gene expression by quantifying alterations in bcl-2 protein levels in two different ways (i) by observing alterations in apoptosis in stressed cells (ii) by returning to the same field of cells after VSOM experiments and observing levels of bcl-2 protein on a cell-by-cell basis using indirect immunofluorescence.

3 Background and significance

3.1 Fluorescence microscope sensitivity and resolution

Recently, it has been demonstrated that a single fluorescent molecule can be detected in aqueous solution at room temperature (Nie et al., 1994). This was done in real time, without statistical analysis on a moving, single-chromophore molecule (fluorescein). Single DNA bases labeled with one fluorescent tag were also observed. To achieve this, a laser confocal microscope with a laser probe volume (or resolution element) of 0.5 femtoliters (5.0×10^{-16} liters) was used with 10 μ L of 3.3×10^{-16} M fluorescein sandwiched between two 0.13 mm thick microscope coverslips. The excitation wavelength was 488nm. A photon-counting Si avalanche photodiode was used as a detector, with a high numerical aperture (NA 1.3) microscope objective lens, and as few optical elements as possible in the optical path. The pH of the solution was 12, and contained 100mM mercaptoethanol to prevent photobleaching by scavenging oxidative species. Fluorescein is a pH sensitive molecule which is very photostable with a high quantum yield under these conditions. Although it was not noted by the authors, coverslips are often chemically treated before these types of experiments in order to remove fluorescent impurities. The authors did note their ability to detect low levels of fluorescent impurities in the aqueous solution.

In this proposal, we will not attempt to detect single molecules of AS-ODNs labeled with a single fluorescent tag for the following reasons. Living cells have a certain inherent level of autofluorescence that can obscure the fluorescence signal from single molecules of antisense compounds labeled with a single fluorescent probe. In addition, it is not appropriate to use intense laser illumination or anti-photobleaching agents when studying living cells. The autofluorescence of one entire cultured NIH 3T3 fibroblast excited at 488nm has been estimated to be equivalent to approximately 34,000 fluorescein molecules, on average. The major sources of autofluorescence in mammalian cells are the flavin coenzymes (FAD and FMN, absorption/emission 450/515nm) and reduced pyridine nucleotides (NADH, absorption/emission 340/460nm). Other biomolecules are also fluorescent, including nicotinamide, adenine nucleotides, riboflavin, porphyrins, and aromatic amino acids such as tryptophan. One can adopt strategies to minimize the contributions of this intracellular background fluorescence. For example, NADH is concentrated in cellular mitochondria; thus, one can avoid making fluorescence measurements in areas of the cell occupied by a mitochondrion. This is

not difficult when performing measurements on living cells (grown on microscope coverslips) using a high NA, oil-immersion microscope objective, where the 2D diffraction-limited resolution interval is approximately 0.2μ . The mitochondrial "compartment" is one cellular compartment we will be monitoring in our experiments.

3.2 Previous collaborations and results

Our group has demonstrated our experience with the detection, manipulation and microdissection of single DNA molecules (Parvin et al., 1997) (included in appendix) [30]. As discussed above, special experimental conditions must be maintained during these experiments. For example, in our DNA microdissection experiments, DNA molecules were stretched and oriented by flow, then fixed in place on a coverslip that had been specially cleaned to decrease fluorescence background. This allowed us to search for stationary fluorescence signal in a specific focal plane (near the coverslip), and no fluorescence signal existed above or below this focal plane that could obscure the signal. In addition, the signal pattern was distinct: linear rods, all of equivalent length, oriented in the same direction. Before illumination, the molecules were layered with a glycerol solution containing a fluorescent dye and an anti-photobleaching compound. The fluorescent dye molecule used for staining (YOYO-1, Molecular Probes, Eugene, OR) bound once every 2-4 base-pairs, so that many fluorochromes were concentrated in a single pixel of the digital image. In addition, the fluorescence of this dye is greatly enhanced when it binds to DNA, so that unbound molecules contribute little to the fluorescence background. In mRNA fluorescence microscope studies, "tracks" of mRNA have been detected suggestive of a transport route from the site of transcription to the nuclear membrane after being induction of the gene by extracellular stimulation (Raap et al., 1991) [33]. Others have reported specific, sensitive, and quantitative detection of mRNA for the measurement of gene expression in individual cells using fluorescence microscopy, in situ hybridization protocols and highly fluorochrome labeled gene probes (Pachmann et al., 1991 [25]). Using a microscope photometer, it was possible to detect between 1 and 20 fluorochrome labeled gene probes above the autofluorescence of fixed cells. In addition, RNA tracks and RNA splicing have been observed in mammalian interphase nuclei after induction, with unspliced transcripts accumulating in one or two discrete sites in the nucleus.

We have demonstrated that single copies of viral genomes inserted into specific sites on human chromosomes can be detected and quantified in metaphase chromosome spreads (Callahan et al., 1992 [8]) (included in appendix). In addition, we have a great deal of experience with quantitative fluorescence microscopy (Callahan et al., 1999 [6]) (included in appendix), and time-lapse videomicroscopy (Barcellos-Hoff, 1992 [4]) of living cells, 3D fluorescence microscope studies (Lesko et al., 1995 [21]) and the use of fluorescence standards (Lesko et al., 1989 [22]) (Kaplan and Picciolo, 1989 [19]). We have also published circular dichroism (CD), NMR, and fluorescence spectroscopy studies of the impressive ability of ODNs to adopt a wide range of conformations (Callahan and Hooker, 1987 [7]; Callahan et al., 1991 [9]; Kan et al., 1991 [18]) even when the ODNs are extensively altered, as in the case of oligonucleotides with methylphosphonate backbones. However, this plasticity of structure comes at a price, because modified AS-ODNs can adopt unforeseen conformations in solution, and bind to unforeseen targets (Yaswen et al., 1993 [43]). In addition, mRNA targets themselves can adopt conformations that make the complementary target sequence inaccessible.

3.3 Sequestration of drugs in lysosomes

Drug delivery problems has unpredicted side effects and are not unique to antisense compounds. These technical difficulties are well known to developers of new drugs, and drug delivery systems. Only the first generation of ODNs are currently in clinical trials, and the insights gained from these trials will lead to chemical modifications that will improve the stability, potency, and safety of AS-ODNs (Temsamani and Guinot, 1997 [36]). Analogous problems have been discussed in one of our recent publications where the amount, distribution pattern, and site of intracellular sequestration were identified in a human glioma cell line for the fluorescent, boronated protoporphyrin (BOPP) (Callahan et al., 1999 [6]) (included in appendix). BOPP is currently a candidate for both boron neutron capture therapy (BNCT) and photodynamic therapy (PDT) of glioblastoma multiforme (GBM). We were able to identify several factors that influenced the uptake, sequestration and retention of BOPP in living cells. Using lysosome or mitochondria-specific fluorescent probes, we were able demonstrate that BOPP accumulated in the lysosomes of human glioma cells *in vitro*, and not in the mitochondria, as reported for C6 rat glioma cells. We were also able to determine that BOPP uptake was LDL-receptor dependent, and was also dependent on the amount of lipoproteins in the medium. This uptake and subcellular trafficking behavior is analogous to that seen for a variety of fluorescently labeled, modified AS-ODNs that demonstrate a vesicular subcellular distribution suggestive of an endosomal/lysosomal compartmentalization after endocytic uptake (Gewirtz et al., 1998 [17]) (Shoji et al., 1991 [35]) (Thierry and Dritschilo, 1992 [38]) (Thaden and Miller, 1993 [37]).

In regards to BOPP, it should be noted that subcellular localization of porphyrins is determined by their different functional groups. Using fluorescence microscopy, researchers have been able develop structure-localization relationships for porphyrins (Woodburn et al., 1991). Porphyrins with predominantly cationic side chains were seen to localize in mitochondria, while those with a more ionic character tended to localize in lysosomes. A third class of compounds showed general cytoplasmic staining. It is of interest to note that BOPP appears able to alter its site of intracellular location depending on the cell type under study and the intracellular environment (i.e., rat glioma versus human glioma cell lines) (Callahan et al., 1999). Structure-activity studies have been performed that attempt to express physicochemical properties of such compounds numerically (e.g., electric charge, pK_a , hydrophilicity-lipophilicity, conjugated bond number, etc) and employ fluorescence microscopy to identify the favored site of intracellular localization (i.e, lysosomes with low internal pH or mitochondria with high internal pH) (Rashid and Horobin, 1990; Rashid et al., 1991). It was noted that inhibition of the lysosomal proton pump could lead to release of acidotropic probes, as these probes diffuse out of the lysosome as its internal pH rises. In addition, for both lysosomal and mitochondrial specific fluorescence probes, it was noted that the proper balance between pK_a , charge, lipophilicity and hydrophilicity was critical for the outcome of the probe- cell interaction. This is reminiscent of current attempts to optimize AS- ODN hydrophobicity and charge by creating hybrid ODNs which contain backbones composed of mixtures of negatively charged phosphorothioate linkages and nonpolar methylphosphonate linkages (Temsamani and Guinot, 1997 [36]).

One important factor of visual servoing (to be followed in this section) will be the exchange of buffers (and compounds) via computer-controlled perfusion pumps. These various extracellular

buffers will be perfused into a temperature controlled microperfusion chamber, and the responses of hundreds of living cells will be monitored and analyzed in real time.

3.4 Previous studies in fluorescently labelled AS-ADNs

We are particularly interested in previous studies that have demonstrated the differential effects of environmental parameters and delivery systems on the intracellular distribution and trafficking of fluorescently tagged AS-ODNs with different backbone compositions. For example, it has been demonstrated using fluorescently tagged and ^{32}P labeled PD and MP (methylphosphonate) AS-ODNs that changes in the uptake and intracellular trafficking of PD and PT (phosphorothioate) ODNs are different than those seen for MP ODNs. This has been observed by varying external parameters such as temperature, pH, or presence of excess unlabeled ODN are varied. In fluorescence microscope studies using $CH^R C5$ cells (multidrug resistant Chinese Hamster Ovary Cells), it was possible to inhibit the uptake of ^{32}P labeled PD ODNs using excess unlabeled PD ODN, but it was not possible to inhibit the uptake of fluorescence tagged MP ODN using excess unlabeled PD ODN. In addition, when the external pH was decreased to pH 5.5, an intracellular pH sensitive probe (BCECF) indicated that the intracellular pH rapidly (within 2 min) decreased to pH 5.7 (Shoji et al., 1991 [35]). Once again, a difference in ODN uptake was observed, with uptake of PD-ODN being completely inhibited, while uptake of MP-ODN was not inhibited. In both cases, MP-ODN was seen to localize in the endosomal/lysosomal compartment. However, others have reported that when MP-ODNs are directly injected into the cytoplasm of several different cell types, they are rapidly accumulated in the nucleus, as are PD and PT ODNs (Chin et al., 1990 [10]; Leonetti et al., 1991). Thus, charge effects of the ODN backbone do not alter the localization of microinjected ODNs into the cell nucleus. However, the 3D intranuclear distribution observed is affected by the chemistry of the internucleoside linkages. For example, PD, and to a lesser extent, PT ODNs colocalize with small nuclear ribonuclear proteins (snRNPs), while MP ODNs colocalize with concentrated regions of genomic DNA (Chin et al., 1990). The nature of the fluochrome used for labeling does not alter the characteristics of nuclear localization (Leonetti et al., 1991). More detailed studies of the in vitro cellular pharmacokinetics of three types of ODNs (including an end-capped, or capPT ODN) have been performed using a liposomal delivery system (Thierry and Dritschilo, 1992 [38]). In these studies, cellular uptake, intracellular stability, efflux rate and intracellular localization were assessed for fluorescently tagged version of these PD and PT ODNs with and without liposome encapsulation. Cellular penetration of fluorescence tagged PT ODNs was greatly facilitated by the use of liposomes created using the method of minimum volume entrapment (MVE). In addition, PD ODNs were protected from degradation (for up to 5 days) in cell culture medium when encapsulated in liposomes.

3.5 Visual servoing

Visual servoing aims at automated manipulation of instrument control parameters based on automatic image interpretation. A simple example of visual servoing is autofocusing for an optical microscope, where the microscope objective is moved automatically along the Z direction to compensate for defocus. In this context, defocus is quantified, and the Z-axis is moved under computer

control for optimum focus. A more complex example includes drift compensation or motion detection as a function of external stimuli for dynamic experiments [27]. This system (currently in use at LBNL) not only detects motion in the scene, but also records and logs pertinent attributes (e.g. size, shape, response, direction of motion). This information is then compared to attributes of similar events that are stored in a database. Another benefit of this level of automation is that these dynamic experiments can be conducted remotely over the wide area network [30]. Automatic drift compensation provides a stationary view of the experiment and eliminates the need for high speed network and/or quality of service.

The proposed research requires close collaboration between biophysicists, chemists, biologists, and computer scientists. The investigators, listed in this proposal, have a proven track record of scientific collaboration [26, 30, 31]. From a computer science perspective, the following components are needed to achieve the research objectives: (1) computer control of the microscope and syringes; (2) detailed segmentation of cells imaged on single or multiple channels; (3) automated annotation of subcellular responses as a function of a compound and its various attributes; (4) offline correlation, clustering, and learning techniques for constructing a model of how various compounds target a specific compartments; (5) online learning techniques for dynamic control and estimation of a policy (schedule) for freeing a compound from a site and guiding it (in a weak sense) to a specific compartment in the cell. The interaction between various system components are shown in Figure 1.

3.6 Relation to other projects

The computational aspect of this proposal will leverage four research programs that are funded through DOE-MICS (*DOE2000 Material and MicroCharacterization Collaboratory*), DOE-OBER (*An Imaging Bioinformatic System for Studying the Effect of Low Dose Radiation*), a DOD breast cancer research grant (*Visual Servoing for Anti Cancer Drug Uptake*), and an LDRD grant to for feature based image representation. The first grant provides the basis for remote collaborative microscopy, seamless data acquisition, and instrument control. The second grant provides the imaging bioinformatic component for annotating data and images and the needed core technology for segmentation of cells. The third grant provides a platform for VSOM that will be available at the end of the current fiscal year. The fourth grant focuses on novel algorithm development for motion tracking and modeling. Our current VSOM grant (funded by the DOD breast cancer research) does not include: (1) database component and population of that database with cell responses; (2) learning, clustering, and data mining in that database; (3) real-time analysis and manipulation of physically separated population of cells; (4) detailed segmentation of subcellular compartment with or without using data fusion technique (images acquired on multiple channels); (5) incorporation of large number of syringes; and (6) study of mitochondrial physiologies or other compartments in the cell. We are confident that by coupling this proposal with our currently funded programs, a new biomedical technology can be demonstrated.

Section 3 provides an overview of background and significance. Section 4 provides a review of core technology for segmentation of cells. Section 5 outlines methods and deliverables.

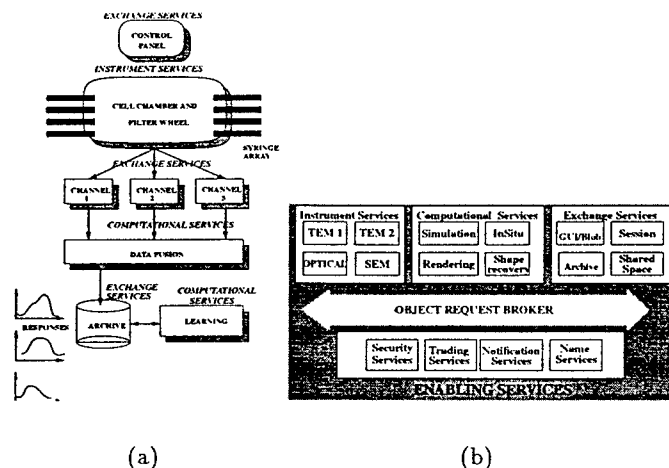


Figure 1: Interaction of various components in the knowledge based VSOM. The italic letters refer to services defined in the distributed architecture (part b funded by DOE-MICS).

4 Preliminary studies

The keys to automated analysis of mRNA expression are subcellular partitioning of cells (segmentation), on-line dynamic and trajectory analysis of antisense compounds, effective storage of computed features, and large scale population studies. Our group has developed a number of novel algorithms to enable measurement of gene expression in different compartments of a cell. These techniques are constantly being refined and updated with new features and capabilities. In sections 4.2 and 4.3, a brief overview of these novel algorithms are presented. One class of algorithms focuses on segmentation of images derived from a single channel. The other class focuses on segmentation of images derived from multiple channels.

This section provides a summary of the system architecture and its current features and then outlines the details of segmentation techniques.

4.1 System architecture

The current functional architecture for visual servoing is shown in Figure 2. It consists of an image-acquisition module, image-analysis module, servoing, and archive. The image-acquisition module provides the means for time-lapsed high resolution video microscopy with six excitation filters. This module has a recipe manager to allow either manual or preprogrammed capture of images at different temporal and excitation frequencies. The analytical module has a pool of unique segmentation algorithms that provide a feature-based summary of images based on an attributed graph model. Accordingly, each node in the graph corresponds to a homogeneous region (e.g., nucleus, cytoplasm) in the image. Attributes of each node include the bounding contours, parametric representation of this contour with hyperquadrics, a number of derived features, and

the response of subcellular compartment under observation. The links in the graph encode the adjacency relationship between various nodes. The attributed graph model completely expresses the structural definition of each cell and its neighborhood. The servoing module controls the concentration of various compounds in the tissue culture vessel by controlling the flow in any of the four syringes that sit next to the microscope. The servoing provides three operational modes with each mode subsequently registered with the recipe-manager: (1) a static recipe in which the flow rate of each compound, its start point in time, and its duration is specified; (2) a dynamic recipe in which the flow rate and its duration are altered as a function of a particular response of the cells under observation; and (3) a modulating recipe under program control that turns the flow on and off at a specified frequency. The archival system stores the images, their computed graph model, and annotation data in a flat file environment. One major feature of our current system is that it can be operated remotely at multiple sites. This unique feature allows researchers to collaborate on a given experiment while sitting at geographically remote locations.

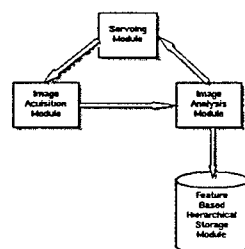


Figure 2: Functional view of the system indicates two unique features: (1) closed loop servo control of compounds being injected into petri dish based on detailed analysis of images; and (2) feature-based storage of images based on computed structural and functional representation of time-lapse video images.

4.2 Segmentation of single-channel data

Our current production use of segmentation algorithms is limited to nuclei observed with fluorescence dye using two different techniques. The first approach is based on a variation of Hough transform that is suitable for a large class of cells as long as they conform to a specifically parameterized geometric model. The second approach focuses on extraction of partial information corresponding to step and roof edges and then groups them through geometric reasoning [13, 14]. The intent is to construct a partitioning that is globally consistent. A list of step edges is constructed by thresholding raw images, recovering corresponding boundaries, and localizing concave corners from their polygonal approximation. These corners provide possible cues to the position where two adjacent nuclei may touch each other. Thresholding separates big clumps consisting of several nuclei squeezed together, but the boundaries between adjacent nuclei cannot be detected because they have higher intensities than background. The partial boundaries between adjacent nuclei can be recovered; however, by extracting crease segments [24, 40, 39], as shown in Figure 3(d). These crease segments correspond to trough edges (positive curvature maxima), but false

creases may also be extracted in the process. Nevertheless, dealing with noise and erroneous segments is a higher-level process that is handled during the grouping process. Our system generates a number of hypotheses for possible grouping of the boundary segments. A unique feature of this system is in hyperquadric representation of each hypothesis and use of this representation for global consistency. The main advantage of such a parameterized representation (as opposed to polygonal representation) is compactness and better stability in shape description from partial information. In this fashion, each step-edge boundary segment belongs to one and only one nucleus while each trough-edge boundary segment is shared by two and only two nuclei. These initial hypotheses and their localized inter-relationship provide the basis for search in the grouping step. This is expressed in terms of an adequate cost function and minimized through dynamic programming. The final result of this computational step is then shown to an operator for verification and elimination of false alarms. An example is shown in Figure 4, where comparison to manual segmentation is shown. A major limitation of this approach is its computational complexity. Grouping of local features is a complex process, and simpler techniques are highly desirable.

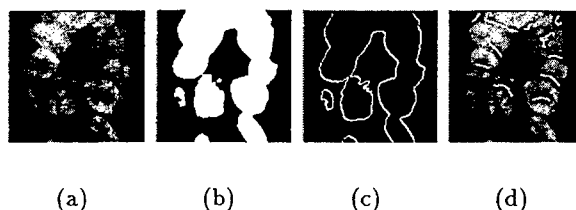


Figure 3: This example demonstrates that segmentation of nuclei with purely global or local operations is not feasible: (a) original image; (b) threshold image; (c) boundary of nuclei; and (d) local troughs.

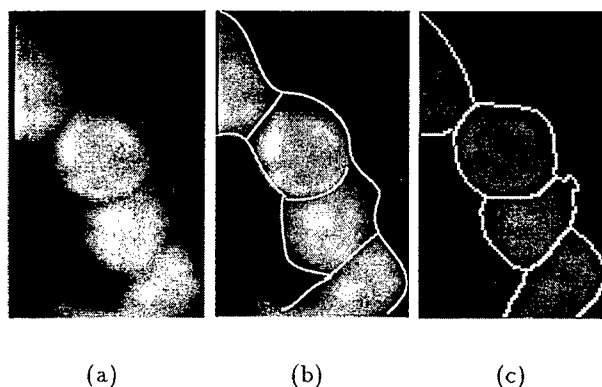


Figure 4: Segmentation results: (a) original image; (b) manual segmentation; (c) our results on segmentation of nuclei.

Recently, we have developed three new techniques. One is based on a new regularized form,

the second on a vector representation of the underlying image followed by feature extraction in vector space, and the third on a geometric and texture model of a cell and its interaction with neighboring cells. The new regularization form has its root in visualization of 3D objects; however, we have also found it to be applicable to segmentation of scientific images. The vector representation of images has its root in analysis of spatio-temporal satellite images [41, 42].

4.2.1 A regularized edge detector based on supremum

Current regularization techniques attempt to minimize an integral such as $\int_R |\nabla f|^2$. Yet, this formulation has no control on the local property of f . In other words, the global average of $|\nabla f|$ may be small, but locally f may change sharply. A way to overcome this issue is to minimize $|\nabla f|$ at every point, which leads to minimization of the supremum of $|\nabla f|$. It is natural to consider the functional $H(f) = \sup_R |\nabla f|$ as a "limit" of the sequence of functionals

$$H_N(f) = \left(\int_R |\nabla f|^{2N} dx \right)^{\frac{1}{2N}}, \quad N = 1, 2, 3, \dots \quad (1)$$

The Euler equation for the minimization of the functional $H_N(f)$ can be expressed as:

$$\begin{aligned} |\nabla f|^{2(N-2)} \left\{ \frac{1}{2(N-1)} |\nabla f|^2 \Delta f \right. \\ \left. + f_x^2 f_{xx} + 2f_x f_y f_{xy} + f_y^2 f_{yy} \right\} = 0 \end{aligned} \quad (2)$$

where a subscript indicates a derivative, such as $f_x = \frac{\partial f}{\partial x}$, $f_{xy} = \frac{\partial^2 f}{\partial x \partial y}$. By removing the first coefficient and letting $N \rightarrow \infty$, we have

$$f_x^2 f_{xx} + 2f_x f_y f_{xy} + f_y^2 f_{yy} = 0 \quad (3)$$

Equation (3) is called the Infinite Laplacian Equation (ILE), which has been studied widely in the literature [1, 2, 3, 15]. Some important properties of the equation [2] are: (1) there is at most one solution and if we redefine the "solution" in a suitable weak sense, then a continuous solution to C^1 does exist; (2) the trajectory of the gradient of f is either a convex curve or a straight line; and (3) there are no stationary points $|\nabla f| = 0$ in R .

The rationale for optimality of the supremum is based on the "equal importance criterion" [11, 12]. This criterion asserts that *every point in R is equally important and contributes similarly to the estimation process. Any other assumption means that we need to know some additional information about the curve.* It is easy to verify that ILE is equivalent to the following equation:

$$\mathcal{J}'(f) = \nabla(|\nabla f|) \cdot \frac{\nabla f}{|\nabla f|} = 0 \quad (4)$$

which implies that along each trajectory of the gradient of f , the magnitude of the gradient is a constant. Figure 5 indicates that minimizing the integral of $|\nabla f|$ aims to minimize the area while minimizing the supremum aims to minimize the maximum. Although the overall integral of $|\nabla f|$ may be larger, the supremum is smaller and the gradient is more likely to concentrate at a smaller

range. It is interesting to note that Equation 3 is equivalent to the zero-crossing ($f_{xx} + f_{yy} = 0$) in the local coordinate system, where the local coordinate system is defined by ∇f .

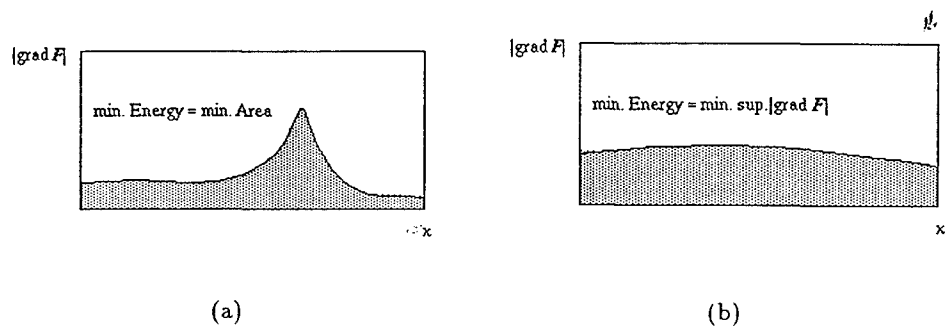


Figure 5: Comparison of our method with traditional regularization terms: (a) solution to minimization of gradient; (b) solution to minimization of supremum.

The edge detection results reveal closed regions. These regions correspond to spatial blobs that are further filtered for size, response, and convexity constraint. An example is show in Figure 6.

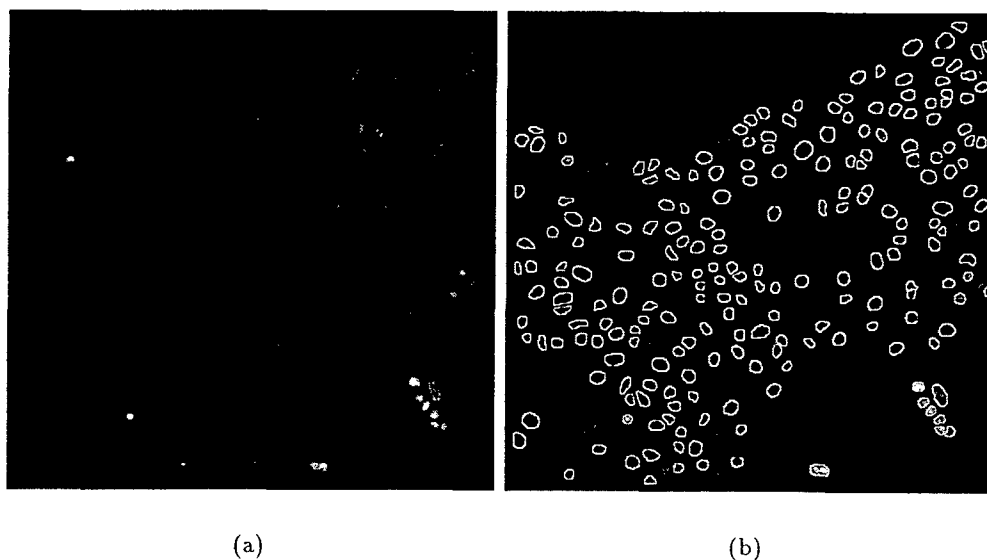


Figure 6: Segmentation result of human epithelial cells at low resolution: (a) original image; (b) extracted nuclei.

4.2.2 Tensor-based feature analysis

Vector field analysis is a well-studied technique in computer vision and pattern recognition as well as other classic fields such as mathematics and physics. Many concepts and tools have been developed for motion based applications. Our work extends the current state of the art to segmentation and interpretation of scientific images. Given an intensity image $f_0(x, y)$, there exists a natural vector field derived from the intensity image, which corresponds to the gradient field rotated by $\pi/2$:

$$\mathbf{v} = \left(-\frac{\partial f_0}{\partial y}, \frac{\partial f_0}{\partial x}\right)$$

The problem here is that the vector field \mathbf{v} is noisy, and some type of regularization needs to be introduced. This can be expressed as

$$\min_{\mathbf{u}} \int \int \|\mathbf{u} - \mathbf{v}\|^2 + \alpha^2 \|\nabla \mathbf{u}\|^2 dx dy$$

where \mathbf{u} is the regularized vector field. An elliptic PDE can be solved iteratively. A first order approximation can be computed by a simple linear (Gaussian) scale space model [23]:

$$f(\cdot; t) = g(\cdot; t) * f_0(\cdot)$$

where

$$g(x, y; t) = \frac{1}{2\pi t} e^{-\frac{x^2+y^2}{4t}}$$

is the Gaussian kernel with standard deviation $\sigma = \sqrt{2t}$.

Singularities of the vector field then provide a compact abstraction for the dense vector representation. These singularities can be characterized by point or linear features. Point features include vortices and saddle points. An example of such a vector field and its singularities (vortices) on a synthetic scene is shown in Figure 7. Once these patterns are detected, the corresponding objects can be extracted. Rao [34] used local Jacobian for feature extraction from the underlying vector field to detect singularities. Our approach is more robust and provides a measure for the size of the vortex as well. The vortex size complements localization of convex blobs eventhough they are connected (or touching one another). This is based on *Jordan index* to localize singularities in the underlying vector field. Let $F = (u, v)$ be a vector field and J be a Jordan curve with no critical point on it. The index of J is defined by

$$\text{Index}(J) = \frac{1}{2\pi} \oint_J \frac{u dv - v du}{u^2 + v^2}$$

At each point P , we choose a small circle of radius R (denoted by J_P^R) around P and compute $\text{Index}(J_P^R)$. The flow field (u, v) can then be classified according to:

1. The index of a vortex is equal to +1 (the classification of singular points in a vector field is given in [34]), and
2. The index of a saddle point is equal to -1.

Note that there is no node in the vector field because its divergence is zero everywhere, i.e.,

$$\text{div} \mathbf{v} = \frac{\partial}{\partial x} \left(-\frac{\partial f}{\partial y} \right) + \frac{\partial}{\partial y} \frac{\partial f}{\partial x} \equiv 0$$

The vortex size is then estimated by a simple search technique. If a point $a(x, y)$ is a vortex, then its size $R^*(x, y)$ can be defined as

$$R^*(x, y) = \max\{R | \text{Index}(J_{(x,y)}^R) = 1\}$$

In other words, $R^*(x, y)$ is the largest R such that the index of $J_{(x,y)}^R$ remains to be 1. Being an integral of the first order partial derivatives, the Jordan index is, in some sense, a function of the intensity image. In contrast, other techniques are based on high order derivatives, which are bound to be more noisy. Figures 7, 8, and 9 show the result of vortices and region segmentation on a synthetic image, nuclei labeled with fluorescent dye, and cells observed with transmission light. The later result is significant because current techniques in localizing individual cells are limited to fluorescent imaging, which adds a layer of complexity to the design of dynamic experiments.

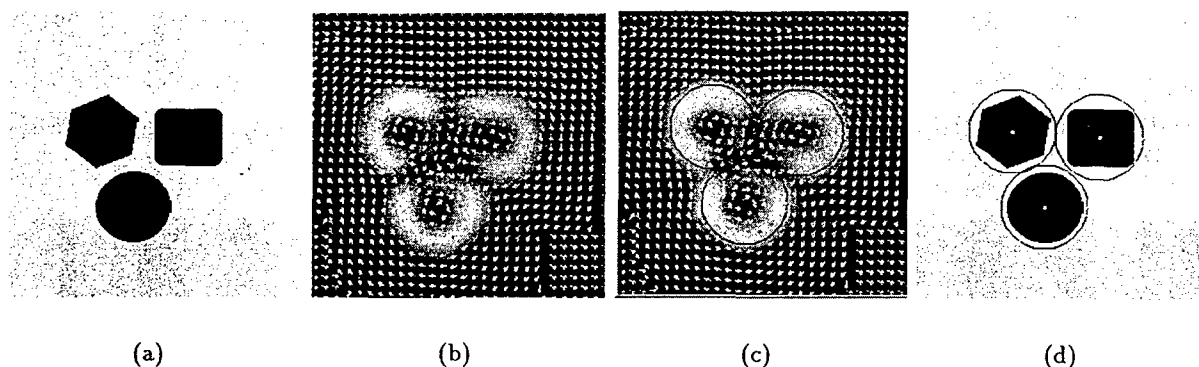


Figure 7: Vector field analysis on a synthetic image: (a) original image; (b) vector field corresponding to the gradient field; (c) detection of vortices from the vector field; (d) localization results.

4.2.3 Geometric and texture model

Although the previous techniques are applicable for localizing nuclei, a more advanced technique is needed for a more detailed segmentation at higher imaging resolution. This is based on a geometric model of the cell, its texture in various compartments, and relationship of its features with respect one another. The geometric model is expressed as a graph, and the texture is computed using an array of orientation and scale specific filters. These local feature activities help collect an ensemble of information that is further refined with dynamic programming [28]. Our preliminary result, shown in Figure 10, indicates reasonable segmentation of nucleus and cytoplasm, which can be used as a basis for computing responses in each of these compartments. Furthermore, responses can be annotated with a proximity filter (distance transform) to reveal whether responses in the

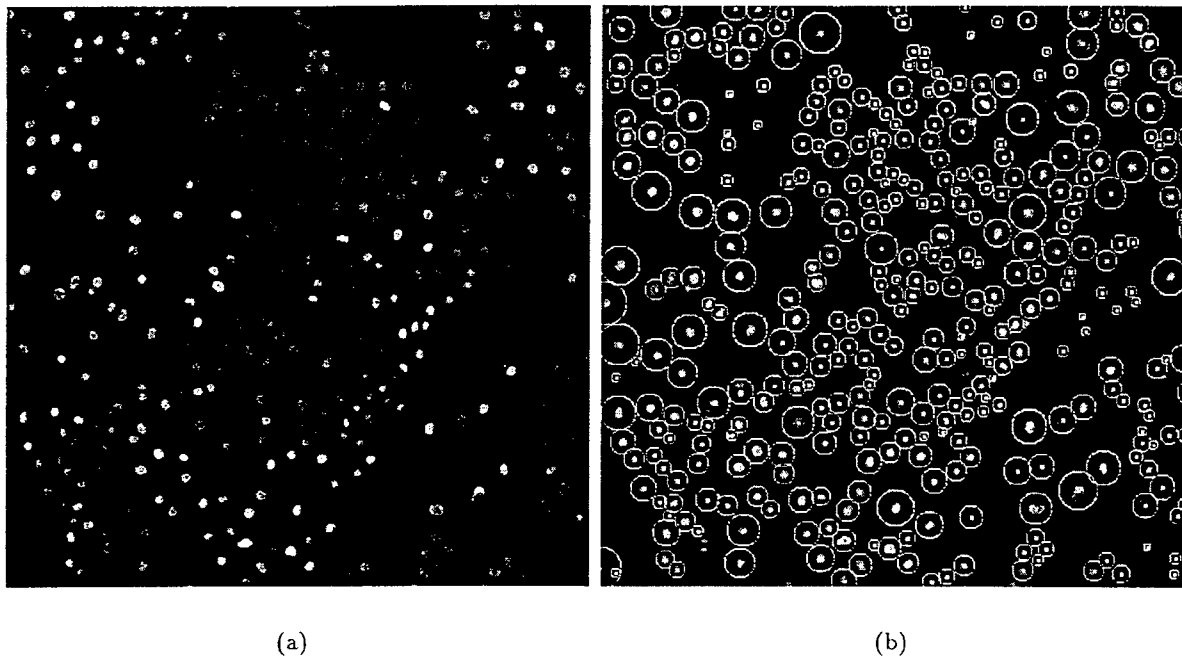


Figure 8: Detection of vortices from nuclei of MCF7 cells: (a) original image; (b) fields of vortices.

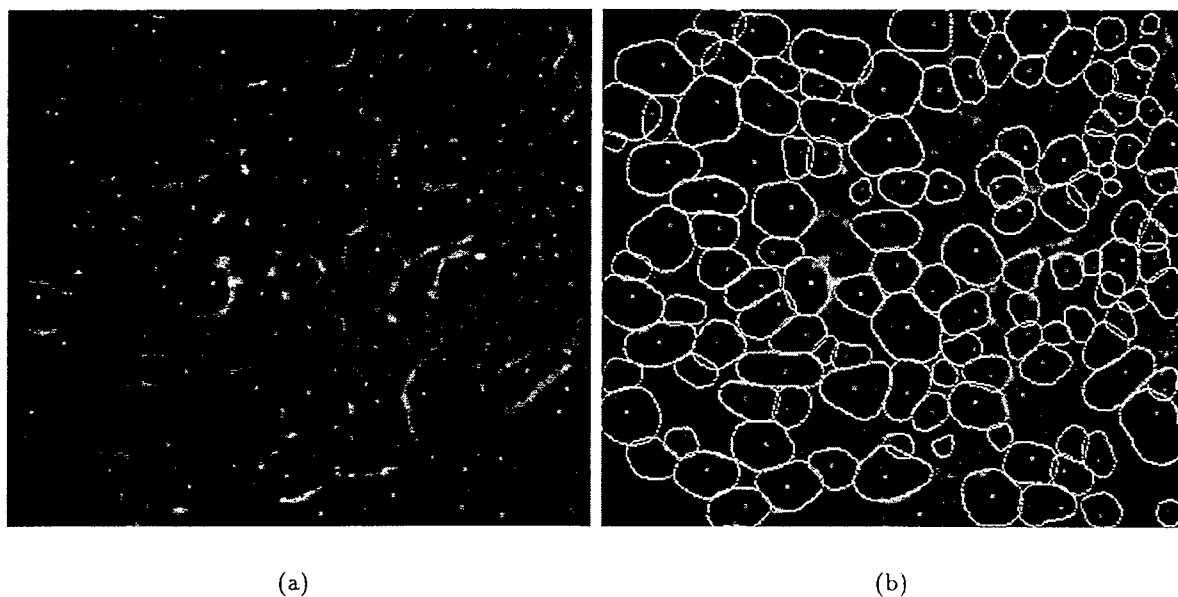


Figure 9: Detection of cells from phase contrast imaging: (a) the original image with detected vortices; (b) cell boundaries from a balloon expansion.

cytoplasm have a preferred localization or are diffused. For example, it is important to know whether the concentration of a particular compound is at lysosome or mitochondrial. In general, preferred uptake at lysosome tends to be of less interest.



Figure 10: Preliminary result for segmentation of MCF7 cells at mid-resolution uses geometric and texture features to delineate sub-cellular structures. The functional response in each compartment can then be measured for large scale statistical analysis as well as visual servoing in real-time.

4.3 Segmentation of multi-channel data

Imaging mode may be multispectral. In this context, a sample is imaged with different dyes and filters to accentuate different cellular components. Here, the system must be able to analyze several channels of data simultaneously, select a specific location in the cytoplasmic region, and make repeated measurements. An efficient approach to fusing images based on a Bayesian framework has been developed. This approach can also be extended to 3D (with confocal microscopes), as demonstrated by our earlier work [29]. The purpose of data fusion is complementary processing of different modalities for segmentation and labeling. From this perspective, the segmentation procedure should label each pixel in the data volume accordingly. A number of ambiguities; however, can complicate the labeling process. These ambiguities can arise from purely local processing and the absence of any high level feedback. The sources for the ambiguities include corruption of data by noise, performance limitation of algorithms for extracting local features, and the existence of nonessential features that impede the labeling task. One aspect of region segmentation is estimating the average intensity of each region by analyzing the histogram. The initial position of the peaks in the histogram are approximated and then refined with least square approximation. The next step of the computational process is to use these peaks as cluster centers to enforce local consistency in the image space. Here, a Bayesian framework is used to label images based on their multiple channel information. Specifically, we use a Bayesian hierarchical model with three levels of hierarchy. The first level is a model for the underlying classification, Z . Under ideal conditions,

observing Z under M different modalities (here, there are three fluorescent images correspond to 360nm, 490nm, and 570nm fluorescent emission, respectively) specifies an ideal representation, X_i , of the data that are corrupted by different types of noise in the imaging system. The third level of the hierarchy corresponds to the actual observation of data Y_i . The first level uses Markov Random Field (MRF) with prior probability density function in the form of Ising model with a positive parameter β . This parameter encourages cooperation among nearby pixels. In a Bayesian framework, β may assume prior ignorance about the scene content. The second level models X as conditionally independent given Z , i.e., $P(X_1, \dots, X_M|Z) = P(X_1|Z) \dots P(X_M|Z)$. This is reasonable because if a classification is labeled as cytoplasm, then the ideal response of the green channel (cytoplasm) and the blue channel (nuclei) will not affect each other. Finally, the third level of hierarchy, Y_i , is modeled as a Gaussian distribution. As a result, Y_i will be a locally blurred representation of X_i . The full model can be written as

$$P(Z, X_i|Y_i) = \prod P(Y_i|Z) \prod P(X_i|Z)P(Z) \quad (5)$$

We use maximum a posteriori (MAP) estimates to obtain X_i and Z . Because MAP computation is inherently infeasible, we use numerical approximation based on iterative conditioning modes (ICM) [5] to find the local optimum. An example of three channel fluorescent image analysis is shown in Figure 11:

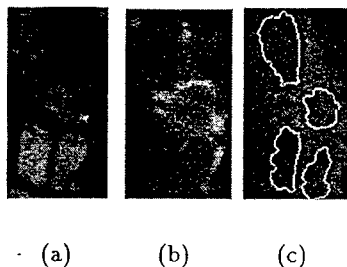


Figure 11: Multiple channel data fusion for segmentation of nuclei: (a) DAPI image (blue channel); (b) Texas Red image (red channel); (c) segmentation results on FITC (green channel).

5 Research design and methods

This section outlines new developments to accommodate specific experiments.

5.1 Detailed segmentation

Although the group has a wide array of computational tools for automated analysis of images, these tools are not sufficient for detailed analysis of various compartments within the cell. Specifically, some form of image restoration and a better segmentation model are Needed. The requirement for image restoration originates from the fact that there could be potential cross-talk between responses

obtained at different focal planes. Furthermore, as Figure 10 shows, different compartments in a cell may not have the necessary clarity and focus at a given focal length. We will incorporate a simple nearest neighbor deconvolution to reduce cross-talk, noise, and improve the required image quality and resolution. Segmentation must be more detailed (e.g., with respect to localizing nucleus, membrane bounding the cytoplasm, mitochondrial, and lysosome). A precise structural definition of these compartments is necessary to measure how (fluorescently) labeled compounds are expressed in each compartment and whether such expressions are diffused in cytoplasm or highly localized. This will be achieved by designing a strategy to couple on-line segmentation (analysis of images) with control of the excitatory filters and perfusion of specific dye into a petri dish. The dye labels a specific area in the cell that is visible at a particular excitation filter. This is another form of visual servoing in which the instrument is placed in a particular state, based on computed features from image content. We will build a real-time computational toolkit to track the trajectory and expression of naked antisense compounds in subcellular compartments. The computed tracking results will then be used to populate the database.

5.2 Feature based image storage

Our current model of storage are based on flat files that is difficult to search and maintain. We propose to leverage an active bioinformatic program to build the required schema for storage handling. The design of current schema for low dose radiation study is shown in Figure 12. This design will be extended to accommodate VSOM and the required chemistry. The intent is to build a feature based spatio-temporal database that will be used for constructing a model of how and where each AS-ODN compound settles in subcellular compartment and what it takes to free it. The proposed multidimensional database, shown in Figure 13, will represent the structure and function of subcellular anatomy, the dose response curve for each compartment, and the trajectory of the compounds from one compartment to next. Each experiment consists of a target frame (image) that corresponds to a specific physical location on the petri dish. The subcellular structures in the cell are segmented and stored as an attribute graph along with the annotation data. The target frame is then observed with time-lapsed video microscopy while compounds are being injected into petri dish under computer control. The response, in each compartment, is recorded and the trajectory of the antisense compound is tracked as it migrates in the subcellular compartment.

The functional view of the stored data will be hierarchical. At the lowest level, raw images and the corresponding physical annotation of images will be stored. At the next level, the attributed graph model (structure), corresponding responses (function), and dynamic annotation of environmental condition (e.g., compound type, flow rate) will be stored. At the next level, the temporal expression of each compartment in a cell will be summarized as a response curve along with trajectory of the compound. These responses may not be similar for all cells under observation. We expect; however, that these response curves will form clusters, with each cluster corresponding to a group of cells in similar state or cell lines of a particular origin. These clusters must be identified for subsequent correlation studies. Each cluster corresponds to a time series event that correspond to a particular compartment in the cells. The average behavior of these responses in each cluster will be represented through single value decomposition. Formally, the observed response is a multivariable

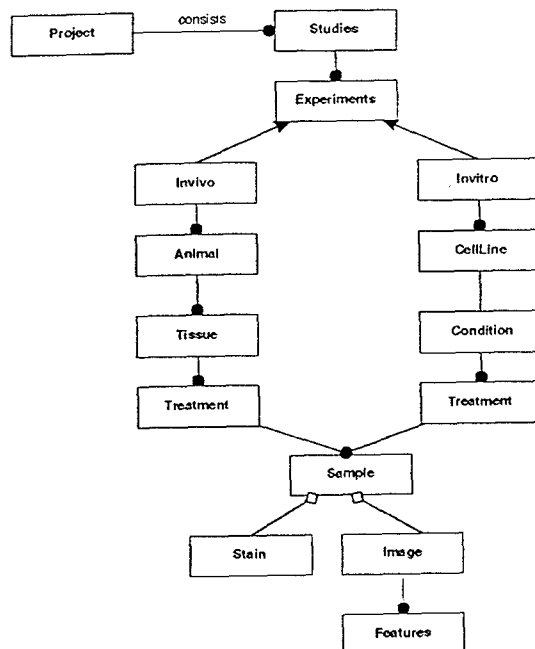


Figure 12: Current schema model for low dose radiation studies (funded through DOE-OBER)

function defined as

$$f_t(Channel, CellType, Compartment, Dye) = f([Dye], \frac{\partial f}{\partial t}, \frac{\partial Flow_{c_i}}{\partial t}, T) \quad (6)$$

Where f is the mean intensity observed in a specific compartment at time t , $[Dye]$ is the concentration of dye, $Channel$ is the position of the excitation filter, T is temperature, and $\frac{\partial Flow_{c_i}}{\partial t}$ corresponds to changes in the flow of compounds being injected. Schema will be developed to capture this time varying information to store the observations into a database for subsequent knowledge discovery. Each experimental cycle generates a fingerprint for each observed cell. These individual responses provide a compact representation of intra-cellular activities in the image space that can be visualized per cell, population of cells, cell types, etc.

5.3 Learning from cell responses

We will extend and apply learning techniques to help refine and design new antisense compounds for targeting mRNA sequence into cytoplasmic or nucleoplasmic compartments of the cell. In this context, computed responses together with their organization and trajectories aid in development of a model and environment in which subsequent stepwise search for design and modification of antisense can take place. The basis for any learning approach is a policy, rewards, values, and a model of environment. One purpose of model reconstruction is to evaluate various policies and reward functions. For example, what are the transition probabilities that describe the state of a

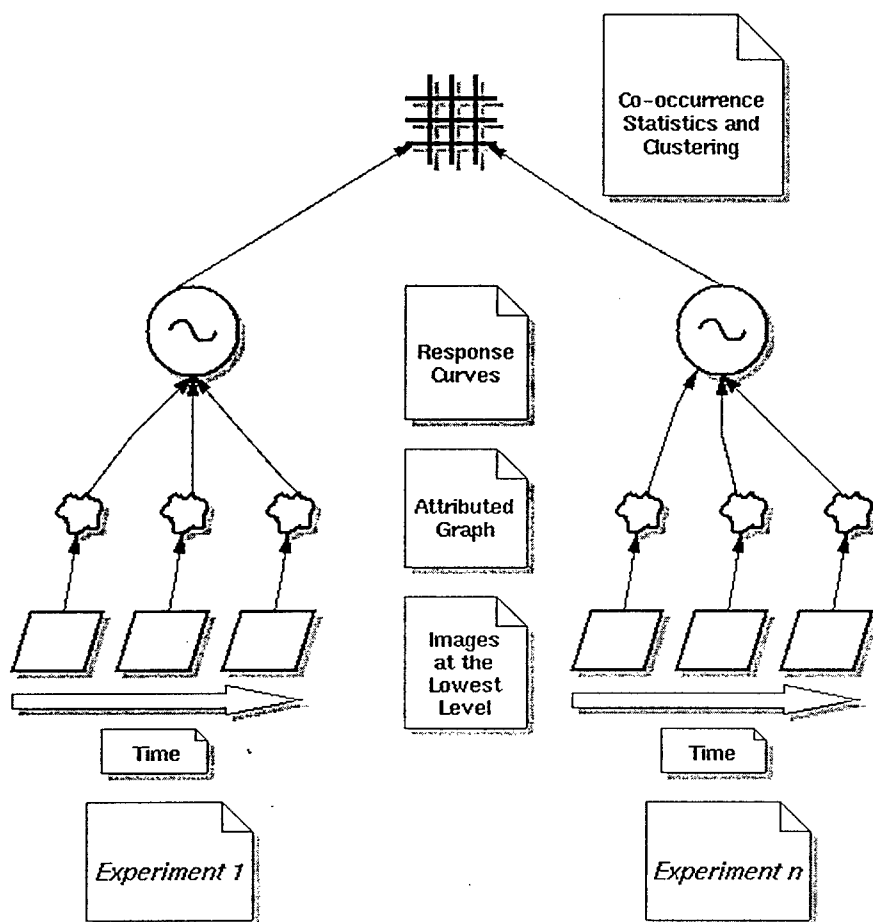


Figure 13: Feature based hierarchical storage of computed structure and function in each compartment of the cell. Each experiment consists of time lapsed video imaging and the required manipulation of perfusion pumps (not shown here). Images are stored at the lowest level. The next level stores the structure and function of the subcellular anatomy as an attributed graph. The third level constructs the corresponding response curves at a specific location and inferred trajectories of the compound. The fourth layer provides a mechanism to construct the transition probabilities together with cross-correlation studies between experiments.

cell as AS-ODN is injected or pH altered in its environment? Or what should be the modulation frequency of a compound (alternating high/low concentration) to track the retention of a particular compound in the cell structure? This step provides the basis for construction of a model and environment. Furthermore, we expect that such a model will vary from one cell-line to another. These variations are significant by their own merit and when quantified, can serve as a valuable validation. The content of a database will provide the basis for evaluation, refinement, and localization of similarity measures. Similarities will be measured by analyzing clusters on the basis of state and action. These clusters aid in computation of co-occurrence statistics over different responses for establish an equivalence classes. Alternatively, a cell response and its corresponding attributes (dynamic annotations) will generate a representation within a sequence. This representation can then be used to construct joint co-occurrence statistics in that sequence together with transition probabilities. The co-occurrence statistics will aid in hypothesizing a binary tree classification of an ensemble of representative features. One utility of this method is in detecting and classifying correlated sequences. Furthermore, once a model is established, co-occurrence statistics will provide a means of detecting outliers. The transition probabilities will provide the knowledge of environment, which can be used for reinforcement learning. In addition, we will explore modeling the cell responses as a time varying linear system. Linear systems are simple and powerful techniques to characterize the behavior of a system. In this context, a state space representation of the system with variable memory (delay) is constructed and parameters of the associated matrices are estimated and validated.

5.3.1 Reinforcement learning

The intent is to use prior knowledge as a starting point to learn how to manipulate an antisense for guiding it into a specific site in a systematic way. This is often referred to as "reinforcement learning" in the literature, which may be modeled as a Markov decision process (MDP). A particular MDP is defined by its state (observed response) and action set that includes modification of antisense by changing its binding constant, altering the concentration of important intra-cellular ions for releasing sequestered antisense from nucleus, etc. The reward in such a system is measured as the changes in computed response or its episodic gradient. Furthermore, the transition probabilities (of the Markov decision process) can be computed from observations made from the same assay in the database. These transition probabilities provide the enabling technology for an optimal policy (schedule). In general, such a policy can be expressed as dynamic programming, Monte Carlo methods, and temporal difference learning. Dynamic programming requires a model of cell response. Such a model can be hypothesized from the database. Presumably, as the database expands, models may become more accessible. Monte Carlo methods do not require a model, but they are not suitable for step-by-step incremental computation. On the other hand, temporal methods require no model and are fully incremental. The PI has extensive experience in expressing a policy based on dynamic programming [14, 28, 32]. Still, all three methods apply to our research agenda. For example, Monte Carlo techniques can be used in one incremental step (or one episode) if sample transition probabilities (not a complete one) exist. And temporal differencing is the combination of Monte Carlo and dynamic programming (i.e., learning directly from raw experience without the model, and then updating estimates based on currently learned estimates).

5.4 Experiments

Our experimental plan is designed to complement the companion grant, "Strategies for Imaging Gene Expression with PET", submitted by S. Taylor, et al. from the LBNL Center for Functional Imaging (LBNL CGI) in which in vivo animal experiments and PET imaging will be performed using radiolabeled AS-ODN. We plan to collaborate closely with this group, and for this reason we will use the same cell line, (BT- 474 cells, breast cancer cells that overexpress the apoptotic bcl-2 protein) and the same three AS-ODN sequences designed to target the bcl-2 protein. Our in vitro technology will allow us to test more modifications of these compounds than is possible in in vivo studies of nude mice bearing BT-474 tumor xenografts. However, many of our joint experiments will include AS-ODN compounds of the same sequence with the same modifications, with the exception of the modification at the 5' terminus of the AS-ODNs, which be a fluorochrome in the case of our experiments but will be one of two radiofluorinated moieties for in vivo PET imaging studies. In both cases, however, a hexyl-amine linker will be attached to the 5'-terminus to facilitate attachment of the fluorochrome and radiolabel. Our proposal and the Taylor proposal are also integrated in several other ways. For example, the two groups will conduct control experiments using the same "sense" sequences that are complimentary to the three AS-ODN sequences we have chosen, and the same non-bcl-2 producing cell line. Further, in the Taylor grant, differential cell sedimentation centrifugation experiments and binding assays using the BT-474 cell line will be performed with both radiolabeled and fluorescence labeled compounds. In addition, both groups will perform studies to determine if the delivery of AS-ODN is enhanced using liposomes and immunoliposomes. The same liposome preparations will be used between our two groups. For our biological endpoint studies, we will in some cases use a non-fluorescent, non- radioactive version of the fluorinated moiety used in the radiolabel studies. In this manner, we will determine the consequences, if any, of different substituents at the 5'-terminus of the AS-ODNs. It will also be possible for our group to determine the amount of signal amplification produced by the β -galactosidase amplification protocol proposed by the Taylor group. AS-ODN sequences to be used:

1. PT-G3139: TCTC CCAG CGTG CGCC AT

The full phosphorothiate of this 18-mer with sequence antisense to the first six codons of the open reading frame of bcl-2 has shown efficacy against the DoHH2 lymphoma implanted in severe immunodeficient mice (Raynaud et al., 1997).

2. PNA-1: CCCC AGCC CCTA CCC

3. PNA-4: AGCG TGCG CCAT CCC

Peptide nucleic acid (PNA) is a modified oligonucleotide in which the entire deoxy-ribose backbone has been replaced with a polyamide (peptide) chain (Gewirtz et al., 1998 [17]; Tamsamani and Guinot, 1997 [36]). These two 15-mer PNA-ODNs have been evaluated in vitro in a cell- free system (Mologni et al., 1999). Of particular interest is the fact that a complete block of mRNA translation is only achieved when both PNA- ODNs are present simultaneously.

5.4.1 VSOM experiments

Flourescence labeled versions of PT-G3139, PNA-1, and PNA-4 will be obtained commercially (Genset, <http://www.gensetoligos.com>) and from the Taylor group. We will also obtain modifications of these AS-ODNs where the backbone consists entirely of PD, PT, MP, or PNA backbone linkages. In addition, we will obtain compounds with various permutations and mixtures of backbone linkages.

Initial experiments will be performed and recorded in the database as a series of single-cell responses. We will use a set of fluorescently labeled AS-ODNs with various modifications of the backbone linkages, as described above. A set of baseline VSOM runs will be performed. In these runs, cells will be grown on microscope coverslips, and a 63X, NA 1.3 oil-immersion objective will be used. Cells will be placed in a temperature controlled microperfusion chamber containing cells at 37 °C. An initial segmentation of the cytoplasmic, nucleoplasmic, and mitochondrial compartment will be performed in the following manner. A computer controlled syringe will inject the fluorescent compound TMRE contained in a D-PBS (Dulbecco's phosphate-buffered saline) buffer containing calcium, magnesium, glucose and pyruvate. The compound TMRE (tetramethyl rhodamine ethyl ester, Molecular Probes, Eugene, OR) is a cationic redistribution dye used to determine the mitochondrial membrane potential according to the Nernst equation (Farkas et al., 1989). Unlike the mitochondrial dye rhodamine 123, TMRE equilibrates rapidly and reversibly into the mitochondria and (to a lesser extent) the cytoplasm. It does not stain the nucleoplasmic compartment. Our ability to perform such segmentation on TMRE stained MCF-7 cells (a human breast cancer cell line) was shown in Figure 10. Next TMRE will be flushed out of the cell using a computer-controlled syringe containing buffer only. TMRE is readily rinsed out of the cell. We will then proceed to inject fluorescently labeled AS-ODN into the microperfusion chamber using yet another computer controlled- syringe. The concentration at which fluorescent signal from the AS- ODN becomes visible will be noted, and the AS-ODN perfusion will be automatically halted. This will complete the first half of a VSOM run.

It should be noted that all digital images will become part of the database so that they make be replayed in order to verify VSOM operation. Thus, multi-channel digital images, experimental parameters, and single-cell responses (5-10 cells at 63X) to computer-controlled compound perfusions will become part of the database.

The second half of these initial VSOM runs will be conducted as follows. The fluorescence distribution pattern of the fluorescently labeled AS- ODN will be compared with either (i) previously observed fluorescence distribution patterns obtained for the same cell type using organelle- specific fluorescence dyes (Molecular Probes, <http://www.probes.com/>) or (ii) the existing fluorescence pattern in a separate fluorescence channel for the current cells, dual-stained with both fluorescent AS-ODN and an organelle-specific fluorescence dye. After the VSOM makes a determination of the AS-ODN location within the cell, it will apply the appropriate compound from the appropriate syringe and observe the effect on AS-ODN distribution within the cell.

In the case of lysosomal sequestration of fluorescently labeled AS-ODN, compounds known to selectively permeablize lysosomes will be perfused into the chamber at a controlled rate by the computer-controlled perfusion pumps. Several compounds, such as the sodium proton ionophore

monesin, have been demonstrated to free fluorescent compounds trapped in the acidic vesicles of human breast cancer cells (Schindler et al., 1996). The amount of monesin (for example), required to free fluorescently labeled AS-ODNs will be logged in the database. The time for redistribution to the next compartment (the nucleus for example) and the resulting pattern of staining in the nucleus will also be recorded.

VSOM perturbations to dislodge AS-ODN compounds from the nucleus will be performed using "clamping" techniques which allow the experimentalist to vary the concentration of intracellular ions such as potassium by simply varying the potassium concentration of the surrounding extracellular medium (Negulescu et al., 1994). These same methods can be used to alter levels of intracellular calcium. The VSOM system will ramp up the concentrations of such ions within the cell in an attempt to interfere with the binding of AS-ODN to basic nuclear proteins. Once again the concentrations and other environmental conditions necessary to dislodge the compounds from the nuclear compartment will be recorded. If these attempts are not successful, on-line hypotonic lysis of the cells will be performed and harsher environmental conditions will be applied.

VSOM perturbations to dislodge cytoplasmic membrane-associated AS-ODN will consist of buffer rinses at nonphysiological pH or rinses with buffer containing trypsin. Once again, quantitative data on the magnitude of perturbation required to free the fluorescently labeled AS-ODN will be recorded on a cell-by-cell basis and will be correlated with the chemical structure of the current AS-ODN.

5.4.2 Physiological and fluorescence assays for apoptosis in living cells

The physiological effects of the AS-ODNs (both fluorescent and nonfluorescent) can be assessed in several ways. In most cases, we will apply an apoptosis-inducing extracellular stress such as UV light, anticancer drugs, or calcium ionophores. If the AS-ODN successfully reduces the amount of bcl-2 protein in BT-474 cells, we will be able to detect a decrease in bcl-2 protein and a decrease in these cells' ability to resist apoptosis. The most direct method is to fix the cells after the experiment, perform indirect immunofluorescence using an antibody for the bcl-2 protein, then return to the same field of cells to quantify the amount of bcl-2 protein, which should be proportional to the observed fluorescence signal on a cell-by-cell basis.

Many other markers for apoptosis exist, both morphological and fluorescent. For example, one of the channels we collect during VSOM experiments is the transmitted light channel, where membrane blebbing can be observed. There are also a variety of antibodies to proteins such as Annexin V, and also DNA stains which reveal the nuclear fragmentation characteristic of apoptosis. In addition, we regularly use cytoplasmic membrane integrity (cell viability) stains such as calcein-AM in one of the fluorescence channels during VSOM experiments. Also of interest to us is the fact that loss of the mitochondrial membrane potential occurs early in apoptosis, and we would be able to detect such changes in the mitochondrial membrane potential by using TMRE, as described above.

5.4.3 AS-ODN Delivery techniques

AS-ODNs will be delivered as naked compound, or encapsulated in liposomes, or they will be injected using a microcapillary positioner we used in our DNAmicrodissection studies.

References

- [1] G. Aronsson. Extension of function satisfying lipschitz conditions. *Ariku för Matematik*, 6:551-561, 1966.
- [2] G. Aronsson. On the partial differential equation $u_x^2 u_{xx} + 2u_x u_y u_{xy} + u_y^2 u_{yy} = 0$. *Ariku för Matematik*, 7:133-151, 1967.
- [3] G. Aronsson. On certain singular solutions of the partial differential equation $u_x^2 u_{xx} + 2u_x u_y u_{xy} + u_y^2 u_{yy} = 0$. *Manuscripta Math*, 41:133-151, 1981.
- [4] M.H. Barcellos-Hoff. Mammary epithelial reorganization on extracellular matrix is mediated by cell surface galactosyltransferase. *Experimental Cell Research*, 34:201-225, 1992.
- [5] J. Besag. On the statistical analysis of dirty pictures. *Journal of Royal Statistical Society B*, 48(3):259-302, 1986.
- [6] D. E. Callahan, T. M. Forte, S. M. J. Afzal, D.F. Deen, S. B. Kahl, K. A. Bjornstad, W. F. Bauer, and E. A. Blakely. Boronated protoporphyrin (bopp) localization in lysosomes of the human glioma cell line sf-767 with uptake modulated by lipoprotein levels int. j. radiation. *Oncology Biol. Phys.*, 45:761-771, 1999.
- [7] D. E. Callahan and T. M. J. Hooker. Conformation of dna in solution: Cd calculations based on crystal structures of b- and z-dna fragments. *Biopolymers*, 26(457):61, 1987.
- [8] D. E. Callahan, A. Karim, G. Zheng, P.O. Ts'o, and Lesko. Quantitation and mapping of integrated human papillomavirus on human metaphase chromosomes using a fluorescence microscope imaging system. *Cytometry*, 13(453):61, 1992.
- [9] D. E. Callahan, T. L. Trapane, P. S. Miller, P. O. Tso, and L.S. Kan. Comparative circular dichroism and fluorescence studies of oligodeoxyribonucleotide and godeoxyribonucleoside methylphosphonate pyrimidine strands in duplex and triplex formation. *Biochemistry*, 30(1650):5, 1991.
- [10] D. J. Chin, G. A. Green, G. Zon, F. C. J. Szoka. and R. M. Strabinger. Rapid nuclear accumulation of injected oligodeoxyribonucleotides. *New Biologist*, 2(1091):100, 1990.
- [11] G. Cong and B. Parvin. Shape from equal thickness contours. In *Proceedings of the Conference on Computer Vision and Pattern Recognition*, 1998.
- [12] G. Cong and B. Parvin. An algebraic solution to surface recovery from cross-sectional contours. *Journal of Graphical Model and Image Processing*, 1999.
- [13] G. Cong and B. Parvin. Model based segmentation of nuclei. In *Proceedings of the Conference on Computer Vision and Pattern Recognition*, 1999.
- [14] G. Cong and B. Parvin. Model based segmentation of nuclei. In *Journal of Pattern Recognition*, 2000.

- [15] L. Evans. Estimates for smooth absolutely minimizing lipschitz extensions. *Electronic Journal of Differential Equations*, <http://ejde.math.swt.edu/Volumes/1993/03-Evans/abstr.html>, 1993(3):1-9, 1993.
- [16] D.L. el al Farkas. Simultaneous imaging of cells and mitochondria membrane potentials. *Biophysical Journal*, 56:1053-1069, 1990.
- [17] A. M. Gewirtz, D. L. Sokol, and M. Z. Ratajczak. Nucleic acid therapeutics: state of the art and future prospects. *Blood*, 92(712):36, 1998.
- [18] L. S. Kan, D. E. Callahan, T. L. Trapane, P.S. Miller, P. O. Ts'o, and D. H. Huang. Proton nmr and optical spectroscopic studies in the dna triplex formed by d-a-(g-a)7-g and d-c-(t-c)7-t. *Journal Of Biomolecular Structure And Dynamics*, 8(911):33, 1991.
- [19] D. S. Kaplan and G. L. Picciolo. Characterization of instrumentation and calibrators for quantitative microfluorometry for immunofluorescence tests. *Journal of Clinical Microbiology*, 27(442):7, 1989.
- [20] J. P. Leonetti, N. Mechti, G. Degols, C. Gagnor, and B. Lebleu. Intracellular distribution of microinjected antisense oligonucleotides. *Proceedings of the National Academy of Sciences of the United States of America*, 88(2702):6, 1991.
- [21] S. A. Lesko, M. E. Callahan, D. E. LaVilla, Z.P. Wang, and Ts'o. P.O. The experimental homologous and heterologous separation distance histograms for the centromeres of chromosomes 7, 11, and 17 in interphase human t-lymphocytes. *Experimental Cell Research*, 219:499-506, 1995.
- [22] S. A. Lesko, W. Li, G. Zheng, Callahan D.E., W.R. Kaplan, D. S. Midden, and P. T. Strickland. Quantitative immunofluorescence assay for cyclobutylidithymidine dimers individual mammalian cells. *Carcinogenesis*, 10(641):6, 1989.
- [23] T. Lindeberg. Scale-space theory:a basic tool for analyzing structures at different scales. *Journal of Applied Statistics*, pages 225-270, 1994.
- [24] O. Monga, S. Benayoun, and O. Faugeras. From partial derivatives of 3d density images to ridge lines. In *Proceedings of the Conference on Computer Vision and Pattern Recognition*, pages 354-359, 1992.
- [25] K. Pachmann, K. Reinecke, B. Emmerich, and E. Thiel. Highly fluorochrome labeled gene probes for quantitative tracing of rna in individual cells by in situ hybridization. *Bioconjugate Chemistry*, 2:19-25, 1991.
- [26] B. Parvin, D. Callahan, W. Johnston, and M. Measter. Visual servoing for micro manipulation. In *Int. Conference on Pattern Recognition*, Austria, 1996.
- [27] B. Parvin and et al. Telepresence for in-situ microscopy. In *IEEE Int. Conference on Multimedia Systems and Computers*, Japan, 1996.

- [28] B. Parvin, C. Peng, W. Johnston, and M. Maestre. Tracking of tubular molecules for scientific applications. *IEEE Transactions on Pattern Analysis and Machine Intelligence*, 17:800-805, 1995.
- [29] B. Parvin, D. Robertson, and W. Johnston. Visualization of volumetric structures from mr images of brain. In *AAAI Symp. on Application of Computer Vision to Medical Imaging*, 1995.
- [30] B. Parvin, J. Taylor, D. Callahan, W. Johnston, and U. Dahmen. Visual servoing for on-line facilities. *IEEE Computer*, 1997.
- [31] B. Parvin, J. Taylor, G. Cong, M. Okeefe, and M.H. Barcellos-Hoff. Deepview: A channel for distributed microscopy and informatics. In *IEEE High Performance Computing and Networking*, 1999.
- [32] B. Parvin and S. Viswanatha. Optimal grouping of line segments into convex sets. In *British Machine Vision Conf.*, 1995.
- [33] A. K. Raap, F. M. van de Rijke, R. W. Dirks, C. J. Sol, R. Boom, and M. van der Ploeg. Bicolor fluorescence in situ hybridization to intron and exon mrna sequences. *Experimental Cell Research*, 197(319):22, 1991.
- [34] A. R. Rao and R. C. Jain. Computerized flow field analysis: Oriented texture fields. *IEEE Transactions on Pattern Analysis and Machine Intelligence*, pages 225-270, 1994.
- [35] Y. Shoji, S. Akhtar, A. Periasamy, B. Herman, and R. L. Juliano. Mechanism of cellular uptake of modified oligodeoxynucleotides containing methylphosphonate linkages. *Nucleic Acids Research*, 19(5543):50, 1991..
- [36] J. Temsamani and P. Guinot. Antisense oligonucleotides: a new therapeutic approach. *biotechnology and applied biochemistry*, 26(2):65-71, 1997.
- [37] J. Thaden and Miller P. S. Photoaffinity behavior of a conjugate of oligonucleoside methylphosphonate, rhodamine, and psoralen in the presence of complementary oligonucleotides. *Bioconjugate Chemistry*, 4(386):94, 1993.
- [38] A. R. Thierry and A. Dritschilo. Intracellular availability of unmodified, phosphorothioated and liposomally encapsulated oligodeoxynucleotides for antisense activity. *nucleic acids research*, 20(5691):8, 1992.
- [39] J. Thirion. New feature points based on geometric invariants for 3d image registration. *International Journal of Computer Vision*, 18(2):121-137, May 1996.
- [40] J. Thirion and A. Gourdon. The 3d matching lines algorithm. *Graphical Models and Image Processing*, 58(6):503-509, 1996.
- [41] Q. Yang and B. Parvin. Detection of singularities from sst data. In *Int. Conf. on Pattern Recognition*, 2000.

- [42] Q. Yang and B. Parvin. Feature-based visualization of large scale geophysical data. In *Proceedings of the Conference on Computer Vision and Pattern Recognition*, 2000.
- [43] P. Yaswen, M. R. Stampfer, K. Ghosh, and J. S. Cohen. Effects of sequence of thioated oligonucleotides on cultured human mammary epithelial cells. *Antisense Research And Development*, pages 67-77, 1993.



DEPARTMENT OF THE ARMY
US ARMY MEDICAL RESEARCH AND MATERIEL COMMAND
504 SCOTT STREET
FORT DETRICK, MARYLAND 21702-5012

REPLY TO
ATTENTION OF:

MCMR-RMI-S (70-1y)

21 Feb 03

MEMORANDUM FOR Administrator, Defense Technical Information
Center (DTIC-OCA), 8725 John J. Kingman Road, Fort Belvoir,
VA 22060-6218

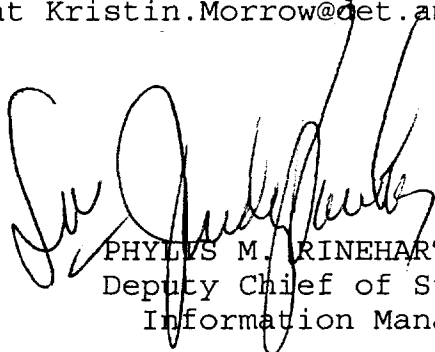
SUBJECT: Request Change in Distribution Statement

1. The U.S. Army Medical Research and Materiel Command has reexamined the need for the limitation assigned to technical reports written for this Command. Request the limited distribution statement for the enclosed accession numbers be changed to "Approved for public release; distribution unlimited." These reports should be released to the National Technical Information Service.

2. Point of contact for this request is Ms. Kristin Morrow at DSN 343-7327 or by e-mail at Kristin.Morrow@det.amedd.army.mil.

FOR THE COMMANDER:

Encl


PHYLLIS M. RINEHART
Deputy Chief of Staff for
Information Management

ADB263458	ADB282838
ADB282174	ADB233092
ADB270704	ADB263929
ADB282196	ADB282182
ADB264903	ADB257136
ADB268484	ADB282227
ADB282253	ADB282177
ADB282115	ADB263548
ADB263413	ADB246535
ADB269109	ADB282826
ADB282106	ADB282127
ADB262514	ADB271165
ADB282264	ADB282112
ADB256789	ADB255775
ADB251569	ADB265599
ADB258878	ADB282098
ADB282275	ADB232738
ADB270822	ADB243196
ADB282207	ADB257445
ADB257105	ADB267547
ADB281673	ADB277556
ADB254429	ADB239320
ADB282110	ADB253648
ADB262549	ADB282171
ADB268358	ADB233883
ADB257359	ADB257696
ADB265810	ADB232089
ADB282111	ADB240398
ADB273020	ADB261087
ADB282185	ADB249593
ADB266340	ADB264542
ADB262490	ADB282216
ADB266385	ADB261617
ADB282181	ADB269116
ADB262451	
ADB266306	
ADB260298	
ADB269253	
ADB282119	
ADB261755	
ADB257398	
ADB267683	
ADB282231	
ADB234475	
ADB247704	
ADB258112	
ADB267627	